UNIVERSITÉ DE MONTRÉAL

EFFECT OF MAGNESIUM CONTENT ON THE SEMI SOLID CAST MICROSTRUCTURE OF HYPEREUTECTIC ALUMINIUM-SILICON ALLOYS

ALIREZA HEKMAT-ARDAKAN

PROGRAMME DE GÉNIE MÉTALLURGIQUE

DÉPARTEMENT DE GÉNIE CHIMIQUE

ÉCOLE POLYTECHNIQUE DE MONTRÉAL

THÈSE PRESENTÉE VUE DE L'OBTENTION

DU DIPLÔME DE PHILASOPHIAE DOCTOR (Ph.D.)

(GÉNIE METALLURGIQUE)

AVRIL 2009

Your file Votre référence
ISBN: 978-0-494-49417-2
Our file Notre référence
ISBN: 978-0-494-49417-2

UNIVERSITÉ DE MONTRÉAL

ÉCOLE POLYTECHNIQUE DE MONTRÉAL

Cette thèse intitulée:

EFFECT OF MAGNESIUM CONTENT ON THE SEMI SOLID CAST MICROSTRUCTURE OF HYPEREUTECTIC ALUMINIUM-SILICON ALLOYS

présentée par: HEKMAT-ARDAKAN Alireza

en vue de l'obtention du diplôme de : Philosophiae Doctor

a été dûment acceptée par le jury d'examen constitué de :

M. TURENNE Sylvain, Ph.D., président

M. AJERSCH Frank, Ph.D., membre et directeur de recherche

M. CHEN X. Grant, Ph.D., membre

Ms. PEKGULERYUZ, Mihriban Ozden, Ph.D., membre

Dedicated to

My lovely wife, Farnaz, my son, Daniel, my daughter, Denise and my parent

ACKNOWLEDGMENTS

I would like to express my sincerest gratitude to the thesis supervisor, Prof. Frank Ajersch for the education, valuable support, helpful suggestions, encouragement and confidence in me. The thesis committee, Prof. Sylvain Turenne (president), Prof. Mihriban Ozden Pekguleryuz and Prof. X. Grant Chen is also acknowledged for their comments and suggestions.

I am grateful to Dr. Ali Shanian, Dr. Shahrooz Nafisi, Dr. Faouzzi Massoud, Dr Kentaro Oishi, Mr. Xichun Liu and all my friends and colleagues for sharing with me their friendship and knowledge. I am thankful to Carole Massicotte and Josée Laviolette, the Ecole Polytechnique's technicians in metallurgical department who provided for me all required facilities.

Finally, I would like to thank my family especially my lovely wife, Farnaz Abbassi-Moghadam for their eternal love and support.

RÉSUMÉ

L'évolution de la microstructure durant le moulage semi solide et le moulage conventionnel a été étudiée pour l'alliage hypereutectique A390 (Al-17%Si-4.5%Cu-0.5%Mg) auquel du magnésium a été ajouté. L'addition de magnésium favorise, lors de la solidification, la formation de la phase intermétallique Mg_2Si au détriment de la phase primaire Si typiquement observée. Il a été démontré que la présence de l'intermétallique Mg_2Si est bénéfique pour la microstructure, pour les propriétés mécaniques et plus particulièrement pour la résistance à l'usure des pièces produites avec l'alliage A390. Pour le moulage semi solide, il est démontré que le Mg_2Si permet d'obtenir une microstructure constituée d'une phase primaire dont la morphologie, la taille et la distribution spatiale sont bénéfiques pour les propriétés mécaniques. La morphologie dendritique de la phase primaire du A390 à forte teneur en magnésium entoure un constituant eutectique composé de fines particules de silicium et de particules de Mg_2Si dont la morphologie est dite en « caractères Chinois ». Cette microstructure est différente de celle typiquement observée pour le A390 conventionnel, dont l'eutectique est essentiellement composé de la phase alpha riche en aluminium et de silicium grossier de forme aciculaire. Pour l'alliage A390 additionné de magnésium, la taille et la morphologie modifiée du silicium eutectique ainsi que la présence de Mg_2Si au sein de la phase primaire permettent d'expliquer que cet alliage résiste mieux à l'usure. De plus, ces mêmes caractéristiques microstructurales ont une influence importante sur les propriétés mécaniques de l'alliage.

La première étape des travaux consiste à étudier les données thermodynamiques qui caractérisent la solidification de l'alliage A390 ayant différentes teneurs en magnésium pour identifier la séquence de formation des phases. L'étude des diagrammes de phases a été réalisée à l'aide du logiciel FACTSAGE pour des conditions thermodynamiques d'équilibre et de non équilibre (Schiel). L'alliage a été caractérisé par un système quaternaire Al-Si-Cu-Mg pour lequel la composition chimique a été fixée à 4.5%Cu et 17%Si. Les proportions de magnésium et d'aluminium (Mg/Al) ont été variées de la façon suivante : 0.5/78, 1/77.5, 2/77, …., 10/68.5 ce qui correspond à des teneurs en magnésium de 1%, 2%, …., 10% respectivement. Pour cette gamme de compositions chimiques, deux compositions critiques ont été identifiées ce qui divise les résultats en trois zones. Ces zones sont caractérisées par une séquence de formation du Mg_2Si bien particulière. Pour une teneur en magnésium entre 0.5 et 4.2%, les résultats thermodynamiques mettent en évidence que le silicium est la seule phase primaire qui se solidifie avant la transformation eutectique. L'intermétallique Mg_2Si n'apparaît que lors de la réaction eutectique ternaire (Liq→Al+Si+Mg_2Si). Pour l'alliage contenant le moins de magnésium (0.5% Mg), il a aussi été observé que la région ternaire est stable dans un intervalle de température plus petit que pour les autres alliages. Cet intervalle de stabilité croît avec l'ajout de magnésium, jusqu'à 4.2%Mg. Il est donc possible d'anticiper que l'alliage A390 conventionnel et l'alliage A390 riche en magnésium auront des microstructures différentes caractérisées par la présence des phases Al+Si et Al+Si+Mg_2Si respectivement. Pour des teneurs en magnésium entre 4.2 et 7.2%, la phase Mg_2Si apparaît lors de la formation du silicium primaire (Liq.→Si+Mg_2Si) ainsi

que lors de la transformation eutectique (Liq→Al+Si+Mg_2Si). Néanmoins, le silicium demeure la première phase à se solidifier. Pour des teneurs en magnésium qui dépassent 7.2%, le Mg_2Si se solidifie en trois étapes à partir d'une réaction primaire (Liq → Mg_2Si), d'une réaction secondaire (Liq. →Si+Mg_2Si) et d'une réaction ternaire (Liq.→Al+Si+Mg_2Si). Au sein de la microstructure de l'alliage, il serait donc possible d'observer du Mg_2Si pro-eutectique de morphologies différentes ainsi que du Mg_2Si eutectique. Ces résultats indiquent que l'intervalle de solidification du Mg_2Si augmente avec l'addition de magnésium. D'un autre côté, la température de la réaction eutectique diminue avec l'ajout de magnésium. Cette diminution est drastique pour des teneurs en magnésium entre 0.5 et 4.2% mais n'est plus significative pour des ajouts supplémentaires de magnésium. Cet effet sur la température eutectique pourrait modifier la morphologie du réseau eutectique. Les résultats thermodynamiques obtenus confirment donc la pertinence d'étudier l'effet du magnésium sur la microstructure de l'alliage A390.

La deuxième étape des travaux a pour but de vérifier expérimentalement les prédictions thermodynamiques obtenues à l'aide du logiciel FACTSAGE. D'abord, les microstructures de trois alliages (A390, A390-6%Mg, A390-10%Mg) ont été étudiées durant le refroidissement continu d'échantillons produits par coulée conventionnelle et rhéocoulée. Les observations réalisées mettent en évidence que l'ajout de magnésium à l'alliage A390 modifie la morphologie des particules de silicium contenues dans le constituant eutectique. Toutefois, aucune différence n'a été mise en évidence en

comparant la morphologie du constituant eutectique des deux alliages auxquels du magnésium a été ajouté (A390-6%Mg et A390-10%Mg).

Durant la solidification des alliages, la température de la transformation eutectique a été mesurée de deux façons. La première méthode de mesure consistait à mettre un thermocouple directement au sein de l'alliage coulé, la deuxième consistait à analyser un petit échantillon par calorimétrie différentielle (DSC). Ces essais ont permis de confirmer que l'ajout de magnésium, jusqu'à concurrence de 4.2%, abaisse la température de la transformation eutectique. Il a aussi été mesuré que la température de transformation eutectique est comparable pour des échantillons dont la teneur en magnésium est de 6% et 10%.

L'effet de l'ajout de magnésium sur la taille et la morphologie de chacune des phases premières de l'alliage a été étudié plus en détails pour l'alliage A390 additionné de 10% de magnésium. Des échantillons de cet alliage ont été transformés à l'état semi solide par deux procédés différents, la rhéocoulée et la thixocoulée, et leurs microstructures ont été étudiées dans des conditions isothermes. Pour les deux types d'échantillons, il a été observé que la morphologie des particules de Mg_2Si est plus globulaire et que leur taille est plus fine que des particules de Si dans l'alliage A390 coulée à partir de l'état semi solide. Il a aussi été mis en évidence que cette modification des particules de silicium est meilleure pour les échantillons produits par thixocoulée.

En plus d'étudier la microstructure, la viscosité à l'état semi solide de deux échantillons (A390 et A390-10%Mg) a été mesurée en utilisant un viscosimètre Couette. Ces manipulations ont été effectuées à une température légèrement au-dessus de la température de transformation eutectique où la fraction solide de phase primaire est maximum. Les résultats montrent que les deux alliages ont un comportement pseudo plastique et que leur rhéologie peut être modélisée par une loi de puissance. Malgré tout, l'alliage A390 a un comportement plus Newtonien que l'alliage A390-10%Mg. Cela s'explique par le fait que, près de la température eutectique, l'alliage qui contient du magnésium a une fraction solide plus élevée que l'autre alliage.

Pour terminer la partie expérimentale du projet, des mesures de duretés ont été effectuées sur trois alliages (A30, A390-6%Mg et A390-10%Mg) à l'état brut de coulé ainsi que suite à un traitement thermique de durcissement structural (T6). Tel que prévu, l'alliage à plus forte teneur en magnésium est caractérisé par une dureté plus élevée. Une augmentation de la dureté va généralement de pair avec une augmentation de la résistance à l'usure, à température intermédiaire et élevée. Il est donc possible de proposer que l'ajout de magnésium à l'alliage A390 permettra d'augmenter sa résistance à l'usure. Cette augmentation de dureté est expliquée par la modification du silicium eutectique, par la présence de la phase intermétallique Mg_2Si, ainsi que par l'augmentation de la fraction solide de phase primaire. En effet, la proportion de phase primaire qui caractérise l'alliage passe de 6.1%, pour l'alliage A390, à 12.2% pour l'alliage A390-10%Mg. Quant au traitement thermique de durcissement structural, il a

pour effet d'augmenter la dureté de tous les échantillons. Toutefois, cette augmentation de dureté est plus significative pour l'alliage A390 conventionnel. Le seul phénomène métallurgique qui puisse expliquer cette différence de duretés est la précipitation des phases intermétallique ainsi que $CuAl_2$, lors du vieillissement des échantillons, au sein de la phase alpha (phase riche en aluminium). Étant donné que l'alliage A390 contient une plus grande proportion de phase alpha que les autres alliages, le durcissement par précipitation aura un effet global plus significatif sur cet alliage. Enfin, il serait intéressant d'approfondir l'étude du comportement des alliages lors du traitement thermique.

ABSTRACT

A comprehensive study of microstructural evolution of A390 hypereutectic aluminum-silicon alloy (Al-17%Si-4.5%Cu-0.5%Mg) with addition of Mg contents up to 10% was carried out during semi solid metal processing as well as conventional casting. By adding Mg into A390 alloy, the Mg_2Si intermetallic phase is promoted to solidify instead of primary silicon and believed to improve the microstructure of casting and semi solid processing of A390 alloy resulting in better mechanical properties particularly wear resistance. Since the size and morphology of the primary phase as well as its distribution in the microstructure plays an important role on improving the mechanical properties, the Mg_2Si intermetallic phase is preferentially formed instead of the primary silicon. On the other hand, the dendritic matrix network of the added Mg alloys has shown that the eutectic microstructure consists of dendritic α-Al as well as skeleton network of the eutectic silicon and the eutectic Mg_2Si with Chinese script morphology when compared to the matrix of A390 alloy which consists of only dendritic α-Al as well as large individual flake eutectic silicon without eutectic Mg_2Si. This findings give remarkable importance to the A390 alloy with high Mg content because the high resistance to wear can be attributed to the modification of the eutectic silicon as well as the presence of eutectic Mg_2Si in the matrix and both of these eutectic structures which have a significant influence on the mechanical properties of these alloys.

As a first step, the FACTSAGE thermodynamic databank and software was applied in order to investigate the phase diagram, the solidification behavior as well as the

identification of the components that are formed during the solidification of A390 alloy with different Mg contents for equilibrium and non-equilibrium (Schiel) conditions. The alloy corresponds to a quaternary system (Al-Si-Cu-Mg) which was calculated for a constant composition (isopleth) of 4.5% Cu and 17% silicon (weight percent) and with measuring $\frac{Mg}{Al}$ ratios of $\frac{0.5}{78}, \frac{1}{77.5}, \frac{2}{77}, \ldots\ldots, \frac{10}{68.5}$ for A390 and with 1%, 2%,....., 10% Mg content, respectively. With the addition of Mg, up to 10% Mg, two critical compositions were identified where within each critical zone, the Mg_2Si particles are solidified by the identical reaction. Therefore, the software indicated that primary silicon is the only primary phase solidified in the microstructure of A390 alloy with Mg content between 0.5 - 4.2 %. In this case the Mg_2Si can only appear in the matrix network with a eutectic morphology due to the ternary reaction of $Liq \rightarrow Al + Si + Mg_2Si$. For the A390 alloy with the lowest limit of Mg value (0.5%), contrary to the binary Al + Si region, the ternary region has the smallest temperature interval. This small region becomes larger when the Mg content increases up to 4.2%. Therefore, it is anticipated that the microstructure of matrix network of A390 alloy and high Mg content alloys consists mostly of the binary Al + Si and the ternary Al + Si + Mg_2Si eutectic phases, respectively. With higher Mg content between 4.2 - 7.2 %, the Mg_2Si intermetallic phase is solidified in the eutectic network according to the ternary reaction together the primary silicon due to the binary reaction of $Liq \rightarrow Si + Mg_2Si$. However the primary silicon is still the first solidified phase in this critical Mg zone. For Mg contents greater than 7.2%, the Mg_2Si solidifies first as a primary phase. In fact, the Mg_2Si is solidified

during the primary, the binary and the ternary reactions and can be observed in the microstructure as a eutectic phase and a pro-eutectic phase with different morphology. This implies that the solidification interval of Mg_2Si increases with addition of Mg. On the other hand, the eutectic reaction temperature is abruptly decreased with the addition of Mg up to 4.2% (first critical Mg value) and then becomes almost constant with higher Mg content. The eutectic network has the highest solid fraction in the microstructure of alloy and is attributed to the reduction of the eutectic reaction temperature by the addition of Mg. The results generated by the FACTSAGE were used as the basis of the experimental work and led to the study of the effect of Mg on the microstructural evolution of A390 alloy.

In the next stage, the experimental tests were carried out in order to verify the accuracy of the results obtained by the FACTSAGE software. The microstructures of the A390 and the 6 and 10 wt% Mg alloys were investigated using conventional casting and rheocasting (stir casting) processes with continuous cooling solidification. The results showed that, for both processes, the microstructure of the eutectic network for high Mg alloys, specifically the eutectic Si phase is modified compared to the eutectic Si in the microstructure of A390 alloy. However the alloys with 6% and 10% Mg have a similar eutectic morphology. The eutectic formation temperature was measured by placing the thermocouple into the melt for determination of the cooling curves. DSC (Differential Scanning Calorimeter) test were also carried out. The results are in good agreement with the FACTSAGE results confirming the reduction of eutectic formation temperature with addition of Mg up to 4.2% and nearly the same temperature for 6 and 10% Mg alloys.

Two semi solid metal processing techniques, Rheoprocessing and Thixoprocessing, were carried out for the 10% Mg alloy at isothermal condition in the semi solid state. In both processes, the morphology and size of the primary Mg_2Si particles change more significantly than the polygonal silicon particles and became smaller and more globular. However, the Thixoprocessed samples showed a better modification of the Mg_2Si particles than Rheoprocessed samples.

The rheological characteristics of the 10% Mg alloy were measured in the semi solid region by using a Couette viscometer and the results were compared to A390 alloy. The viscosities were measured for continuous cooling of the alloy at a constant shear rate and also in a series of step change experiments at constant temperature with variable shear rates. It was showed that the flow behavior of A390 alloy in the semi solid region near to the eutectic reaction temperature, where the maximum solid fraction of the primary silicon phase occurs is more Newtonian than for the 10% Mg alloy. The reason is due to the higher solid fraction of the 10% Mg alloy compared to the A390 alloy at the temperature near the eutectic reaction. However, both alloys were shown pseudo-plastic behavior and their flow behaviors can be presented by the power law equation.

Finally, the hardness of the A390 and the 6 and 10% Mg alloys was evaluated for conventionally cast samples and after T6 heat treatment. As expected, the high Mg content alloys showed higher hardness values compared to the A390 alloy. This is a significant finding because A390 is used in high wear resistance applications at medium or elevated temperature. Therefore, the A390 alloy with higher Mg addition can improve

the wear resistance of this alloy. The reason for the increased in hardness of Mg can be attributed to the modification of eutectic silicon in the matrix, the presence of eutectic Mg_2Si in the matrix as well as the increase of solid fraction of primary phases from 6.1% for A390 to 12.2% for the 10% Mg alloy.

The T6 heat treatment increased the value of hardness for all samples. However, contrary to the as-cast samples, the hardness of A390 alloy in T6 condition shows higher increase than the high Mg alloys. This phenomenon can be attributed to the precipitation hardening of α-Al phase during the heat treatment. Since the matrix of A390 consists of more α-Al phase when compared to the high Mg content alloys, the increases in hardness of A390 alloy is more significant.

CONDENSÉ EN FRANÇAIS

Les alliages hyper eutectiques Aluminium Silicium tels que le A390 (Al-17Si-4.5Cu-0.5Mg) sont utilisés dans des applications qui requièrent un haut degré de résistance à l'usure et la corrosion, bonnes propriétés mécaniques et faible dilatation thermique. Leurs propriétés sont d'un intérêt particulier pour l'industrie automobile pour la production des composants légers fabriqués à partir de ces alliages tels que les bielles, pistons, compresseurs pour climatiseurs et le bloc-moteur. Les bonnes propriétés mécaniques et une haute résistance à l'usure sont attribuées essentiellement à la présence des particules de silicium primaire qui sont très dures et distribuées dans la microstructure. Par conséquent, la taille et la morphologie du silicium primaire dans les alliages hyper eutectiques Al-Si joue un rôle important sur les propriétés mécaniques des alliages. En raison du grand intervalle de solidification de ces alliages, le silicium premier devient grand pendant la solidification au cours du moulage conventionnel. En effet, au cours de la condition de travail, les fissures se forment sur le grand particules de silicium premier et la concentration de contrainte sera plus sévère à l'interface entre ces particules et la matrice Par conséquent, la modification de la microstructure de silicium primaire est nécessaire afin d'obtenir la meilleures propriétés mécaniques.

En vue de modifier la microstructure, la mise en forme à l'état semi solide est utilisée comme une puissante alternative au moulage conventionnel. Il est divisé en deux procédés distincts: Rhéocoulée et Thixomoulage. En rhéocoulée, l'alliage est brassé par un agitateur au cours de solidification afin de produire des microstructures non

dendritique, puis la gelée semi solide produite par brassage est directement coulée en moule (Rhéocoulée) ou moulée par injection (Rhéomoulage). En thixomoulage, le lingot qui présente la microstructure souhaitable (non dendritique) est réchauffé jusqu'à l'état semi solide et ensuite façonné en pièces. Les lingots doivent être préalablement traités afin de produire des matières avec les microstructures appropriées.

D'autre part, il a été démontré que les alliages hyper-eutectiques aluminium silicium à haute teneur en Mg possèdent un fort potentiel de résistance à l'usure en raison des excellentes propriétés mécaniques et physiques de la phase intermétallique Mg_2Si qui est formée au cours de la solidification. En termes de propriétés et de comportement lors de la solidification, des grandes similitudes existent entre de Mg_2Si et le Si. Toutefois, elles ont différentes évolutions microstructurals au cours de la mise en forme à l'état semi solide. Il semble que l'ajout de magnésium peut améliorer la microstructure de l'alliage A390 traité et coulé à l'état semi solide ainsi que conventionnel par la formation de la phase intermétallique Mg_2Si au lieu de Si. En outre, la microstructure dendritique du réseau eutectique de l'alliage A390 à haute teneur en Mg a montré une forme modifiée de silicium eutectique en réduisant la température de la réaction eutectique. Par conséquent, la microstructure de la coulée conventionnelle ou la gelée semi solide de l'alliage A390 à haute teneur en Mg montre la modification remarquable résultant en grande dureté et une bonne résistance à l'usure.

La présente thèse étudie l'effet de l'addition de Mg sur la réduction de la densité ainsi que la modification de la microstructure de l'alliage hyper-eutectique d'aluminium

silicium A390 (Al-17Si-4.5Cu-0,5Mg) au cours de la coulée conventionnelle ainsi que lors de la mise en forme à l'état semi solide.

Les recherches sont nécessaires afin d'établir les relations entre les paramètres du procédé semi solide, la composition chimique, la microstructure et leurs conséquences en propriétés mécaniques particulièrement la dureté et la résistance à l'usure. Les principaux objectifs de cette thèse sont d'étudier premièrement, la caractérisation thermodynamique de l'alliage A390 avec différentes teneurs en Mg à l'aide du logiciel FACTSAGE afin de bien comprendre et comparer le diagramme de phase et le comportement de solidification. Dans cette thèse, l'effet de Mg contenu, jusqu'à 10%, sur le chemin de la solidification de l'alliage A390, Al-17% Si-4.5% Cu-0.5% Mg (wt%), est étudié par le logiciel FACTSAGE développé par le groupe CRCT à l'École Polytechnique de Montréal selon le Fslite base de donnée (base de données pour les alliages métalliques légers). Le logiciel FACTSAGE ont montré que la solidification de l'alliage A390 se fait de façon séquentielle, où les réactions primaire, binaire, ternaire et quaternaire se produisent à des températures de 653.1, 566.2, 502.4 et 496.9 °C, respectivement. En ajoutant du Mg, jusqu'à 10%, deux compositions critiques ont été détectées à 4.2% et 7.2% Mg où la température des réactions liquidus, binaires et ternaires est changée. En effet, dans chaque zone critique (entre 0.5% et 4.2%, entre 4.2% et 7.2%, entre 7.2% et 10%), la particule Mg_2Si est solidifiée par une réaction identique. Par exemple, le logiciel indique que le silicium primaire est la seule première phase solidifiée dans la microstructure des alliages avec la valeur de Mg entre 0.5 – 4.2%. Dans ce cas, le Mg_2Si ne peut être apparu dans la matrice avec la morphologie

eutectique due à la réaction ternaire Liq $\rightarrow$ Al + Si + Mg_2Si. Lorsque la valeur de Mg varie entre 4.2-7.2%, la phase intermétallique de Mg_2Si est solidifiée dans le réseau eutectique (par la réaction ternaire) ainsi qu'avec le silicium primaire selon la réaction binaire Liq $\rightarrow$ Si + Mg_2Si. Toutefois, le silicium primaire est encore la seule première phase solidifiée dans cette zone critique de Mg. Pour une teneur du Mg de plus de 7,2%, la phase Mg_2Si se solidifie aussi en tant que première phase. En fait, le Mg_2Si est solidifié lors des réactions primaire, binaire et ternaire et peut être observé dans la microstructure comme phases eutectiques et primaires avec différentes morphologies.

À la plus faible valeur de Mg, tel que la composition de l'alliage A390 (0,5% Mg), la zone ternaire est la plus petite région au cours de la solidification contrairement à la région binaire Al + Si. Cette zone devient plus grande lorsque le contenu Mg augmente jusqu'à 4,2%. Par conséquent, il est prévu que la plupart des réseaux dendritiques de la matrice de l'alliage A390 et de l'alliage A390 à haute teneur en magnésium soient constitués d'eutectique binaires Al + Si et ternaire Al + Si + Mg_2Si, respectivement.

Cela indique que la température de la formation d'eutectique diminue en augmentant la teneur de Mg. Le logiciel a montré que la température d'eutectique diminue brusquement jusqu'à 4,2% de Mg (première valeur critique de Mg) et devient alors presque constante. Par conséquent, la modification de la morphologie d'eutectique qui possède le plus de fraction solide dans la microstructure est attribuée à la diminution de la température de la formation d'eutectique pour l'alliage A390 avec l'addition de Mg.

Les résultats obtenus par FACTSAGE ont été utilisés comme la base pour l'étude expérimentale sur le rôle de Mg en évolution microstructurale.

À la première étape du travail expérimental, la densité des alliages A390, 6% et 10% de Mg, a été mesurée par le principe d'Archimède. L'aluminium est un métal très léger (2700kg/m3 par comparaison à l'acier 7800kg/m3) soit environ un tiers du poids de l'acier. Étant donné que les densités du silicium (2,33 g/cm^3) et du Mg_2Si (1,99 g/cm^3) sont plus petites que celle de l'aluminium pur, l'alliage A390 ainsi que les alliages 6% et 10% de Mg devraient être plus légers par rapport à l'aluminium pur et la valeur de densité diminue avec la teneur en Mg. Cela nous incite à mesurer la densité des alliages en utilisant le principe d'Archimède. Le calcul de la densité des alliages A390, 6% et 10% de Mg indique les valeurs 2,68, 2,58 et 2,51 g/cm^3, respectivement.

À l'étape suivante, les microstructures des alliages A390 ainsi que celles des alliages avec 6 et 10% de Mg additionnel ont été étudiées au cours de la coulée conventionnelle et de la rhéocoulée en refroidissement continu. Les coulées conventionnelles ont été produites avec deux vitesses de refroidissement: $-0,15 \pm 0,05\ ^{o}C\ s^{-1}$ (refroidi dans le four) et $-1,0 \pm 0,2\ ^{o}C\ s^{-1}$ (refroidi à l'air).

Les échantillons rhéocoulées ont été soumis à une vitesse de rotation de 260 tr/min à l'aide d'un agitateur. Dans le cas de la coulée conventionnel, le microstructure des échantillons à haute vitesse de refroidissement est plus fine que les échantillons à faible taux de refroidissement.

Toutefois, avec l'addition de Mg, la morphologie du silicium eutectique est effectivement modifiée de manière significative. La raison est due à la diminution de la température de la réaction eutectique causée par l'ajout de Mg à l'alliage A390. Cette température a été mesurée en plaçant le thermocouple dans la bain d'alliage liquid, ainsi que par l'essai DSC (Differential Scanning Calorimeter). Un bon accord était observé entre les résultats obtenus par FACTSAGE, l'essai DSC et les courbes de refroidissement continu confirmant la diminution de la température eutectique avec addition de Mg jusqu'à 4,2% et près de la même température pour les alliages contenant 6% et 10% de Mg.

En outre, l'addition de Mg change la réaction eutectique constituant la matrice à partir de la réaction binaire (Al + Si) à une réaction ternaire (Al + Si + Mg_2Si). La morphologie de la phase eutectique pour le cas binaire du A390 composé de silicium aciculaire alors que pour le cas ternaire, la constituant eutectique composé de fine particules de silicium et de particule de Mg_2Si dont la morphologie est dite en 'caractères Chinois'.

Dans le cas des échantillons rhéocoulées durant le refroidissement continu, la grande ségrégation des phases première a été observée pour la microstructure des trois échantillons (A390, 6% et 10% Mg) en raison du cisaillement imposé lors de la solidification. Par conséquent, la microstructure contient deux régions différents: la région près de la paroi du creuset (couche extérieur) où toutes les phases primaires sont concentrées dans cette région et la région située à côté de l'agitateur (couche intérieur)

que ne présente pas aucune phases primaires. Dans la couche intérieur, la phase α-Al aggloméré avec la morphologie globulaire sont présents dans la microstructure.

Pour l'alliage A390, la fragmentation du silicium eutectique s'est produite en condition cisaillée par rapport à l'échantillon non cisaillé. Pour les alliages avec 6% et 10% de Mg, la silicium eutectique en 'caractères Chinois' est aussi fragmentée.

Pour tous les échantillons cisaillés ou non cisaillés, la morphologie du silicium eutectique est transformée par l'addition de Mg dans l'alliage A390. Cela peut modifier considérablement la microstructure de l'alliage car la phase eutectique constitue la partie principale de la microstructure. En outre, la fraction solide de la phase primaire augmente avec l'addition de Mg. Par conséquent, il est prévu que l'addition de Mg peut augmenter la dureté de l'alliage A390 et améliorer le comportement à l'usure. Pour les échantillons rhéocoulés, la grande ségrégation des phases primaires dans la couche extérieure indique que cette région est plus dure que la couche intérieure (près de l'agitateur). Il est nécessaire de noter que la forme de l'agitateur peut affecter cette ségrégation.

Afin de vérifier l'évolution microstructurale ainsi que la taille et la morphologie de chaque particule en particulier les phases primaires tels que la particule silicium et la particule Mg_2Si qui sont dispersées dans le réseau dendritique de la matrice, les deux procédés, rhéocoulée et thixocoulée, en condition isotherme à l'état semi solide ont été effectuées pour l'alliage avec 10% de Mg.

Pour l'essai thixocoulée, d'abord, l'alliage 10% de Mg a été directement versé à l'état liquide dans un moule d'acier avec la cavité cylindrique. Les échantillons ont ensuite été chauffés à la température de 560 °C à laquelle les phases liquide, Mg_2Si et Si coexistent ainsi que la température de 540 °C (liquide + Mg_2Si + Si + Al). Ces températures sont situées au-dessus et en dessous de la température de la réaction eutectique. Puis la semi-solide est tenue à la température isotherme pendant 30, 60 et 180 minutes.

Pour l'essai rhéocoulée, l'alliage de 10% de Mg a été refroidi à vitesse constant à l'état liquide jusqu'à la température isotherme de 540 °C. Ensuite, la semi-solide est brassé en vitesse de rotation de 260 tr / min à la condition isotherme pendant 30, 60 et 120 minutes.

L'évolution de la microstructure ont montré que la morphologie des particules de α-Al est plus globulaire et que leur taille est plus grande que des particules de α-Al thixocoulée à la même condition isotherme.

Pour les deux procédés avec différentes températures isothermes, 540 °C ou 560 °C, la morphologie et la taille de particule Mg_2Si varie plus facile que de silicium polygonal et deviens plus fine et plus globuleuse. Toutefois, les échantillons de procédé thixocoulée ont montré la transformation de particule Mg_2Si plus que les échantillons rhéocouée. C'est un avantage le plus important de l'alliage à haut teneur en Mg.

À la prochaine étape, la caractérisation rhéologique de l'alliage avec 10% de Mg a été mesurée à l'état semi-solide durant refroidissement continu ainsi que en condition isotherme à l'aide d'un viscosimètre Couette. Les courbes de viscosité en fonction de la

température étaient comparées avec celle de l'alliage A390. Les résultats ont montré que le comportement de l'écoulement de l'alliage A390 à l'état semi solide en condition isotherme est plus Newtonien que de l'alliage avec 10% de Mg. La raison est due à la grande fraction solide de la phase primaire (12,2%) pour l'alliage avec 10% de Mg par rapport au A390 avec 6,9% fraction solide seulement. Toutefois, les deux alliages ont montré un comportement pseudo plastique présenté par la loi de puissance.

Enfin, la dureté de l'alliage A390 ainsi que 6 et 10% de Mg a été mesurée au cours de la coulée conventionnelle et après le traitement thermique T6. Tel que prévu, les alliages à forte teneur en Mg ont montré la valeur de dureté la plus élevée par rapport de l'alliage à faible teneur. Par conséquent, l'alliage à haute teneur en Mg peut améliorer la résistance à l'usure de l'alliage hyper-eutectique Al-Si. La raison pour augmentation la dureté peut être attribuée à la modification du silicium eutectique, la présence d'eutectique Mg_2Si dans la microstructure des alliages à haute teneur en Mg ainsi que l'augmentation de la fraction solide de la phase primaire de 6,1% à 12,2% en augmentant de Mg de 0.5% à 10%.

Pour terminer la partie expérimentale du projet, des mesures de duretés ont été effectuées sur trois alliages (A30, A390-6%Mg et A390-10%Mg) à l'état brut de coulé ainsi que suite à un traitement thermique de durcissement structural (T6). Tel que prévu, l'alliage à plus forte teneur en magnésium est caractérisé par une dureté plus élevée. Cette augmentation de dureté est expliquée par la modification du silicium eutectique, par la présence de la phase intermétallique Mg_2Si, ainsi que par l'augmentation de la

fraction solide de phase primaire. En effet, la proportion de phase primaire qui caractérise l'alliage passe de 6.1%, pour l'alliage A390, à 12.2% pour l'alliage A390-10%Mg. Quant au traitement thermique de durcissement structural, il a pour effet d'augmenter la dureté de tous les échantillons. Toutefois, cette augmentation de dureté est plus significative pour l'alliage A390 conventionnel. Le seul phénomène métallurgique qui puisse expliquer cette différence de duretés est la précipitation des phases intermétallique ainsi que $CuAl_2$, lors du vieillissement des échantillons, au sein de la phase alpha (phase riche en aluminium). Étant donné que l'alliage A390 contient une plus grande proportion de phase alpha que les autres alliages, le durcissement par précipitation aura un effet global plus significatif sur cet alliage.

Les conclusions suivantes ont été obtenues grâce à cette étude:

- En augmentant la teneur en Mg de l'alliage A390 (Al-17Si-4.5Cu-0.5Mg) de 0,5% à 10%, la densité de l'alliage diminue de 2,68 g/cm^3 à 2,51 g/cm^3.
- En utilisant le logiciel FACTSAGE, les deux valeurs critiques de Mg sont détectées à 4,2% et 7,2% pour l'alliage hyper-eutectique Al-Si avec différent teneur en Mg où la température de liquidus, des réactions binaires et ternaires est changée. Selon ces points critiques, la zone de précipitation de la phase intermétallique Mg_2Si augmente avec la teneur en Mg au cours de la solidification.
- En ajoutant de Mg plus de 7.2% à l'alliage A390, la phase intermetallic Mg_2Si solidifie au lieu de la silicium primaire.

- Les courbes de la fraction liquide en fonction de la température calculée par le logiciel FACTSAGE indiquent que l'ajout de magnésium diminue la température de réaction eutectique de 17 °C lorsque la teneur en Mg de l'alliage A390 augmente à 10%.
- Les résultats obtenus par le logiciel FACTSAGE sont en bon accord avec l'essai DSC (Differential Scanning Calorimeter) et les courbes refroidissement mesuré par un thermocouple au cours de la solidification des alliages.
- Les résultats expérimentaux ont montré que la variation de la vitesse de refroidissement entre $-0,15 \pm 0,05$ $^{o}C\ s^{-1}$ (refroidi dans le four) et $-1,0 \pm 0,2$ $^{o}C\ s^{-1}$ n'a pas d'effet significatif sur la température de réaction eutectique.
- L'observation microscopique pour les échantillons coulée conventionnelle durant la refroidissement continue ont déterminé que la morphologie du silicium eutectique transform de façon significative avec l'addition de Mg à partir de grande aciculaire et séparé entre eux à une morphologie tellement fine et connecté entre eux comme le réseau eutectique. La raison est due à la diminution de la température eutectique par l'ajout de Mg.
- Les autres phases intermétalliques telle que θ-$CuAl_2$, Q-$Cu_2Mg_8Si_6Al_5$ et β-Al_5FeSi (très défavorable pour les propriétés mécaniques) ont également été identifiées dans la microstructure de l'alliage A390. En ajoutant de Mg, la phase β-Al5FeSi est transformé en phase π- $Al_8FeMg_3Si_6$ sans effet défavorable.
- L'observation microscopique des echantillons rhéocoulée et thixocoulée en condition isotherme à l'état semi solide pour l'alliage avec 10% de Mg ont

montré que la morphologie et la taille des particules α-Al rhéocoulée sont plus sphériques et plus grandes que des particules α-Al thixocoulée à la même condition isotherme.

- Pour les deux procédés, la morphologie et la taille des particules Mg_2Si varient plus significative que des particules silicium polygonal et deviennent plus fine et plus globuleuse. Cependant, les échantillons de procédé thixocoulée ont montré la modification de la particule Mg_2Si plus que les échantillons de procédé rhéocoulée.
- l'alliage à plus forte teneur en magnésium est caractérisé par une dureté plus élevée. Cette augmentation de dureté est expliquée par la modification du silicium eutectique, par la présence de la phase intermétallique Mg_2Si, ainsi que par l'augmentation de la fraction solide de phase primaire.
- La traitement thermique augment la dureté de tous les échantillons. Toutefois, cette augmentation de dureté est plus significative pour l'alliage A390 conventionnel. Le seul phénomène métallurgique qui puisse expliquer cette différence de duretés est la précipitation des phases intermétallique ainsi que $CuAl_2$, lors du vieillissement des échantillons, au sein de la phase alpha (phase riche en aluminium).

TABLE OF CONTENTS

LIST OF FIGURES

LIST OF TABLES

CHAPTER 1

ORGANISATION OF ARTICLES AND THESIS STRUCTURE

The first section of the thesis presents the introduction and the objectives (chapter 1 and 2). The literature review is in chapter 3 and the methodology in chapter 4. Chapter 5 presents the results in the form of 3 papers that have been submitted for publication. The results of the rheological characteristic, microstructural evolution and the hardness tests are in preparation for publication.

The literature review of chapter three consists of three sections. Section 3-1 presents the principles of semi Solid Metal (SSM) processing with a brief explanation of Rheocating and Thixoforming, non-dendritic solidification and related phenomena. The importance of rheology in semi solid metal processes and the main parameters that determine the viscosity are discussed in terms of metallurgical and process variables that characterize semi solid metal slurries. Section 3-2 presents the solidification characteristics and the thermodynamic evaluation of hyper-eutectic Al-Si alloys with addition of Mg. First, the most common Al-Si alloys used for SSM process like A356 or A357 Hypoeutectic Al-Si alloys containing 6-7% Si, 0.5% Mg as well as A390 hypereutectic alloy (Al-17%Si-4.5%Cu-0.5%Mg) is presented. Eventually the thermodynamic properties are presented by isopleth diagrams and the solidification paths of the A390 and alloys with added Mg are investigated using the Factsage® software. At the end of this section the similarity between hypereutectic Al-Si and Al-Mg_2Si alloys is discussed. Section 3-3 shows the

flow behavior as well as the mechanical properties of Al-Si alloys such as wear resistance, hardness, stresses (yield stress, ultimate tensile stress) and their relation to the morphology and the particle size of primary phase.

Chapter 4 presents methodology and experimental procedures used in this study.

Chapter 5 presents the main body of this thesis corresponding the results and scientific findings divided into 4 main sections. The experimental tests and scientific findings are started in sections 5-3 to 5-6. At the end of each section an article is presented. The following is brief description of sections 5-3 to 5-6:

- Section 5-3: The effect of Mg content, up to 10 wt%, on the solidification path of A390 hypereutectic Al-Si alloy, Al-17%Si-4.5%Cu-0.5%Mg (wt%), are investigated by using thermodynamic calculation package, FACTSAGE. The phase diagram, solidification behavior as well as the microstructure constituents during solidification of A390 with different Mg content at the equilibrium and non-equilibrium (Scheil) conditions are studied. An article "Thermodynamic evaluation of hypereutectic Al-Si (A390) alloy with addition of Mg" was submitted to the journal (ACTA MATERIALLIA). The results obtained from this series of experiments were used as the basis of the experimental works and led to study of the role of Mg in microstructural evolution of A390 alloy.
- Section 5-4: The evolution of the eutectic microstructure of A390 and of 6 and 10 wt% Mg alloys are investigated by using two processing routes, conventional

and SSM processes. An article "Effects of Mg content on the evolution of eutectic microstructure for conventionally cast and rheocast hypereutectic Al-Si alloy" was submitted to the journal (ACTA MATERIALLIA).

- Section 5-5: This section is divided in two parts. In the first part, the flow behavior or rheological characterization of A390 alloy with 10% Mg is evaluated in the semi solid state for isothermal cooling conditions and during continuous cooling and compared to the A390 alloy. In the second part, the evolution of the semisolid microstructure of A390 and 10% Mg alloy are investigated for two different processes for isothermal conditions: rheoprocessing using a stirrer, and partial remelting after fast cooling in steel mould of (thixoprocess). An article "Effect of isothermal ageing on the semi solid microstructure of rheoprocessed and partially remelted of A390 alloy with 10% Mg addition" was already submitted to the journal of (MATERIAL CHARACTERIZATION) corresponding to the experiments carried out on with 10% Mg alloy.
- Section 5-6: Finally, the hardness of A390, 6% and 10 wt% Mg alloy conventionally cast was measured. The hardness results of the as cast samples are compared with T6 heat treated samples.

Chapter 6 is a general discussion and a summary of results obtained in this study. Chapter 7 presents the conclusions and suggestions for future work.

CHAPTER 2

INTRODUCTION

As the trend of automakers towards weight reduction continues, the need to replace the iron and steel components with lighter materials has led to the increased use of aluminum and magnesium castings in automobiles. To produce these lightweight components, the automakers are using manufacturing processes that can produce near-net shape components with the goal of achieving superior properties. Such efforts led to the discovery of semi solid metal (SSM) casting process [1]. The SSM processing, invented at MIT in the early 1970's, has been accepted as an economically attractive and powerful alternative to conventional casting. It consists of two steps: rheocasting and thixoforming. Rheocasting involves the application of shear force during solidification to produce non-dendritic semisolid slurry that can be transferred directly into a mould or die to produce a component. In fact, an agitator stirs the alloy during solidification in order to produce non dendritic microstructure and then the slurry is directly poured into die. During thixoforming reheated ingots (feedstocks) with desirable microstructure are shaped into parts at semi solid state. The cost of handling liquid metal thus can be saved and existing forming facilities may be adapted to this process. The ingots, however, must be previously processed through rheocasting or other microstructural modification processes such as Magnetohydrodynamic (MHD) stirring [2], cooling slope casting (CS) [3], strain induced melt activated (SIMA) [4] as well as re-crystallization and partial

melting (RAP) [5] in order to produce feedstocks with appropriate microstructure as a starting material for thixoforming process.

One of the main objectives of SSM casting process, with specific emphasis on Al-alloys, is to achieve globular structure of the primary phase in order to improve the mechanical properties and rheological (flow) behavior of alloys. This latter is a quite important property in die filling and thin wall casting and near net shape forming where more globular and finer particles lead to better flow behavior.

The present thesis examines the effect of Mg addition on the reduction of density as well as the modification of microstructure of A390 (Al-17Si-4.5Cu-0.5Mg) hypereutectic Aluminum-Silicon alloy in conventional and SSM casting processes. The research efforts are necessary to establish the relationships between SSM process parameters, the chemical composition, the microstructure and their consequence on mechanical properties particularly hardness and wear resistance. In fact, hypereutectic alloys such as A390 alloy are used in applications that require high resistance to wear and corrosion, good mechanical properties, low thermal expansion and reduced density. Its properties are of particular interest to the automobile industries for the production of fuel-efficient vehicles using light weight components produced from these alloys such as connecting rods, pistons, air conditioner compressors, cylinder liner and engine blocks [6]. The incentive to produce alloys with low density and better mechanical properties than A390 alloy by adding the Mg content can be lead to many promising results using semi solid processing.

Good mechanical properties and high resistance to wear are essentially attributed to the presence of hard primary silicon particles distributed in the matrix of hypereutectic Al-Si alloys such as A390 alloy which can also be called are in-situ natural Si/Al-Si composite (the silicon acting as the reinforcing phase in the fine matrix of Al-Si) [7]. Therefore, the size and morphology of primary silicon in hypereutectic Al-Si alloys play an important role on mechanical properties of the alloys. However, the mechanical properties of hypereutectic Al-Si alloys in conventional casting are not optimized due to the relatively large size of primary Si particles which adversely affect the application of alloy. Wear tests indicate that the cracks nucleate on the large primary silicon and the resultant stress concentration will be more severe at the interface between coarse Si phases and the matrix relative to that present between fine Si particulates and the matrix [8]. Briefly, under destructive actions, the large primary silicon is detached from matrix while the fine and modified silicon is strongly bound to the matrix result in improving the mechanical properties. The phosphorus modifier can change the morphology and size of the primary silicon and improve the mechanical properties.

The advantages of A390 alloy with modified microstructure are:

- High resistance to wear as a result of fine silicon
- High resistance to corrosion.
- High hardness and strength.
- Low thermal expansion coefficient.
- Low weight and good castability.

As a result, it is very attractive to the automotive industry in heavy wear applications at elevated medium temperatures. The disadvantages of conventionally cast of A390 alloys are:

- Large solidification interval (150°C). Coarse network of primary silicon with a high volume fraction of binary eutectic phase (about 88%) result in poor mechanical properties.
- Low ductility and toughness.
- Significant Si segregation.
- High degree of shrinkage.

On the other hand, the hypereutectic Al-Si alloys do not lend itself to SSM process [9] because the modification of size and morphology of primary silicon using semi solid processes requires strong external forces as well as prolonged time.

By increasing Mg content of hypereutectic Al-Si alloys, a new alloy is formed due to formation of Mg_2Si intermetallic particles (density: 1.99 gr/cm^{-3}) with a high potential in wear resistant because it contributes to a lower density, high hardness, lower thermal expansion coefficient, with an equilibrium interface, excellent workability due to high morphology deformation during metallurgical processes with a potential for cost reduction [10]. In terms of properties and solidification behavior, great similarities exist between Mg_2Si and Si [11]. Both intermetallic Mg_2Si and non-metallic Si have shown the faceted morphology during slow cooling rate with $\{001\}$, $\{111\}$ [12-13] and $\{111\}$ close-packed facets [14-15], respectively (see Fig. 31).

However, they have a different microstructural evolution during semisolid processing. It seems that the addition of Mg can improve the semi solid processing and casting of A390 alloy (Al-17%Si-4.5%Cu-0.5%Mg) by promoting the formation of primary Mg_2Si intermetallic phase instead of primary Si particle. Moreover, the dendritic network of matrix with a eutectic microstructure has shown a modification of eutectic microstructure specifically eutectic silicon for A390 alloy with high Mg content alloys. The reason for the eutectic modification is due to the decrease of the eutectic formation (reaction) temperature when adding Mg into A390 alloy, resulting in a fine skeleton network of the eutectic silicon, compared to large flake and individual eutectic silicon in A390 alloy. Therefore, the microstructure of the conventional or semi solid casting processes of A390 with high Mg content shows a significant modification in the matrix network and results in high hardness and good wear resistance.

The main objectives of this thesis is to investigate first, the thermodynamic properties of the A390 alloy with different Mg content using the FACTSAGE software in order to determine the phase diagram and solidification behavior. Subsequently, the microstructural evolution of A390 alloy with different Mg content, using two processing routes, SSM and conventional casting, for continuous and isothermal cooling conditions. Finally, the hardness of these alloys as an important parameter is studied in order to improve their wear resistance.

The following specific objectives are targeted to justify the implementation of this project:

- Producing the alloy lighter than A390 by increasing Mg content of A390 alloy (density of Mg_2Si is 1.99 gr/cm^{-3} compared to Si: 2.33 gr/cm^{-3}) and measuring the density of A390 alloy with different Mg contents.
- Thermodynamic characterization and analysis of the solidification behavior including the transition (formation) temperatures and their corresponding binary, ternary and quaternary reactions of the base alloy with variable Mg content using the Factsage® simulation.
- Comparing the phase diagrams of the base alloy with variable Mg content in order to determine the critical Mg compositions that can significantly affect the phase diagrams.
- Microstructural characterization of the base alloy with different Mg content of the primary phase, the matrix microstructure with different intermetallic phases during conventional and SSM casting processes for continuous cooling condition.
- Comparison of the size and the morphology of the eutectic Si present in the matrix for different Mg contents and investigation of the effect of Mg on the eutectic formation temperature.
- Microstructural evolution of A390 alloy for different Mg content using thixoprocess and rheoprocess at isothermal conditions in the semi solid state with different processing time.
- Characterization of viscosity of A390 alloy with different Mg content for "step change", isothermal shearing as well as continuous cooling shearing experiments using a Couette rheometer.

- Characterization of hardness of the Mg alloys for the as cast and as-T6 heat treatment condition.

A comprehensive study of the effect of Mg variation on thermodynamic behavior of A390 alloy has not been previously investigated. The modification of the eutectic network of A390 alloy with additions of Mg is a new contribution to the alloy development. Promoting the formation and the morphological evaluation of the primary and eutectic Mg_2Si intermetallic phases during conventional and semi solid processes is also original. Previous studies have focused on the modification of primary Si or Mg_2Si particles using specific modifiers [16-21]. Same studies have reported on semi solid processing of A390 alloys [22-24] as a new structural modification process but no studies have been carried out on casting and semi solid processing of A390 with high Mg contents.

It is necessary to note that the A390 (with 0.5% Mg) alloy with the added 6% or 10% Mg show the characteristics of new alloys completely different with A390 due to transformation of silicon particle to Mg_2Si intermetallic phase. However, for simplicity, they are called A390 + 6% and A390 + 10% Mg.

Chapter 3

Literature review

3-1 Principles of Semi Solid Metal (SSM) processing

3-1-1 Introduction

Semisolid metal (SSM) processing is a relatively new technology for metal forming. Different from the conventional metal forming technologies which use either solid metals (solid state processing) or liquid metals (casting) as starting materials, SSM processing deals with semisolid slurries, in which non-dendritic solid particles are dispersed in a liquid matrix. Therefore, it offers several potential advantages such as energy saving for forming, reduction of microsegregation and porosity, especially for near net shape manufacturing of components and finally good mechanical properties due to their globular microstructure compare with conventional casting with dendrite structure.

The original experiment leading to the discovery of this process was performed in 1972 by Spencer et al. [1]. They used Sn–15Pb alloy as a model system to evaluate the viscosity of the partially solidified alloy using a Couette viscometer. They discovered that when the dendritic structure is sheared, the dendrites are transformed to a non dendrite (rosette or globular) form and the semi solid alloy has a greatly reduced viscosity and exhibits thixotropic behavior.

Semi solid processing in generally is carried out using two typical methods of forming: rheocasting and thixocasting.

Rheocasting involves the application of shear during solidification to produce non-dendritic semisolid slurry that can be transferred directly into a mould or die to produce a component. The alloy is stirred by an agitator during the solidification and then directly cast (rheocasting) or injected (rheoforming) into die.

Thixoforming is a near net shape process where the feedstock (billet) with a non-dendritic structure is used as a starting material. The feedstock is reheated to the semi solid state and formed to a shape. This feedstock can be obtained by using mechanical or Magneto-Hydrodynamical (MHD) stirring during solidification or other processes such as cooling slope casting (CS) [3], strain induced melt activated (SIMA) [4] as well as re-crystallization and partial melting (RAP) [5].

Thixoforming has advantages compared to other processes because the material is injected at lower temperatures, allowing for laminar material flow rather than the highly turbulent flow of conventional die casting processes. Accordingly, the thixoforming process reduces the defects associated with die-casting such as gas porosity, shrinks porosity, poor fill, tearing and sticking and results in components with excellent mechanical properties and functional performance with low total manufactured costs.

3-1-2 Rheocasting processes for achieving non-dendritic structures

Fig. 1.a schematically illustrates the simple "batch rheocaster," in which a crucible of molten liquid is mechanically stirred while being cooled [25]. A second type of process known as the "continuous rheocaster" illustrated in Fig. 1.b has the following characteristics:

(1) Higher shear rate is readily achievable.

(2) The stirring is well below the surface of the metal, thus minimizing air entrapment.

(3) Cooling rate can be high so as to achieve a fine structure.

The third type of process (Fig. 1.c) is vigorous electromagnetic stirring used in continuous casting. This process is of considerable technological importance today, since it permits production of large tonnage using a variant of a well-established technology and it is applicable to high-temperature melting such as steel. It avoids any problem of wear or erosion since it does not require any agitator and results in better mixing because it acts effectively on the whole of the semi solid slurry contrary to the case of mechanical mixing with agitator. Fig. 1.d shows two typical methods of forming in SSM processes i.e rheocasting and thixoforming.

The rheocasting process offers several advantages over thixocasting:

1- Reduced process complexity – A multi-station heating system is not required, nor is a robotic transfer system.

2- Increased shot size flexibility – There are no shot size restrictions related to the billet height to diameter ratio.

3- Alloy modifications can be made in house.

4- Solid fraction can be tailored to the application – Billets have a narrow solid fraction working range.

5- Unrestricted metal suppliers – Die cast ingots are readily available from several sources and cost less than the specially prepared thixocasting billet.

6- In house scrap recycling – Scrap can be remelted and used again, whereas in thixocasting, the metal must be returned to the supplier to be recycled into new billets.

Rheocasting is based on direct casting of the mush, slurry, while solidification is in progress. Thixoforming and thixomolding however, deal with reheating of the feedstock materials to the mushy state temperatures and injecting the reheated alloy within close die, thixocasting (thixomolding) or within open die, thixoforging.

Another completely different approach used to obtain non-dendritic structure has been termed "strain-induced melt activation" (SIMA). In this case, an alloy billet or bar (usually of relatively small cross section) is cold worked to a critical level so that, on reheating into the liquid-solid zone, the desired spheroidal structure is obtained. In fact, residual strain is stored in a billet and a global structure is evolved by the strain energy stored in the billet after reheating. There include two steps in SIMA process [26].. In the first step of plastic deformation, there are two mechanisms to control the deformation,

slip or cross-slip or twinning in grain and grain rotation. The deviatory stress will benefit to slip or cross-slip or twinning in grains, and the hydrostatic stress will benefit to rotation of gain. In the second step of heating, the grain boundary will melt first and the shape of the grains will be globe.

Recently, the "slurry on demand" processes such as NRC (New Rheo-Casting) and SEED (Swirled Enthalpy Equilibration Device) have been developed for new applications of semi solid forming process. NRC uses a cup for each shot and a conventional automatic ladling system, which pours molten metal into the cup. This process produces semi-solid slurry including globular crystals directly from molten metal without stirring technique.

SEED process consists of two steps: The initial step involves extracting specified amount of heat from the molten metal by swirling to generate liquid-solid slurry, i.e. mushy structure, followed by drainage of remaining liquid to produce a compact free standing feedstock for rheocasting operation.

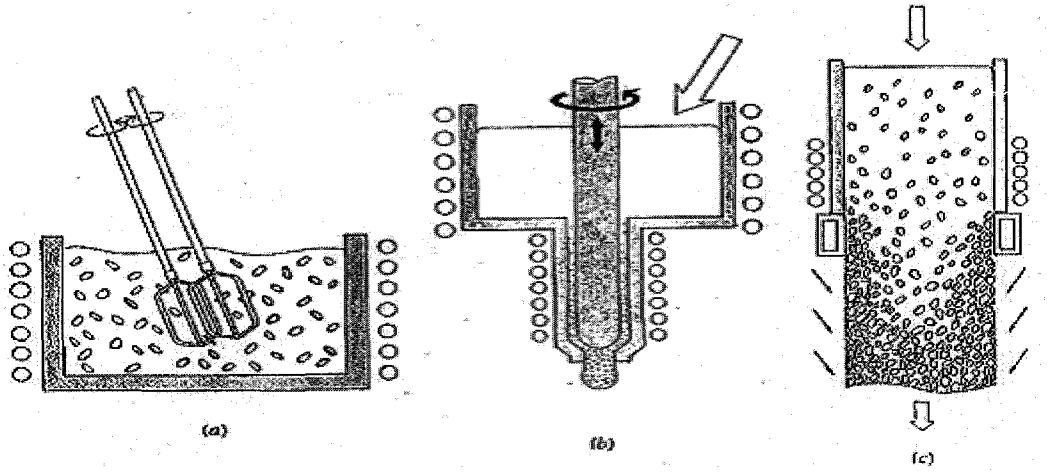

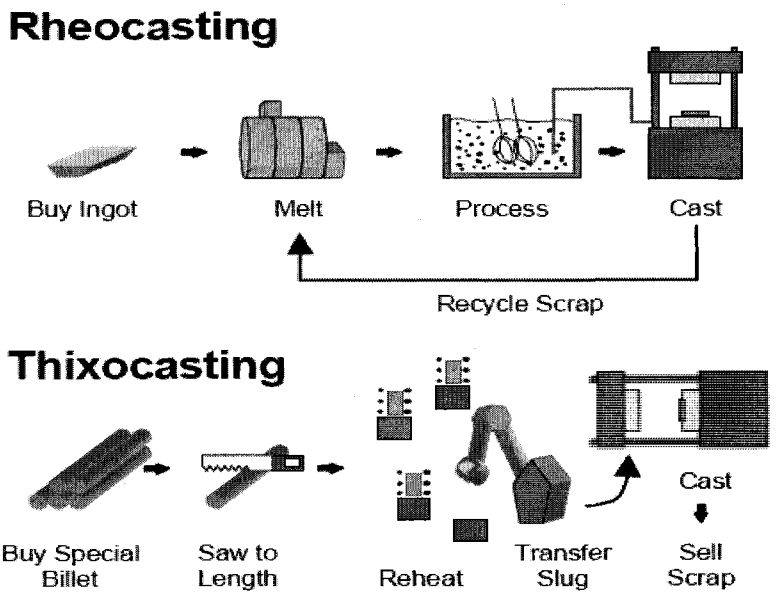

(d)

Fig. 1: Schematic diagram of method of producing of non-dendritc structure by rheocasting a) bath b) continuous and c) electromagnetic stirring with continuous casting [25] and (d) two typical method of forming.

3-1-3 Non-dendritic (globular) Solidification

During dendritic solidification, a number of processes take place simultaneously in the semi solid region. These include crystallization, solute redistribution, ripening, interdendritic fluid flow, and the solid movement. The dendrite structure which forms, is greatly affected by convection during the early stages of solidification. With vigorous convection and slow cooling, the grains become spheroidal. Semi solid alloys with this microstructure possess rheological properties, which are quite different from those of dendritic alloys. They behave thixotropically and the apparent viscosity can vary over a wide range of shear rate depending on processing conditions.

Vigorous convection is achieved by using external forces such as mechanical or electromagnetic stirring. Generally, the alloy is sheared in the liquid state and the alloy is then slowly cooled into the solidification range while it is being sheared [25]. The shear stress increases only very slowly as temperature is decreased below the liquidus and is an order of magnitude smaller than alloys that are cooled to the given temperature for the non-sheared case. The grain structure obtained in these early experiments was non-dendritic and the material was found to consist of a liquid like slurry, with an apparent viscosity lower than for the dendritic case.

3-1-4 Physical mechanism associated with non-dendritic solidification

As solidification begins, vigorous agitation results in the formation of new grains from initial dendrite fragments as shown in Fig. 2.a [25]. The early growth of each dendrite

fragment then continues dendritically as shown schematically in (Fig. 2.b). With continuing shear and time during solidification, the dendrite morphology changes to the form of a "rosette" (Fig. 2.c), as a result of ripening, shear and abrasion with other grain ripening proceeds during further cooling (Fig. 2.d) and with sufficiently slow cooling and high shear, the particles become spheroidal (or in some case, ellipsoidal), often with a small amount of entrapped liquid, as shown in (Fig. 2.e).

The extent to which the morphology evolves from that of Fig 2.a to that of Fig. 2.e increases with increasing shear rate and with decreasing cooling rate. Fig. 2.f schematically shows the morphological transition from dendritic to spherical via rosette with increase in shear rate. The fragmentation of dendrite particles, the collision of particles as well as the shallow temperature gradient encourage the equiaxed growth (rosette or globular) during solidification with shear.

Spencer et al. [1] observed the spherical morphology of primary Al crystal under high shear rates and suggested that the morphological change from dendritic to spherical grains occurs through the initial deformation of individual dendrites followed by the total collapse of the dendritic structure.

Vogel et al. [27], and Dohetry et al. [28], on the other hand, proposed that the fragmentation of metallic dendrites could occur by dendrite arm bending during stirring, creating boundaries within the dendrite and complete wetting by the liquid phase leading to eventual break up of dendrites. (Fig.3)

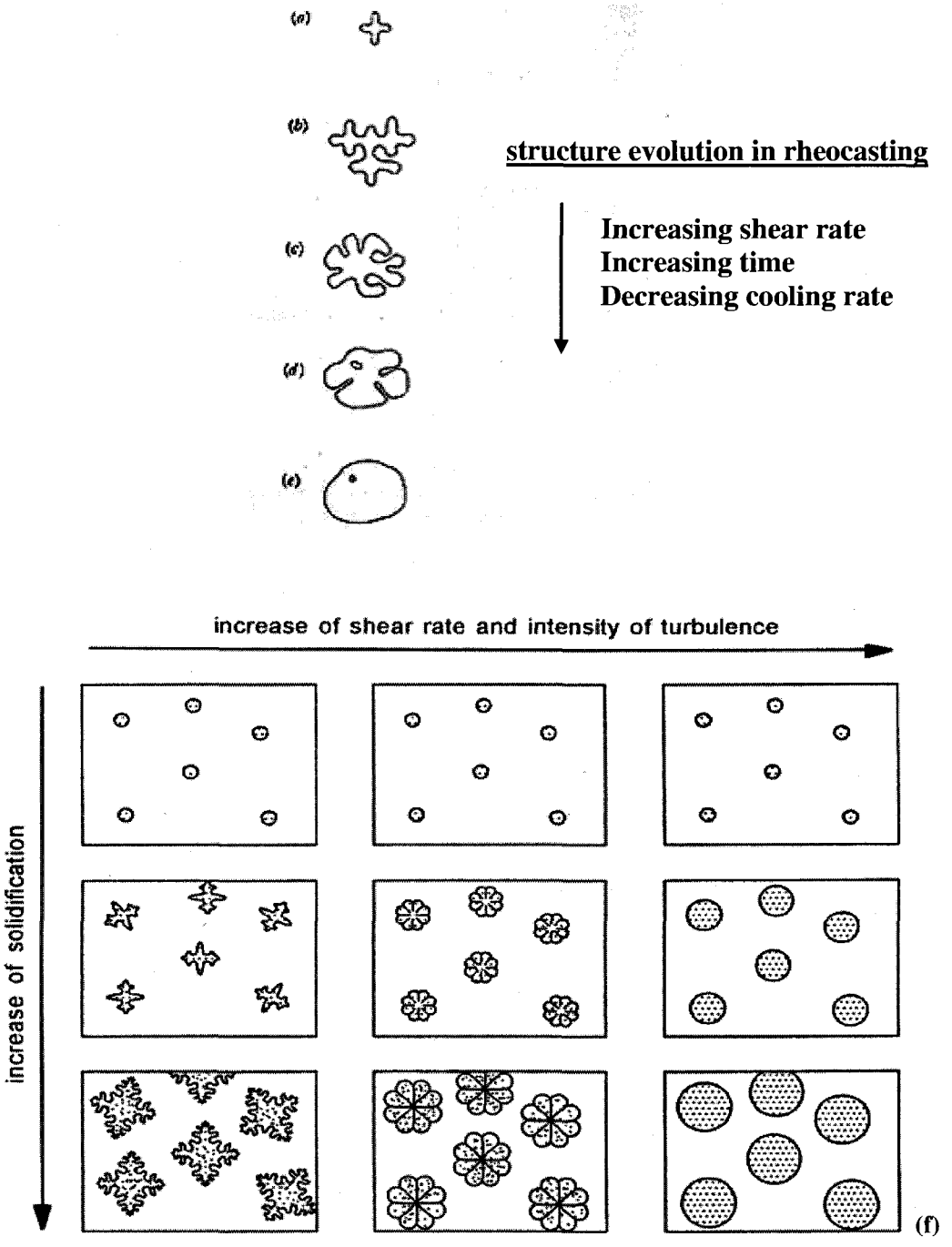

Fig. 2: Globularisation mechanism a) initial dendrite fragment b) dendrite growth c) rosette d) ripened rosette and e) spheroid [25] and (f) Schematic illustration of morphological transition from dendritic to spherical via rosette with increase in shear rate [85].

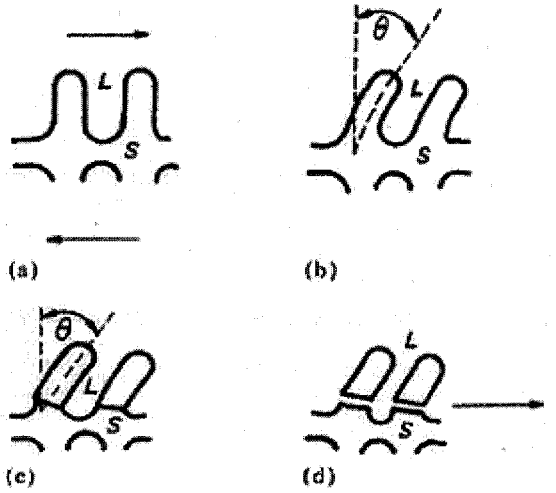

Fig. 3: Dendrite fragmentation mechanism [27].

3-1-5 Rheology of Suspensions

The implication of rheology in semi solid metal processes is the study of how matter deforms and flows. This is part of physical sciences dealing with simultaneous deformation and flow of materials and is quantitatively expressed in terms of stress–strain–time relationships which are influenced by a range of process parameters including temperature [29]. Shear flow is an important type of deformation in rheology and may be visualized as a process in which infinitely thin, parallel planes slide over each other as in a pack of rigid cards.

With such simple definition, the rheology and mechanical properties of materials is closely tide up with materials' viscosity and deformation behavior within mushy state.

3-1-5-1 Viscosity

Viscosity is the main parameter for characterizing the rheology of semi solid metallic alloys and plays an important role equivalent to that of "fluidity" concept in liquid metals. Viscosity is an indication of SSM capability in filling the mold and determines the required force for deformation and flow of materials [30] and the viscometry is identified as an appropriate route for the rheological studies of materials.

Based on Newton's law, viscosity is a constant to show the capability of momentum diffusion through the body of material by relating the shear stress to the velocity gradient within forming material.

$$\tau = \eta\left(\frac{\partial V}{\partial y}\right) = \eta\dot{\gamma} \tag{1}$$

Where $\left(\frac{\partial V}{\partial y}\right)$ is the local velocity gradient also represent the shear rate $\dot{\gamma}$, τ is the shear stress and η is the viscosity. In Newtonian fluids the viscosity, η, is a constant but for non-Newtonian fluids it is a function of physical properties of the fluid and testing conditions including particle size and distribution, microstructural degeneration, temperature, shear force and shear rate, Fig.4. They can be described mathematically as follows:

$$\tau = k(\dot{\gamma})^n \tag{2}$$

Where τ is the shear stress, $\dot{\gamma}$ is the shear rate and k and n are two solid-fraction dependant factors. We can calculate the viscosity of non-Newtonian fluids where $\eta = \frac{\tau}{\dot{\gamma}}$ such that:

$$\eta = k\dot{\gamma}^{n-1} \tag{3}$$

Depending on the values of n, the flow behavior can be divided to the power-law (pseudo plastic), dilatant or Newtonian fluids as shown in Table 1. Typically, n is called the power-law index or degree of pseudoplasticity for shear thinning or pseudoplastic fluid (metal semi solid materials) when n lies between 1/2 and 1/3 ($0< n <1$).

Knowledge of viscosity for mass producers of metallic components is equivalent to die filling characteristics, since lower viscosity causes better movement of material through the die. Lower viscosity results complex thin wall component production with lower machine pressure and reduced rejects and scraps.

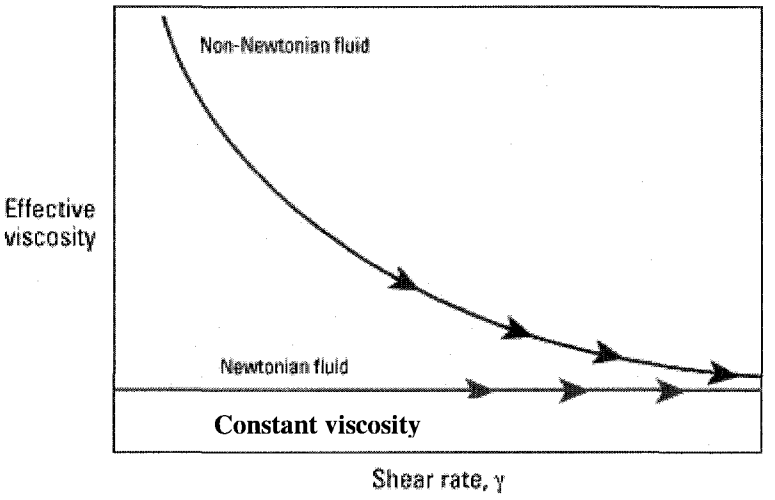

Fig. 4: The viscosity of Non-Newtonian fluids varies with shear rate.

Table 1: Value of n for various type of fluid

n	Type of fluid
<1	Pseudoplastic (most common)
1	Newtonian fluid
>1	Dilatants

3-1-5-2 SSM materials

Generally all types of materials whose solidification extends over a temperature range, mushy zone, are suitable for SSM processing. This is particularly true for metallic alloys having a wide solidification range with dendritic growth [31]. The mushy zone contains the solid and liquid phases simultaneously. A wider solidification range is translated into easier and more controllable "*mush*". The alloys with narrow solidification range or single point transformation such as eutectic alloys can not be processed by SSM.

The ability of metallic alloys to be SSM processed was initially discovered by Spencer et al. [1]. during continuous hot-tearing test of solidifying Sn–15% Pb. They found sheared dendritic alloys with broken dendrites having lower viscosity, close to oil viscosity at room temperature. This simple but important concept opened up new frontiers to casting engineers where near or net-shape parts could be fabricated at lower temperatures, by the so-called rheocasting and thixoforming processes.

The flow and deformation of metallic alloys "rheological behavior" are entirely dependent on the viscosity which itself varies with both metallurgical and process parameters. The following sections give a brief account of the effects of both sets of parameters on the viscosity of SSM slurries.

3-1-5-3 Metallurgical parameters

The most important metallurgical characteristics of SSM alloys to have an effect on viscosity are as follows.

3-1-5-3-1 Solid Fraction: One of the most important parameters affecting viscosity of the mush is the solid fraction of the primary phase, e.g. α-Al dendrites in case of hypo-eutectic and primary silicon in the case of hyper-eutectic Al–Si alloys (Fig. 5).

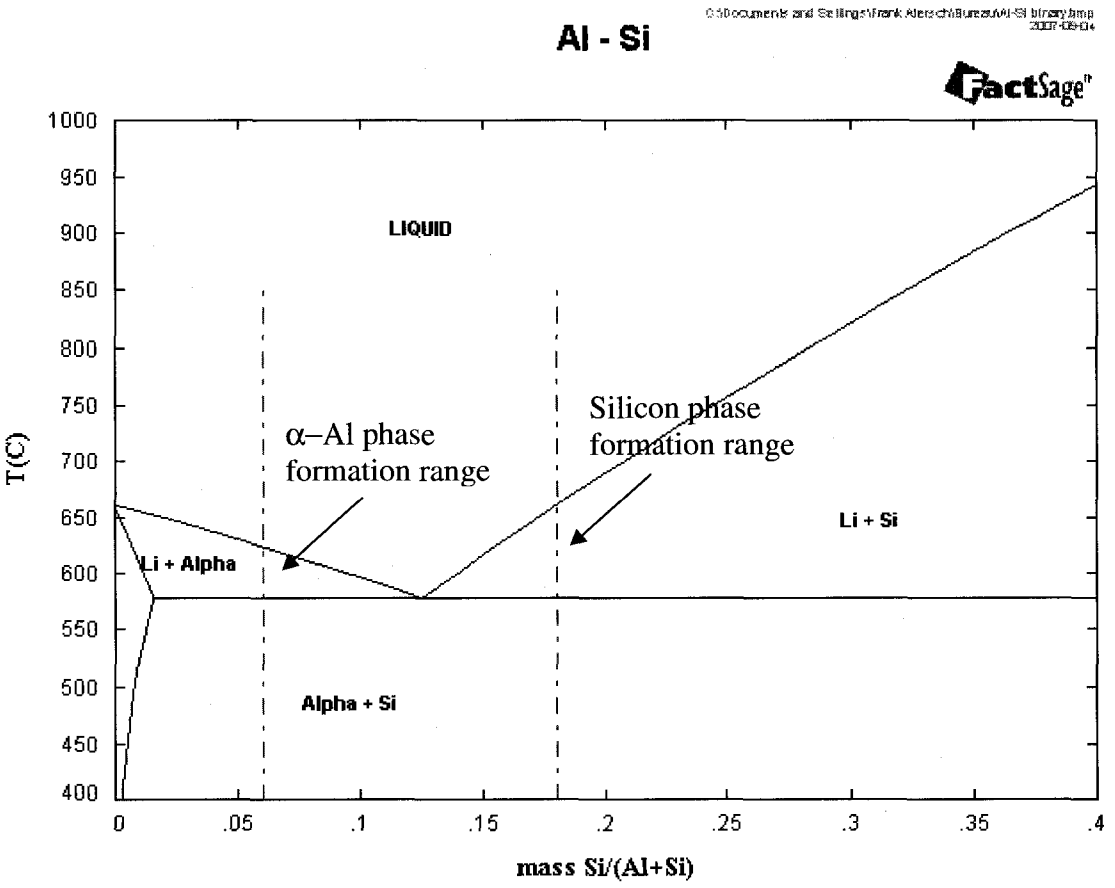

Fig. 5: Schematic representation of mushy zone and solidification range, formation of α phase and primary silicon in binary Al–Si alloys.

Solid fraction may be calculated by the Scheil equation as follow:

$$f_s = 1 - \left(\frac{T_m - T_L}{T_m - T} \right)^{1/(1-K)} \quad (4)$$

Where f_s, T_m, T_L and k are the fraction solid, melting point of solvent (for example, for Al–Si alloys, it is 660 °C, the melting point of Al), liquidus temperature of the alloy and equilibrium partition ratio, respectively. Thermal data during solidification extracted from cooling curve by using DSC (Differential scanning calorimetry) and image analysis of the resulting structure may also be used to calculate and measure solid fraction.

The Factsag software developed by the group CRCT of *Ecole Polytechnique de Montréal* was also used to calculate the phase diagrams and the solid fraction for the case of Scheil (non-equilibrium) or equilibrium conditions.

It is necessary to note that the viscosity of the semi solid slurry is a direct function of the solid fraction. Viscosity rises up steadily with increasing of solid fraction up to the dendrite coherency point (DCP) [32], after which increases abruptly as schematically shown in Fig. 6. As solidification proceeds, both the solid and liquid within the mushy zone move to compensate for solidification shrinkage, but there is a point during solidification where the solid can no longer move easily and the already solidified segment tends to develop strength and a 3D solid skeleton is formed. This is the dendrite coherency point, which marks the transition from mass feeding to interdendritic feeding during solidification.

In SSM processing, the DCP is postponed due to the forced convection or shallow temperature gradient within the melt. The break down of dendrites due to stirring coupled with multi-directional growth of fragmented dendrites due to more uniform temperature distribution within the mold, shallow temperature gradient, resulting from forced convection, encourages the formation of globular grains, thus postponing the rapid rise of viscosity to higher fractions of solid.

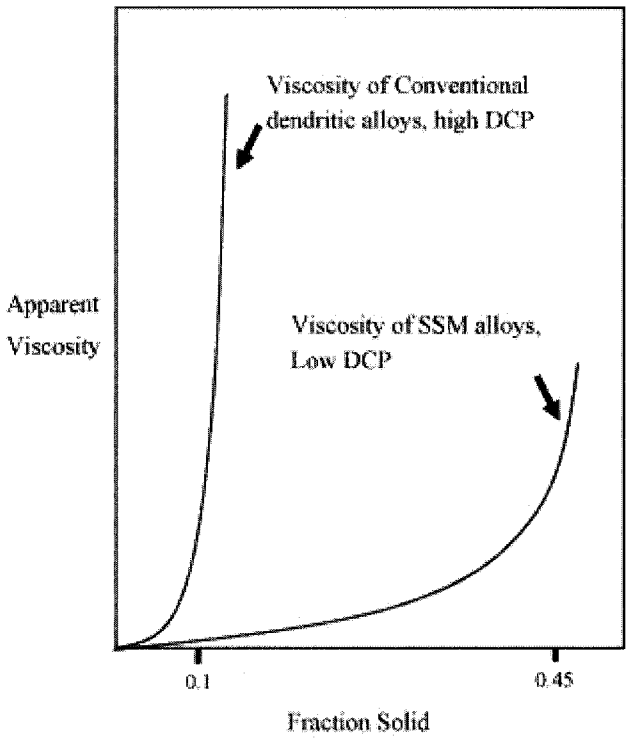

Fig. 6: Schematic representation of viscosity changes with fraction solid at different DCP points [32].

3-1-5-3-2 Primary phase morphology

The morphology of primary phase has a pronounced effect on the flow behavior of semi solid metal slurries. It is found that dendritic structures at the same solid fraction exhibit flow resistance approximately several orders of magnitude greater than the dendrite structures [33]. In fact, the globular particles move easier over each other than dendritic phases which tend to interlock during application of external force, resistance against flow. Therefore, a good understanding of the effect of particle morphology on the rheological behavior is not only of scientific interests but also has great significance on the development of new SSM processes. Fig. 7 shows the microstructures of A356 alloy after different applied pressure for parallel plate compression test [33].

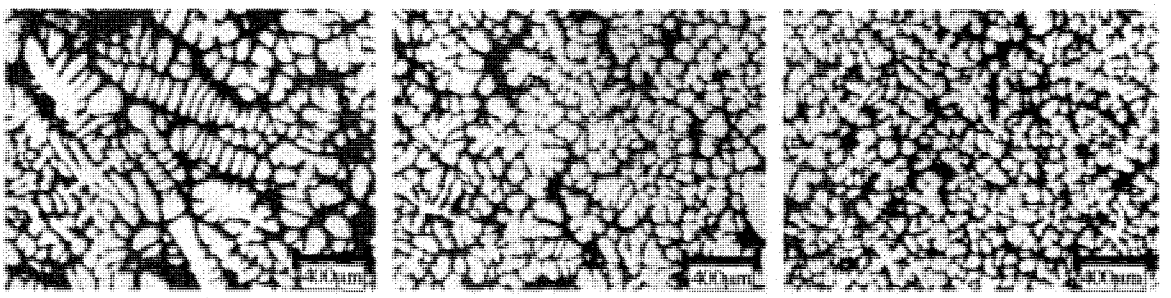

Fig. 7: Effect of different morphology of the primary phase (α-Al) on microstructure of A356 hypo-eutectic Al-Si alloy at fraction solid of 0.33, parallel plate compression method [33].

3-1-5-3-3 Particle size and distributions

It is expected to have better flow for finer microstructure as there is easier movement and less collision amongst particles resulting in lower viscosity [25]. In addition, a uniform distribution of individual particles within semi solid slurries is another important issue for researchers. There are always tendencies for the suspended particles in the liquid matrix to agglomerate. Such tendency is intensified with application of external forces on the semi solid slurry. The dynamic interaction among solid particles causes the formation of agglomerates of particles within the semi solid slurries and makes the flow of mush harder. After a while under the influence of viscous forces, a dynamic equilibrium is established between the agglomeration and deagglomeration processes, where the viscosity reaches a steady state and uniform distribution of particles observed [34].

3-1-5-3-4 Alloy chemistry

Effects of solute elements on reducing grain size and consequently improving mechanical properties of as-cast products are well-established facts [35]. The alloy chemical composition directly affects the amount of solidified primary phase within the mushy zone. It is generally believed that small additions of alloying elements interferes with grain growth and provide conditions required for new nuclei to form, i.e. to promote the formation of finer grains. In fact, they restrict the growth of grains. The solutes form an enriched boundary layer ahead of the solidification front in which the

actual temperature is lower than the solidification temperature due to constitutional undercooling zone [36] which is responsible for dendritic growth. In other words, alloy chemical composition, the type and quantity of solute elements can control constitutional undercooling and thus the growth rate and morphology of primary phase for dendritic or non-dendrite growth. On the other hand, certain elements are growth poisoner and do interfere with grain growth as well.

3-1-5-3-5 Pouring temperature

The pouring temperature or superheat is one of the important parameters that affect the evolution of primary phase during solidification. Several researchers have investigated the effect of pouring temperature on the microstructure of as-cast semi solid metals in recent years. Low superheats are instrumental in establishing shallower temperature gradient within the slurry, thus encouraging equiaxed (globular) growth [37]. In fact, a shallow temperature gradient removes directional heat extraction from the melt and prevents the formation of columnar dendrites within the slurry. This is an effective way to control the morphology of primary phase in SSM processing. Fig. 8 shows the effect of pouring temperature on microstructural evolution of A356 Al–Si alloy [38]. This figure confirms the importance of superheat for microstructural evolution of as-cast billets and clearly shows a more globular structure of α-Al for billets poured at lower temperatures, where more globular primary phase particles formed within SSM slurries.

It is necessary to note that this process is not SSM process. In this experiment, the evolution of microstructure for A356 alloy (with melting point of 619 ^{0}C) is investigated as a function of different pouring temperature.

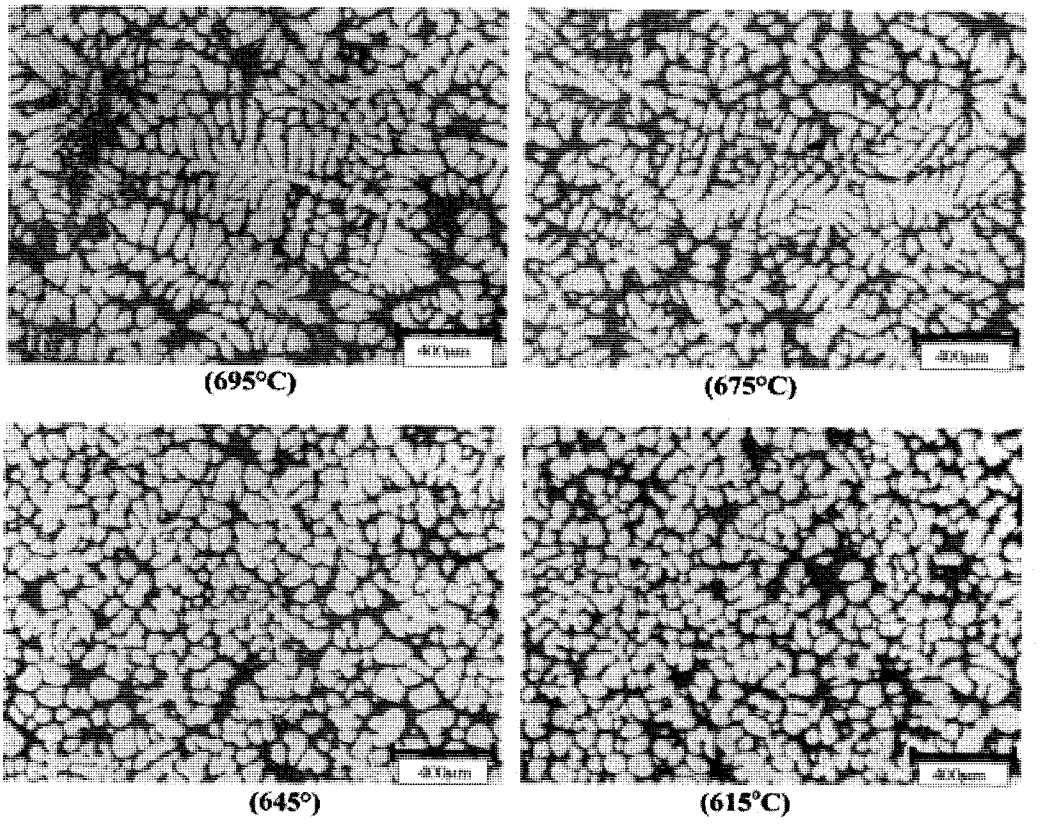

Fig. 8: The effect of pouring temperature on the Al–Si 356 alloy microstructure [38].

3-1-5-4 Process parameters

In addition to the metallurgical characteristics of SSM alloys, the process parameters such as temperature or shear rate could also influence the viscosity and thus the flow behavior of SSM slurries. The following process parameters are discussed briefly.

3-1-5-4-1 Shear stress and shear rate

One of the most important factors affecting the viscosity of SSM slurries is the applied shear stress. It imposes laminar or turbulent flow within the slurry and induces disintegration of dendrites and the agglomeration or deagglomeration of the dendrite fragments, the main drive for fine distribution of primary phase particles. The applied shear force could eventually establish some sort of equilibrium between agglomeration and deagglomeration phenomena within SSM slurries (steady state) and prevent the formation of bulky particles; the main obstacle to SSM slurry flow within mold cavity. The term "apparent viscosity" used for SSM slurries expresses the viscosity of steady-state flow and varies with shear rate and solid fraction (Fig. 9). However, before reaching equilibrium, the viscosity can go through a transient state and varies for different shear rates or fractions solid (Fig. 10).

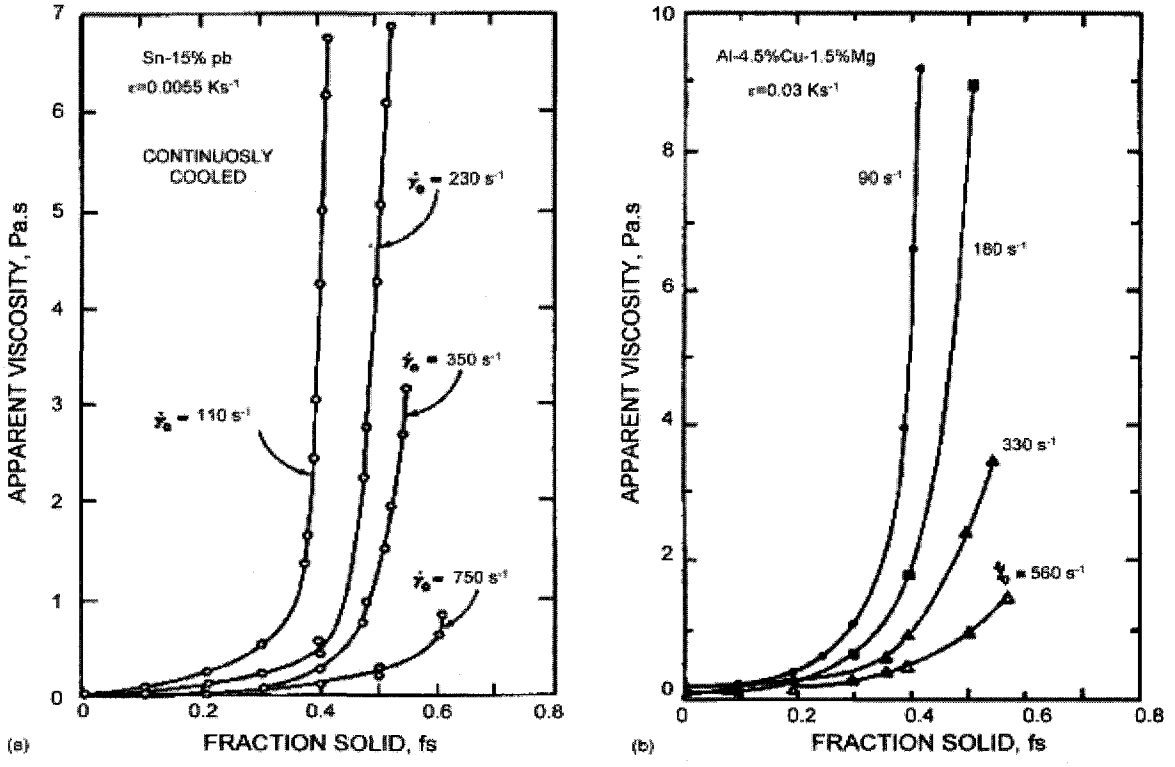

Fig. 9: Apparent viscosity vs. fraction solid at different shear rate: (a) Pb–15% Sn [39] and (b) Al–4.5% Cu–1.5% Mg [40].

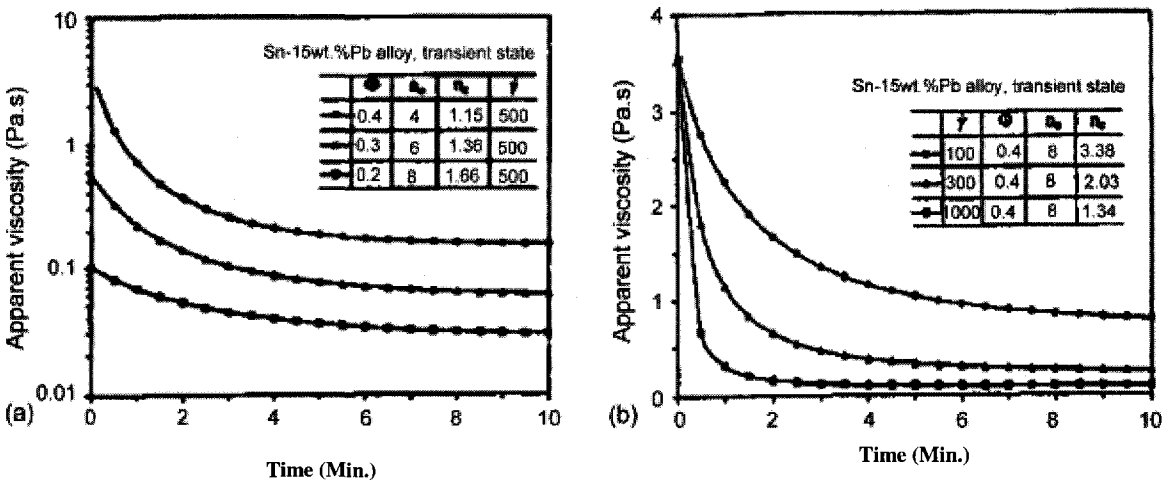

Fig. 10: (a) Calculated transient state viscosity for Sn–15% Pb alloys with different solid fraction under shear rate 500 s^{-1} as function of shearing time (b) with constant 0.4 fraction solid under different shear rates as function of shearing time ($\dot{\gamma}$ is shear rate and $\phi$is fraction solid) [33].

3-1-5-4-2 Temperature

Temperature is as important as solid fraction and plays the same role on viscosity. Higher temperature generally results in lower solid fraction and better deformability and flow. The temperature is related to the fraction solid according to the phase diagram and the effect on viscosity in the semi solid state is related to the form and nature of the solidification. However, there is an inverse relationship for temperature and viscosity, where higher temperatures impart lower viscosity values. This equation is defined according to Arrhenius model and is only valid for systems where there is not any phase change due to temperature variation as, for instance, in polymeric materials.

$$\eta = \eta_0 \exp\left(\frac{\Delta E}{RT}\right) \tag{5}$$

where T is temperature, μ_0 is a coefficient, E is the activation energy (could be positive or negative depending on increasing or decreasing the rates of reaction with increasing temperature) and R is the universal gas constant.

3-1-6 Viscometer

There are several test procedures to study the visco-plastic behavior of SSM slurries. These methods are based on measuring the viscosity of slurries and are divided into two

main categories depending on the fractions solid, low fraction solid up to 0.4, and high fraction solid, in excess of 0.4–0.5.

The simplest methods to measure the viscosity of low fraction solid slurries are the direct methods where the induced torque in the slurries is measured. In general, there are two types of viscometers, the "Couette" and "Searle" types. In Couette type viscometers, the liquid is between an outer cylinder (cup) and inner cylinder (bob). Rotation of the cup while holding the bob stationary produces a shear stress on the surface of the bob which is measured as torque (Fig 11.a).

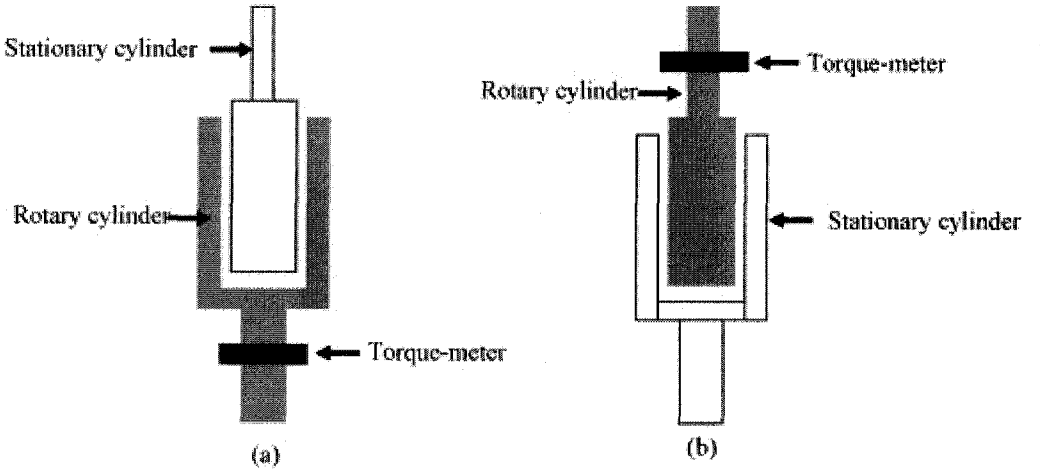

Fig. 11: The types of viscometers: (a) Couette type with rotary outer cylinder and (b) Searle type with rotary inner cylinder.

In a Searle type viscometer, the cup is stationary and the bob or inner cylinder rotates and induces shear to the melt or slurry (Fig 11.b). In both systems, the temperature of slurry is maintained at a constant value during stirring the process by using thermocouples. The apparent viscosity is calculated by a set of equations given below using the torque (T) data [41]:

$$\tau = \frac{T}{2\ \pi r^{2} L} \tag{6}$$

$$\dot{\gamma} = \frac{2\Omega}{r^{2}}\left(\frac{r_i^{2} r_o^{2}}{r_o^{2} - r_i^{2}}\right) \tag{7}$$

$$\eta = \frac{T}{4\pi L\Omega}\left(\frac{1}{r_i^{2}} - \frac{1}{r_o^{2}}\right) \tag{8}$$

where T is the measured torque, L the liquid height inside the cylinder, $\dot{\gamma}$ the shear rate, Ω the angular speed of rotor, η the apparent viscosity, r_i the inner cylinder radius, r_o the outer cylinder radius and r is the actual annular gap radius. For the solid fraction of 0.45 or more, viscosity is not generally measured by the rotational viscometers and can be measured by the parallel plate compression test as it is shown in Fig. 12. In this method a dead weight is applied on the top surface of SSM slug and its deformation behavior is investigated by analyzing strain variation with time. The resulted strain–time graph is further treated mathematically to determine the exponent, i.e. viscosity.

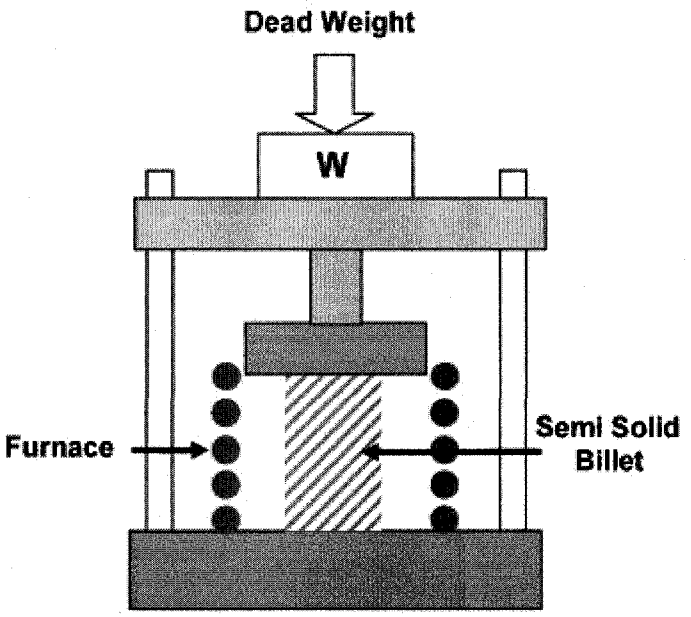

Fig. 12: The schematic diagram of a simple parallel plate compression test machine

3-2 Solidification characterization and thermodynamic evaluation of hyper-eutectic Al-Si alloys

3-2-1 Al-Si alloys

Use of cast Al-Si alloys in recent years has been expanding widely in automobile and general engineering industry. In fact, silicon is one of the most significant alloying elements incorporated in Al-alloys. Its addition is to improve castability, fluidity, reduce shrinkage and to render superior mechanical properties. The Al-Si alloys with the silicon content greater and smaller than 11.2 wt% are called hyper-eutectic and hypo-eutectic alloys, respectively (see Fig. 5). Although most of the alloys being used are hypoeutectic, the hypereutectic alloys have been gaining in popularity during the past twenty five years. Being one of a few alloying elements that do not increase the density of aluminum alloys, silicon in hypereutectic aluminum alloys also imparts to them a unique wear resistance due to the high hardness of solid silicon crystals dispersed in the matrix.

Normally, hypoeutectic Al–Si alloys form coarse columnar, and equiaxed α-Al grains during solidification depending on cooling rate and heat extraction whereas the faceted, star shape or polygonal silicon forms during solidification of hypereutectic alloys as primary and acicular shape as eutectic phase. A356 (Al-7%Si-0.3%Mg) hypoeutectic alloy and A390 (Al-17%Si-4.5%Cu-0.5%) alloys are two general alloys used for SSM processes. Fig. 13 shows the microstructure of conventional and SSM of A356 and A390 alloys.

A390 alloy is generally alloyed with copper and magnesium to provide better mechanical properties. Most of the primary silicon crystals exhibit the basic characteristics of octahedral growth resulting in faceted crystal with $\{111\}$ planes [42] as it is shown in Fig. 14.

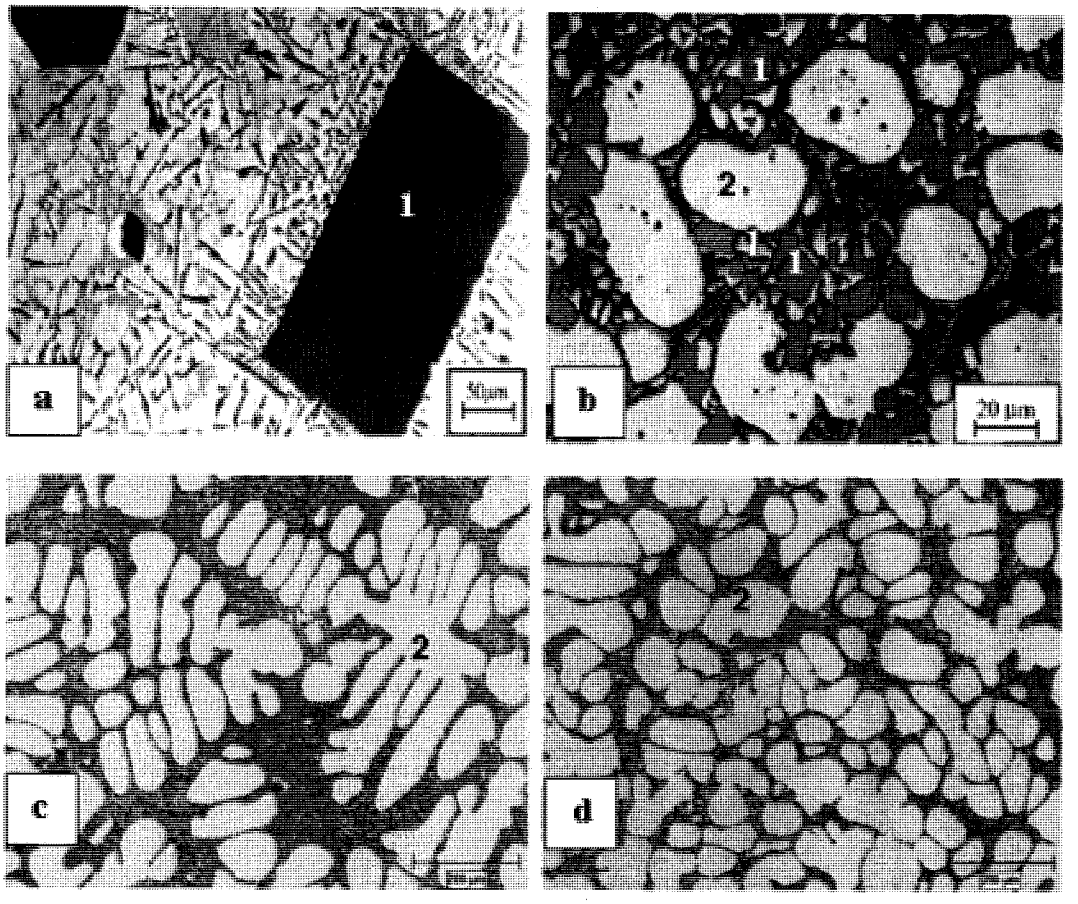

Fig. 13: Optical micrographs showing the microstructures of: (a) typical conventional [43], A390 alloy and (b) SSM cast billets, A390 (c) typical conventional, A356 alloy and (d) SSM cast billets, A356 [42].

1: Primary Si
2: α-Al

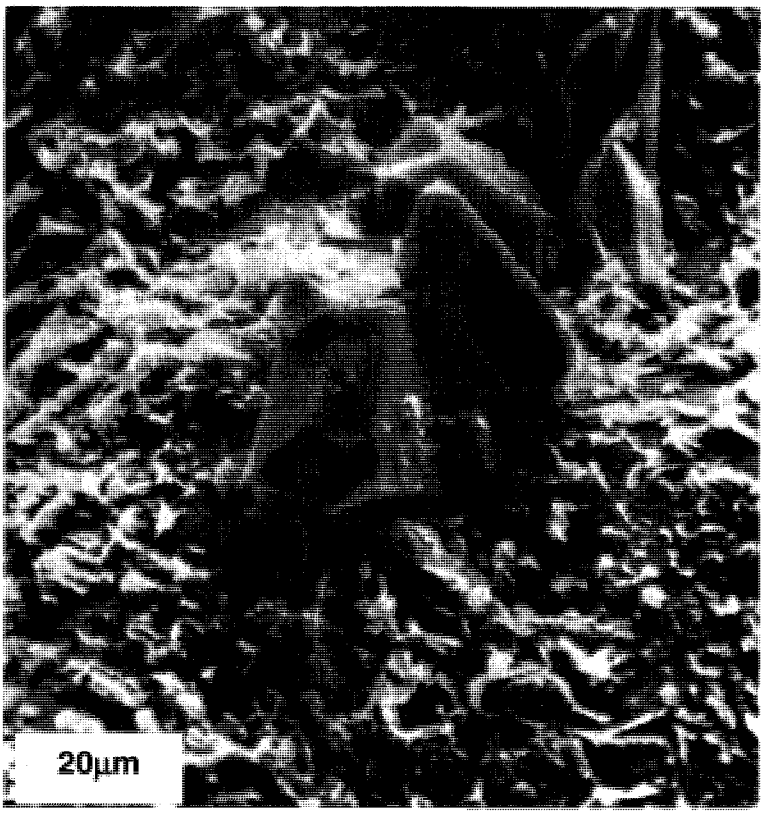

Fig. 14: SEM micrograph of Al-17%Si with faceted morphology of primary silicon

The addition of 4.5% Cu to the binary hyper-eutectic Al-Si is necessary in order to stabilize the α-Al phase in the semi solid state, making the Al-Si more readily thixoformable [44]. As it is shown in Fig. 15, for hypereutectic region of the binary Al-17%Si alloys, the semi solid zone consists of only "Liquid + Si" and the solidification becomes complete with the binary eutectic reaction at 577 °C. Therefore the binary alloy is not suitable for SSM processing due to the lack of α-Al in the semi solid state. According to the phase diagram of the Al-17%Si-5%Cu alloy, the binary eutectic reaction occurs in a temperature range between 566 °C-502 °C in the "Liquid + Si + Al" region where α-Al co-exists with Liquid + Si in the semi solid state. Usually the semi

solid process is carried out in this temperature range where the final solid fraction can be controlled by the α-Al solid fraction in this region. Generally, the thixoforming process is carried out at solid fraction between 30%-50% because values higher than 50%, die filling problems can occur due to the high viscosity. For solid fraction smaller than 30%, die filling becomes turbulent which results in reduced mechanical properties. For Al-17%Si-5%Cu alloy this range of solid fraction is located in the "Liquid + Si + Al" zone as it is shown in Fig.15. Microstructural observation confirms the presence of α-Al in forms of both eutectic and individual grains in the matrix. In fact, in the region of "Liquid + Si + Al" the α-Al solidifies with two morphologies: the grains of α-Al and eutectic α-Al (see Fig.16). The addition of 2% Mg appears to weaken considerably the network of primary Si, and enhances the flow properties (the flow resistance when it is injected into the mold) of the semi solid material on shearing [44]. H.V. Atkinson et al. [45] have observed that for alloy with more than 27% silicon, the primary silicon forms a three dimensional network, with enough strength to hinder flow in the semi solid state, but that the presence of Mg inhibits this formation. When Al-30%Si-5%Cu and Al-30%Si-5%Cu-2%Mg alloys were rapidly compressed in the semi solid state after holding at various times and temperatures, the initial resistance to flow decreased for Mg containing alloys where no networks are observed and a much smaller peak loads were measured. As described before, the importance of the presence of primary α-Al along with the primary Si in hyper eutectic Al-Si alloys is essential in order to control the solid fraction by α-Al

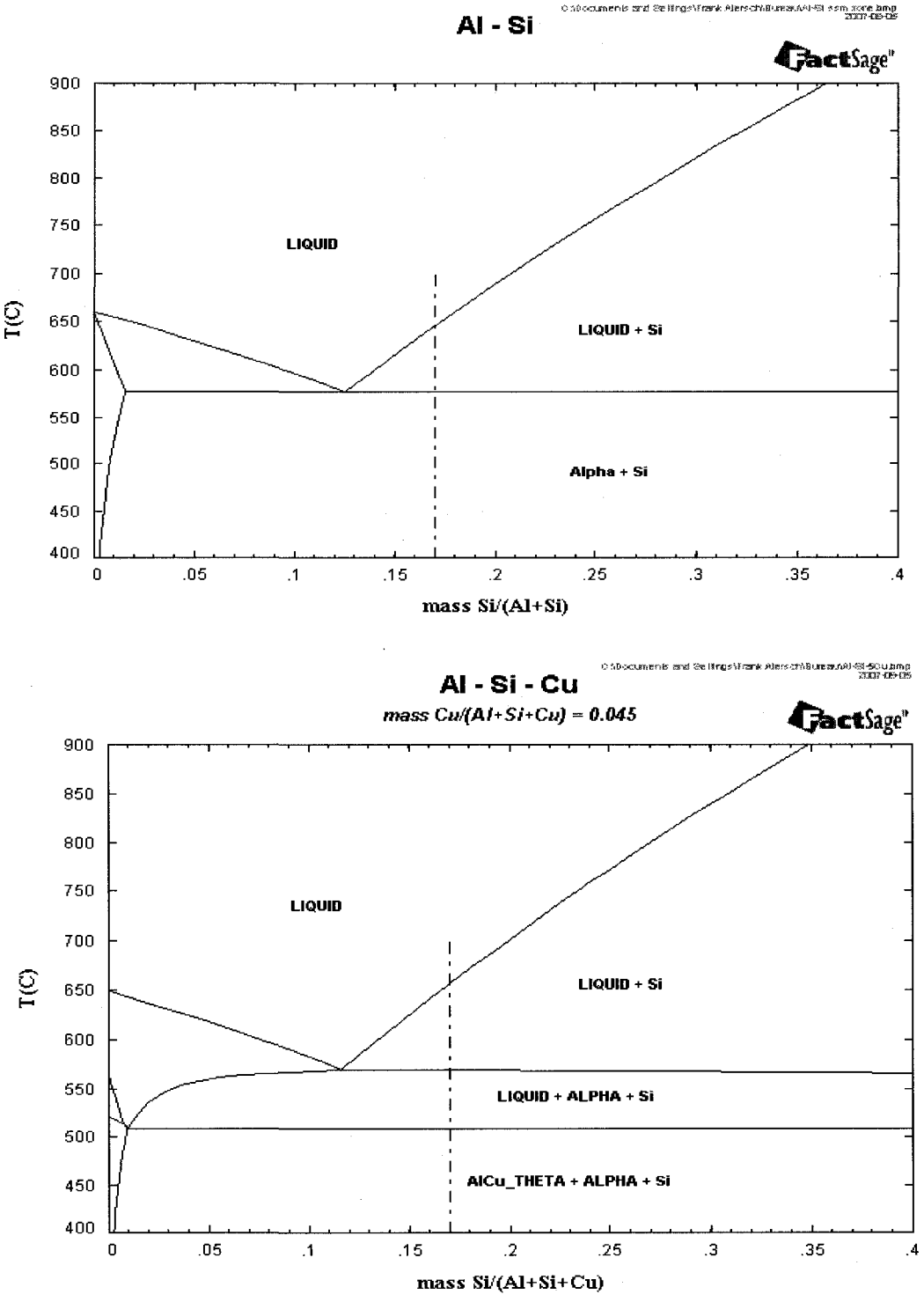

Fig. 15: Dash-dot lines indicate the solidification path of binary Al-17%Si and Al-17%Si-5%Cu alloys. The SSM is applied in the liquid + alpha + Si zone that can not be appeared for binary alloy.

Generally, non equilibrium solidification (high cooling rate) produces α-Al grains in the structure that can not be predicted by phase diagram. Because the phase diagram only shows the alpha phase in the SSM zone as a result of binary eutectic reaction of matrix (Liquid → Alpha + Si). However, the α-Al is observed in the form of eutectic as well as the equiaxed (dendrite or globular) grain in the microstructure (see Fig.16).

The presence of alpha aluminum phase in the form of separate particles is probably due to the degree of undercooling. H.S. Kang et al. [46] have observed various microstructural transitions for different levels of undercooling. For near-eutectic Al–13 wt%Si binary alloys, a phase change from eutectic to primary α-Al dendrite plus eutectic and a morphological change from α-Al dendrite to equiaxed (globular) Al grains were observed with increasing undercooling levels as shown in Fig. 16. Based on the competitive growth principle, i.e. the principle that the most preferred microstructure is that possessing the highest growth velocity at a given undercooling, microstructural transitions can be expected. The results of the calculations on the growth velocity of each phase at different undercoolings are represented in Fig. 17.

Another region of interest is the region around the primary silicon particles. This region is a silicon-depleted zone and susceptible for nucleation of the α-Al phase. For this reason the microstructure of hyper-eutectic Al-Si alloys contain primary silicon surrounded by α-Al phase (Fig. 21.a). This α-Al can not be predicted by phase diagram. For example, the solidification path of binary hyper-eutectic Al-Si alloys only shows the precipitation of primary silicon in the matrix consist of eutectic network of Al + Si.

However, the microstructure of these alloys confirms the presence of two different α-Al phases morphology. The α-Al around the silicon is believed to be formed at a temperature near the eutectic [50].

Macrosegregation of primary silicon is common in hypereutectic alloys. The effect is more pronounced at higher silicon content. Primary silicon was also found to nucleate preferentially at the mould wall causing silicon-depleted zone at the inner region of the casting resulting in precipitation of α-Al.

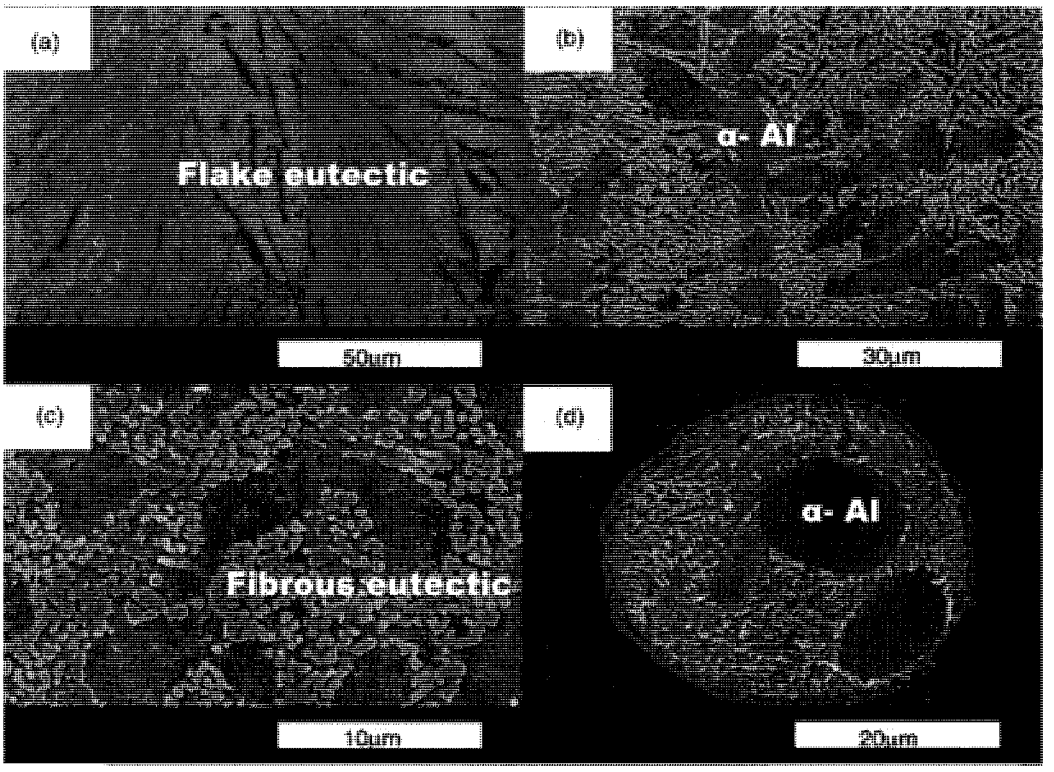

Fig. 16: The effect of an undercooling on microstructures of Al–13 wt%Si (SEM image). Increasing the undercooling from (a) to(d) [46].

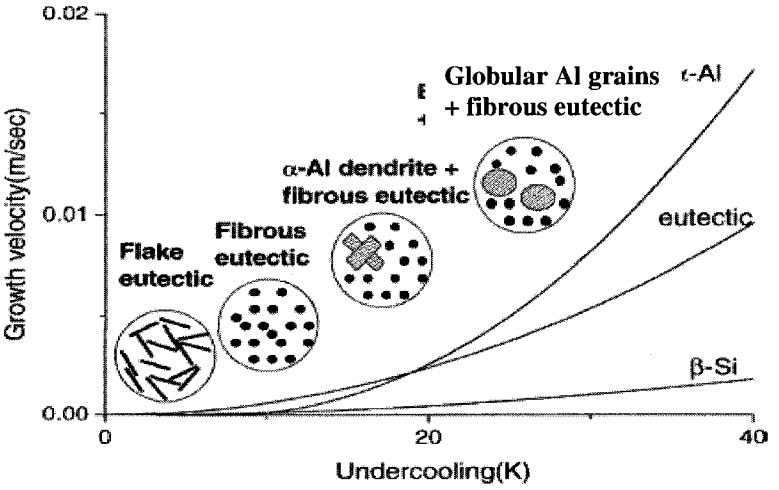

Fig. 17: Crystal growth velocities in undercooled Al–13 wt%Si alloy and the experimentally observed microstructures [46].

3-2-2 A390 alloy

Hypereutectic alloys such as A390 (Al-17Si-4.5Cu-0.5Mg) are used in applications that require high resistance to wear and corrosion, good mechanical properties, low thermal expansion and reduced density. These properties are attracting the attention of automobile manufactures since high fuel-efficiency; low energy consumption and low air pollution are possible via vehicle weight reduction. The most common applications are components such as pistons, air conditioner compressors, cylinder liner and engine blocks [47]. The good mechanical properties and high resistance to wear are essentially attributed to the presence of hard primary silicon particles distributed in the matrix. Therefore, the size and morphology of primary silicon in hypereutectic Al-Si alloys

determine the influence on the mechanical properties of the alloys. However, high latent heat and consequent large solidification interval (about 150 ° C) result in excessive growth of the silicon particles in the melt, which adversely affect the application of alloy. In service conditions cracks can nucleate on the large primary silicon and the resultant stress concentration will be more severe at the interface between coarse Si phases and the matrix relative to that present between fine Si particulates and the matrix [48] and would result in worse mechanical properties. In the conventional casting process, the primary silicon in hypereutectic Al-Si alloys exhibits a variety of the morphologies such as plate-shaped crystals of hexagonal form, octahedral equi-axed crystals, star-like crystals containing two to five radiating twin planes with {1 1 1} close-packed facets. Semi Solid Metal (SSM) processing have been utilized to suppress the formation of the coarse, brittle, primary silicon phase.

3-2-3 Semi solid metal processing of hypereutectic Al-Si alloy [49]

3-2-3-1 Rheocasting

Ichikawa et al. [86] studied the effect of shearing and phosphorous treatment on the particle size of primary silicon for binary hyper-eutectic Al-Si alloy. The solidifying alloys were sheared in a concentric cylinder rheocaster at ultra high speed and a fixed cooling rate of 3 ^{0}C/min. The results indicate that silicon particle size in the untreated alloys with Si content up to 21 wt% can be refined by shearing. Particle size slightly decreases with increasing shear rate. However, no significant refining effect was

obtained in sheared alloys with phosphorous addition. Smith et al. [49] used a graphite paddle to stir a solidifying Al-19 %Si and observed the microstructure. They concluded that agitation can either refine or coarsen the primary silicon. At the early stage of solidification when the solid volume fraction is low, the coalescence of primary silicon crystals is the dominating mechanism. Fragmentation of primary crystals, however, becomes the dominating mechanism at higher volume fraction solid. The aggregates of silicon crystals were also found to be more spherical at lower cooling rate. Fig.18 is a schematic representation of such aggregate at an early stage and the corresponding microstructure evolution during continuous cooling with agitation.

Arakane et al. [87] studied the effect of rotation speed and gap width (concentric cylinder rheocaster of 50 mm diameter of inner cylinder) on the primary silicon particle size in Al-20 wt.% Si alloy. The speed of rotation varied from 8 to 167 rev per second and the gap varied from 2.5 mm to 7.5 mm. Fig. 19 shows their results together with an adaptation of their result in terms of shear rate. It is clear that particle size become smaller at higher speeds of rotation and at smaller gap width.

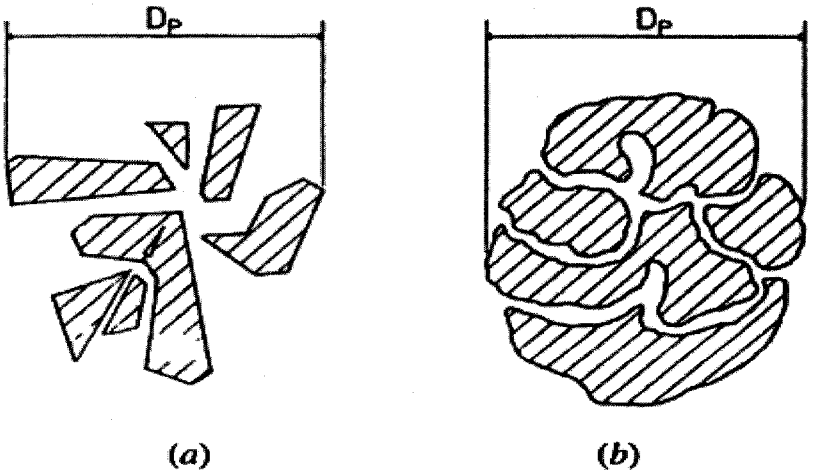

Fig: 18: Typical shapes of primary silicon particles in stirred slurry (a) at an early stage of solidification and (b) at a larger stage, near the eutectic temperature. [49]

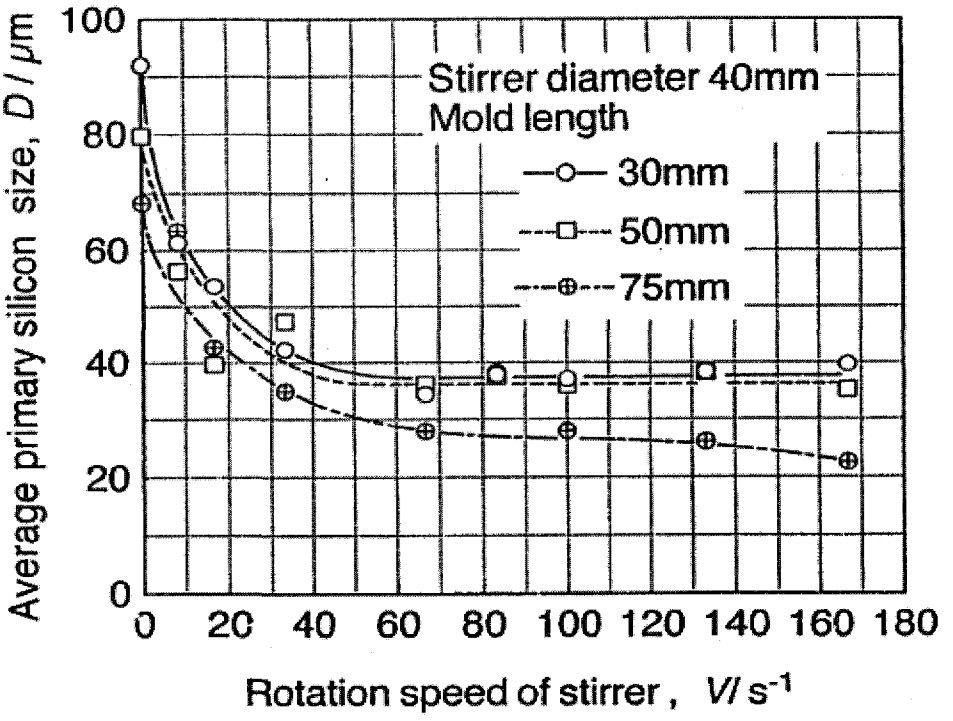

(a)

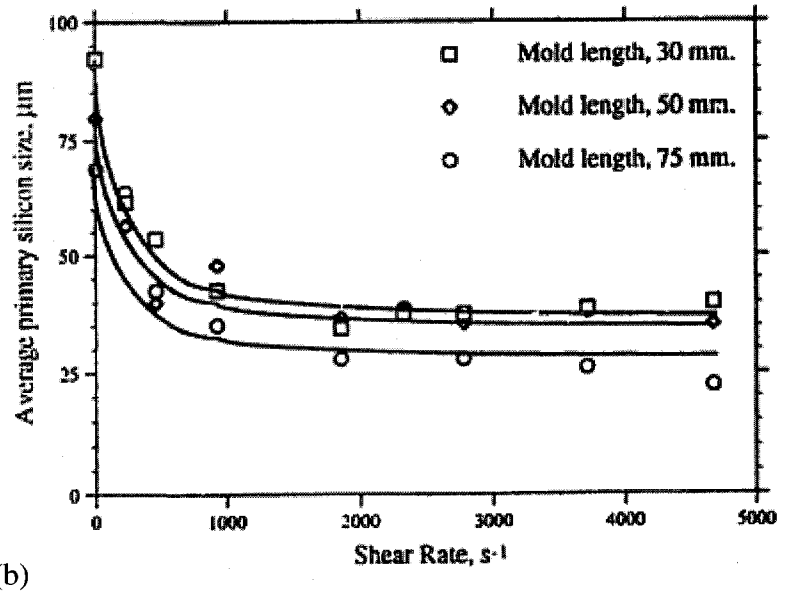

(b)

Fig. 19: (a) Average primary silicon size of Al-20% Si versus rotation speed of stirrer. (b) A reconstructed plot in terms of shear rate [49]

3-2-3-2 Thixoforming

The thixoforming of A390 hypereutectic Al-Si alloy was carried out by Birol [50] and compared with die casting. In his study, A390 alloy feedstock as starting material for thixoforming process (see section 3-1-2) was produced using a cooling slope (CS) casting technique and then thixoformed successfully at a temperature of 844 K (571 ^{0}C), which is much lower than the typical die casting temperatures employed for this alloy. He showed that the thixoformed part was metallurgically sound and free from porosity compared to die-cast part.

The cooling slope (CS) casting process, Fig. 20, was employed to produce the non-dendritic feedstock. The CS casting involved pouring the partially molten alloy with a small fraction of Si crystals over a 0.05m wide and 0.5m long, inclined steel plate into a permanent mold with a diameter of 0.03 m and a depth of 0.15 m. The cooling plate was adjusted at 60° with respect to the horizontal plane and was cooled with water circulation underneath (Fig. 20). The best as-cast microstructural features were obtained with a pouring temperature of 858K (585 ^{0}C) and a cooling length of 0.3 m. The feedstock was sectioned into 35 mm long slugs. The slugs were then held at 844 (571 ^{0}C) ±1K for 300 s to allow spheroidization of the grains. The thixoforging operation was carried out using a laboratory press. A pneumatic cylinder was used to provide the forging load (15 kN) and the maximum speed of the ram was 0.5 m/s. The die was pre-heated to 723 K (450 ^{0}C). Fig. 21 shows the microstructure of CS cast ingot and the thixoformed and die cast A390 part.

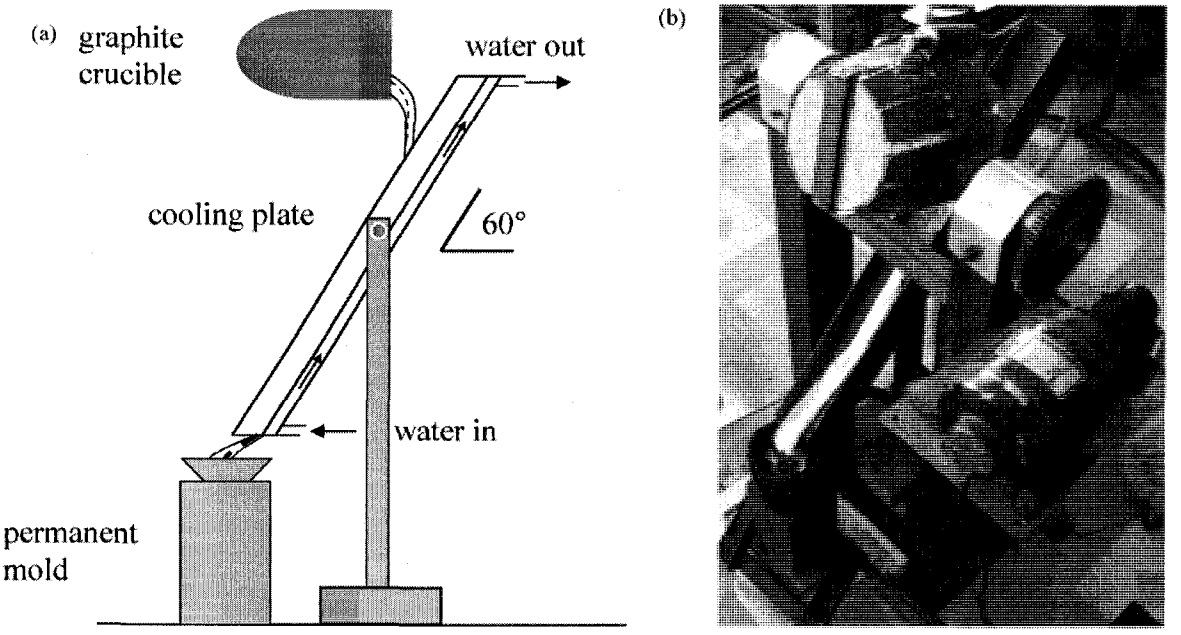

Fig.20: Cooling slope casting unit used by [50].

The CS-cast ingot is characterized by a dispersion of primary Si particles in a matrix of Al–Si eutectic and some intermetallic particles (Fig. 21a).

The primary Si particles exhibited polyhedral morphologies and were of sizes ranging from several to 3×10^{-5} m. Low pouring temperature and high cooling rates are responsible for the small size of the primary Si particles which are almost invariably surrounded by α-Al rosettes (Fig. 21a). The Si depletion around primary particles in the melt before pouring is believed to be responsible for the shift in local chemistry which facilitates the formation of primary aluminum dendrites–rosettes.

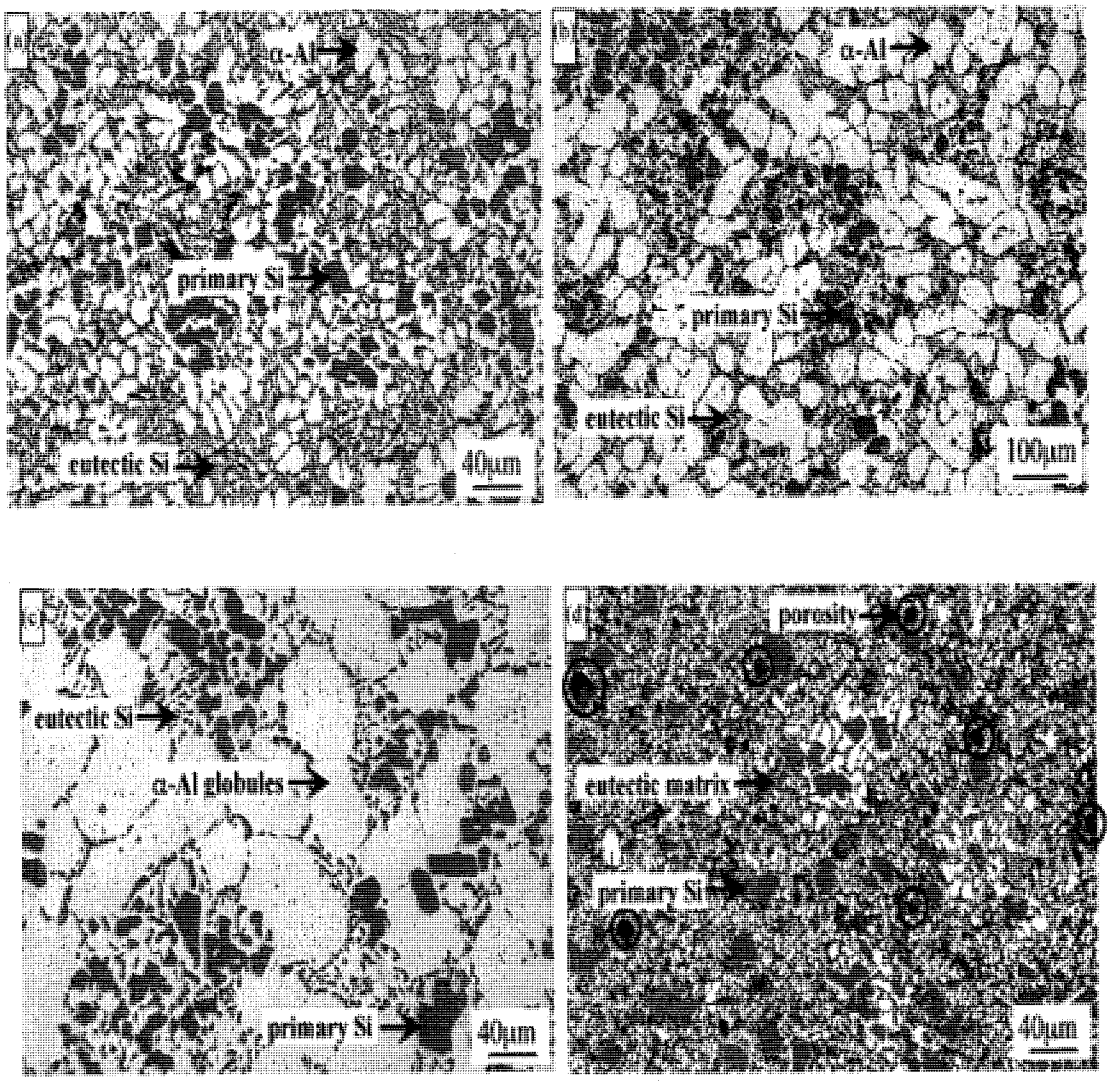

Fig. 21: Microstructure of (a) CS cast ingot, (b,c) thixoformed and (d) die cast A390 part [50]

The solidification structure was largely modified, due to the reduced latent heat and the rapid solidification which prevail under thixoforming conditions. The aluminum globules were found to vary between 5×10^{-5} and 10×10^{-5} m in diameter. The thixoformed A390 part was perfectly sound, free of porosity, in contrast to the die cast sample of the same alloy which revealed both micro and macro-porosity (Fig. 21d). However, the matrix structure in the die-cast sample was much finer. It was shown that the hardness of the thixoformed part is somewhat higher than that of the die-cast part. Finally, it was concluded that thixoforming offers as an attractive alternative in the production of these alloys, as it can overcome the problems encountered in die casting of hypereutectic Al–Si alloys.

3-2-4 Thermodynamic evaluation (Factsage software)

Before investigating the rheological characteristics of A390, it was necessary to determine the thermodynamic characteristics and solidification path of the alloy in order to identify the compounds and phases that are formed during the solidification period based on the calculated phase diagram. The composition of A390 corresponds to a quaternary system of Al-Si-Cu-Mg in the Al-rich corner. We will begin by presenting the calculated diagrams relevant to our study that will give us a base for comparing with the model.

3-2-4-1 Quaternary Al-Si-Cu-Mg

Different intermetallic phases can appear [51] for the quaternary system depending on the alloy composition according to the reactions shown in Table 2. This table shows the all reactions carried out for quaternary system. However, in the case of A390 alloy, the reactions related to the phases such as $CuAl_2$, Mg_2Si, $Cu_2Mg_8Si_6Al_5$ takes place which are the most common phases observed in the microstructure of A390 alloy [52, 53, 54]. The other reactions may carry out for other compositions out of rich corner of aluminum.

Table 2: Phases present in Al-Si-Cu-Mg. [51]

Reaction		%Mg(L)	%Si(L)	%Cu(L)	T
eutectic	Liq. $\rightarrow Al + Mg_5Al_8 + Mg_2Si + CuMg_4Al_6$	33.0	0.3	1.5	446
peritectic	Liq.+ $CuMgAl_2 \rightarrow Al + Mg_2Si + CuMg_4Al_6$	25.5	0.3	10.0	467
eutectic	Liq. $\rightarrow Al + Mg_2Si + CuMgAl_2$	10.5	0.3	23.0	516
eutectic	Liq. $\rightarrow Al + CuAl_2 + Mg_2Si + CuMgAl_2$	$\approx$6.5	$\approx$0.3	30-33	500
eutectic	Liq. $\rightarrow Al + CuAl_2 + Mg_2Si$ (quasiternary)	31.5	3.9	31.5	515
peritectic	Liq.+ $Mg_2Si \rightarrow Al + CuAl_2 + Cu_2Mg_8Si_6Al_5$	2.2	6.0	28.0	512
eutectic	Liq. $\rightarrow Al + CuAl_2 + Cu_2Mg_8Si_6Al_5$ +Si	2.2	6.0	28.0	507
peritectic	Liq.+ Mg_2Si +Si $\rightarrow$ Al + $Cu_2Mg_8Si_6Al_5$	3.3	9.6	13.8	529

3-2-4-3 Calculated phase diagram

The objective of this section is to calculate phase diagrams using the Factsage software (version 5.4.1) developed by the group CRCT of *Ecole Polytechnique de Montréal.* In the aluminum rich corner, the thermodynamic data of the Al liquid phases, Al (fcc) and Si (diamond) as well as the intermetallic phases such as Mg_2Si and θ-Al_2Cu, were used to model the phase diagrams of Al-Si-Cu-Mg according to the Fslite (Factsage light metal alloy database) database. The FactSage FSlite light alloy database has been derived from the database that resulted from the European COST Action 507 (*COST 507, Thermochemical database for light metal alloys*) [55]. However, it has been much improved by corrections of the original data and by many additions in terms of binary and higher order subsystems. Some amendments and some updates were incorporated in this upgraded light alloy database to calculate the binary, ternary and quaternary diagrams. The database is generally valid for the temperature range of approximately 200°C to 1800°C and all ranges of composition. For some alloys with high melting point metals, the data was still found to be reliable. In the calculations, the liquid phase was described using a simple substitutional solution approach based on the Redlich-Kister-Muggianu polynomial expression. Most of solid solution phases were described using sub-lattice models which include interstitials and vacancies where appropriate.

3-2-4-2-1 The quaternary Al-Si-Cu-Mg

The solidification path of A390 alloy is shown in Fig. 22 and indicates the binary, the ternary and the quaternary reactions. Fig. 23 indicates the transition temperatures between 700 ° C and 25 ° C for A390 alloy. Consequently, the solidification path confirms that the Si starts to precipitate from the liquid phase at 653,1 ° C and continues down to the 566,2 ° C with maximum solid fraction of 6.1%. At this point a dendritic network of α-Al and eutectic Si start to form and continues down to 502,4 ° C where 88% liquid changes to this network. The ternary eutectic reaction takes place according to following reaction:

$$\text{Liq.} \rightarrow \text{Al} + \text{Si} + \text{Mg}_2\text{Si} \qquad (9)$$

The ternary eutectic zone continues down to the temperature of 496, 9 ° C and only 2.0% of the liquid changes to ternary phases. The solidification becomes complete according to the quaternary reaction and the last liquid (3.9%) changes to:

$$\text{Liq.} \rightarrow \text{CuAl}_2\ (\theta) + \text{Al} + \text{Si} + \text{Mg}_2\text{Si} \qquad (10)$$

Other studies [52, 53, 54] have reported that the quaternary reaction proceeds according to the following equation:

$$\text{Liq.} \rightarrow \text{CuAl}_2\ (\theta) + \text{Al} + \text{Si} + \text{Cu}_2\text{Mg}_8\text{Si}_6\text{Al}_5 \qquad (11)$$

It should be noted that the quaternary compound ($Cu_2Mg_8Si_6Al_5$, Q phase) is not included in the Factsage database and is therefore not considered in the calculated diagram. However, the microstructural observation shown in Fig. 24 indicates the presence of the $Cu_2Mg_8Si_6Al_5$ phase associated with $CuAl_2$ in the solidified microstructure.

On the other hand, no Mg_2Si has been reported by other studies in the microstructure of A390 alloy implying any Mg_2Si is thoroughly transformed to the Q phase [12] according to the following reaction [56]:

$$\text{Liq.} + Mg_2Si \rightarrow CuAl_2\ (\theta) + Al + Si + Cu_2Mg_8Si_6Al_5 \qquad (12)$$

This reaction (see Table 2) must be placed between reactions (1) and (3) in order to transform all Mg_2Si to phase Q.

It was observed that the $Cu_2Mg_8Si_6Al_5$ typically nucleates on θ-Al_2Cu in a form of blocky or thick needle-like structures [57]. The θ-Al_2Cu phase precipitates in both a blocky and eutectic ($Al+Al_2Cu$) forms or as a mixture of both types depending on the cooling rate Fig. 24 a,b [58]. The precipitation of $Cu_2Mg_8Si_6Al_5$ is reported to take place at the end of the $Al+Al_2Cu$ eutectic region or at the end of the solidification of A390 alloy [58].

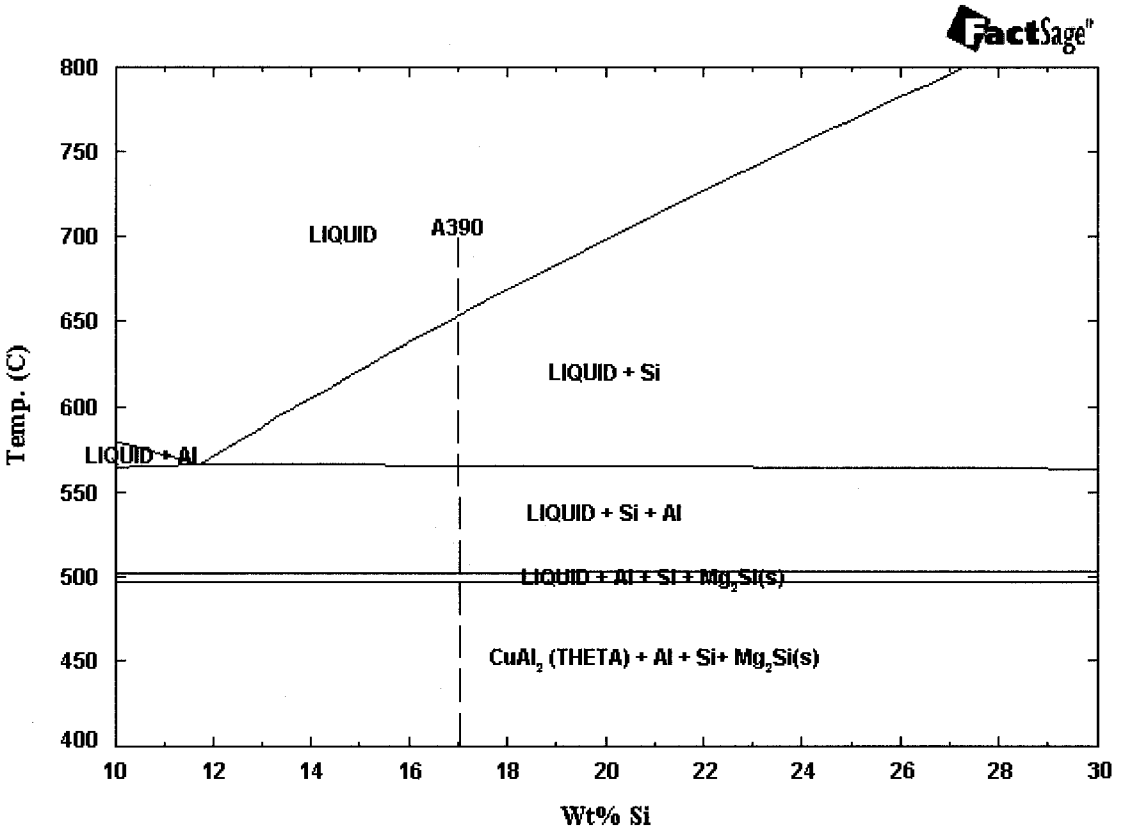

Fig. 22: A vertical section of Al-Si-Cu-Mg system at 4.5%Cu and 0.5%Mg. Dashed line indicates the solidification path of A390 alloy at 17% Si.

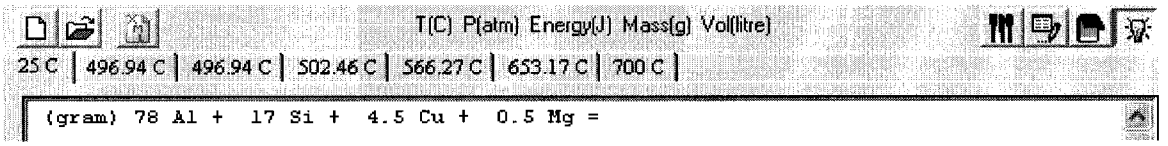

Fig. 23: Transition temperatures for A390 alloy between 700˚C of 25˚C.

According to the solidification path of A390 calculated by Factsage software (Fig. 22), the silicon start to precipitate as primary crystals at 653 ° C and the binary Al-Si eutectic forms at 566 ° C. The silicon that precipitates as a primary phase has a faceted morphology as shown in Fig. 24c and the eutectic morphology has a coarse plate-like crystals, Fig. 24 d, e. The Mg_2Si phase is rarely observed in microstructure of A390 alloy as explained before. However, due to the non-equilibrium cooling it can be observed in form of Chinese script [57] as shown in Fig. 24 f. Many studies have confirmed the close similarity between hypereutectic Al-Si alloys and Al-based composites with similar composition [59] where the primary silicon plays the role of reinforcing phase in this composite.

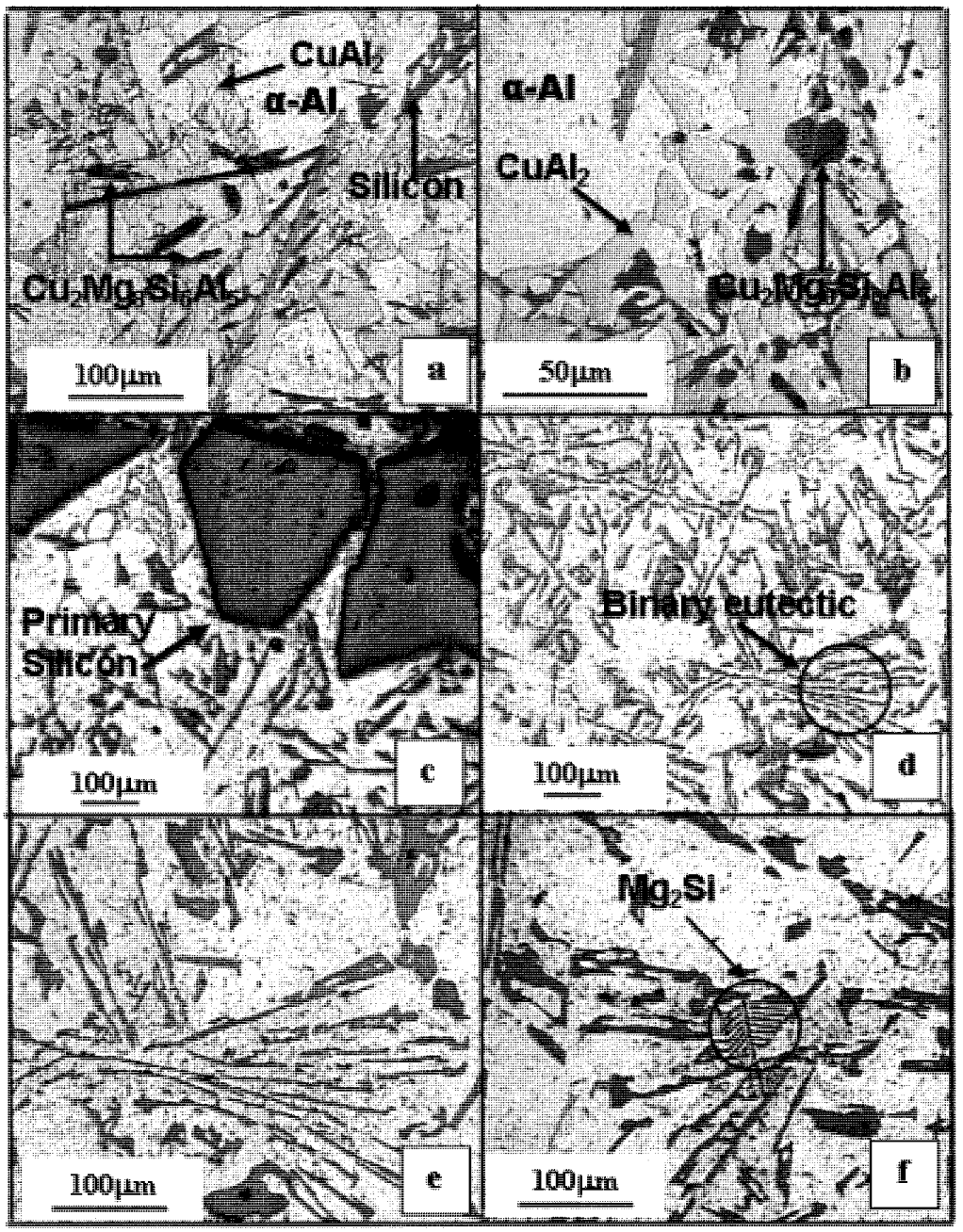

Fig. 24: Microstructure of as cast A390, (a) precipitation of Al_2Cu and $Cu_2Mg_8Si_6Al_5$ (dark blocky) (b) same region, high magnification (c) primary faceted silicon (d) plate-like crystals of eutectic Si (e) same region, high magnification and (f) Mg_2Si [88].

Table 3 shows the liquid fraction, the compositions as well as the solid fraction with the percentage of each solid constituent during the transformation reactions of A390 alloy. It should be noted that the binary and ternary reactions take place at the temperature interval between isotherm 566.2-502.4 °C and 502.4-496.9 °C, respectively. However the quaternary reaction occurs at an isothermal temperature of 496.9 °C corresponding to the final solidification.

According to Table 3 the binary reaction has the highest contribution in forming solid phases Si + Al (88.0 %) whereas the ternary reaction has a much smaller contribution (2.0 %) in forming Al + Si + Mg_2Si phases. The microstructure of the solidified eutectic therefore consists of a dendritic network where the most predominant phases observed are Al + Si as shown in Fig.24,

Table 3: The liquid and solid fraction as well as corresponding compositions for each transition reaction for A390 alloy.

A390	liquid Fraction (%)	reaction	Solid Fraction (%)	Solid composition (%wt)			
Temperature (°C)				Al	Si	θ*	Mg_2Si
653,1	100	Primary silicon	0	-	-	-	-
566,2	93,9	Binary Al+Si	6,1	-	100	-	-
502,4	5,9	Ternary Al+Si+Mg_2Si	94,1	83,2	16,8	-	-
496,9+δT	3,9	Quaternary	96,1	83,1	16,7	-	0,2
496,9-δT	0	Al+Si+Mg_2Si+Q**	100	81,4	16,2	2,1	0,3

* θ = Al-Cu (θ) or $CuAl_2$

** Q = $Cu_2Mg_8Si_6Al_5$

3-2-4-2-1-1 Effect of Cu content

An isopleth diagram is a vertical section of ternary or quaternary phase diagram at a fixed value of a solute component. The isopleths of the quaternary Al-Si-Cu-Mg system with a section at 4.5%Cu and 0.5%Mg is shown in Fig. 22. The variation of Cu changes the Si content in the liquid phase when the binary and ternary reactions are started. The corresponding temperatures are also changed. However, there is no effect on the quaternary reaction as shown in Table 4 and Fig 25. For the system of alloys Al-17%Si-X%Cu-0.5%Mg (X = 4.5%, 7%, 10%, 15%, 20%), the temperature of the binary reaction as well as the silicon content in the liquid both decrease with increasing the Cu content.

For a value of copper up to 7.2%, the ternary reaction is given as liquid$\rightarrow$ Al(S) + Si + Mg_2Si, which is the same as A390 alloy. However, the alloys with more than 7.2% Cu, the ternary reaction is transformed to liquid$\rightarrow$ Al(S) + Si + θ-$CuAl_2$. This implies that the value of 7.2% Cu is a critical point to enlarge the zone of θ-$CuAl_2$ solidification.

Table 4: Effect of Cu variation on silicon content in liquid of binary, ternary and quaternary eutectic and corresponding temperature for Al-17%.Si-n%Cu-0.5%Mg (n=4.5,7,10,15,20) alloys.

	Start of binary reaction		Start of ternary reaction		Quaternary reaction	
%Cu	T (°C)	%Si *	T (°C)	%Si*	T (°C)	%Si*
4.5 **	566	11.7	502	7.8	496	7.1
7	561	11.1	499 ***	7.0	496	7.1
10	554	10.6	501	6.9	496	7.1
15	542	9.4	503	6.8	496	7.1
20	529	8.3	504	6.7	496	7.1

*** Silicon content in liquid at the first precipitation of binary, ternary and quaternary eutectic**

**** A390 composition**

***** With increasing the copper content from 7%, ternary eutectic changes to**
Liquid→ Al(s) + Si + θ-$CuAl_2$

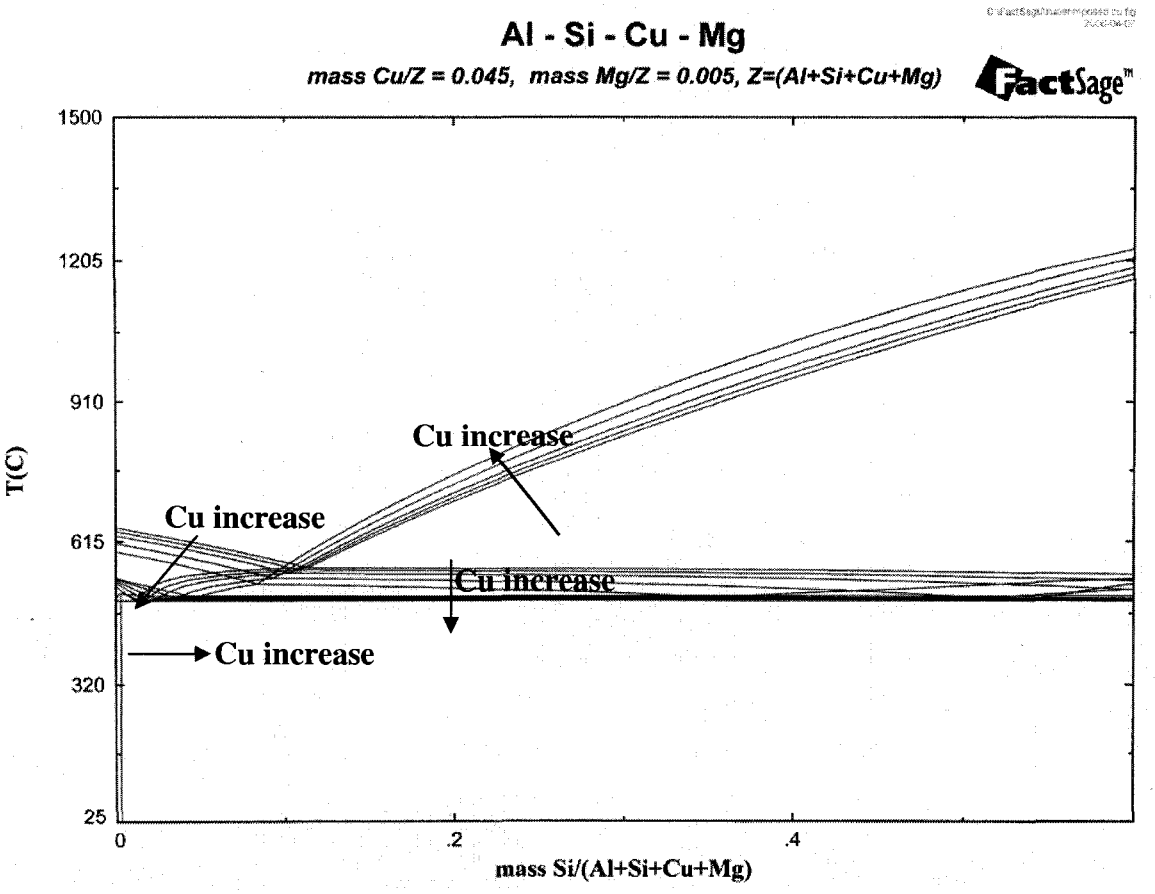

Fig. 25: Effect of copper variation on the phase diagram of Al-Si-XCu-0.5%Mg (X = 4.5%, 7%, 10%, 15%, 20%).

3-2-4-2-1-2 Effect of Mg content and property of Mg_2Si particle

The isopleths of the system of Al-Si-4.5%Cu with variable Mg contents was investigated for values of 0.5%, 1%, 3%, 5% and 10% Mg and the transition temperatures shown in Table 5. Very interesting results were obtained with variation of Mg content. The results indicate that with the addition of Mg, the Mg_2Si intermetallic phase first appears in the ternary eutectic zone for 3% Mg as shown in Fig. 26. For 5% Mg content shown in Fig. 27, the Mg_2Si intermetallic phase appears in the both binary and ternary reactions. For 10% Mg content, the Mg_2Si is solidified as primary phase as well as during the binary and ternary reactions as shown in Fig. 27. This implies that the formation range of Mg_2Si intermetallic particle can be significantly increased with addition of Mg. The results obtained at this step has led to the identification of two critical Mg contents, at 4.2% and 7.2%, where at each critical point the Mg_2Si is solidified according to new reaction.

This is principally due to the transformation of the phase silicon to form Mg_2Si with the addition of Mg. The melting point of Mg_2Si is about 1102°C [60] and this encourages the Mg_2Si to be formed as a primary phase at high temperature level. Fig. 28 shows the binary Mg-Si alloy and the composition of the Mg_2Si intermetallic phase.

The solidification path of A390 (Al-17%Si-4.5%Cu-0.5%Mg) alloy and alloy with 10% Mg content (Al-17%Si-4.5%Cu-10%Mg) can be compared in Figs. 22 and 29, respectively. The solidification paths were shown by dash-dot lines in the isopleth diagrams. The first important difference is due to the precipitation of the primary phase.

As explained before, the silicon and Mg_2Si particles are the primary phases solidified in A390 and 10% Mg containing alloys, respectively. The second difference during their solidification paths is the microstructure of matrix. After precipitating the primary silicon phase in A390 alloy, the biggest region is binary region where the liquid is changed to dendritic aluminum and eutectic silicon. The ternary and quaternary reaction has no significant effect (or low solid fraction) in formation of matrix. Therefore, it is anticipated that matrix of A390 forms of binary Al + Si. However, for 10% Mg alloy, the ternary Al + Si + Mg_2Si forms the matrix of alloy because it is the biggest eutectic region. Therefore, the eutectic Mg_2Si is appeared in the microstructure of A390 alloy with 10% Mg content.

Table 5: Effect of Mg variation on silicon content in liquid of binary, ternary and quaternary eutectic and related temperature for Al-Si-4.5%Cu-n%Mg systems at 17%Si.

	Start of binary reaction		Start of ternary reaction		Quaternary reaction	
%Mg	T (°C)	%Si [1]	T (°C)	%Si[1]	T (°C)	%Si[1]
0.5[2]	566	11.70	502	7.49	496	7.1
1	564	11.75	526	9.65	496	7.1
3	555	12.20	546	12.08	496	7.1
5	565[3]	13.76	549	12.51	496	7.1
10	588	15.65	549	12.43	496	7.1

1- Silicon content in liquid at the first precipitation of the binary, ternary and quaternary eutectic.
2- A390 composition.
3- At Mg content higher than 4.2% the Binary eutectic reaction changes to (Liquid → Si (S) + Mg2Si (S)) instead of (Liquid → Al (S) + Si (S)).

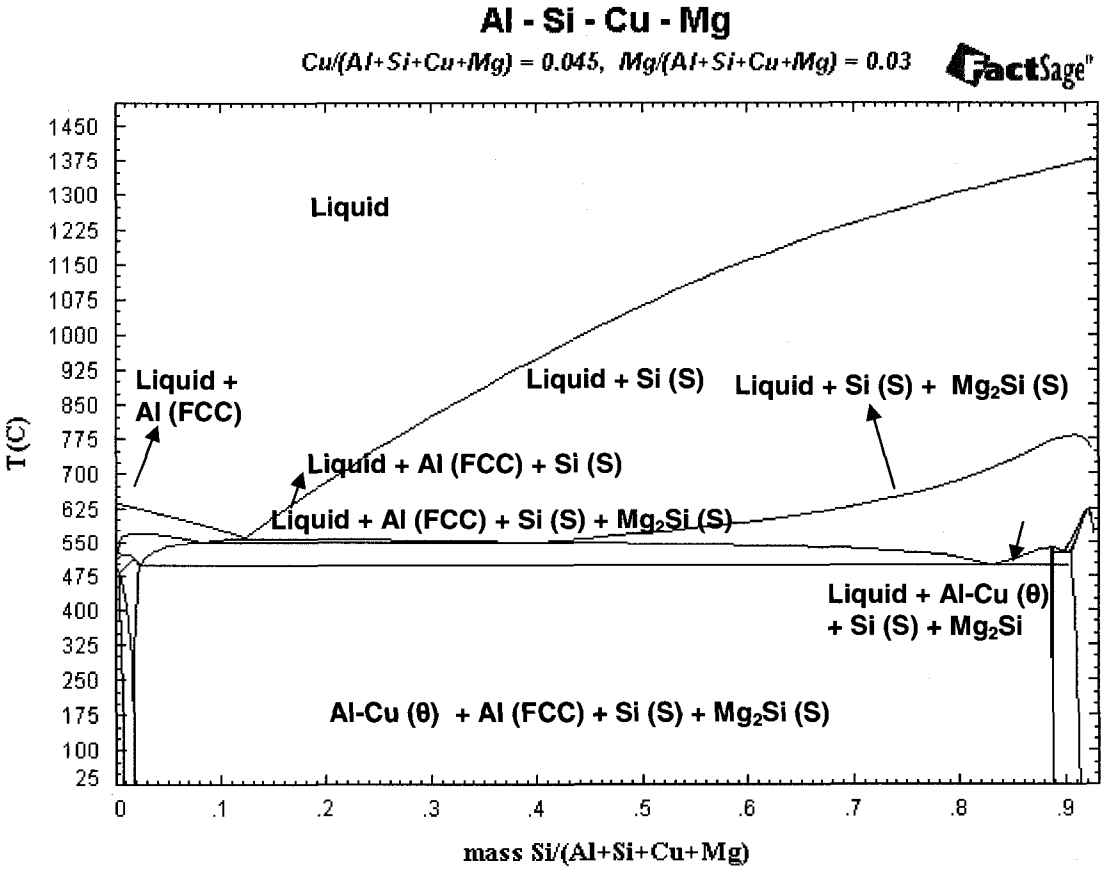

Fig. 26: A vertical section of Al-Si-Cu-Mg system at 4.5%Cu and 3%Mg.

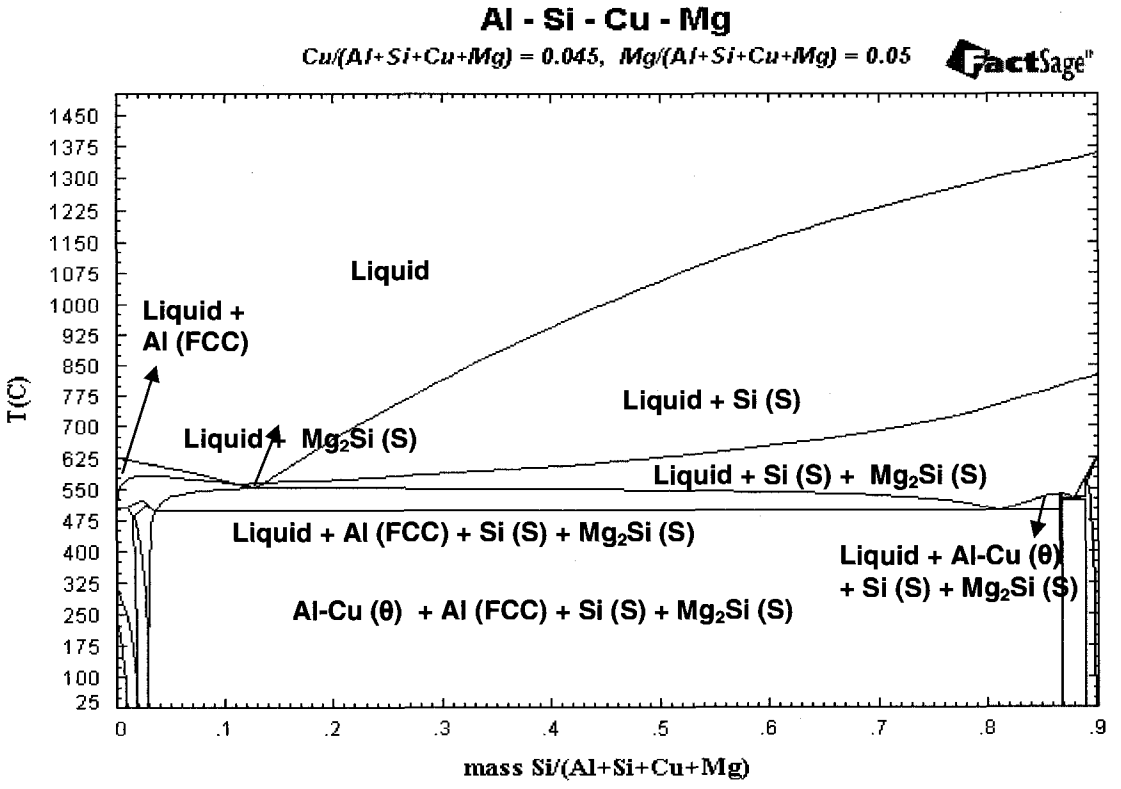

Fig. 27: A vertical section of Al-Si-Cu-Mg system at 4.5%Cu and 5%Mg.

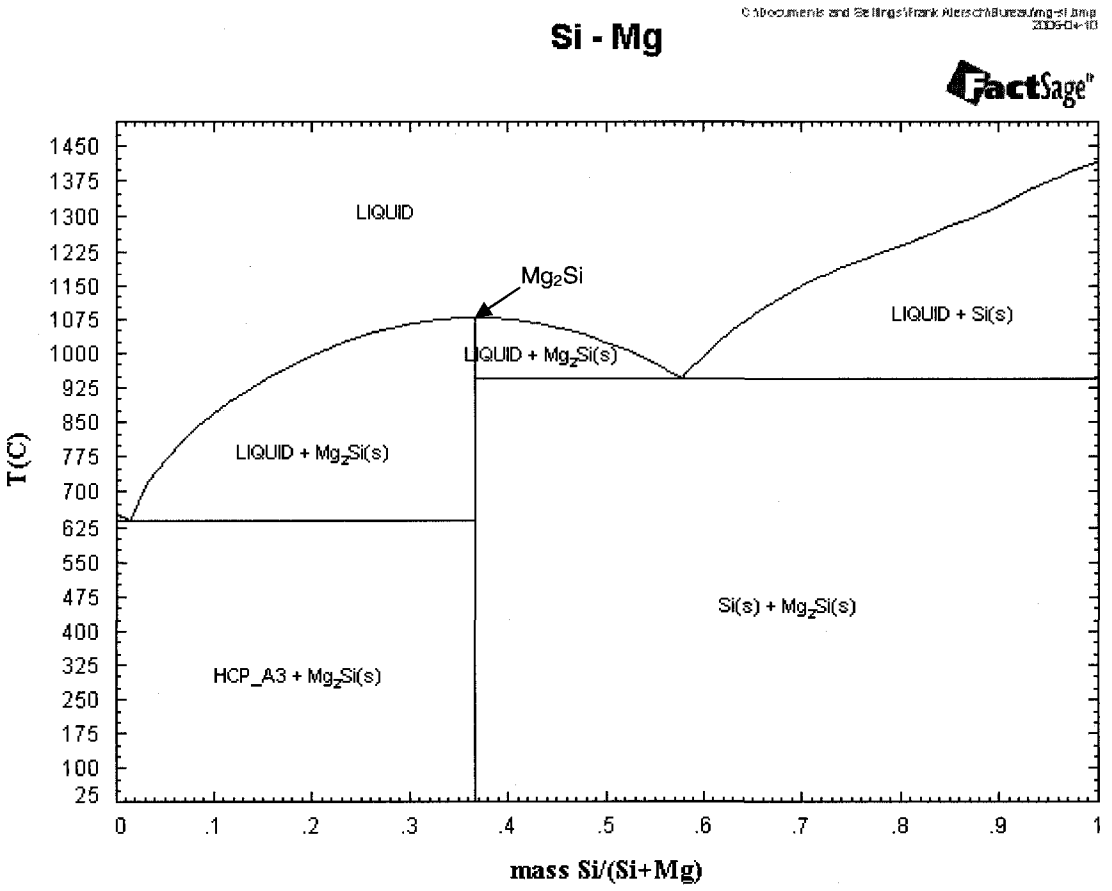

Fig. 28: Binary Si-Mg phase diagram

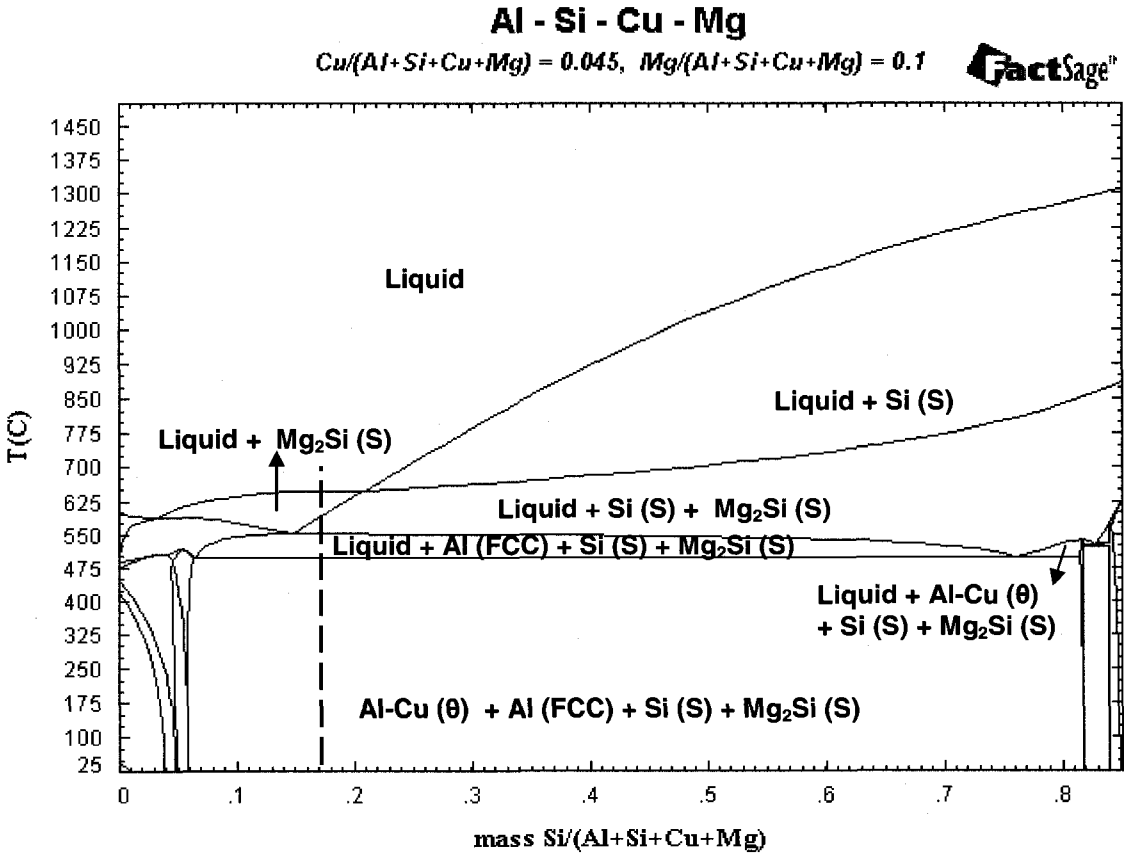

Fig. 29: A vertical section of Al-Si-Cu-Mg system at 4.5%Cu and 3%Mg and solidification path at 17%Si

3-2-5 Similarities between hypereutectic Al-Si and Al-Mg_2Si alloys

Hypereutectic Al-Si alloy with high Mg content has high potential as a wear resistant material because the intermetallic compound of Mg_2Si exhibits high melting temperature, low density, high hardness, low thermal expansion coefficient, equilibrium interface, excellent workability as well as the potential for cost reduction [61]. Both hypereutectic Al-Si alloy and Al- Mg_2Si alloy can be called in situ metal matrix composite (MMCs) because the hard particles of silicon and Mg_2Si are dispersed in the metal matrix and act as a reinforcing phase resulting in better mechanical properties particularly wear resistance. The term 'in situ' implies that these hard particles is formed naturally during solidification process contrary to most composites where the reinforcement fibres such as SiC or Al_2O_3 are externally added in to molten metal matrix. Most of the application of these alloys are in automotive industry for parts such as piston, engine block and break disk materials that require significant wear resistance at medium or elevated temperatures. Both the size and morphology of the reinforcement phases (Si or Mg_2Si) strongly affect the mechanical properties. The studies carried out by author show that the modification of Mg_2Si particles can be achieved more easily in comparison to the silicon particle during semi solid metal processing. To produce the Mg_2Si intermetallic, a lorge amount of Mg has to be added to the hypereutectic Al-Si as indicated in Table 6. The chemical composition of Al-Mg_2Si alloy and Fig. 30 shows the as-cast microstructure of this alloy according to [62]. Microstructure consists of Mg_2Si, alpha aluminum and eutectic silicon phase.

Table 6: Chemical composition of Al-Mg_2Si alloy or Mg_2Si/Al composite. [62].

Materials	Al	Mg	Si	Cu	Cr	Zn	Ni	Fe
Al-Si-Mg-Cu	Bal.	13.276	11.281	3.523	<0.005	<0.023	<0.001	0.325

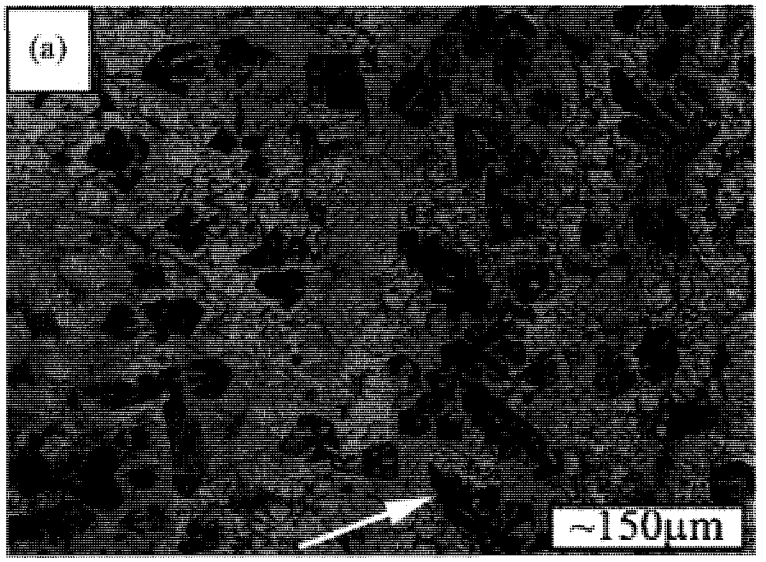

Fig. 30: Microstructure of as-cast Al-Mg_2Si alloy consists of Mg_2Si, alpha aluminum and eutectic silicon phase. [62].

In terms of properties and solidification behavior, similarities exist between Mg_2Si and Si. The simple cubic lattice of Mg_2Si, which has a high symmetry results in better ductility [63] and the very low density, makes it suitable as a reinforcing compound. Epitaxial growth of Mg_2Si on Si (111) occurs with a low lattice mismatch. Analysis of the diffraction pattern shows that the strong diffraction spots coincide with the diffraction spots of Mg_2Si [111] zone [64]. This means that the polygonal Mg_2Si has a faceted morphology similar to the Si particle

The most important advantage of Mg_2Si particle is its very low density of 1.99 $g.cm^{-3}$ (Si = 2.33 $g.cm^{-3}$). The growing demand for more fuel-efficiency vehicles to reduce energy consumption and air pollution is a challenge for the automotive industry [65]. Another advantage is its good response to morphology modification when SSM processing is used. This means that its morphology quickly changes to spheroidal particle in a thixocasting process, which improves the mechanical properties. In contrast, the large size of primary Si particles formed on solidifying A390 is not suitable for SSM process requiring time and high amount of energy to modify the morphology of Si to form a fine and globular microstructure. Fig. 31 shows the SEM images and Table 7 compares the physical properties of silicon and Mg_2Si particles.

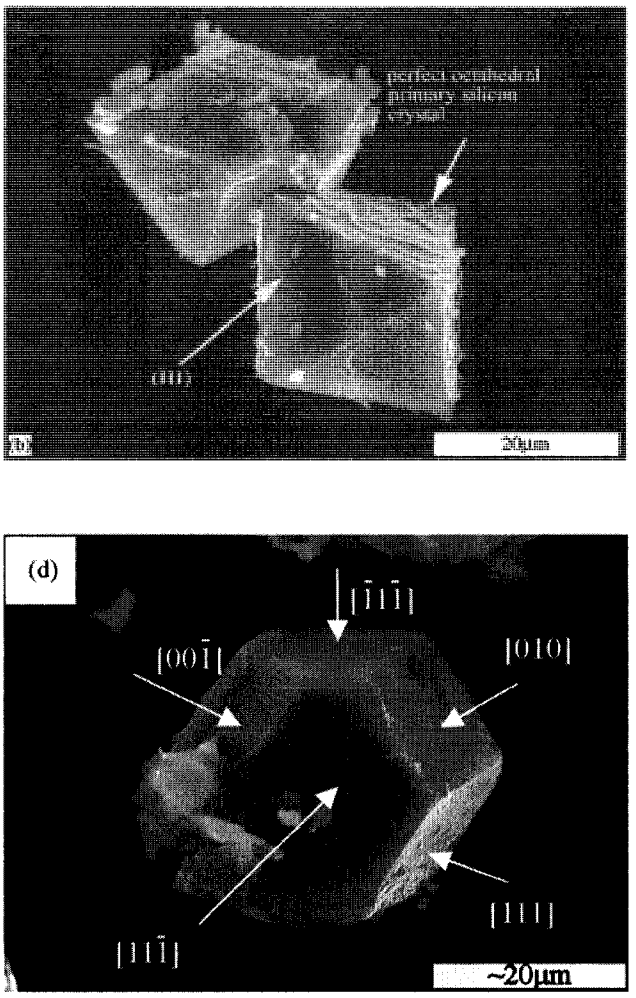

Fig. 31: SEM images of silicon and Mg_2Si showing polygonal particles.

Table 7: Physical property of silicon and Mg_2Si particles

Phases	Crystal structure	Lattice parameter (nm)	Density ($g\,cm^{-3}$)	C.T.E[a] ($10^{-6}\,k^{-1}$)	Elastic modulus (Gpa)	Melting point ($^{\circ}C$)
Mg_2Si	Cubic	0.635	1.99	7.5	120	1085
Si	Cubic	0.542	2.33	3.06	112	1411

3-3 Mechanical properties of Al-Si alloys

3-3-1 Viscosity (flow behavior)

3-3-1-1 Hypoeutectic alloy A356

As it was described in section 1-4-3-2, the morphology of primary phase has a pronounced effect on the flow behavior of semi solid metal slurries. The apparent viscosity is an indication of the capability in filling the mould and determines the required force for deformation and flow of materials in the SSM processing. It has found that dendritic structures at the same solid fraction exhibit flow resistance approximately several orders of magnitude greater than the equiaxed or globular structures [33]. In fact, the globular particles move easier over each other than dendritic phases which tend to interlock during application of external force, resistance against flow.

S. Nafisi et al. [66] show the effect of morphology and particle size of primary α-Al on flow behavior of A356 alloy with and without grain refiners such as Ti-B and Sr by using a parallel plate compression test (see section 3-1-6 for definition of this test). They revealed that the lower resistance to flow shown in Fig. 32 is due to the smaller particle size of the primary α-Al phase. Furthermore the grain refined alloy results in finer and more spherical primary α-Al particles with a greater solid–liquid interfacial area where the interparticle liquid film can assist solid particles gliding over one another. Strain–time graphs were used to calculate the viscosity of alloy and confirmed that non-modified alloy has the highest apparent viscosity.

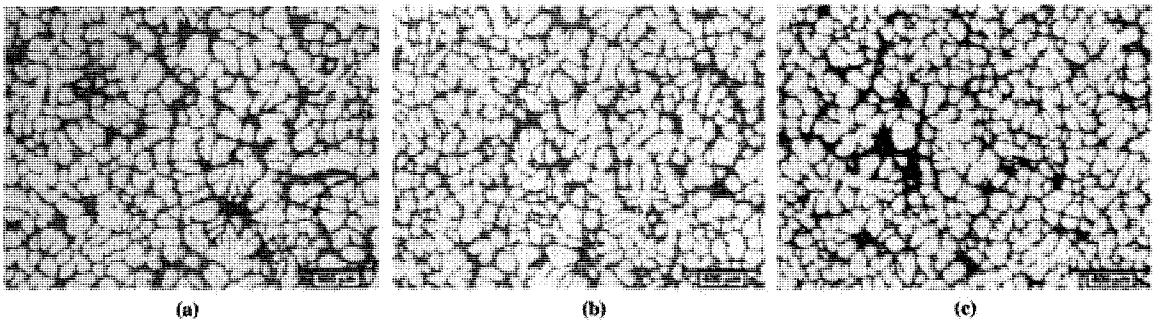

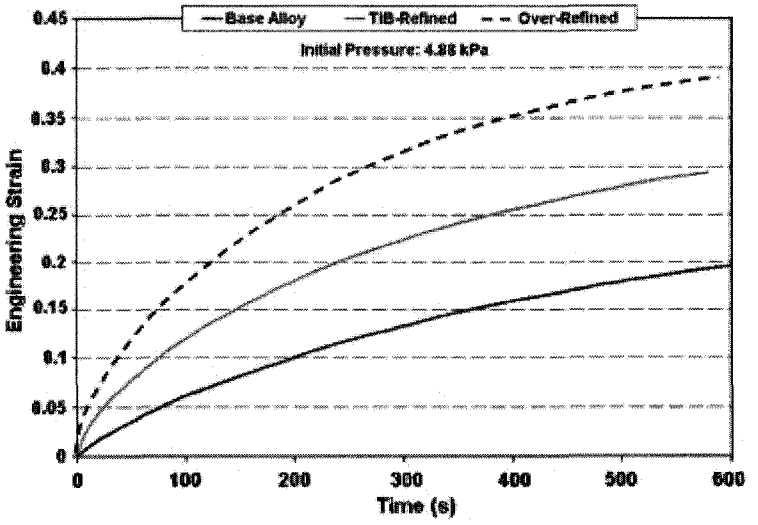

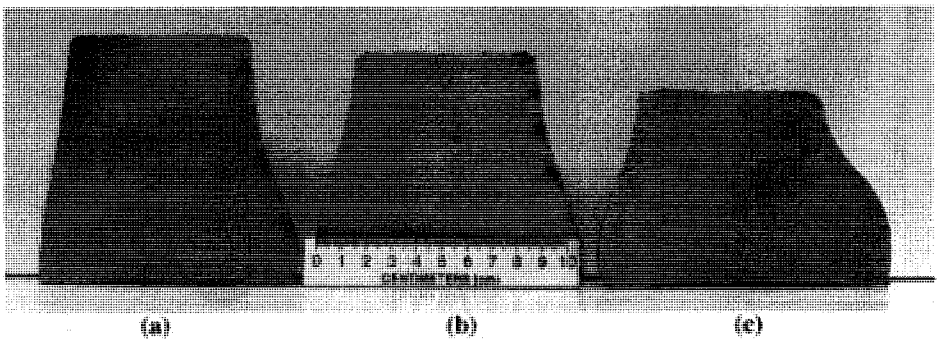

Fig. 32: Comparison of deformation behavior of A356 aluminum alloy by parallel plate compression test at 598 ± 2 °C due to microstructural evolution of quenched samples: (a) untreated alloy, (b) grain refined with 620 ppm Ti, 110 ppm B, and (c) combined treatment, 610 ppm Ti, 100 ppm B, 160 ppm Sr [66].

3-3-1-2 Hypereutectic alloy A390

Lashkari et al. [67] have investigated the flow behavior of thixocast A390 hypereutectic Al-Si alloy in the semi solid state also using the parallel plate compression test. Liquid A390 alloy was poured at 700 °C, at about 62 °C superheat, into a refractory coated cylindrical metallic mold, held at 25 °C, supported by a copper plate at the bottom of the mold. The cylindrical samples of 60mm diameter and 70mm height were cut from the bottom section of the castings. The cast samples were then reheated in a resistance furnace, at a rate of 37 °C /min to mushy zone temperatures of 552, 558, 560 and 561.5 ±1 °C representing solid fractions of 0.6, 0.5, 0.4 and 0.3 respectively. The reheated samples were quickly transferred and compressed uniaxially and isothermally in the parallel-plate compression-test machine.

Fig. 33 shows the evolution of the microstructures obtained at different conditions for the as-cast case and for the samples reheated at different semi solid temperatures. As expected, the as-cast microstructure, shown in Fig. 33a, shows some primary Si particles in the matrix, surrounded by α-Al phase which is preferentially formed due to deficit of Si in the liquid around the primary Si crystals.

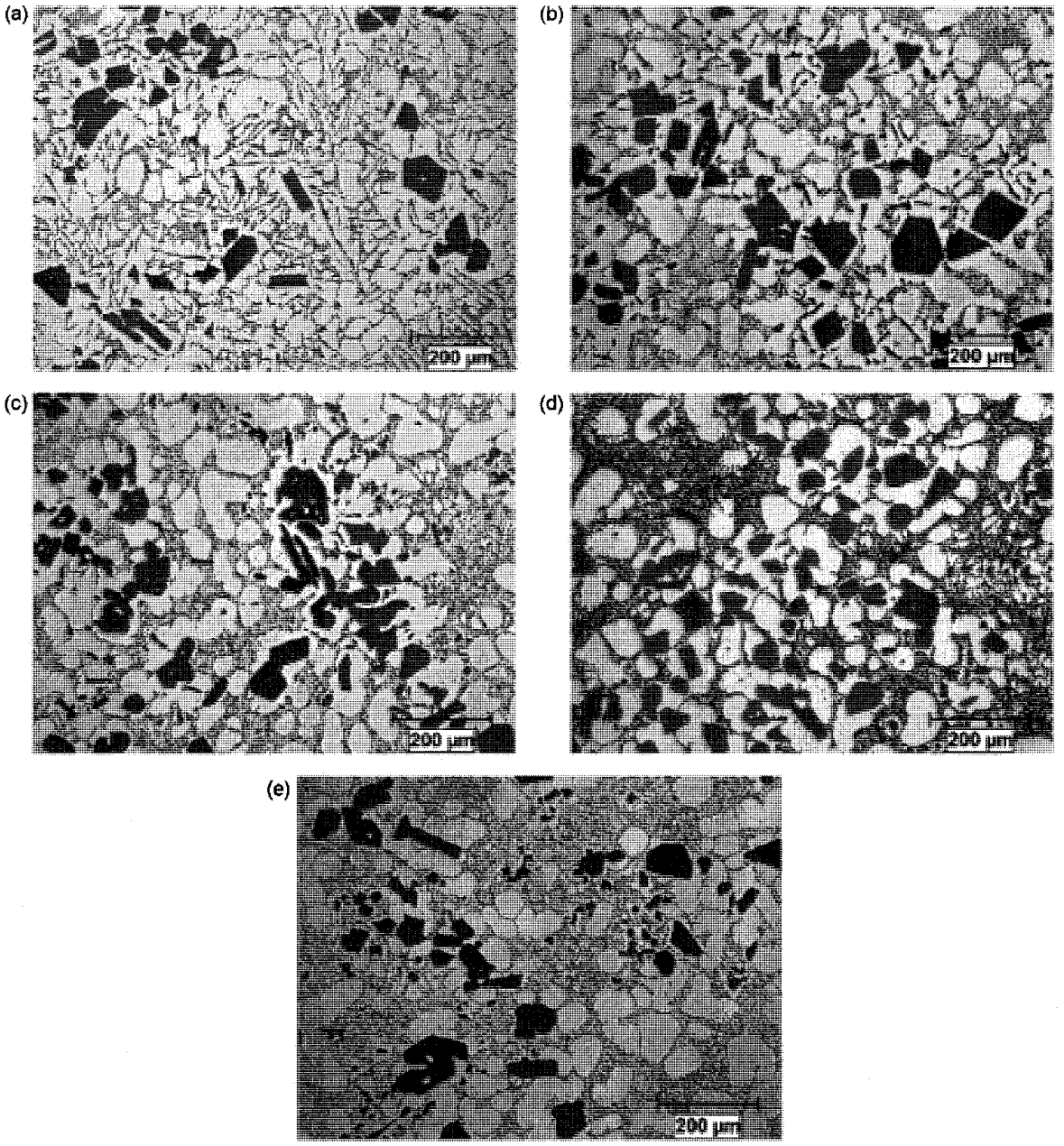

Fig. 33: (a) As-cast A390 alloy poured in 60mm diameter metallic mold, (b) sample reheated to 552 °C, (c) sample reheated to 558 °C, (d) sample reheated to 560 °C, (e) sample reheated to 561.5 °C. [67]

The remaining liquid transforms according to the eutectic reaction. The elevated cooling rate does not produce a suitable microstructure of α-Al and Si phases for semi solid processing. Therefore, reheating of the samples was carried out to produce a microstructure of this alloy facilitating the deformation at high solid fractions.

Fig. 33b shows a reheated microstructure at the beginning of the eutectic transformation 552°C, where the Cu and Mg enriched eutectic region remelts and the growth of the α-Al and Si phases proceeds by a diffusion process. The estimated amount of solid phase (α-Al + Si) at this temperature was calculated to be 0.6, where the semi solid samples are still not easily deformed. Increasing the temperature to 561.5 °C reduces the amount of α-Al fraction solid which remelts in combination with the Si eutectic phases, but the primary Si phase still remains due to the precipitation of the Si eutectic around this pre-existing phase. The resulting structure improves the deformation behavior of the slurry represented by a decrease in the viscosity. Fig. 33c–e demonstrates the phase transformation resulting from higher reheating temperatures. The graphs presented in Fig. 34 are typical strain-time behavior of the thixocast samples reheated at different temperatures, representing different solid fractions. The instantaneous change in the billet height is registered during parallel plate compression test and converted into engineering strain using the following simple equation;

$$e = 1\text{-}h/h_0 \qquad (13)$$

where h_0 and h are the initial and instantaneous heights (mm) of the specimen during compression, respectively.

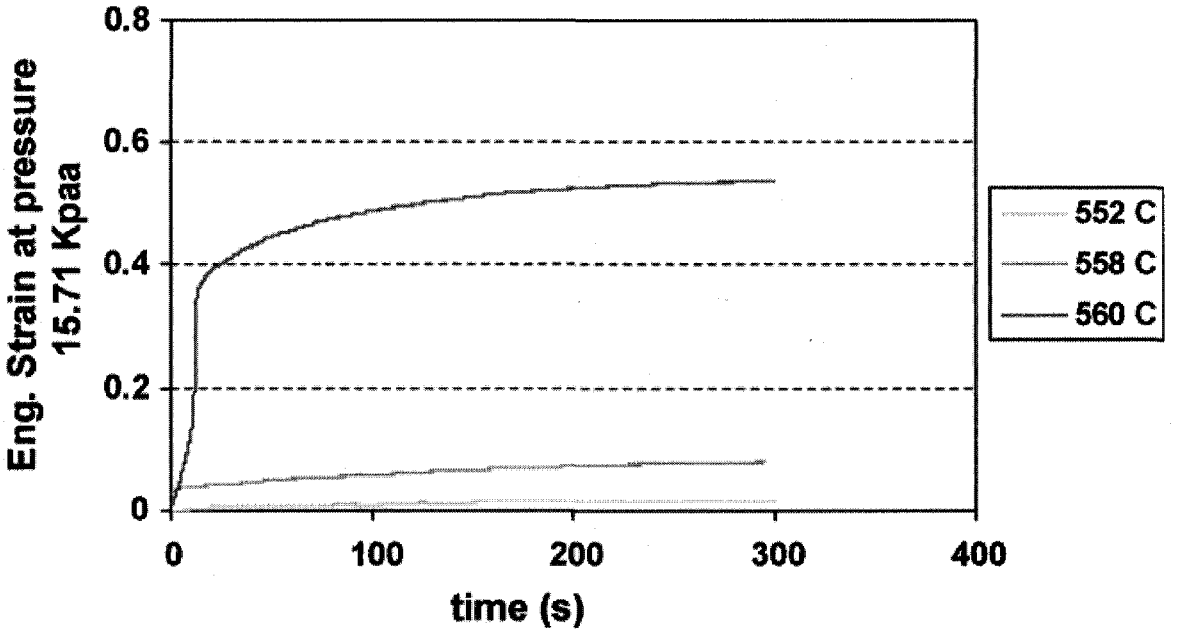

Fig. 34: Engineering strain as a function of time at different reheating temperature, representing different solid fractions of partially solidified A390 [67].

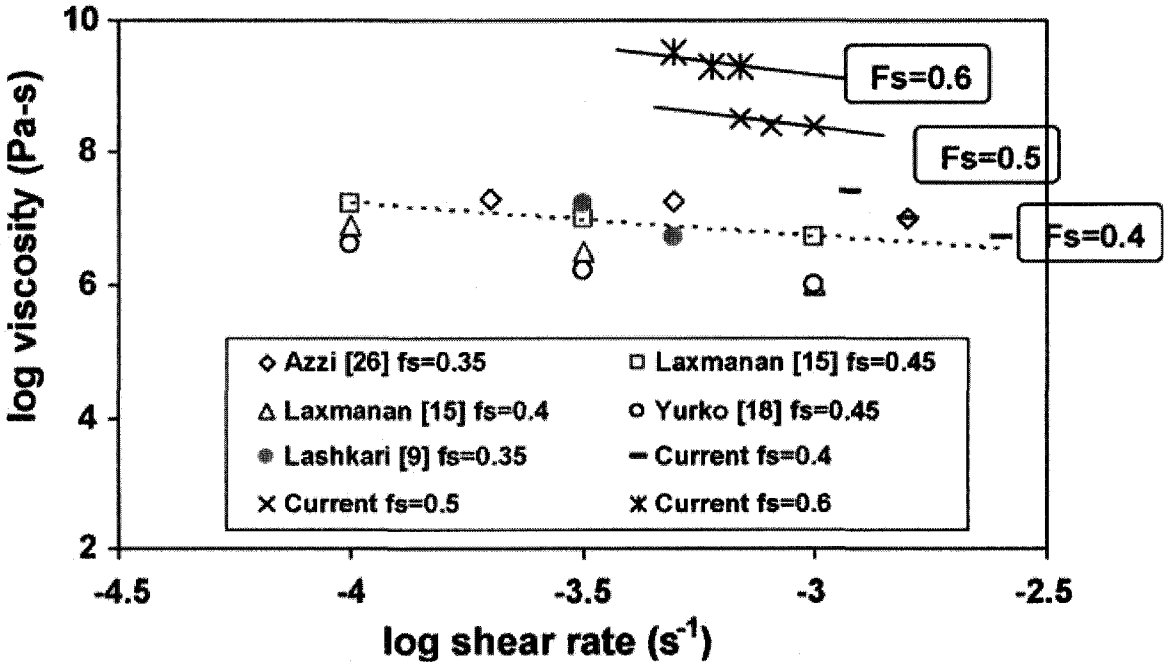

Fig. 35: Viscosity plots as a function of shear rate for different solid fraction. [67]

The difference in the solid fraction, composed of primary Si particles and α-Al phase, has a distinct effect on the engineering strain. The higher solid fraction at 552 ˚C shows the lowest deformation rate, while the lower *fs* at 560 ˚C deforms at a much higher rate. The deformation rate appears to be an important parameter in differentiating between structures at these temperatures. This implies that the control of the reheating temperatures resulted in the formation of a range of primary α-Al and Si phase particles with a combined solid fraction can significantly change the flow behavior (viscosity) of hypereutectic Al–Si alloy as it is shown in Fig. 35. This figure shows the viscosity as a function of shear rate applied by compression test for different solid fractions. First, at the same solid fraction, with increasing shear rate, the value of viscosity decreases. This is a characteristic of pseudo-plastic fluids defined by power law equation. Second, at the

same shear rate, the value of viscosity increases when the solid fraction increases. This mean in order to control the value of viscosity, the semi solid temperature have to be tightly controlled.

3-3-2 Hardness

3-3-2-1 Effect of silicon on hardness of Al-Si alloys

The effect of Si content on the hardness of as thixoformed and T6 heat treatment AlSiCuFe alloys was investigated by Birol et al. [68]. Four alloys were selected for this investigation with chemical compositions indicated in Table 8. Ingots of these alloys were melted and then were cooled to within 5–15 °C of their liquidus points before they were poured into a permanent mould in order to produce non-dendritic ingots for thixoforming. The ingots were thixoformed after they were heated in-situ in the semisolid range, between 568 and 573 °C, for 5min in a laboratory press. A second set of thixoformed samples were heat-treated to the T6 temper, by solutionizing at 500 °C for 1 h, followed by forced air cooling before ageing at 175 °C for 8 h.

As-cast microstructures of four ingots with different Si are illustrated in Fig. 36. The alloy 1 (Fig. 36a) exhibits a coarse dendritic structure of the α-Al solid solution with an interdendritic network of Al–Si eutectic phase, confirming its hypoeutectic composition. Intermetallic particles, found by XRD and metallographic analysis to be of the β-Al_5FeSi and $CuAl_2$ variety, were also noted at interdendritic sites.

Table 8: Chemical compositions of the alloys used in the present work [68].

Alloy	Si	Fe	Cu	Mn	Mg	Cr	Ni	Zn
1	8,52	1,099	2,940	0,1712	0,1532	0,018	0,046	0,975
2	12,65	1,109	2,600	0,1813	0,1193	0,019	0,040	0,907
3	16,32	1,056	2,934	0,1708	0,1395	0,018	0,047	0,953
4	19,73	1,044	2,623	0,1635	0,1049	0,019	0,044	0,893

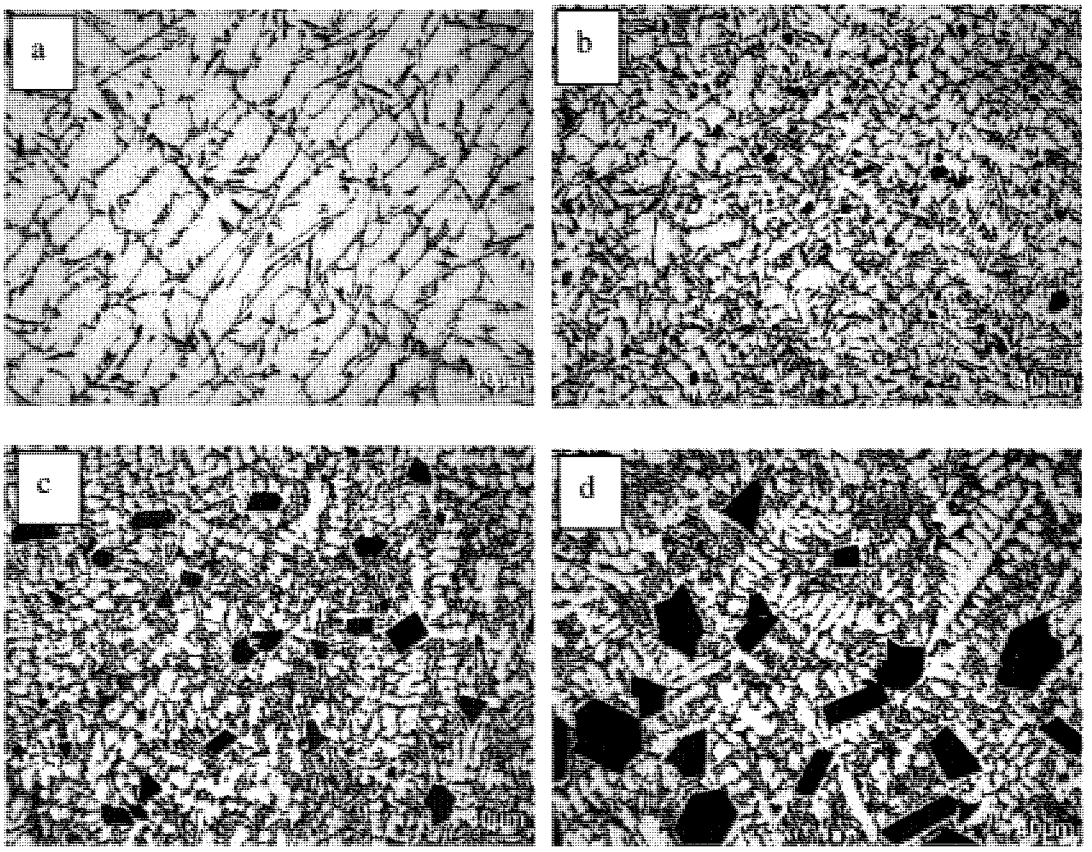

Fig. 36: As-cast microstructures of the AlSiCuFe alloys: (a) alloy 1, (b) alloy 2, (c) alloy3 and (d) alloy 4. [68]

Alloy 2 is dominated by a uniform distribution of Si platelets and needles in an aluminum solid solution matrix (Fig. 36b). Several small primary Si particles place this alloy very near, yet slightly above the eutectic point. An increasing number of coarse blocky Si particles is noted in the next two hypereutectic alloys (Fig. 36c, d). These particles are larger in size, occupy a greater volume fraction and have thus become the predominant feature in alloy 4 which contained 20 wt% Si (Fig. 36d).

Marked changes are noted in all alloys after thixoforming as shown in Fig. 37. The eutectic Si plates and needles in the cast ingots are largely modified into compact blocky particles after semisolid soaking while the aluminum solid solution matrix is rearranged into a more or less uniform distribution of α-Al globules. Hence, a variety of features in the cast alloys are replaced by a simple mixture of α-Al globules and predominantly compact blocky Si particles, regardless of the Si level (Fig. 37a). The latter are bigger and more frequent in the hypereutectic alloys while α-Al globules become smaller with increasing Si content.

High temperatures and long soaking times involved in the solution heat treatment apparently promoted rounding of the Si particles, the interglobular ones in particular. The primary Si particles and Fe/Cu-based intermetallics, on the other hand, resisted spheroidization during the solution treatment. The very fine intraglobular particles which are noted after the T6 treatment are Mg_2Si particles which have precipitated during quenching from the solution heat treatment.

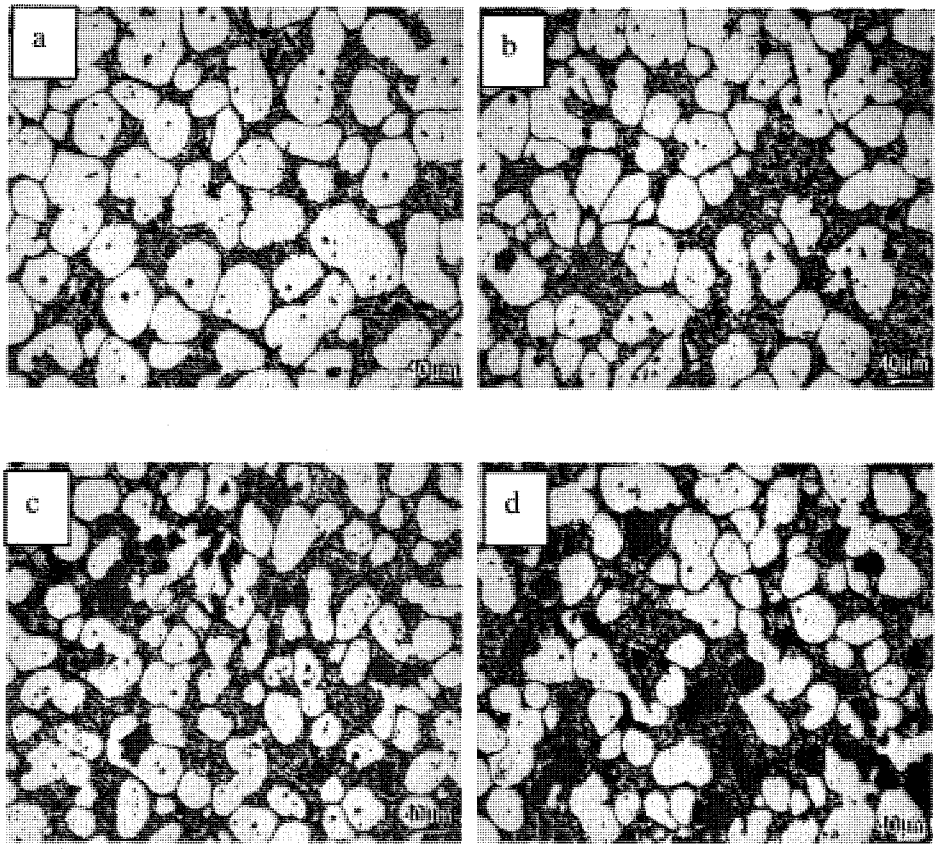

Fig. 37: Microstructures of thixoformed alloys: (a) alloy 1, (b) alloy 2, (c) alloy 3 and (d) alloy 4. [68]

Fig. 38 shows the results of hardness of alloys in the thixoformed and heat treatment conditions. The hardness of the thixoformed parts which ranged between 82 and 96HB increased to 121–131HB after the T6 heat treatment, increasing with Si content both in the thixoformed state and after the T6 treatment. This indicates that the increase of Si content results in the precipitation of hard polygonal primary silicon which significantly increases the value of hardness.

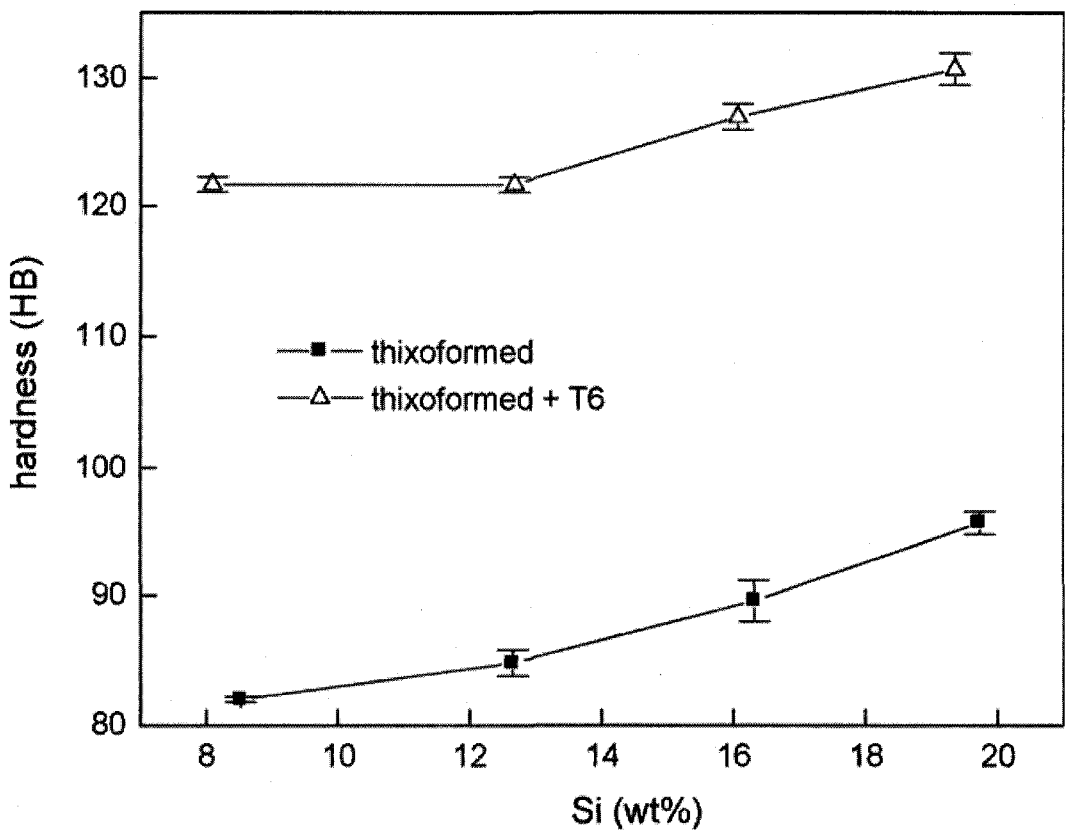

Fig. 38: Change in hardness with Si content in thixoformed and heat-treated alloys. [68]

3-3-2-2 The role of primary Si on hardness of Al-Si alloys

Silicon crystals possess very high hardness (12,000 MPa Vickers) and contribute the abrasive-wear resistance to the cast parts of alloys. The size and morphology of primary silicon strongly affect the hardness of hypereutectic Al-Si alloys. It was found that increasing the silicon content in hypereutectic alloys can improve the wear resistance of the castings. Another advantage of increasing the silicon content is that the casting can be lighter due to the lower density of this element (2.33 g. cm^{-1}) compared to that of aluminum (2.7 g. cm^{-1}). Hardness of these alloys was investigated by Q.C. Jiang et al.

[69] for Al-20%Si and Al-29%Si alloys. They have drastically modified the morphology from irregular shapes, such as star like and coarse platelet to regular (polygonal) morphologies by using a refiner. Primary silicon sizes in modified Al–20wt.%Si and Al–29wt.%Si alloys (approximately 20 and 35 μm, respectively) are smaller than those in unmodified Al–20wt.%Si and Al–29wt.%Si alloys (approximately 100 and 250 μm, respectively). Fig. 39 shows the SEM micrograph of the morphology and size of primary Si for the case of modified and non-modified alloys of Al–20wt.%Si and Al–29wt.%Si [69]. Ambient temperature hardness (HB) of the unmodified and modified alloys is given in Table 9. The Brinell hardness values of modified Al–20wt.%Si and Al–29wt.%Si alloys are increased by 15.8% and 32%, respectively. These values are the results of the refinement of primary silicon. On account of crack propagation, primary silicon phase cannot be effectively bound by the matrix. In fact, the crack nucleate at the interface of large primary silicon with fine matrix and stress concentration will be more severe at interface between large primary silicon and fine matrix results in separating the large primary silicon from matrix during wear test. It can be observed that modified primary silicon phase is strongly bound by the matrix in their position persisting the destructive action. On the other hand, the finer primary silicon phase suppressed crack propagation at the finer primary silicon/matrix interface [69].

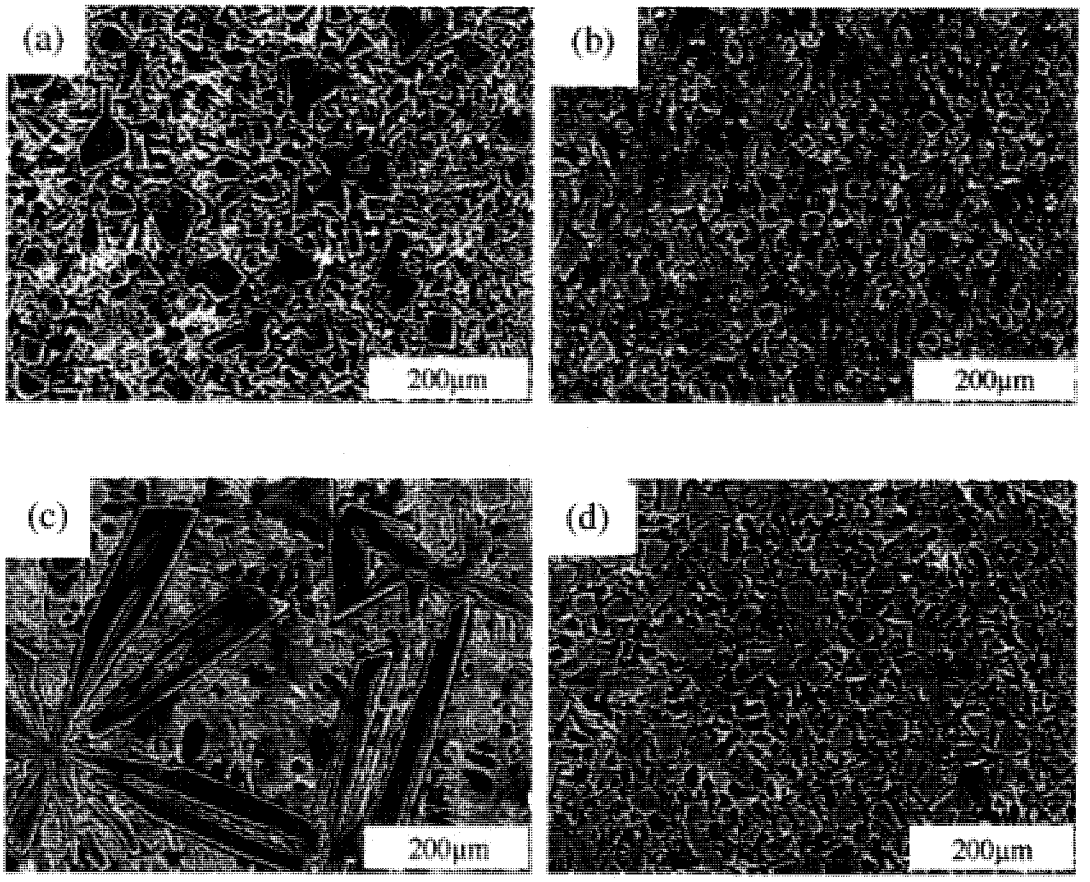

Fig. 39: SEM micrographs of Al–Si alloys: (a) unmodified base alloy (Al–20wt.%Si) (b) modified alloy (Al–20wt.%Si) (c) unmodified base alloy (Al–29wt.%Si) and (d) modified alloy (Al–29wt.%Si) [69].

Table 9: Ambient temperature hardness (HB) of the unmodified and modified of Al–20wt.%Si and Al–29wt.%Si alloys [69].

Material	**Hardness (HB)**
Unmodified Al–20wt.%Si alloy	83.0
Modified Al–20wt.%Si alloy	96.1
Unmodified Al–29wt.%Si alloy	97.7
Modified Al–29wt.%Si alloy	129.0

3-3-3 Strength (Yield stress, Ultimate Tensile stress) and Elongation Toughness

The tensile strength of test specimens increases with decreasing silicon particle size. Mandal et al. [49] measured tensile strength in binary hypereutectic Al-Si alloys with silicon content from 17 to 22 wt. % and found that beyond 22 wt.% the average hardness of casting reaches a plateau at about 120 BHN and the tensile strength-particle size correlation is:

$$\text{Tensile strength (in MPa)} = 252.8\text{-}3.73\,\bar{d} \qquad (14)$$

Where average particle size, $\bar{d}$, is in μm.

J. Valer et al. [70] studied the strength of hypereutectic Al-Si alloys using SSM. The 3 hypereutectic alloys (Al-25Si-5Cu (%wt), Al-25Si-5Cu-2Mg and Al-30Si-5Cu) were studied for two different conditions: as-extruded and extruded + thixoformed. They have also compared the effect of alloy elements such as Mg, with comparing alloy 1 with alloy 2, as well as the effect of Si, comparing alloy 1 with 3 for different forming routes.

Mean values of tensile strengths are reported in Table 10. It was observed that there is an improvement in the strength, after thixoforming for the three alloys. Thixoforming has an effect equivalent to a heat treatment but results in a decrease in elongation [70]. In the case of the Al-25Si-5Cu-2Mg composition, probably due to the Mg induced precipitation results in solidification of eutectic Mg_2Si intermetallic phase, higher

strength values were measured but the specimens broke without any significant elongation.

Table 10: Tensile test results. [70]

Material	Extruded			Thixoformed		
	$\sigma_{0.2\%}$ (MPa)	σ_{UTS} (MPa)	Elongation (%)	$\sigma_{0.2\%}$ (MPa)	σ_{UTS} (MPa)	Elongation (%)
25Si/5Cu	149	249	2.6	266	290	0.5
25Si/5Cu/2Mg	154	254	1.5	—	296	—
30Si/5Cu	147	200	0.8	175	235	0.4

In Fig. 40 histograms of particle size distribution for thixoformed Al-25Si-5Cu, Al-25Si-5Cu-2Mg and Al-30Si-5Cu alloys are compared. The coarsest Si particles correspond to the A1/30Si/5Cu alloy with some particles larger than 30 μm (mean particle size: 10.5 μm).

The thixoforming process does not have a significant influence on fracture toughness, as can be observed in the data reported in Table 11. Although a refining Si particle would be expected to improve ductility and toughness of these materials, this is not the case at least in the studied alloy, but this could be due to a Si particle clustering phenomena which produces a large tri-axial stress field in the matrix around the clustered particles. In order to obtain better ductility and toughness values, clustering of Si particles in alloys with high Si content be avoided during the processing route. This calls for an improvement in the semisolid processing.

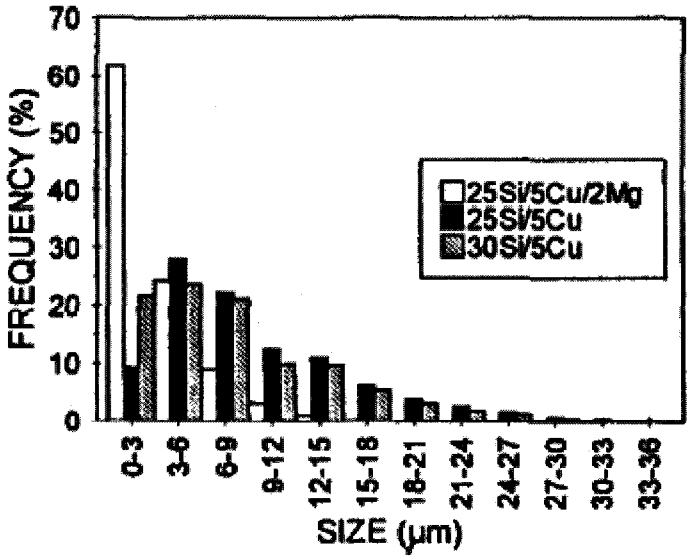

Fig. 40: Histograms of the maximum dimension of primary Si particles in thixoformed Al-25Si-5Cu, Al-25Si-5Cu-2Mg and Al-30Si-5Cu alloys [70].

Table 11: Fracture Toughness Results [70].

Material	Condition	K_Q (MPa√m)	K_{Ic} (MPa√m)	Si_{fract} (%)	Si_{local} (%)	Si_{frac}/Si_{local}
25Si/5Cu	extruded	7.9 8.9		— —	— —	— —
	thixoformed		10.3 9.6 10.5	63 60 75	28.6 28.6 29.3	2.2 2.1 2.6
25Si/5Cu/2Mg	extruded	11.3 8.8 9.4				
	thixoformed		8.7 7.2 6.8	64	24.5	2.6
30Si/5Cu	extruded	9.3 9 9.7 9.6				
	thixoformed	9.4 10.7		50	31	1.6

3-3-4 Wear behavior of hypereutectic Al-Si alloys

There may be number of phases in cast Al–Si alloys such as primary α-Al and eutectic aluminum and silicon as well as inter-metallic constituents according to the alloy composition. Silicon has a profound effect on wear resistance of these alloys. The presence of impurities, metallic debris, and hard dust particles in lubricant may cause abrasive wear and adversely affect the life of components [71-72]. The pin on disc (POD) apparatus is a quick, easy and commonly used method for investigating the abrasive wear characteristics of aluminum alloys [73-77]. As the name implies, such apparatus consists essentially of a "pin" in contact with a rotating disc. A schematic diagram of wear testing machine is shown in Fig. 41. In a typical pin-on-disc experiment, the wear is continuously measured by determining the amount of removed material by weighing and/or measuring the profile of the resulting wear track.

Changes in the coefficient of friction are frequently indicative of a change in wear mechanism, although marked changes are often seen during the early stages of wear tests as equilibrium conditions become established. The good mechanical properties and especially high resistance to wear attributed to hypereutectic Al-Si alloys such as A390 are essentially due to the presence of hard primary silicon particles distributed in the matrix. Therefore, the size and morphology of primary silicon in hypereutectic Al-Si alloys determine the influence on the mechanical properties of the alloys. However high latent heat and consequent large solidification interval (about 150 °C) result in excessive growth of the silicon particles in the melt, which adversely affect the application of alloy.

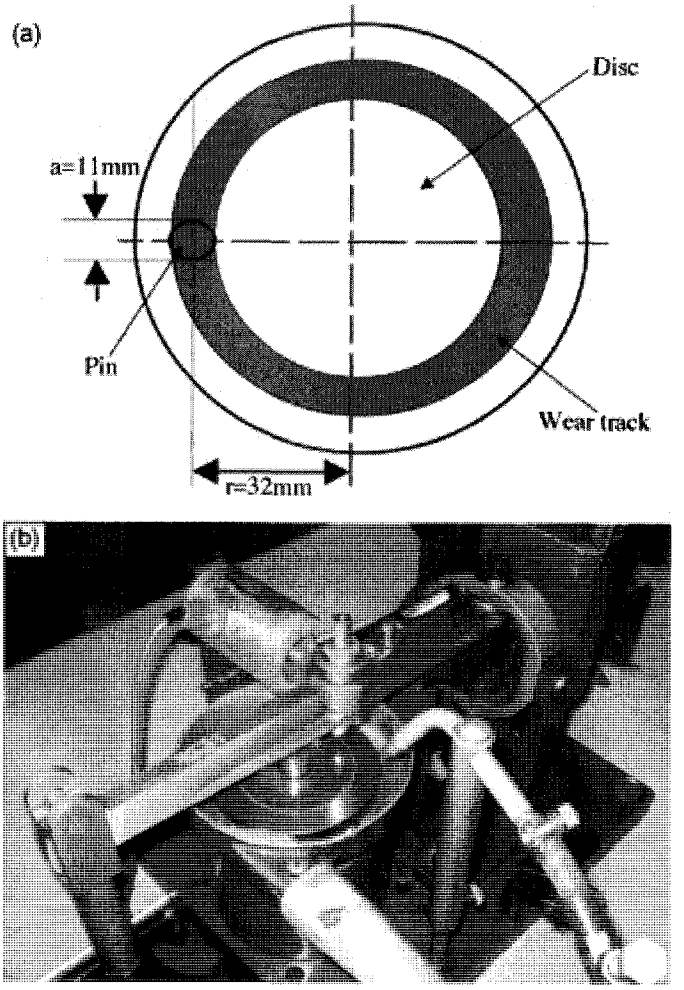

Fig. 41: Pin-on-disc testing machine: (a) schematic diagram and (b) photography.

In fact, in wear applications, the crack nucleates on the large primary silicon and the resultant stress concentration will be more severe at the interface between coarse Si phases and the matrix when compared to fine Si particulates and results in poorer mechanical properties.

L.Lasa et al. [78] used a POD wear test to investigate the wear behavior of eutectic and hyper eutectic Al-Si alloys formed by different processing techniques that produced different particle size. The chemical compositions of the alloys and processing route are shown in Table 12. Alloys H1, H2 and HS were cast in permanent metallic moulds, alloys Thixo1 and Thixo2 were thixoformed, alloys SQ1 and SQ2 were produced using squeeze casting and finally, alloys LF1 and LF2 were cast using lost-foam technology. It is important to note that in all the alloys with the exception of HS, phosphorus was used as primary silicon refiner. The microstructures of the alloys are shown in Fig. 42.

The microstructure of thixoformed alloy, Thixo1, exhibits a very homogeneous microstructure. The aluminum phase forms globules, the primary silicon particles are fine and homogeneously distributed in the aluminum matrix. The eutectic silicon forms small polygonal particles instead of the needle-like network observed in the other alloys. Since the size and the distribution of the primary silicon particles control the wear to a great extent, the volume fraction of these particles together with the mean particle size (D_p) and the interparticle distance (λ) were measured for all alloys, Table 13. The large primary silicon particle size of alloy HS is in contrast with the small size and high concentration of silicon particles in observed thixoformed alloys.

Table 12: Chemical composition (wt.%) and processing route of the alloys [78].

Alloy	Processing route	Chemical composition (wt.%)					
		Si	Mg	Cu	Ni	Fe	Ti
H1	Ingot metallurgy	12.85	1.30	1.37	–	0.11	0.11
H2	Ingot metallurgy	12.29	1.30	4.40	–	0.12	0.11
HS	Ingot metallurgy	15.90	1.20	4.71	0.00	0.12	0.11
Thixo1	Thixo forming	15.30	0.58	4.38	< 0.42	0.21	0.16
Thixo2	Thixo forming	15.70	0.54	4.60	4.10	0.20	0.17
LF1	Lost foam	12.64	1.09	4.39	–	0.13	0.13
LF2	Lost foam	16.11	1.04	4.04	–	0.13	0.13
SQ1	Squeeze casting	16.20	1.16	0.70	–	0.13	0.11
SQ2	Squeeze casting	19.85	1.13	0.66	–	0.14	0.11

The coefficient of wear of all alloys tested by POD test is shown in Fig. 43. This confirms that different processing routes affect the wear resistance. Comparing the acquired results for coefficients of wear, the thixoforming process route comprises superior wear resistance due to the fine and homogeneously distributed Si particles in the aluminum matrix.

It is shown that at lower disc speed (0.089 m/s), the wear rate for all the alloys was low and very similar. As the test went on, a wear transition was observed in most of the alloys. This transition was attributed to a progressive break down of the oxide layer. The alloys with high concentrations of silicon particles continued to wear at a slow rate even after the break down of the oxide layer because the wear was limited by the wear rate of the hard silicon particles. The alloys with low fractions of silicon particles suffered severe wear because the softer aluminum matrix was responsible for carrying the load.

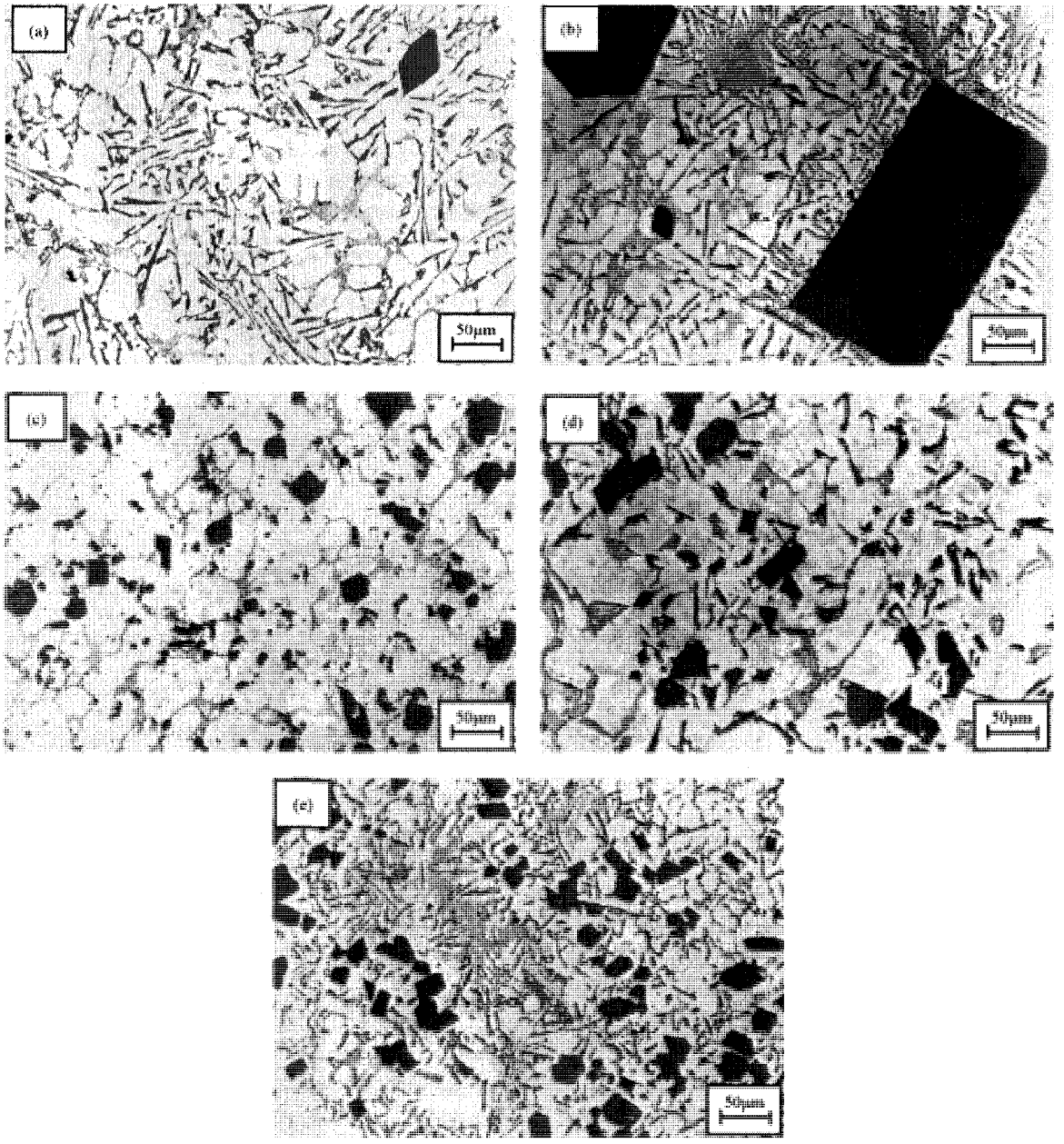

Fig. 42: Microstructure of the alloys: (a) H2, (b) HS, (c) Thixo1, (d) LF1, and (e) SQ2 in as-received condition [78].

Table 13: Primary silicon content and size of the primary silicon particles in the nine alloys [78].

Material	Part (mm^2)	$\%Si_{prim}$	D_p (μm)	λ (μm)
H1	8.4	0.9	35.3	3668.6
H2	6.0	1.0	44.2	3931.6
HS	1.5	2.2	121.0	5249.9
Thixo1	866.4	13.4	11.6	74.6
Thixo2	858.7	13.5	11.8	75.0
LF1	108.2	4.9	23.1	426.3
LF2	138.0	9.3	29.1	272.2
SQ1	336.4	7.2	15.1	190.8
SQ2	211.3	12.0	25.5	181.5

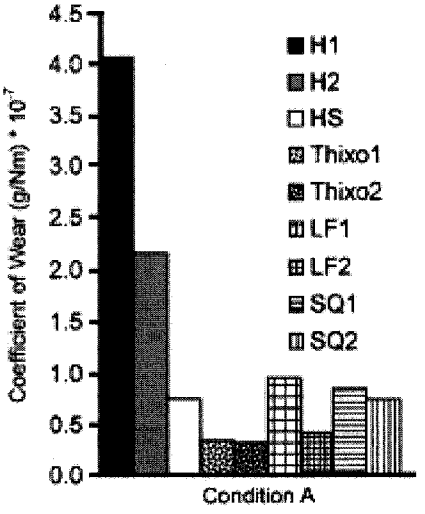

Fig. 43: Average coefficient of wear of the alloys [78].

They have also shown the effect of size and morphology of primary silicon on wear behavior. Fig. 44 shows the loss of pin height as a function of test distance for different alloys and processing routes. The wear rate of the alloys is very similar until about 500 m. At this stage, alloy H1 suffers a transition and the wear rate accelerates progressively until around 1300 m. After this distance, the wear rate stabilizes and continues at a constant rate until the end of the test. The differences in overall wear coefficients can be linked to the distance at which transition takes place. In the case of both thixoformed alloys and in alloy LF2, no transition is observed. Many of the primary silicon particles, especially the biggest ones, are damaged during the wear test as can be seen in Fig. 45. The damage on the particles was probably caused by their collision with abrasive hard particles from the disc. From the above explanations, the outstanding wear resistance of both thixoformed alloys and lost-foam alloy LF2 can be explained by the copper which results in the formation of a strong oxide layer. If the oxide layer was disrupted, the high concentration of primary silicon particles and their homogeneous distribution limited the extent of wear. Moreover, the small size of the silicon particles made them tougher and consequently much harder to break, limiting the abrasion of the particles by microcracking.

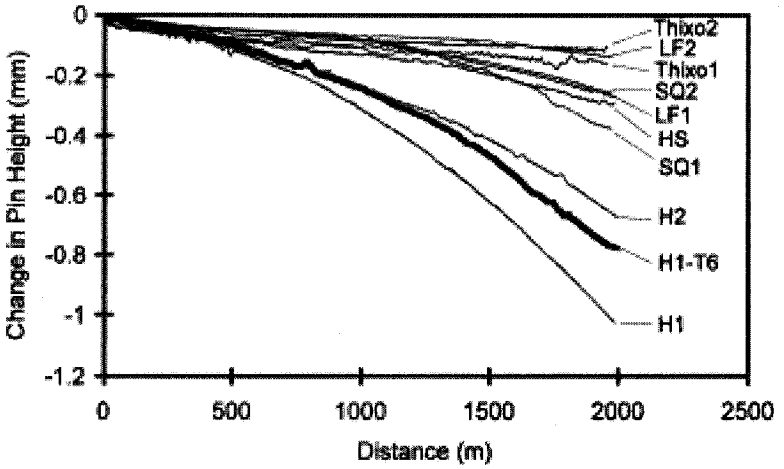

Fig. 44: Loss of pin height as a function of test distance for different alloys and processing routs.

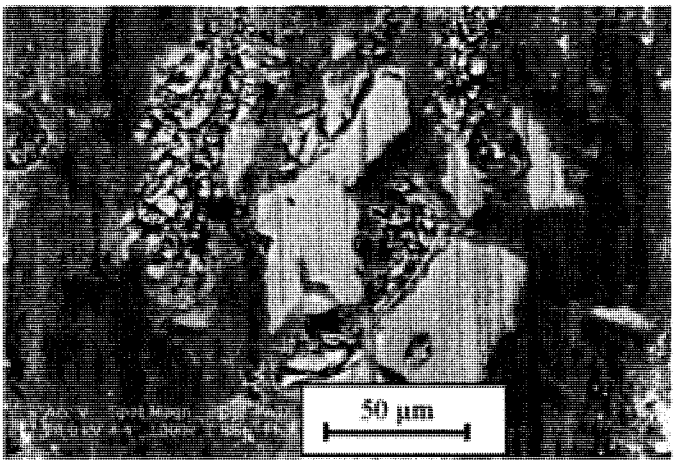

Fig. 45: Cracked primary silicon particles in alloy LF2 after wear test

Dwivedi [79] has also reported the influence of alloying elements on wear behavior of binary (Al–17%Si) and multi-component (Al–17Si–0.8Ni–0.6Mg–1.2Cu–0.6Fe) cast hypereutectic aluminum alloys using POD wear test. Fig. 46 shows the wear rate-sliding speed at 30 N contact load for binary and multi component alloy. It is confirmed that multi-component alloy is subjected to lower wear rate than binary alloys under identical sliding conditions. Fig. 47 shows the variation in the friction coefficient with sliding speed at constant contact loads (30 N) for both the alloys. Increase of sliding speed decreases the friction coefficient for both the alloys until seizure or smearing of metal on disc is started. Friction coefficient for binary alloy under similar sliding condition was found higher than the multi-component alloy. It was therefore concluded that wear rate of both the binary and multi-component hypereutectic Al–17%Si alloys initially decreases with increase in sliding speed up to a critical speed, it then increases. In this experiment, wear rate of binary alloy was somewhat higher than multi-component alloy under identical sliding condition and the presence of alloying elements (Cu, Mg) increases the wear and seizure resistance. The friction coefficient was found higher for binary Al–Si alloy than the multi-component alloy.

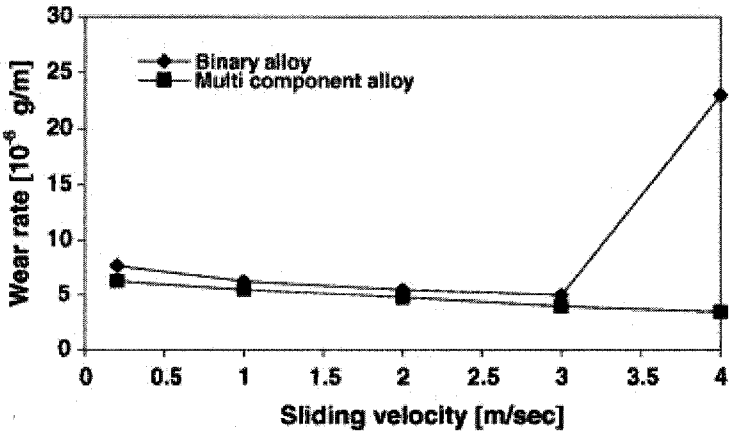

Fig. 46: The wear rate-sliding speed at 30 N contact load for binary and multi component alloy. [79]

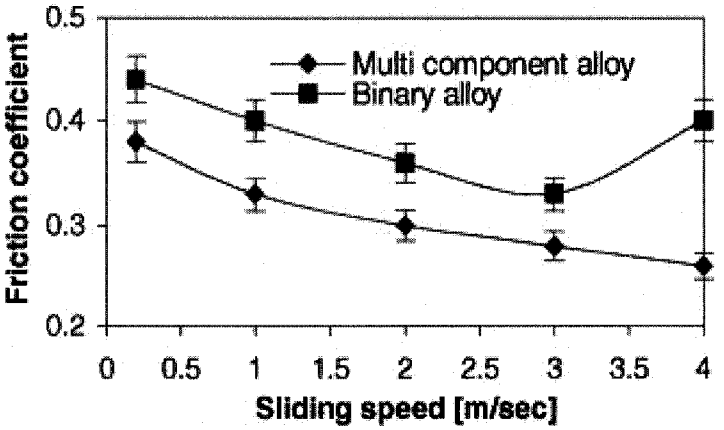

Fig. 47: Friction coefficient vs. sliding speed relationship for binary and multi component alloy at 30 N load. [79]

3-3-5 Conclusions about wear behavior of hypereutectic Al-Si alloy

The POD wear tests indicates that

- The size and the distribution of the primary silicon particles are the important factors that determine wear.
- Cracks nucleate on the large primary silicon crystal and the resultant stress concentration will be more severe at the interface between coarse Si phase and the matrix compared to fine Si particulates and the matrix.
- A wear transition at a point where wear abruptly decreases is observed in most of the hypereutectic Al-Si alloys. This transition is attributed to a progressive break down of the oxide layer.
- The alloys with high concentrations of silicon particles continued to wear with a slow rate even after the rupture of the oxide layer (transition) because the wear is limited by the wear rate of the hard silicon particles.
- The alloys with low fractions of silicon particles suffered severe wear because the softer aluminum matrix is responsible for carrying the load.
- Alloying elements have significant influence on wear behavior of binary (Al–17%Si).
- Friction coefficient for binary alloy under similar sliding condition was found to be higher than the multi-component alloy.

CHAPTER 4

METHODOLOGY AND EXPRIMENTAL PROCEDURES

This section presents the methodology and the experimental procedures used for carrying out the research activities related to the study of the effect of Mg content on microstructure of hypereutectic Al-Si alloys during conventional and semi-solid casting processes. It is believed that the addition of Mg can improve the semi solid processing and casting of A390 alloy by promoting the formation of primary Mg_2Si intermetallic phase instead of Si. A comprehensive study of the thermodynamic evaluation of hypereutectic Al-Si alloy with addition of Mg was first carried out using the Factsage software. The results were then compared with DSC (Differential Scanning Calorimeter) tests of the same alloys. Subsequently the microstructural characterization (particularly the eutectic network) of the base alloy (A390) as well as of alloys with 6% and 10% Mg was studied for conventional and SSM forming processes under continuous cooling. In this case, first the eutectic reaction temperature was measured from cooling curves by placing a thermocouple in the melt and the results are compared with the Factsag thermodynamic prediction as well as with the DSC tests. The modification of eutectic microstructure specifically eutectic silicon for A390 alloy and 6% and 10% Mg alloys was investigated and identified with their eutectic-formation temperature. The microstructure of the primary phases, mainly silicon and Mg_2Si, of A390 alloy and 10% Mg alloy was compared for two SSM casting processes at isothermal conditions: rheoprocess and partial remelting of rapidly solidified samples (thixoprocess). The 10%

Mg alloy was chosen due to the presence of both silicon and Mg_2Si particles in the microstructure of this alloy in both the primary and eutectic phases. A through investigation is carried out on microsrtucatural evolution of this alloy during SSM processes especially the coarsening of the primary particles for different isothermal holding times in the semi solid state. Moreover, the rheological characterization (viscosity) of the A390 alloy and 10% Mg alloy was compared in the semi solid state according to different rheological tests such as "step change", isothermal shearing and continuous cooling shearing tests. Eventually, the hardness tests were carried out for the conventionally cast and after T6 heat treatment of the base alloy (A390) as well as for the 6% and 10% Mg alloys.

4-1 Alloys under study

Commercial ingots of A390 alloy produced by Alcan Inc. were used as the base alloy. Table 14 shows the chemical composition of this alloy. This is a hypereutectic Al-Si alloy with primary silicon-phase dispersed in the matrix of eutectic Al-Si. Most of the primary silicon crystals exhibit the polygonal faceted crystal [80].

SSM processes, particularly thixoprocess, must be carried out at a solid fraction between 30%-50% [81]. Die filling problems can occur for values higher than 50%, due to the high viscosity of slurry, whereas for values lower than 30%, the flow behavior cannot easily be controlled resulting in turbulent die filling. Therefore, the binary hypereutectic Al-17%Si alloys cannot be used for thixoprocess due to the low solid fraction of primary

silicon (maximum 7%) present in the semisolid zone i.e. "Liquid + Si". The presence of 5% Cu in the composition of A390 alloy is necessary in order to stabilize the α-Al phase in the semi solid zone of "Liquid + Si + Al" [82] and makes the alloy thixoformable (see chapter 3, section 3-2-1 and Fig.15.a, b). On the other hand, the addition of only 2% Mg appears to weaken the Si network considerably, and enhances the flow properties of the semi solid material on shearing.

Table 14: Chemical analysis of A390 alloy (%wt)

Si%	**Cu%**	**Mg%**	**Fe%**	**Mn%**	**P%**	**Ti%**	**Al**
17.4	4.58	0.58	0.29	0.012	0.0003	0.02	Bal.

4-2 Thermodynamic evaluation of the alloy system

This section represents calculated phase diagrams of the A390 alloy for quaternary Al-Si-Cu-Mg system and to analysis the effect of the Mg variation on the solidification path using the Factsage software (version 5.4.1) developed by the CRCT group of Ecole Polytechnique de Montréal [55]. This thermodynamical simulation can identify the compounds and phases as well as the transition temperatures and reactions that are formed during the solidification interval of the A390 alloy and the alloys with increasing Mg content based on a calculated phase diagram.

The isopleth diagram (vertical section of the quaternary Al-Si-Cu-Mg system at 4.5% Cu and 0.5% Mg) was calculated. The solidification path at 17% Si indicates the solidification behavior of the A390 alloy as a base alloy (sections 3-4-2 and 5-3 present a comprehensive studies of thermodynamic evaluation). The calculation of isopleths were also calculated for alloys with Mg contents of 1%, 2%, 3% ....up to 10% (weight percent) in order to compare the effect of Mg on the solidification behavior in terms of the transition temperatures and the reactions that occur during the solidification. For example, the calculation can determine value of the Mg content when the primary silicon phase transforms to the primary Mg_2Si or the Mg content where the matrix is changed from a binary microstructure to a ternary microstructure. The results obtained by Factsage were used as the basis of the experimental work and led to study the effect of Mg on the microstructural evolution.

4-3 Preparing the high Mg content alloys

The base alloy (A390) was melted in a resistance furnace as shown in Fig. 48. It was first heated to 750°C which is about 100°C above the liquidus temperature. Pure Mg (99.999%) or AZ91 Mg base alloy was then added into melt to increase the Mg content to 6 and 10 wt%. Pieces of pure Mg or AZ91 alloy were cut and wrapped with aluminum foil before melting and then submerged into a molten A390 alloy using a stainless steel rod until it was totally melted. In order to account for the oxidation loss, an additional amount of 20% Mg was added to the melt. Silicon and copper were also added to the melt in order to keep the chemical composition of these elements the same

as for the A390 composition. The melt is degassed with argon and stirred for two minutes before pouring into a steel mould to form three 35 ∅× 120 mm cylindrical samples (Fig. 48). These ingots were used as the starting material for conventional and SSM casting processes.

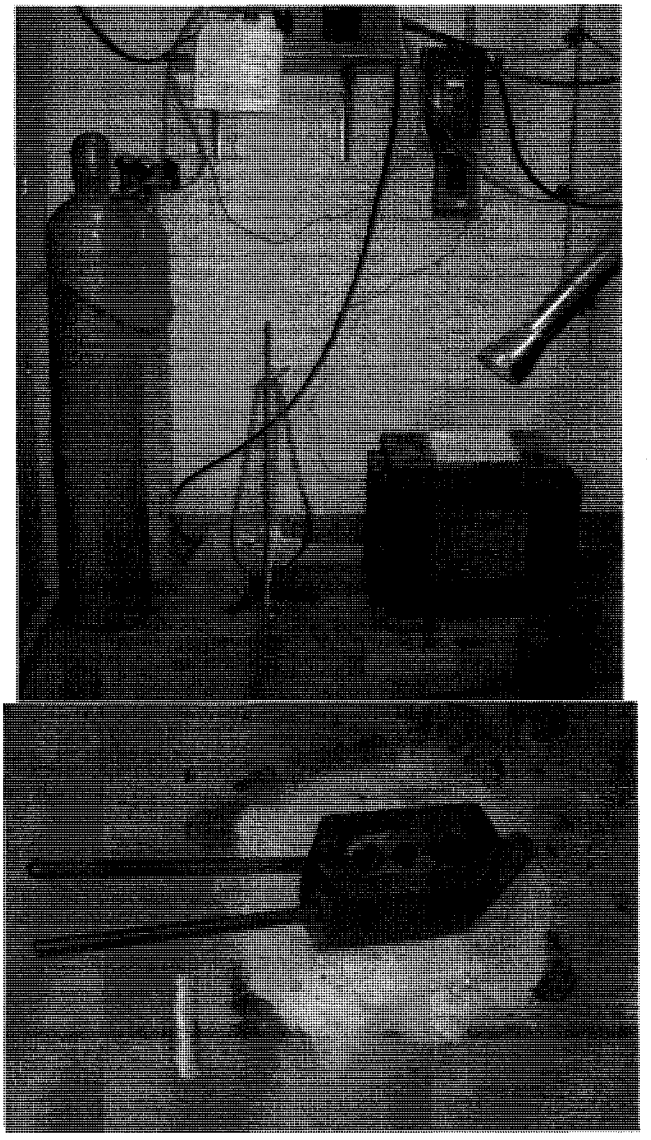

Fig. 48: The furnace and mould used for preparing the added Mg alloys.

4-4 Measurement of density by Archimedes's principle

Light weight is perhaps aluminum's best known characteristic and with a density of 2.7 g/cm^3 is approximately 35% that of steel. Since the density of both silicon (2.33 g/cm^3) and Mg_2Si (1.99 g/cm^3) are smaller than the pure solid aluminum, the A390 as well as the 6% and 10% Mg alloys are expected to be lighter alloys when compared to pure aluminum. The density of alloys was measured using Archimedes's principle where a body immersed in a fluid is buoyed up by a force equal to the weight of the displaced fluid. The density can be measured by determining the Buoyant Force. Fig. 49 shows how buoyant force is measured.

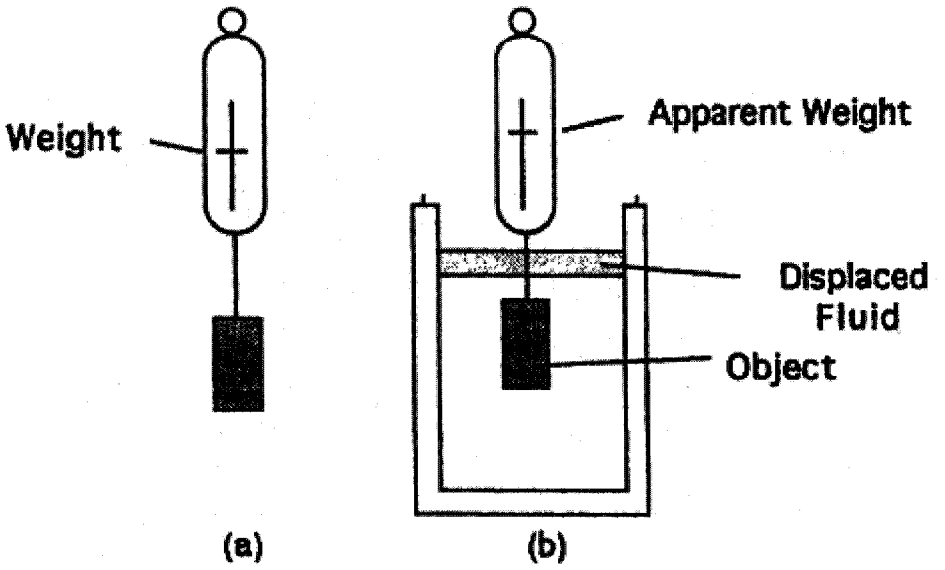

Fig. 49: Measuring buoyant force with spring scale.

In Fig. 49a, the scale reads the weight of the object in air. In Fig. 49b, the buoyant force of the displaced liquid acts upward on the object, and the scale reads less than in Fig. 49a by an amount equal to the buoyant force. We call this second reading the *apparent weight* of the object. The buoyant force is calculated as:

$$\text{Buoyant Force} = \text{Weight} - \text{Apparent Weight} \tag{15}$$

Using water, the density of object (ρ) is measured by following equation:

$$\rho = \frac{\text{Weight}}{\text{Weight} - \text{ApparentWeight}} \rho_{\text{Water}} \tag{16}$$

The calculated density for the A390 and the 6% and 10% Mg alloys are 2.68 g/cm^3, 2.58 g/cm^3 and 2.51 g/cm^3, respectively. These alloys are all lighter than pure aluminum confirming a super light alloy characterization.

4-5 Microstructural characterization

Microstructural examination of A390 and the 6% Mg and 10% Mg alloys was carried out for samples formed by conventional casting, rheocasting and partial remelting (thixocasting) processes under continuous cooling as well as isothermal conditions.

For conventional casting, 60 grams of the A390, 6% Mg and 10% Mg containing alloys were placed in a graphite crucible (internal diameter, 28 mm, wall thickness, 5 mm and height, 120 mm), heated to 700 °C in a resistance furnace. The samples were degassed

with argon and stirred two minutes before sampling followed by continuous cooling from the liquid state in a furnace at a controlled cooling rate of -0.15± 0.05 $^{o}C\ s^{-1}$ or air cooled with a cooling rate of -1.0± 0.2 $^{o}C\ s^{-1}$. A K-type thermocouple was quickly immersed into the melt at a position about 10 mm from the bottom in the center. Temperatures were recorded using a data logging system with a 15 per second sampling rate in order to trace the cooling curve.

Metallographic specimens for the conventionally cast samples were prepared by sectioning transversely at the level of 10 mm from the bottom (the level of the thermocouple) of samples. The specimens were polished conventionally for microstructural analyses and etched by using 0.5% HF solution agent. The morphology was examined by optical and scanning electron microscopy (JEOL JXA-840) with energy disperse X-ray analysis (EDX) accessory, operated at 15 and 20 kV.

The rapid solidification (chill cast), solidification using addition of microstructure modifiers and even rheocasting process can be used for making a billet suitable as a starting material for thixoforming process [81]. Therefore, the ingots prepared in this study can also be used as a starting material for thixocasting due to rapid solidification process from liquid into steel mold.

In this study, the thixocasting process is carried out for the A390 and for the 10% Mg alloy. The billet of 10% Mg alloy produced in section 4-3 is placed in a graphite crucible and is heated in a resistance furnace to a semi solid temperature of 560° C and 540° C

which correspond to solid fractions of 10% and 55%, respectively. Subsequently, the variation of microstructure is investigated for different ageing times of 30 minutes, 60 minutes and 180 minutes. At the end of each isothermal period, a sample is quickly removed from the semi-solid slurry by a small spatula and quenched in the water.

All thixocasting specimens were prepared for microstructural observation by using optical microscopy. Microstructural characterization such as the size, volume fraction and shape factor of the primary particles were determined by an image analysis system (CLEMEX).

For the rheoprocessed samples, a spirally grooved cylindrical agitator was used in continuous cooling for A390, the 6% and 10% Mg alloys as well as for the isothermal tests. Each test contained 150 gram of each alloy in a graphite crucible with inner diameter of 41 mm, 10 mm wall thickness and height of 120 mm. Subsequently, the samples are heated to 700 ° C and then held at this isothermal temperature for a period of 5 minute.

For the continuous cooling tests, the alloy was cooled in the furnace at a rate of -0.15 ± 0.05 $^{o}C\ s^{-1}$ (the cooling rate is the same as for the conventionally cast tests cooled in the furnace) and sheared at an average rate of $\dot{\gamma}_{ave} = 52\ s^{-1}$ (rotation speed = 260 rpm). Two K-type thermocouple were located in the crucible wall and were used to measure the temperature near the surface and the bottom positions of the sample. Argon gas is

introduced into the furnace chamber in order to prevent sample oxidation. The tests are stopped when the upper limit of the viscometer torque was reached.

For the rheoprocess of samples, the samples were first heated to 700°C and were then continuously cooled from the liquid state without stirring at a rate of -0.15± 0.05 $^{o}C\ s^{-1}$ down to the semi solid temperature of 540 °C. A spiral grooved cylindrical agitator was then immersed into the semi solid material and rotated at 260 rpm. The variation of microstructure of the alloys was investigated for stirring times of 30 minutes, 60 minutes and 120 minutes.

4-6 Rheological characterizations

4-6-1 Apparatus

A HAAKE RV12 Couette type viscometer (coaxial rotating cylinder) was used to measure the rheological characteristic (apparent viscosity) of the semi-solid slurry. A schematic diagram of the apparatus used in this study is shown in Fig. 50. The viscometer consists of a rotating spindle with a rotational speed controller, variable from 0.01 to 512 rpm. The speed may be maintained constant or varied with the speed controller. This is coupled to the torque sensor, which makes it possible to measure a torque from 0 to 4.9 N.cm using a torsion spring with a maximum angle of torsion of 0.5^{0} when it is subjected to the maximum torque. The angle of torsion is directly proportional to torque and transformed by a magnetic sensor. The machine measures the

required torque in the semi solid material for maintaining the rotation speed of agitator at constant level.

The material to be tested was placed in a graphite crucible and was heated in the resistance furnace with precise temperature control zones. The furnace temperature is controlled in the three zones: in the middle of the central zone of the furnace where the heating element is located at the bottom of the upper zone of furnace and at the top of the lower zone of the furnace. The temperature of the melt was measured using by two thermocouples placed in the crucible wall near the bottom and near the surface of the melt. The height of the crucible and support is fixed, so that the sample was positioned in the central zone of furnace where the temperature variation is less than 1^0C. During the test, the semi solid alloy as well as the graphite crucible was protected against oxidation by a flow of argon gas introduced into the bottom of furnace. The rotational speed, the torque as well as the temperature are recorded using data acquisition software.

The calculation of viscosity of semi solid slurry was carried out by measuring the torque applied on the viscometer spindle. This is made possible using the dimensionless power number, P_0, and Reynolds number defined as follows:

$$P_0 = \frac{C}{\rho \Omega^2 r_a^5} \tag{17}$$

Where C, ρ, Ω and r_a are torque, density, rotational speed (angular speed)and stirring radius, respectively as determined from the calibration [83].

The Reynolds number can be calculated as:

$$\mathrm{Re} = \left(\frac{P_0}{K}\right)^{\frac{1}{a}} \tag{18}$$

Where K and a are constants that depend on stirring geometry. In this study K = 842.3 and a = -0.995.

Thus, the viscosity was calculated by the following equation:

$$\mu = \frac{\rho \Omega \, r_a r_c}{\mathrm{Re}} \tag{19}$$

Where r_c is the crucible radius.

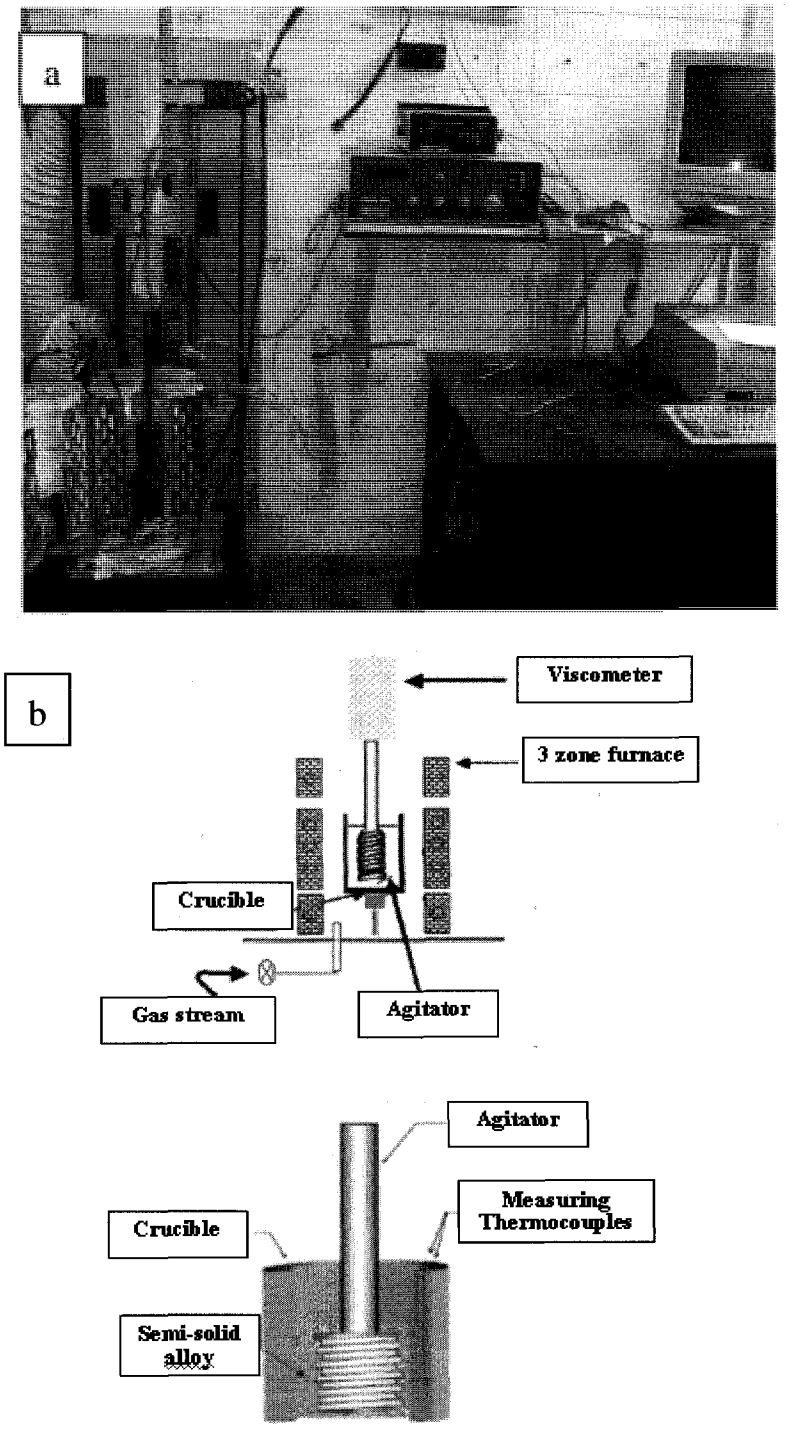

Fig. 50: A photo (a) and schematic diagram (b) of the apparatus used in this study

4-6-2 Methodology and process parameters

The rheological behavior of the test alloys was investigated for continuous cooling, isothermal as well as "step change" experiments.

For the continuous cooling experiments, the samples of the alloy (A390 and 10% Mg alloys) were placed in a graphite crucible and heated in a resistance furnace up to 700 ° C then held at the given temperature and stirred at maximum rotation velocity of 512 rpm for a period of 10 minutes in order to achieve a homogeneous liquid composition. After this period, the alloy was continuously cooled at a rate of -0.15 ± 0.05 $^{o}C\ s^{-1}$ while stirring at the constant rotation speed of 512, 256, 128, 64 and 32 rpm in separate tests. The test was stopped when the upper limit of the viscometer torque is reached and the measured values were used to calculate the apparent viscosity alloys as a function of temperature for different shear rate.

For the isothermal or shear step tests, the samples were also heated to a temperature near 700 ° C and then continually cooled at -0.15 ± 0.05 $^{o}C\ s^{-1}$ without shearing to a temperature in the semi solid state. In this case, the variation of viscosity of alloy as a function of time was measured at the semi solid temperature of 550 ° C, the temperature close to the eutectic reaction temperature of matrix with a solid fraction of almost 12%, while the semi solid was stirred at the rotation speed of 260 rpm. The shearing continues till the torque reached a constant value (shear step tests). The variation of apparent

viscosity vs. time, at given temperature, was investigated in order to characterize the "thixotropic behavior" of alloys.

The "step change" test makes it possible to evaluate the viscosity variation at isothermal conditions and at a fixed solid fraction when the rotation speed (or shear rate) is suddenly changed. In this case, the viscosity curve is divided to two sections: the transient state viscosity and steady state viscosity. The transient state viscosity occurs at the time when the rotation speed changes. When the viscosity no longer varies with prolonged shear time at a constant shear rate, the steady state viscosity is reached as shown in Fig. 51. The results obtained from these tests are used to create a curve of viscosity versus shear rate. This curve characterizes the rheological behavior of alloy (the degree of deviation from Newtonian behavior) in the semi solid state at fixed solid fraction. The rheological behavior in the semi solid state can be described by power law equation ($\eta = k\dot{\gamma}^{n-1}$ see section 3-1-5-1 about viscosity) where n is called the power law index. For metals, in the semi solid state, the value of n is less than 1 and the rheological behavior becomes Pseudo-plastic. In this case, with increasing the shear rate $\dot{\gamma}$, the apparent viscosity η decreases. When n = 1, the viscosity does not vary with shear rate and is called Newtonian. Therefore the experimental viscosity vs. shear rate curve resulting from the "step change" test can determine the power law equation of the alloy for fixed solid fraction when the steady state viscosity is plotted against the shear rate. For the evaluating the pseudo-plasticity of the present alloys, these tests were carried out for the A390 and the 10% Mg alloy at the semi solid temperature close to the

eutectic temperature, 566 °C and 550 °C, respectively. The thixotropy value of these alloys for variable shear step changes was obtained but not quantified in these tests.

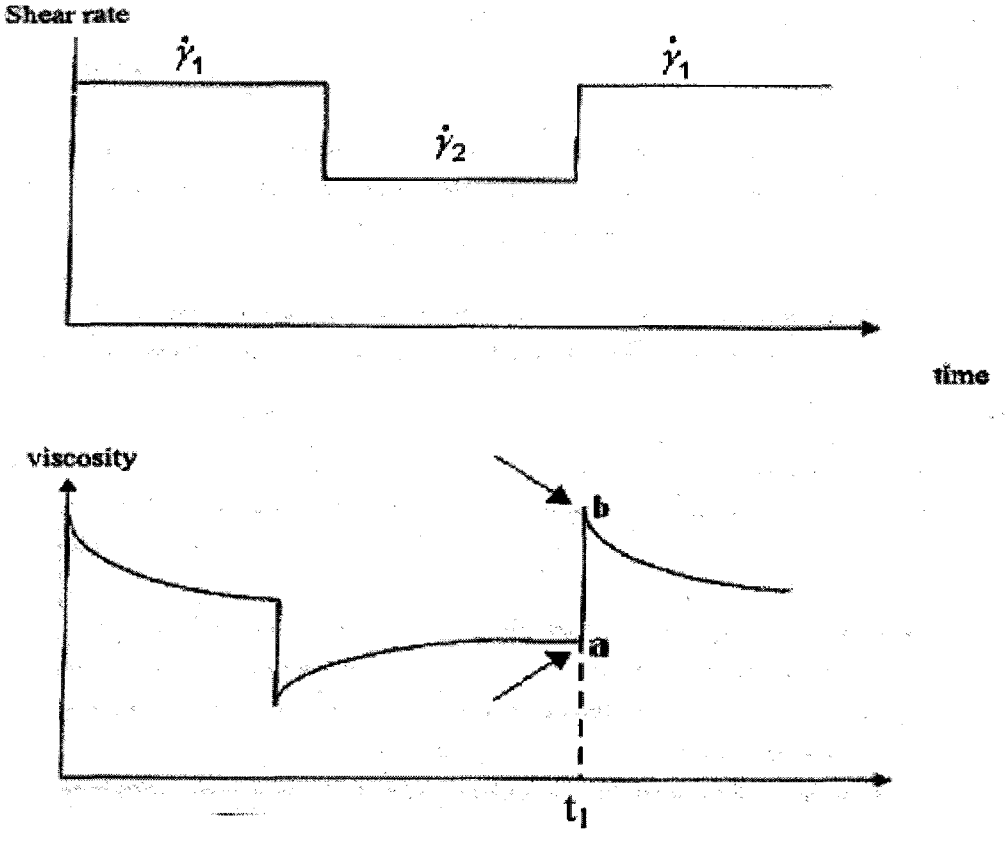

Fig. 51: The viscosity behavior during "step change" test. Points (a) and (b) indicate the steady state for $\dot{\gamma} = \dot{\gamma}_2$ and transient viscosity, respectively, when the shear rate increases from $\dot{\gamma}_2$ to $\dot{\gamma}_1$ at t_1.

4-7 Measurement of hardness

In order to measure the hardness, the samples of A390, 6% and 10% Mg alloys were cast into a standard ASTM permanent mold cast for the tensile bar specimens at the aluminum research center of University of Quebec at Chicoutimi (CURAL). The hardness of the samples for the as-cast as well as after T6 heat treatment was measured. A standard heat treatment procedure for all alloys consisting of 8 hours solutionzing at 495 °C, quenching in the water and followed with another 8 hours ageing at 175 °C, was carried out. Six cylindrical samples (∅ 0.5×0.5) of as-cast and heat treatment were prepared for the hardness tests using a Mitutoyo ATK-600 equipment shown in Fig. 52, and measured by the Rockwell B standard (100 kg load and 1/16 inch ball). The results were converted to standard Brinell HB (500 kg load and 10 mm ball).

Fig. 52: Hardness tests were measured by using Mitutoyo ATK-600

CHAPTER 5

RESULTS AND SCIENTIFIC FINDINGS

5-1 Introduction

The results are presented in the form of three submitted papers and two papers in preparation for publication.

The first paper presents the thermodynamic evaluation of the A390 alloy with addition of Mg content, up to 10%, carried out by the Factsage simulation.

The second paper involves the modification of eutectic silicon dispersed in the matrix of the A390, 6 and 10% Mg alloys during conventional and rheocast processing for continuous cooling conditions. Paper 1 showed that the addition of Mg can reduce the eutectic nucleation temperature (or eutectic formation temperature) and results in a significant modification of the eutectic silicon in the matrix from a coarse, flake like eutectic with large inter-flake space to a fine skeleton network with Chinese script form. Experiments was carried out to measure the eutectic nucleation temperature by cooling curve test and comparing the results with DSC (Differential Scanning Calorimeter) tests and the Factsage software simulation. The microstructures for conventional and rheocast processes for continuous cooling condition are also presented in this paper.

The third paper consists of a through investigation of microstructural constituents particularly the primary silicon and Mg_2Si phases that are formed during the two semi-

solid processes at isothermal condition. The effect of ageing on the microstructure in the semi-solid state with and without stirring is presented.

Two papers in preparation are presented in the standard form. They consists of the rheological characterization of A390 alloy and 10% Mg alloy for continuous cooling and isothermal shear step tests. The second paper presents the results of the hardness of A390, 6% Mg and 10% Mg alloys for as-cast and T6 heated treatment samples.

Paper 1

Thermodynamic evaluation of hypereutectic Al-Si (A390) alloy with addition of Mg content

Alireza Hekmat-Ardakan and Frank Ajersch

Submitted for publication in Acta Materialla

Feb 2009

5-2 Thermodynamic evaluation of hypereutectic Al-Si (A390) alloy with addition of Mg

Alireza Hekmat-Ardakan and Frank Ajersch
École Polytechnique de Montréal, Dép. de Génie Chimique
Montréal, QC, Canada, H3C 3A7

Abstract

In the present work the thermodynamic evaluation of hypereutectic Al-Si alloys with up to 10% Mg were investigated using the Factsage® software. Two critical compositions were detected at 4.2% and 7.2% Mg where the formation temperatures (liquidus, start of the binary and of the ternary reaction) are changed. These variations can be also defined by considering the ZPF (Zero Phase Fraction) line of Mg_2Si for Al-17Si-4.5Cu alloys with increasing Mg content. For Mg contents less than 4.2%, the ZPF line of Mg_2Si corresponds to the ternary reaction whereas for Mg from 4.2% to 7.2% the ZPF line of Mg_2Si corresponds to binary eutectic. Above 7.2% Mg and up to 10% Mg, the ZPF line of Mg_2Si corresponds to the liquidus line. In addition, the calculated liquid fraction vs. temperature curves has shown a decrease of the eutectic formation temperature (Knee point temperature) with the addition of Mg content up to 4.2% Mg. This temperature becomes almost constant up to 10% Mg. The calculation of eutectic formation temperature shows a good agreement with DSC (Differential Scanning Calorimeter) tests.

Keywords: Thermodynamic, Factsage, Aluminum alloys, Eutectic solidification, Magnesium

1. Introduction

Hypereutectic alloys such as A390 (Al-17Si-4.5Cu-0.5Mg) alloy or metal matrix composite (silicon acts as a reinforcing phase in the matrix of Al-Si) are used in applications that require high resistance to wear and corrosion, good mechanical properties, low thermal expansion and reduced density. Their properties are of particular interest to the automobile industry for the production of fuel-efficient vehicles using light weight components produced from these alloys such as connecting rods, pistons, air conditioner compressors, cylinder liners and engine blocks [1]. The good mechanical properties and high resistance to wear are essentially attributed to the presence of hard primary silicon particles distributed in the matrix. Therefore, the size and morphology of primary silicon in hypereutectic Al-Si alloys influence the mechanical properties of the alloys. However, the mechanical properties of hypereutectic Al-Si alloys such as A390 alloy are not optimised due to the large size of primary Si which adversely affects the application of this alloy. In service conditions, cracks can nucleate on the large primary silicon particles and the resultant stress concentration will be more severe at the interface between coarse Si phases and the matrix relative to that present between fine Si particulates and the matrix [2]. It has been shown that in-situ Mg_2Si/Al–Si composite has a high potential for wear resistance applications similar to Si/Al-Si composite because the intermetallic compound Mg_2Si also exhibits a high melting temperature, low density, high hardness, low thermal expansion coefficient, equilibrium interface, excellent workability with a potential for cost reduction [3]. In terms of properties and solidification behaviour, great similarities exist between Mg_2Si and Si [4]. The most

important advantage is the possibility of producing very light components due to the low density of Mg_2Si (1.99 $g.cm^{-3}$) compared to Si = 2.33 $g.cm^{-3}$ which can contribute to the light weighting of the vehicles [5].

By increasing the Mg content of hypereutectic Al-Si alloys, the silicon is consumed to form Mg_2Si. To better understanding the solidification behaviour and compound formation of alloys with higher Mg content, an investigation of the thermodynamic properties and the solidification path was carried out by using the Factsage® software developed by the CRCT group at *Ecole Polytechnique de Montreal* using the Fslite (Factsage light metal alloy database) database. The FactSage's FSlite light alloy database was derived from the European COST Action 507 (COST 507, Thermochemical database for light metal alloys) [6]. The alloy corresponds to a quaternary system (Al-Si-Cu-Mg) which was calculated for a constant composition (isopleth) of 4.5% Cu and 17% silicon (weight percent) and with $\frac{Mg}{Al}$ ratios of $\frac{0.5}{78}, \frac{1}{77.5}, \frac{2}{77}, \ldots\ldots, \frac{10}{68.5}$ representing 0.5%, 1%, 2%,……., 10% Mg content, respectively. Commercial A390 alloy normally contains other elements such as Mn, Ni, Pb, Sn, Sr, Ti, Zn. These constituents are minor and are generally less than 0.02 % and are not included in the thermodynamic analysis. Since the amount of elements do not change the phase diagram to very significant extent.

2. Results and discussion

2.1. Thermodynamic predictions

The calculated isopleth phase diagram of the basic A390 alloy, without trace elements, (Al-17Si-4.5Cu-0.5Mg) is shown in Fig. 1 where the dashed line at 17% Si indicates the regions of the formation of primary Si as well as the binary, ternary and quaternary reactions that occur at transition temperatures of 653.1, 566.2, 502,4 and 496,9 °C, respectively. Consequently, the solidification path confirms that the Si starts to precipitate as a primary phase from the liquid phase at 653.1 °C and continues down to 566.2 °C with maximum solid fraction of 6.1%. At this point, which is also called "knee" point, a dendritic network of α-Al and eutectic Si start to form and continues down to 502.4 °C where 88% liquid changes to this network. The ternary reaction takes place below this temperature to form Mg_2Si:

$$\text{Liq.} \rightarrow \text{Al} + \text{Si} + Mg_2Si \qquad (1)$$

This ternary eutectic zone is very small and continues down to the temperature of 496.9 °C where only 2.0% of the remaining liquid changes to form the ternary phases. The solidification becomes complete with quaternary reaction where the last remaining liquid (3.9%) solidifies corresponding to reaction (2) as follow:

$$\text{Liq.} \rightarrow CuAl_2\ (\theta) + Al + Si + Mg_2Si \qquad (2)$$

Other studies [7-10], have reported that the quaternary reaction proceeds according to the following reaction:

$$\text{Liq.} \rightarrow CuAl_2\ (\theta) + Al + Si + Cu_2Mg_8Si_6Al_5 \qquad (3)$$

The quaternary compound, $Cu_2Mg_8Si_6Al_5$ called the Q phase, is not included in the Factsage database and is therefore not considered in the calculated diagram. However, microstructural observation identifies the presence of the $Cu_2Mg_8Si_6Al_5$ phase and is associated with $CuAl_2$ in the solidified microstructure [10, 11]. Also, Mg_2Si has not been reported by other studies implying that any Mg_2Si is transformed to the Q phase [12] according to reaction (4):

$$\text{Liq.} + Mg_2Si \rightarrow CuAl_2\ (\theta) + Al + Si + Cu_2Mg_8Si_6Al_5 \qquad (4)$$

According to Backerud et al., [12], reactions 1, 4 and 3 occur at 555, 512 and 507 °C, respectively. Fig. 2 shows the result of DSC (Differential Scanning Calorimeter) test carried out for commercial A390 alloy (Al-17.4%Si-4.58%Cu-0.58%Mg-0.32%Fe-0.02%Mn-0.02%Ti-0.0003%P) at a cooling rate of 0.15 °C /s. The DSC test indicates that the temperature of the reactions 1, 4 and 3 occur at 538.2, 505.2 and 499.6 °C, respectively. The Q phase which solidifies at the end of solidification was not taken into account in the thermodynamic prediction and was found to have no significant effect on our investigation, particularly for high Mg content alloys, where reaction (1) predominate

the Mg_2Si precipitation. Factsage® predicts that the formation temperature of reaction (1) increases abruptly from 502.4 to 526.6 °C when the Mg content increases from 0.5 to 1% as it is shown later on in Table 3.

Table 1 shows the calculated liquid fraction, the compositions as well as the solid fraction with the percentage of each solid constituent during the transformation reactions of the basic A390 alloy. It should be noted that the binary and ternary reactions take place at the temperature intervals between 566.2-502.4 °C (binary) and 502.4-496.9 °C (ternary), respectively. However the quaternary reaction occurs at an isothermal temperature of 496.9 °C at the end of solidification. The binary reaction has the highest contribution to form solid phases Si + Al (88.0 %) whereas the ternary reaction has a much smaller contribution (2.0 %) in forming Al + Si + Mg_2Si phases. The microstructure of the solidified eutectic therefore consists of a dendritic network where the most predominant phases observed are Al + Si.

The liquid phase fraction and solid phase fraction of each constituent in the solidification interval are also shown in Fig. 3 for the basic A390 alloy using equilibrium conditions. It can be observed that the liquid fraction decreases slowly down to 566.2 °C (knee point) during the precipitation of primary silicon. With decreasing temperature the liquid fraction decreases rapidly down to 502.4 °C where the ternary reaction occurs. This reaction does not have a significant effect on the liquid fraction curve as previously indicated. Finally, the solidification becomes complete at the isothermal quaternary reaction. This figure also indicates that the main intermetallic phase in microstructure at

this stage is $CuAl_2$ (θ). These diagrams are calculated for equilibrium conditions, where the cooling rate is slow enough to include diffusion in the solid state throughout the solidification. The final structure will consist of solids of a composition corresponding to the end of the eutectic temperature tie line and liquid of eutectic composition [13]. Fig. 4 compares the fraction liquid of the basic A390 alloy for equilibrium and the Scheil condition where there is no diffusion in the solid phase. The Scheil and equilibrium curves are coincident for liquid fractions up to about 50%. However for less than 50%, the equilibrium curve results in a smaller amount of liquid at a given temperature. The calculations show significant decrease of solid fraction at the solidus temperature. At the equilibrium condition the solidification rate becomes more pronounced due to the diffusion effect in solid. This is valid only for very slow rates of temperature decreases. For non-equilibrium cooling, more liquid is present during the final stage of solidification compared to equilibrium cooling. This results in a microstructure with precipitation of intermetallic compounds such as θ-$CuAl_2$, $Cu_2Mg_8Si_6Al_5$ (Q phase) as a result of the quaternary eutectic reaction as compared to the equilibrium microstructure shown in Table 2.

With higher Mg content, the calculated formation temperatures showed two critical Mg values at 4.2% and 7.2%. The transition temperatures including the liquidus, start of binary and ternary as well as their reactions were determined at these critical points. Table 3 shows the variation of these temperatures for variable Mg contents, starting with the basic A390 alloy. Up to 4.2% Mg, both the liquidus temperature and the start of the binary reaction temperature decrease while the start of the ternary reaction temperature

increases. The binary and ternary reaction temperatures are almost at the same value for 4% Mg with a difference of only 1.7 °C. The variation of the Mg content has no effect on the isothermal quaternary reaction temperature (solidus). For Mg contents between 4.2% and 7.2%, the liquidus temperature continues to decrease whereas the start of binary reaction (Liq. → Mg_2Si + Si) temperature increases. At this range of Mg content, the start of the ternary reaction temperatures does not change with varying Mg content as shown in Fig. 5. Between 7.2% and 10%, the Mg_2Si intermetallic phase starts to precipitate as a primary phase from the liquid phase. The liquidus temperature increases and the temperature of the start of the binary reaction decreases once more while the temperature of the ternary remains constant as before. With decreasing binary reaction temperature and increasing liquidus temperature, the solid fraction of the primary Mg_2Si notably increases at this range of Mg content.

With the addition of Mg, the Mg_2Si intermetallic phase first appears only in the ternary eutectic zone up to 4.2% Mg. With Mg contents between 4.2% and 7.2%, solid Mg_2Si appears in the both binary and ternary reactions. Above 7.2% Mg, it solidifies as a primary phase as well as during the binary and ternary reactions. This implies that the formation range of Mg_2Si intermetallic particle can be significantly increased with addition of Mg as shown in the shaded zone of Fig.5.

These variations can also be represented by using the ZPF (Zero Phase Fraction) concept [14] for Mg_2Si and Al. Fig.6 shows the ZPF line for the Al-Si-4.5%Cu system with 0.5, 6 and 10% Mg. These compositions were selected to illustrate the position of the ZPF

line for each critical range of Mg. The solidification path at 17% Si indicates that the variation of Mg content has significant effect on the ZPF line of Mg_2Si. In Fig.6.a, at 0.5% Mg, the ZPF line of Mg_2Si phase represents the temperature of the ternary reaction (Liq. $\rightarrow$ Al + Si + Mg_2Si). For Mg content from 4.2% to 7.2% represented by Fig.6.b for 6% Mg, the ZPF line of Mg_2Si represents the binary reaction temperature Liq. $\rightarrow$ Mg_2Si + Si. For Mg contents of more than 7.2% Mg (Fig.6.c) the ZPF line of Mg_2Si phase corresponds to the Liquidus temperature and the Mg_2Si intermetalic phase formed as a primary phase. As shown in Fig.6.c, Mg_2Si intermetallic precipitates as a primary phase for alloys with a Mg content grater than 7.2% Mg.

Table 4 shows the liquid fraction and the compositions at transition temperatures as well as the solid fraction with the percentage of each solid constituent for the 10% Mg alloy. The calculated results indicate that the solidification starts with the precipitation of Mg_2Si from the liquid. Subsequently, the pro-eutectic silicon solidifies along with the Mg_2Si down to the eutectic formation temperature of 549.2 °C. At this point the eutectic network starts to form according to ternary eutectic reaction. The calculated liquid fraction demonstrates that 82.3% of the liquid phase is transformed to ternary eutectic phases (Al, Si and Mg_2Si) and the resulting eutectic solidification structure for high Mg content alloys corresponds to the ternary reaction. In terms of liquid fraction, the Knee point decreases with increasing the Mg content and corresponds to the temperature of the ternary reaction for alloys containing more than 4.2% Mg. When comparing the liquid fractions vs. temperature curve of the basic A390 alloy (Fig.3) to the alloy with

10% Mg (Fig. 7), it can be observed that the start of the binary eutectic reaction occurs at 566.2 °C (knee point) for the case of the basic A390 alloy. Primary Si is the only pro-eutectic phase in the microstructure with maximum solid fraction of 6.1%. However, for the case of the alloy compositions with 10% Mg the knee point represents start of ternary reaction at 549.2 °C and the pro-eutectic phases consist of mixture of Mg_2Si and Si with maximum solid fraction of 10.1% and 2.1%, respectively. At 10% Mg, the solidification starts with the precipitation of Mg_2Si down to 588.9 °C with a maximum solid fraction of 6.3%. Subsequently, silicon solidifies along with the Mg_2Si down to knee point.

Fig.7 also indicates that the solidification rates of Si and Mg_2Si during solidification interval are very similar. The binary Al-Si and quasi-ternary Al- Mg_2Si systems have a lot of similarities where growth rates are characterized by the faceted structure of the primary phases and the non-faceted as eutectic phase [4]. Fig. 8 compares the liquid fraction vs. temperature curves of the basic A390, 6% Mg and 10% Mg alloys according to the Scheil prediction. It is clearly shown that the variation of Mg content significantly decreases the eutectic formation temperature at knee point shown in Fig.9. This temperature decreases rapidly up to 4.2% Mg and become nearly constant at 549 °C. Fig. 10 shows the results of DSC test for the 6% Mg and 10% Mg alloys. The DSC tests indicate that the knee point occurs at 563.09 °C, 545.23 and 543.63 °C for the basic A390, 6% and 10% Mg alloys, respectively, which is in good agreement with Factsage calculation shown in Fig.8.

3. Conclusions

Thermodynamic computations using Factsage have shown that the solidification of basic A390 (Al-17Si-4.5Cu-0.5Mg) alloy proceeds sequentially where the primary, binary, ternary and quaternary reactions occur at formation temperatures of 653.1, 566.2, 502.4 and 496.9 °C, respectively. With hyper-eutectic alloys up to 10% Mg, two critical compositions were detected at 4.2% and 7.2% Mg where the formation temperatures for the liquidus, the start of the binary and of the ternary reaction are changed. These variations can be also defined by considering ZPF (Zero Phase Fraction) line of Mg_2Si for Al-17Si-4.5Cu alloy with increasing Mg content. For Mg contents less than 4.2%, the ZPF line of Mg_2Si corresponds to the ternary reaction, whereas for Mg from 4.2% to 7.2% the ZPF line of Mg_2Si correspond to the binary eutectic reaction. Above 7.2% Mg and up to 10% Mg, the ZPF line of Mg_2Si corresponds to the liquidus line.

The liquid fraction vs. temperature curves for the solidification of the basic A390, 6% Mg and 10% Mg alloys calculated according to the Scheil equation indicates that the eutectic formation temperature (knee point) for the 6% Mg and 10% Mg alloys occurs at the same temperature of 549 °C which is 17 °C lower than the eutectic formation temperature of A390 alloy at 566 °C. A modification of eutectic Si in the matrix can therefore be expected due to the effect of temperature on eutectic nucleation. The eutectic nucleation temperature has been shown to have a direct effect on the number of potential nuclei found in the melt [15]. There are fewer barriers for nucleation with increasing nucleation temperature and thus greater number of isolated eutectic Si

particles may form. It is therefore anticipated that reduction of the knee temperature with increasing Mg content can modify the eutectic silicon phase. As a result, the solidified microstructure of the basic A390 alloy corresponds to the binary eutectic structure of Al + Si whereas for alloys with Mg contents greater than 4.2% a solidified ternary structure of Al + Si + Mg_2Si is formed.

Acknowledgments

The authors gratefully acknowledge the financial support from the Fonds Quebecois de Recherche sur la Nature et les Technologies (FQRNT) and Natural Sciences and Engineering Research Council (NSERC) of Canada. The authors thank Pro. Arthur D. Pelton, Director of the research center of CRCT (Centre for Research in Computational Thermochemistry) for constructive suggestions about FACTSAGE.

List of Figures

Fig 1: Isopleth of the Al-Si-4.5%Cu-0.5%Mg system (basic A390 alloy) and the solidification path at 17% Si calculated by Factsage.

Fig. 2: DSC (Differential Scanning Calorimeter) test carried out for commercial A390 alloy (Al-16.7%Si-4.58%Cu-0.58%Mg-0.32%Fe-0.02%Mn-0.02%Ti-0.0003%Ti) at a cooling rate of 0.15 °C/s.

Fig. 3: The variation of liquid fractions and other solidified phases with temperature in the solidification interval for the basic A390 alloy (Insert: detail of area at high solid fraction).

Fig. 4: The liquid fractions of the basic A390 alloy for the equilibrium and Scheil (no-diffusion) conditions.

Fig. 5: The effect of Mg content on the transition reactions and related temperatures for Al-17% Si-4.5% Cu alloys. Critical points occur at 4.2% and 7.2% Mg. The shaded zone shows the solidification interval of Mg_2Si intermetallic phase for different Mg alloys.

Fig.6 : Effect of Mg content on the isopleth phase diagram showing the ZPF (Zero Phase Fraction) lines of Mg_2Si and Al for alloy with a) 0.5% Mg (basic A390), b) 6%Mg and c) 10%Mg.

Fig. 7: Liquid fraction and other phases solidified in the solidification interval for 10% Mg alloy.

Fig. 8: The liquid fraction of basic A390, 6% Mg and 10% Mg alloys during solidification interval according to the Scheil condition.

Fig. 9: The variation of knee point temperature of alloys with increasing the Mg content calculated using Factsage.

Fig. 10: DSC results of 6% Mg (a) and 10% Mg (b) alloys for a cooling rate of 0.15 $^{o}Cs^{-1}$

Table 1: The liquid and solid fractions for basic A390 alloy transition reactions.

reactions	A390	Liquid Fraction (%)	Liquid composition (%wt)				Solid Fraction (%)	Constituent percentage (%wt)			
	Temperature (°C)		Al	Si	Cu	Mg		Al	Si	θ*	Mg_2Si
Primary Si	653.1	100	78	17	4.5	0.5	0	-	-	-	-
Start of binary	566.2	93.9	83.0	11.6	4.9	0.5	6.1	-	100	-	-
Start of ternary	502.4	5.9	62.8	7.5	27.1	2.6	94.1	83.2	16.8	-	-
Quaternary	496.9	3.9	61.5	7.2	28.9	2.4	96.1	83.1	16.7	-	0.2
	496.9-δT	0	-	-	-	-	100	81.4	16.2	2.1	0.3

*θ = $CuAl_2$

Table 2: Comparison of the weight percent of the intermetallic phases θ and Q solidified at the equilibrium and the Scheil cooling condition calculated by Factsage®

Phases / Cooling condition	θ	Q
Equilibrium	2.1%	0.3%
Scheil	6.66%	0.6%

Table 3: Effect of Mg variation on the formation temperatures, 4.2% Mg and 7.2% Mg.

%Mg	$T_{Liquidus}$ (°C)	Start of binary reaction	Start of ternary reaction	Quaternary reaction temperature
		T (°C)	T (°C)	T (°C)
0.5*	653.1	566.2	502.4	496.9
1	649.7	564.0	526.6	496.9
2	642.8	559.6	541.4	496.9
3	635.7	555.2	546.7	496.9
4	628.4	551.0	549.3	496.9
4.2**	626.9	550.2	549.7	496.9
5	620.9	565.8	549.8	496.9
6	613.2	584.6	549.7	496.9
7	605.4	600.7	549.6	496.9
7.2***	603.8	603.7	549.6	496.9
8	617,0	599.8	549.5	496.9
9	632.2	594.5	549.3	496.9
10	646.1	588.9	549.2	496.9

*A390 composition
** First critical point
*** Second critical point

Table 4: The liquid and solid fractions for A390 + 10%Mg alloy transition reactions.

Reactions	A390+10%Mg	Liquid Fraction (%)	Liquid composition (%wt)				Solid Fraction (%)	Constituent percentage (%wt)			
	Temperature (°C)		Al	Si	Cu	Mg		Al	Si	θ*	Mg_2Si
Primary Mg_2Si	646,1	100	68,5	17	4.5	10	0	-	-	-	-
Start of binary	588,9	93,6	73.1	15.6	4,8	6,5	6,3	-	-	-	100
Start of ternary	549,2	87,8	77,9	12,4	5,1	4,6	12,2	-	21,2	-	78,8
Quaternary	496,9	5,5	61,5	7,1	28,9	2,5	94,5	72,8	11,2	-	16
	496,9-δT	0	-	-	-	-	100	71,1	10,8	2,8	15,3

- θ = $CuAl_2$

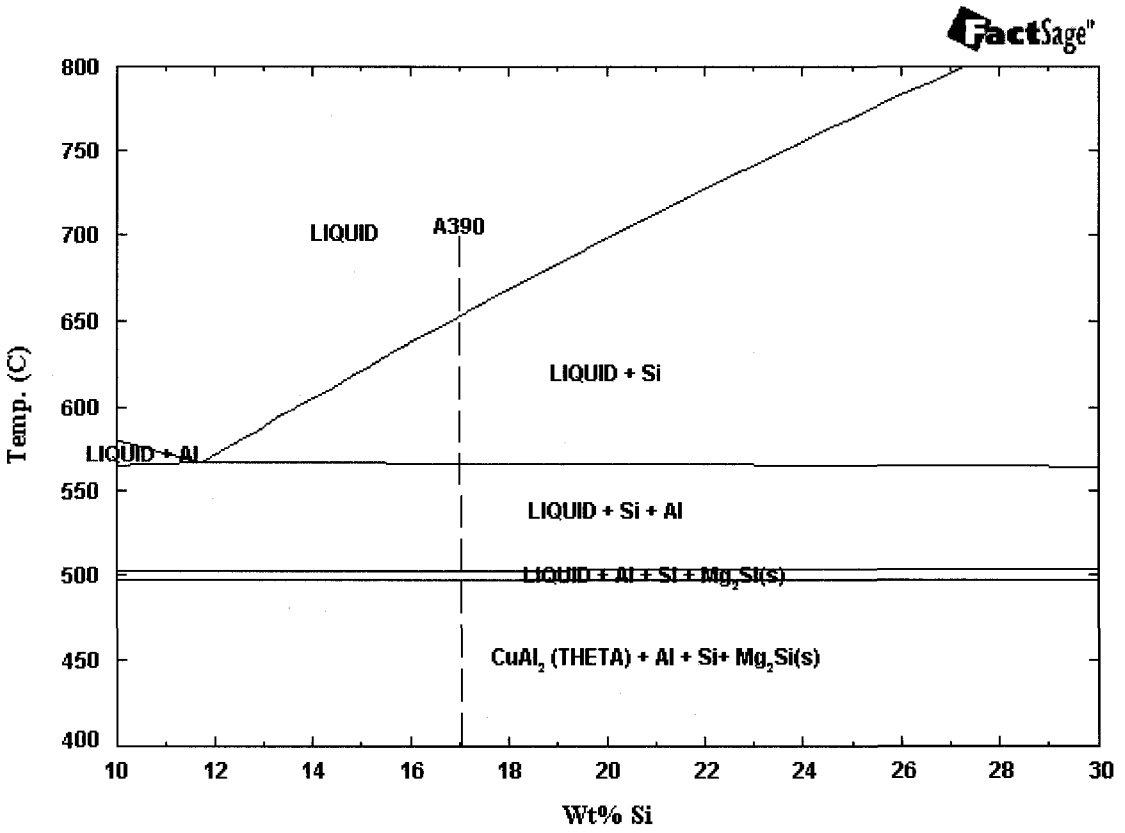

Fig. 1: Isopleth of the Al-Si-4.5%Cu-0.5%Mg alloy (basic A390) and the solidification path alloy at 17% Si calculated by Factsage.

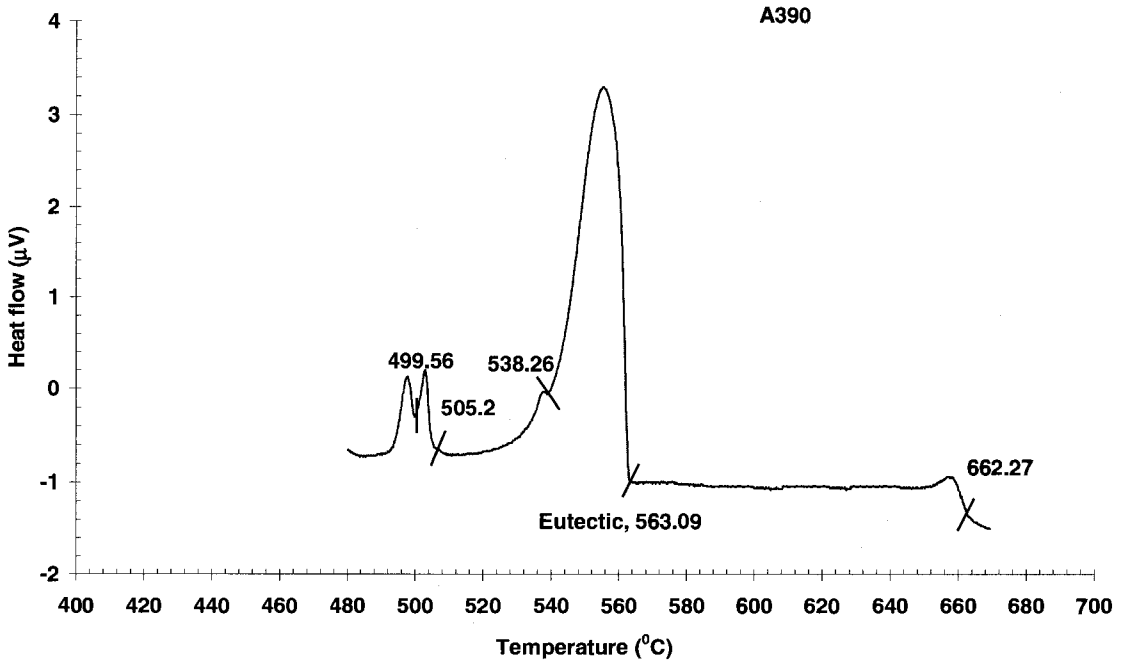

Fig. 2: DSC (Differential Scanning Calorimeter) test carried out for commercial A390 alloy (Al-16.7%Si-4.58%Cu-0.58%Mg-0.32%Fe-0.02%Mn-0.02%Ti-0.0003%Ti) at a cooling rate of 0.15 ° C/s.

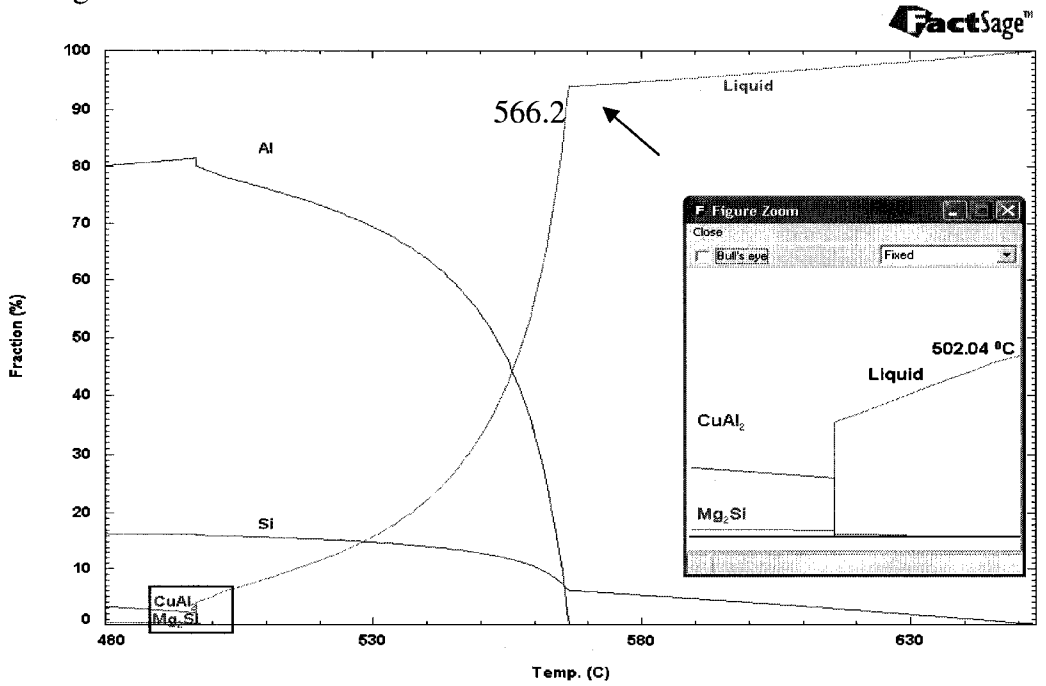

Fig. 3: The variation of liquid fractions and other solidified phases with temperature in the solidification interval for the basic A390 alloy (Insert: detail of area at high solid fraction).

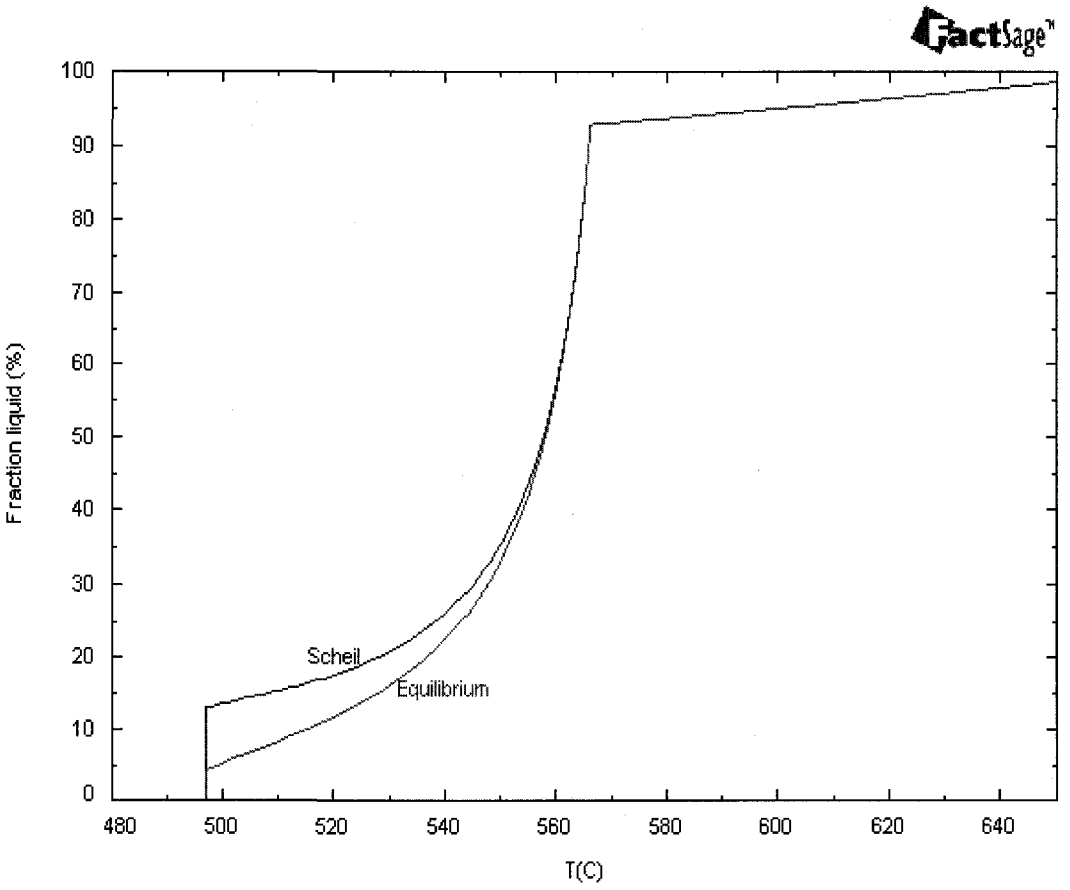

Fig. 4: The liquid fraction of the basic A390 alloy for the equilibrium and Scheil (no-diffusion) conditions.

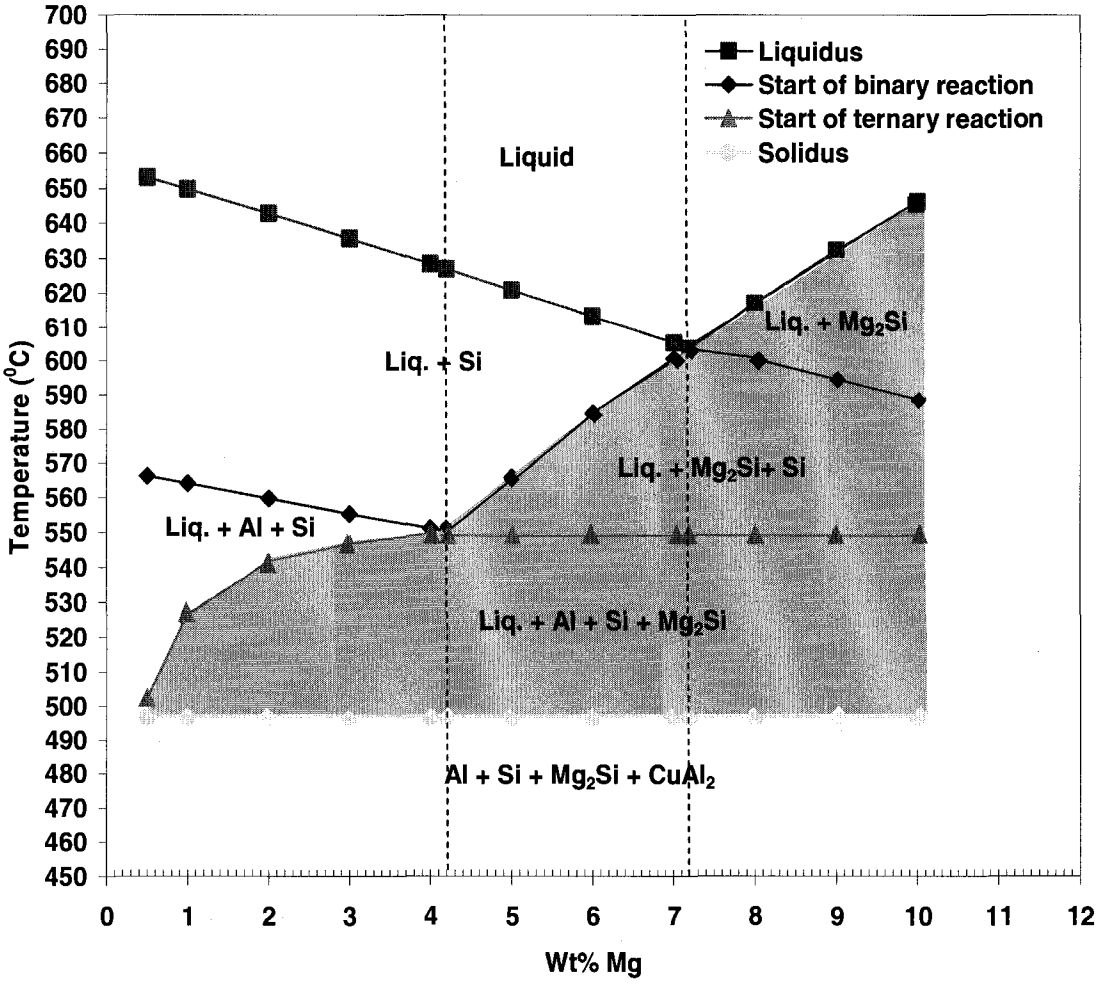

Fig. 5: The effect of Mg addition on transition reactions for Al-17% Si-4.5% Cu alloys with different Mg content. Critical points occur at 4.2% and 7.2% Mg. The shaded zone shows the solidification interval of Mg_2Si intermetallic phase for different Mg alloys.

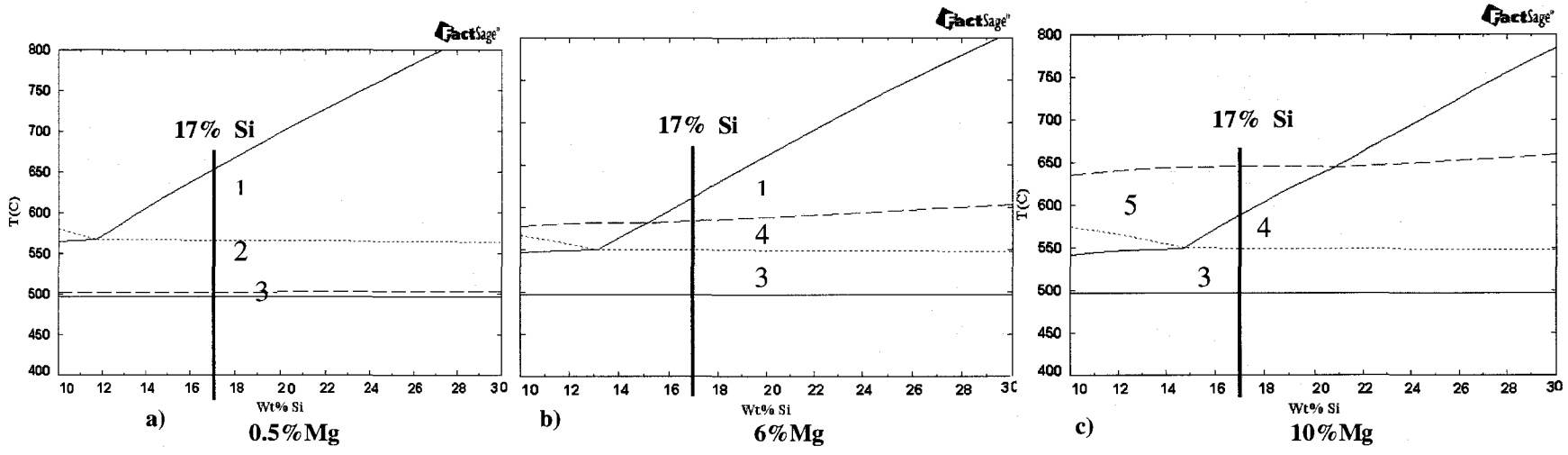

ZPF line of Mg_2Si - - - - - - - - ZPF line of Al .....

1- Liquid + Si
2- Liquid + Al + Si
3- Liquid + Al + Si + Mg_2Si
4- Liquid + Si + Mg_2Si
5- Liquid + Mg_2Si

Fig.6 : Effect of Mg content on the isopleth phase diagram showing the ZPF (Zero Phase Fraction) lines of Mg_2Si and Al for alloy with a) 0.5% Mg (basic A390), b) 6%Mg and c) 10%Mg.

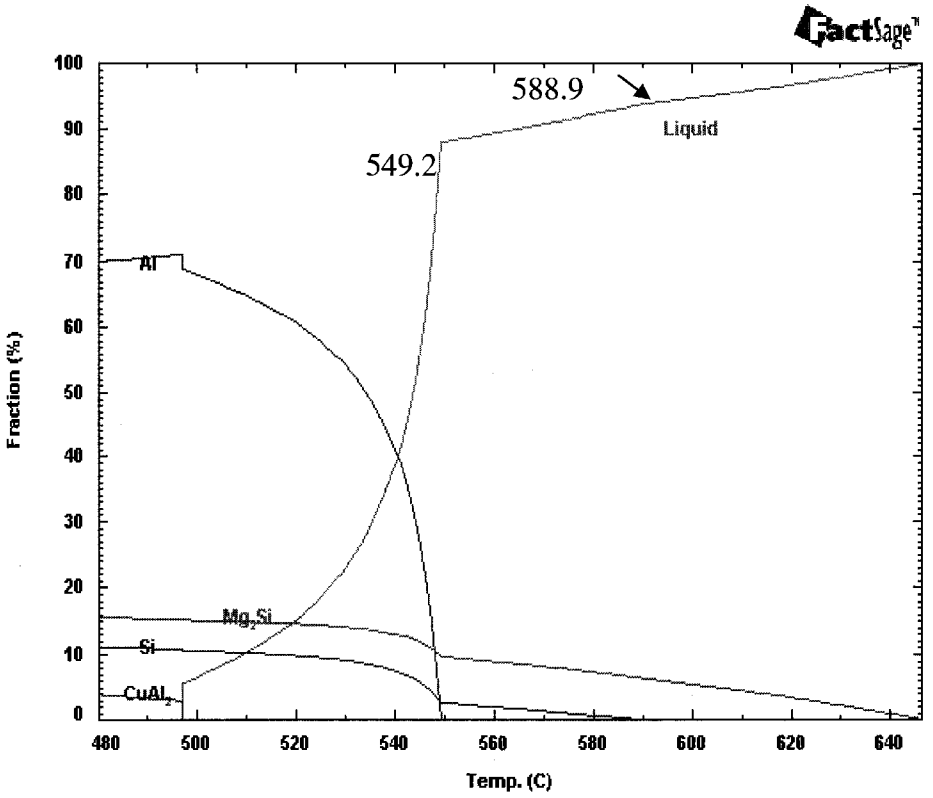

Fig. 7: Liquid fraction and solidified phases in the solidification interval for 10% Mg alloy.

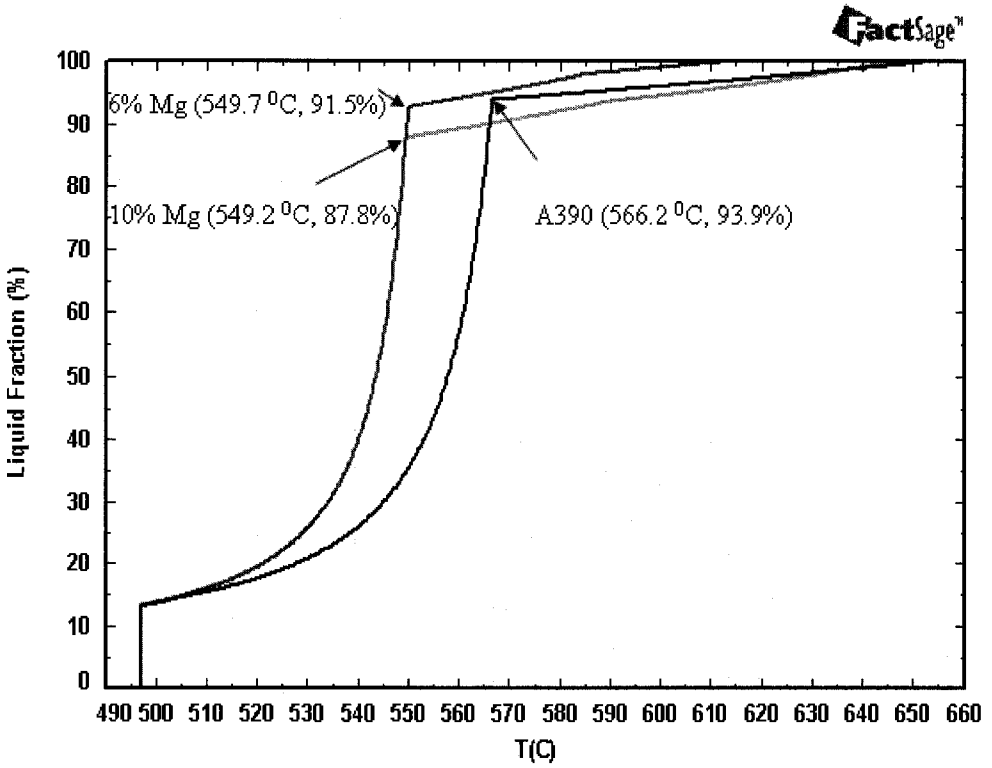

Fig. 8: The liquid fraction of basic A390, 6% Mg and 10% Mg alloys during solidification interval according to the Scheil condition.

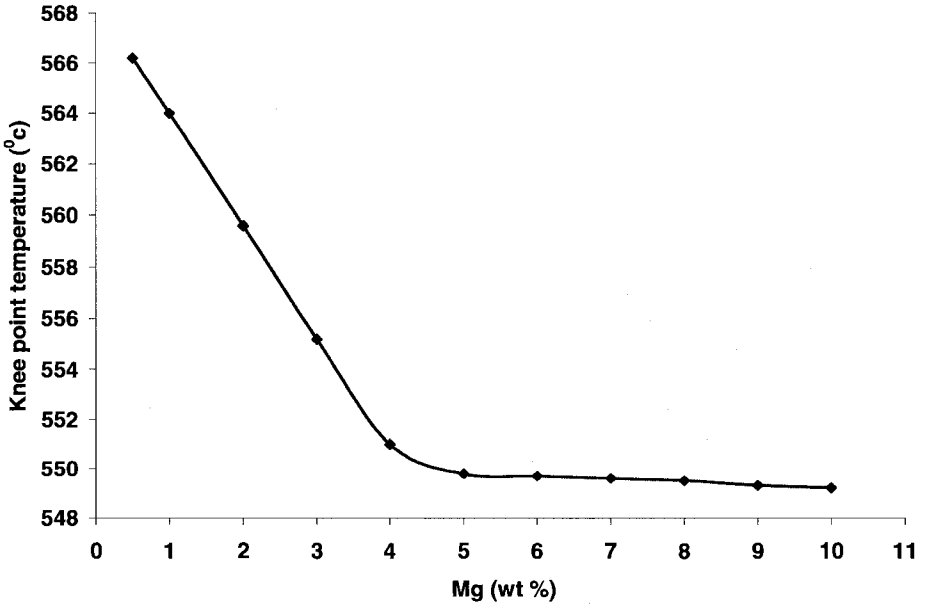

Fig. 9: The variation of knee point temperature of alloys with increasing the Mg content calculated using Factsage.

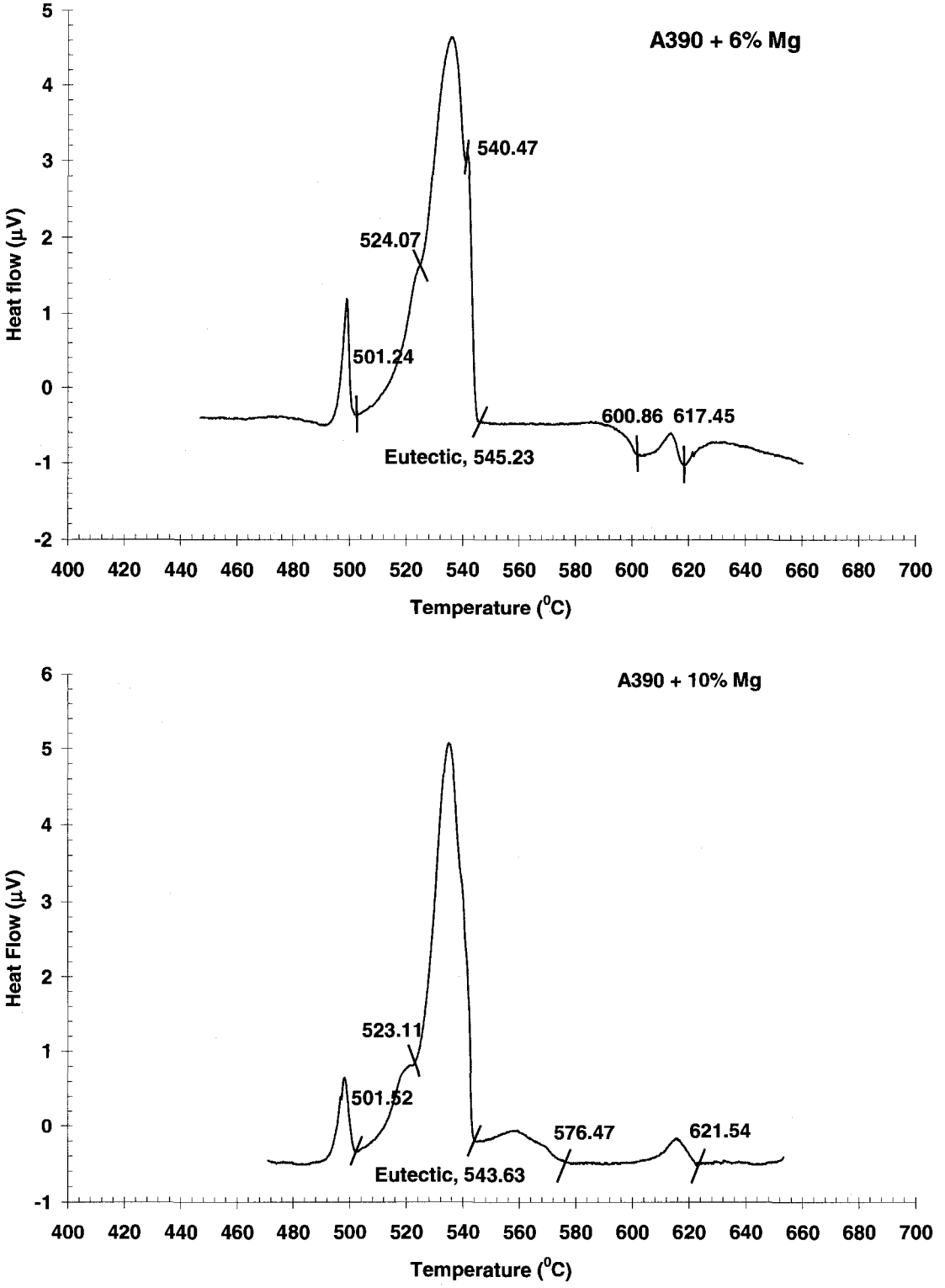

Fig. 10: DSC results of (a) 6% Mg and (b) 10% Mg alloy for a cooling rate of 0.15 $^{o}Cs^{-1}$

References

[1] L. Lasa and J.M. Rodriguez-Ibab, *Mater Sci Eng A* **363** (2003), p. 193.

[2] Wang Feng, Yajun Ma., Zhengye Zhang, Xiaohao Cui and Yuansheng Jin, *Wear* **256** (2004), p. 342.

[3] Y.G. Zhao, Q.D. Qin, Y.Q. Zhao, Y.H. Liang and Q.C. Jiang, *Materials Letters* **58** (2004), p. 2192.

[4] J. Zhang, Z. Fan, Y.Q. Wang and B.L. Zhou, *Mater Sci Eng A* **281** (2000), P. 104.

[5] Q.D. Qin, Y.G. Zhao and W. Zhou, *Wear* **264** (2008), p. 654.

[6] Christopher W. Bale and Arthur D. Pelton, FACTSAGE 5.4.1, C.R.C.T (Centre of Research for Computational Thermochemistry), École Polytechnique de Montréal. http://www.crct.polymtl.ca.

[7] L.F. Mondolfo, Manganese in aluminum alloys, Syracuse University, USA. Publisher: The Centre (1978).

[8] P. Kapranos, D.H. Kirkwood, H.V. Atkinson, J.T. Rheinlander, J.J. Bentzen, P.T. Toft, C.P. Debel, G. Laslaz, L. Maenner, S. Blais, J.M. Rodriguez-Ibabe, L. Lasa, P. Giordano, G. Chiarmetta and A. Giese, *J Mater Proc Tech* **135** (2003), p. 271.

[9] L. Lasa and J. M. Rodriguez-Ibabe, *Mater Charac* **48** (2002), p. 371.

[10] Jian Li, M. Elmadagli, V.Y. Gertsman, J. Lo and A.T. Alpas, *Mater Sci Eng A* **421** (20060, P. 317.

[11] M. Elmadagli and A.T. Alpas, *Wear* **261** (2006), p. 367.

[12] Lennart Backerud, GuoCai Chai and Jarmo Tamminen; Solidification Characteristics
of Aluminum Alloys, Amer Foundry Society Publisher, Volume 2; University of Stockholm; Sweden (1993).

[13] D. Liu, H.V. Atkinson and H. Jones, *Acta Mater* **53** (2005), P. 3807.

[14] J.E. Morral and H. Gupta, *Scr Metall et Mater* **25** (1991), P. 1393.

[15] S. Nafisi and R. Ghomashchi, *Mater Sci Eng A* **415** (2006), p. 273.

Paper 2

Effects of Mg content on the evolution of eutectic microstructure for conventionally cast and rheocast hypereutectic Al-Si alloy

Alireza hekmat-Ardakan and Frank Ajersch

Submitted for publication in Acta Materialla

Feb 2009

5-3 Effects of Mg content on the evolution of eutectic microstructure for conventionally cast and rheocast hypereutectic Al-Si alloy

Alireza Hekmat-Ardakan and Frank Ajersch
École Polytechnique de Montréal, Dép. de Génie Chimique
Montréal, QC, Canada, H3C 3A7

Abstract

In this paper, the evolution of the eutectic microstructure of A390 alloy and alloys containing 6 and 10 wt% Mg was investigated for two types of castings. Conventional castings were produced with two different cooling rates: -0.15± 0.05 $^{o}C\ s^{-1}$ and -1.0± 0.2 $^{o}C\ s^{-1}$. The rheocast samples were subjected to a rotation speed = 260 rpm. For the conventionally cast alloys, the microstructure of the high cooling rate samples is finer than for low cooling rate samples. However, with addition of Mg, the morphology of eutectic silicon significantly changes from large individual flakes to a fine, skeleton network with a Chinese script morphology, similar to the eutectic Mg_2Si. The reason is due to the decrease of the eutectic formation temperature caused by addition of Mg. With Mg addition, the eutectic reaction is also changed from a binary (Al + Si) to a ternary (Al + Si + Mg_2Si) reaction. For the case of the rheocast samples, the eutectic silicon becomes fragmented, with the manifestation of globular alpha aluminium phase particles. The evolution of the primary phases for the two types of castings was analysed in order to determine the effect of the Mg content on the microstructural evolution.

Keywords: Aluminium alloys, Rheocasting, Eutectic solidification, Magnesium, Casting.

1. Introduction

Hypereutectic aluminium–silicon alloys can be considered in-situ composite alloys where the silicon acts as the reinforcing phase [1] with excellent wear and corrosion resistance. These composites are a class of materials with excellent combinations of mechanical and physical properties for various applications in the automotive industry. However, the mechanical properties of Si/Al-Si composites are not optimized due to the large size of primary silicon particles [2]. For example, the machinability of unmodified hypereutectic Al–Si alloy is difficult due to the presence of coarse primary silicon and long needlelike eutectic silicon [3]. Modification of both eutectic and primary silicon microstructure is necessary in order to obtain a better surface finish and further improvement in mechanical properties.

It has been shown that hypereutectic aluminium–silicon alloys with high Mg content are also in situ Mg_2Si/Al-Si composite with a high potential for wear resistance material because of the excellent physical and mechanical properties of the Mg_2Si intermetallic phase that is formed on solidification [4]. This phase has a high melting point (1085 ^{o}C), very low density (1.99×10^3 kg/m^{-3}), high hardness (4.5×10^9 Nm^{-2}), a low thermal expansion coefficient (7.5×10^6 K^{-1}) and a reasonably high elastic modulus of 120 GPa [5]. A thermodynamic analysis of the Al-17%Si-4.5%Cu system increasing content of Mg can transform the matrix structure from binary Al + Si eutectic to ternary Al + Si + Mg_2Si eutectic [6]. This eutectic Mg_2Si has been identified to be of the form of Chinese script type particles [5]. Both of these eutectic structures in the eutectic matrix have a

significant influence on the mechanical properties of these alloys. According to the thermodynamic predictions using the FACTSAGE software, the binary and ternary eutectic reactions start at liquid fractions of 93.9% for A390 and 87.8% for A390 with 10% Mg alloy, respectively, based on the Scheil cooling condition where there is no diffusion in the solid phase [7]. For basic A390 alloy, 81% of liquid is solidified as a result of the binary reaction whereas 75.4% of liquid is solidified as a result of the ternary reaction for the 10% Mg alloy. For equilibrium condition, these values increase to 88% and 82.3%, respectively [6]. Therefore, the modification of the eutectic microstructure, specifically the eutectic silicon, plays an important role in improving mechanical properties. Superior properties have been attained by semi solid metal (SSM) processing resulting in globular structure of primary phase as well as in a fragmentation of large needlelike eutectic silicon in the matrix. This improvement of mechanical properties is also due to pseusoplastic behaviour of the alloy in the semi solid state and results in better die filling. This paper presents the results of the effect of Mg content on the eutectic microstructure of hypereutectic Al-Si alloy conventionally and rheocast (stir cast) samples.

Fig.1 compares the liquid fraction vs. temperature curves for the three alloys according to the Scheil prediction. The points indicated by an arrow on these curves show the starting point of the eutectic formation in the matrix after the solidification of primary phases becomes complete. This point is called "knee" point. For A390 the knee point is due to the start of binary reaction at 566.2 ^{o}C (liquid $\rightarrow$ Al + Si), whereas for the 6% and

10% Mg alloys, the knee point represents the start of ternary reaction at 549.7 °C and at 549.2 °C for the reaction liquid $\rightarrow$ Al + Si + Mg_2Si. The calculations show that the 6% Mg alloy significantly decreases the knee point temperature (up to first critical point at 4.2% Mg, [6]). This decrease is almost constant up to 10% Mg. The knee point also indicates that the pro-eutectic phase for A390 is primary Si with a solid fraction of f_s = 6.1%. For the 6% Mg alloy, the solid fraction of the pro-eutectic phases consist of $(f_s)_{Si}$ = 3.9% and $(f_s)_{Mg_2Si}$ = 3.1% whereas for the 10% Mg alloy, $(f_s)_{Si}$ = 2.1% and $(f_s)_{Mg_2Si}$ = 10.2%. For alloy with Mg content more than second critical point at 7.2%, the Mg_2Si intermetallic compound solidifies as the primary phase [6].

2. Experimental procedures

The 6 and 10 wt% Mg alloys were produced by adding AZ91 Mg-base alloy to A390 alloy (Table 1). The AZ91 alloy was wrapped in aluminium foil and added to the melt of A390 alloy at 750 °C. In order to account for the oxidation loss, an additional amount of 20% Mg was added to the melt. Silicon and copper were also added to the melt in order to keep the chemical composition of these elements the same as for the A390 composition. The melt was degassed with argon and stirred for two minutes before pouring into a steel mould to form three 35 ∅× 120 mm cylindrical samples. After preparing the conventionally cast alloys, each specimen was cut to the weight of 60 gram and put into a graphite crucible with 28mm inner diameter and 5mm wall thickness and heated up to 700 °C, degassed with argon and stirred for two minutes before sampling.

Samples were prepared with two cooling rates, high cooling rate (HCR) and low cooling rate (LCR). For HCR samples, the graphite crucible containing different Mg alloys were transferred to the cooling station where K-type thermocouple was quickly immersed into the melt at a position about 10 mm from the bottom in the center. Temperatures were recorded using a data logging system at 15 per second intervals. For the HCR cooling tests, the cooling rates averaged $-1.0 \pm 0.2\ ^{o}C\ s^{-1}$ for the region above the liquidus temperature. For the low cooling (LCR) rate tests, the samples were cooled in the furnace at a controlled cooling rate of $-0.15 \pm 0.05\ ^{o}C\ s^{-1}$. In the previous studies, the DSC (Differential Scanning Calorimeter) measurements were also carried out for these alloys with cooling rate of $0.15\ ^{o}C\ s^{-1}$ [6].

A HAAKE RV12 viscometer with a spirally grooved cylindrical agitator was used for the semi solid processed samples. Each test consisted of 150 gram of alloy contained in a graphite crucible with inner diameter of 41 mm, 10 mm wall thickness and height of 120 mm. Subsequently, the samples were heated to 700° C and then held at this isothermal temperature for a period of 5 minutes. After this period, the alloy was continuously cooled in furnace at a rate of $-0.15 \pm 0.05\ ^{o}C\ s^{-1}$ (same as for conventional casting) and sheared at an average rate of $\dot{\gamma}_{ave} = 52\ s^{-1}$ (rotation speed = 260 rpm) as shown in Fig.2a. Two K-type thermocouples located in the crucible wall were used to measure the temperature the near the surface and the bottom positions. Argon gas was introduced into the furnace chamber in order to prevent sample oxidation. The tests were stopped when the upper limit of the viscometer torque was reached.

Metallographic specimens for the conventionally cast samples were prepared by sectioning transversely at the level of the thermocouples (10 mm from the bottom of crucible). The rheocast specimens were prepared by sectioning the samples as shown in Fig. 2b. The specimens were polished conventionally for microstructural analyses. All samples were etched by using 0.5% HF solution agent. Optical and Scanning Electron microscopy (SEM) with EDX (Energy Dispersive X-ray) analysis were employed to characterize the microstructure.

3. Results and discussion

Fig. 3 shows the cooling curves for A390, 6% Mg and 10% Mg alloys, for the air cooled (HCR) condition, as measured by a thermocouple at the center of the melt. Fig 4 compares the detail of the eutectic segment of the cooling curves at the HCR and LCR cooling condition for A390, 6% Mg and 10% Mg samples. As confirmed by thermodynamic prediction the addition of Mg, up to 6% significantly reduces eutectic reaction temperature and it is almost constant between 6% and 10% Mg. The results of the DSC test carried out in a previous study [6] also confirms the decrease of the eutectic reaction temperature with variation of Mg content. There is good agreement between thermodynamic prediction, the cooling curve tests and DSC results as shown in Table 2. Table 2 also indicates that the values of the eutectic temperature are very similar for both LCR and HCR conditions. However, for both cases, the value of eutectic reaction temperature significantly decreases for the 6% Mg alloy and then gradually decreases up to 10 % Mg.

3.1. Conventionally cast microstructures

Fig.5 shows the BSE (back scattered electron) image of the microstructure of A390 alloy for the LCR sample showing the form of the intermetallic compounds together with an EDX analysis. The microstructure consists of the primary polygonal silicon phase and the eutectic matrix containing mainly of binary Al + Si as well as the intermetallic phases, $CuAl_2$ (θ), $Cu_2Mg_8Si_6Al_5$ (Q) and Al_5FeSi (β). Other studies have also observed these microstructures with the presence of the Q phase associated with the θ phase [8, 9]. However the main intermetallic phase in these alloys is θ phase.

The result of the thermodynamic computation [6] shows that the Q phase does not appear because it is not in the Factsage database and would therefore not appear in the phase diagram of the quaternary Al-Si-Cu-Mg system. It should be noted that the mixed alloys (A390 and AZ91) contain amounts of Fe, Zn and etc, which also react to form of intermetallics. The platelet Fe-containing phase, β-Al_5FeSi, is the most common Fe intermetallic phase and contributes to the decrease of the mechanical properties of Al–Si based cast alloys [10, 11, 12]. With increasing Mg content, as predicted by thermodynamic data, the Mg_2Si intermetallic phase first appears in the matrix to a form of eutectic morphology and then as a primary phase in the microstructure. The microstructure of these three alloys for LCR and HCR conditions are compared in Fig.6 at low magnification of 50X. For both cooling conditions, the morphology of grey primary silicon particles remained polygonal, whereas Mg_2Si crystals (dark particles) are either in the form of dendritic crystals with entrapped liquid [13, 14] or in the form of

compact polygonal shapes. The polygonal form is more predominant at the HCR condition. J. Zhang et al. [15] have shown that morphology of Mg_2Si primary phase changes with increasing cooling rate when using a copper mould. The white α-Al grains can be also identified in all samples. It can be clearly observed that the eutectic morphology at high magnification (200X) for both the HCR and LCR samples are significantly changed with the addition of Mg, particularly at 6% Mg when compared to A390 alloy as shown in Fig.7. The grey eutectic silicon together with the α-Al grains show a coarse flake structure for A390 alloy cooled at both low and high rates (Fig.7a, b). However, the eutectic microstructure for 6% Mg alloys (Fig.7c, d) and 10% Mg alloys (Fig.7e, f) are similar and the eutectic silicon transforms into a fine, skeleton network with a Chinese script morphology, similar to the dark eutectic Mg_2Si.

The matrices of A390 and of the 10% Mg alloy at LCR condition are compared in Fig.8 using SEM images. The modification of the eutectic silicon is due to the decrease of the eutectic temperature with addition of Mg. Nafisi et al. [16] also investigated the effect of the reduction of eutectic temperature on modification of eutectic silicon morphology of A356 Al-Si alloy when Sr is added as modifier. In fact, they have attributed this temperature reduction to the eutectic nucleation temperature which has a direct effect on the number of potential nuclei found in the melt. This results in fewer barriers for nucleation with increasing nucleation temperature and thus a greater number of isolated eutectic Si particles may form, which result in the flake morphology [16] that was observed for A390 alloy. On the other hand, the interlamellar spacing λ and growth

velocity ν can be related by well known relation of $\lambda^2\nu$ = constant [17]. Consequently the variation in the spacing indicates a varying growth velocity which also depends on formation temperature. For A390 alloy the eutectic silicon reaction temperature is much higher than for the 6% and 10% Mg alloys, as shown before. The Factsage calculation for Scheil solidification of A390 alloy indicates that 73.5% of eutectic silicon phase is already solidified whereas the eutectic silicon for 6% and 10% Mg alloys is still liquid at 549 °C. The morphology of the eutectic silicon for A390 and 6% Mg alloys in HCR condition is compared by SEM image in Fig.9 where the surface were deep etched using 0.5% HF solution.

The intermetallic phases indicated by arrows in Fig.8 are solidified from the remaining liquid at the end of the solidification. As it was shown in Fig.5b, the small white blocky θ-$CuAl_2$ is the main intermetallic phase observed along with black blocky of $Cu_2Mg_8Si_6Al_5$ (Q phase) and plate-like β-Al_5FeSi. A new Fe-intermetallic phase was identified for the higher Mg-containing alloys where the β-Al_5FeSi formed in A390 is transformed to the quaternary intermetallic phase π-$Al_8FeMg_3Si_6$. It is difficult to detect this phase at low magnification using optical microscopy. Fig. 10 shows the SEM image of 10% Mg alloy at the LCR condition with optimum color-contrast showing the π phase associated the θ phase.

3.2 Rheocast microstructure

As described in the experimental procedure, the cooling condition for the rheocast samples is similar to the LCR condition with stirring during the continuous cooling solidification. A large segregation of primary phases was detected in the microstructure of the rheocast samples due to the shear force imposed on slurry during solidification. As a result, the microstructure is different in two distinct regions. The first region, at a radial distance between 2-3 mm adjacent to the crucible wall (near crucible zone shown in Fig. 2b) is the region where the all primary phases are concentrated as shown in left side images of Fig.11 for A390, 6% and 10% Mg alloys. The inner region next to the stirrer (the radial distance between crucible wall and stirrer is 8 mm) shows no primary phases. In this region, the globular α-Al grains from the matrix form aggregates as shown in right side images of Fig. 11. When the primary phases in the first region are compared with non sheared LCR samples in Fig. 6, it is clear that the solid fraction of primary phases is much higher in the rheocast (sheared) samples due to the segregation caused by the shear forces. The primary silicon of sheared A390 alloy (Fig.11a) also agglomerates. All three sheared samples show the increase of the size of the silicon particles when compared to the non sheared samples. This implies that the average shear rate of $\dot{\gamma} = 52$ s^{-1} cannot fragment the hard polygonal silicon but rather facilitates their growth. Lee et al [18] have proved that for hypereutectic Al-15.5%Si alloy, the significant fragmentation and changes of primary Si morphology occur during the isothermal stirring but little change is observed when a sample has been continuously cooled at a shear rate of $\dot{\gamma}$ =

200 s^{-1} and cooling rate of -0.03 $^{o}C\ s^{-1}$. Contrary to primary silicon, this higher shear rate is able to fragment the dendrite morphology of Mg_2Si primary phase crystals with entrapped liquid, as observed in Figs. 6c, e and forms polygonal shapes as shown in the micrographs. Therefore, the particle size of Mg_2Si primary phase for the high Mg-containing rheocast alloys samples (Figs.11c, e) is finer than for the non shared samples. In the inner region, the agglomerated α-Al grains are present only in the eutectic phase matrix. At high magnification these aggregates are separately shown from the matrix region because of their different microstructural characterises as shown in Fig. 12. The left and right hand images in Fig. 12 represent the region of the aggregated α-Al grains and the regions between these aggregations, respectively. For A390 alloys (Figs. 12 a, b) there is no significant difference due to the high fraction of α-Al grains in matrix. For the high Mg-containing alloys of 6% and 10% Mg, as shown in Figs. 12 c, d and Figs. 12 e, f, respectively, the α-Al grains are generally surrounded by intermetallic phases, mainly by the θ-phase. The fraction of silicon and Mg_2Si eutectic phases in the region of the aggregated α-Al grains is much smaller than in the region between these aggregates. Fragmentation of the eutectic silicon for the sheared A390 sample (Fig. 12b) occurred when compared to the non sheared sample as show in Fig. 7a. For the higher Mg content alloys, the skeleton network of eutectic silicon observed for the LCR condition, is completely destroyed and fragmented as shown in Figs 12d, f. For the rheocast samples with different Mg content, the morphology of eutectic silicon remains as individual flakes which become finer with increasing the Mg content.

Generally, the conventionally cast microstructures indicate that the eutectic morphology is significantly changed from a coarse flake structure to a fine and skeleton form with the addition of Mg to A390 alloy. This significant change of microstructure of the alloy occurs because the eutectic phase forms the main component of the microstructure. In addition, the solid fraction of primary phase increases with the addition of Mg as described previously. Therefore, it is expected that the addition of Mg to A390 alloy can increase the hardness of alloy, resulting in improving the wear behaviour, a very important property in application of this alloy.

For the rheocast tests, a large segregation of primary phases was detected in the microstructure of samples adjacent to the crucible wall. This indicates the outer layer of samples becomes harder than the inner layer (near to the stirrer) as a result of the geometry of the agitator used in this study. Finer and more fragmented eutectic silicon was observed for in the inner layer high Mg content alloys.

5. Conclusions

The thermodynamic prediction shows good agreement with cooling curve data and DSC experiments for the detection of starting point of eutectic formation of A390 alloy and for 6% and 10% Mg alloys. A reduction of the eutectic reaction temperature was detected for the 6% Mg alloy when compared to the A390 alloy. The eutectic temperature of 10% Mg alloy also showed no significant difference with the 6% Mg. This implies that beyond the 6% Mg content, the eutectic reaction temperature is almost

constant. For conventionally cast samples, large and individual flake eutectic silicon phase particles were observed in A390 alloy for both HCR and LCR samples. With the addition of Mg content the eutectic silicon particles change to a fine, skeleton network with Chinese script morphology, similar to the eutectic Mg_2Si. Primary Mg_2Si can also be formed as dendritic crystals with entrapped liquid as well as in polygonal shapes. However, the primary silicon morphology remains polygonal for both cooling rates. For the rheocast samples (rotation speed = 260 rpm, $\dot{\gamma}_{ave}$ = 52 s^{-1}), significant segregation was observed in the three samples due to the shear forces imposed during the solidification and the microstructure is different for two distinct regions. Almost all primary phases are concentrated in the region near the crucible wall (outer layer) whereas the second region (inner layer) next to the stirrer, shows no primary phases. Agglomerated α-Al grains with a globular morphology are present in the eutectic phase matrix. The increase of the size of the silicon particles was observed for sheared samples and implied that the average shear rate of $\dot{\gamma}$ = 52 s^{-1} cannot fragment the hard polygonal silicon but rather facilitates their growth. However, this shear rate is able to fragment the dendrite morphology of Mg_2Si primary phase crystals with entrapped liquid, and allows them to form of polygonal shapes. In contrast, fragmentation of the eutectic silicon for the sheared A390 sample was observed when compared to the non sheared sample. For the alloy with higher Mg alloys, the skeleton network of eutectic silicon observed in LCR condition is completely destroyed and fragmented.

Acknowledgements

The authors gratefully acknowledge the financial support from the Fonds Quebecois de Recherche sur la Nature et les Technologies (FQRNT) and Natural Sciences and Engineering Research Council (NSERC) of Canada.

List of figures

Fig.1: The liquid fraction versus temperature curves of A390, 6% Mg and 10 wt% Mg alloys calculated according to the thermodynamic predictions using the FACTSAGE software for the Scheil condition.

Fig. 2: (a) Schematic diagram of the apparatus used in this study and (b) the location of the sampled regions.

Fig. 3: Cooling curves for A390, 6% Mg and 10% Mg alloys for high cooling rate (HCR) condition as recorded from the thermocouple at the center of graphite crucible.

Fig. 4: The eutectic segment of the cooling curves tested at HCR (left curves) and LCR (right curves) for A390, 6% Mg and 10% Mg alloys

Fig.5: BSE (back scattered electron) image of A390 alloy for conventionally cast low cooling rate (LCR) sample. a) Large faceted primary silicon (1). ¨The matrix consists of binary Al + Si eutectic as well as the additional phases found in location A. b) Magnified zone of location A showing θ-$CuAl_2$ (2), Al (3), $Cu_2Mg_8Si_6Al_5$ (Q phase, 4) and β-Al_5FeSi (5) as well as c) the EDX (energy dispersive x-ray) analysis of phases (2), (4) and (5).

Fig.6: Overall microstructure of A390 alloy (a, b), 6% Mg alloy (c, d) and 10% Mg alloy (e, f) for different cooling rates. Right images for HCR samples and left images for LCR

samples. The light grey phase is silicon, the dark phase is Mg_2Si and white phase are α-Al grains.(50X).

Fig. 7: The eutectic microstructure of A390 alloy (a, b), 6% Mg alloy (c, d) and 10% Mg alloy (e, f) alloys for different cooling rates. Right images for HCR samples and left images for LCR samples. Light grey phase is silicon, dark phase is Mg_2Si and white phase are α-Al grains (200X)

Fig.8: Comparison of the eutectic and intermetallic (arrows) microstructures solidified at LCR condition for (a) A390 alloy and (b) 10% Mg alloy at the same magnification.

Fig.9: Deep etched images showing the morphology of the eutectic Si in A390 alloy (a) and 6% Mg alloy (b) for HCR condition at the same magnification.

Fig.10: The π-$Al_8FeMg_3Si_6$ phase observed in the 10% added Mg alloy at LCR condition.

Fig.11: The stir cast microstructure of A390 alloy (a, b), 6% Mg alloy (c, d) and 10% Mg alloy (e, f). Left images represent the region near to the crucible wall (outer layer) and right images belong to the region near to the stirrer (inner layer).

Fig.12: The microstructures near the stirrer (inner layer) for stir cast samples. A390 alloy (a, b), 6% Mg alloy (c, d) and 10% Mg alloy (e, f). Left images represent the region within agglomeration of the α-Al grains. Images at the right show the region of eutectic microstructures.

Table 1: Chemical analysis of A390 base alloy and AZ91 Mg alloy (wt.%).

	Al	Si	Cu	Mg	Fe	Mn	P	Ti
A390	Bal.	17.4	4.58	0.58	0.32	0.02	0.0003	0.02

	Mg	Al	Mn	Zn	Si	Ni	Cu	Fe
AZ91	Bal.	9.3	0.12	0.62	0.02	0.0006	0.0007	0.0046

Table 2: Comparison of the eutectic reaction temperature determined by thermodynamic prediction using Factsage, the measurement of cooling curves at LCR (-0.15 ± 0.05 °C s^{-1}), HCR (-1.0 ± 0.2 °C s^{-1}) and DSC test with cooling rate of 0.15 °C s^{-1} for three alloys.

	Predicted (°C)	Tested (°C) LCR	Tested (°C) HCR	DSC (°C) [7]
A390	566.2	563 ± 1	564 ± 1	563.09
+6% Mg	549.7	545 ± 1	544 ± 1	545.23
+10% Mg	549.2	543 ± 1	542 ± 1	543.63

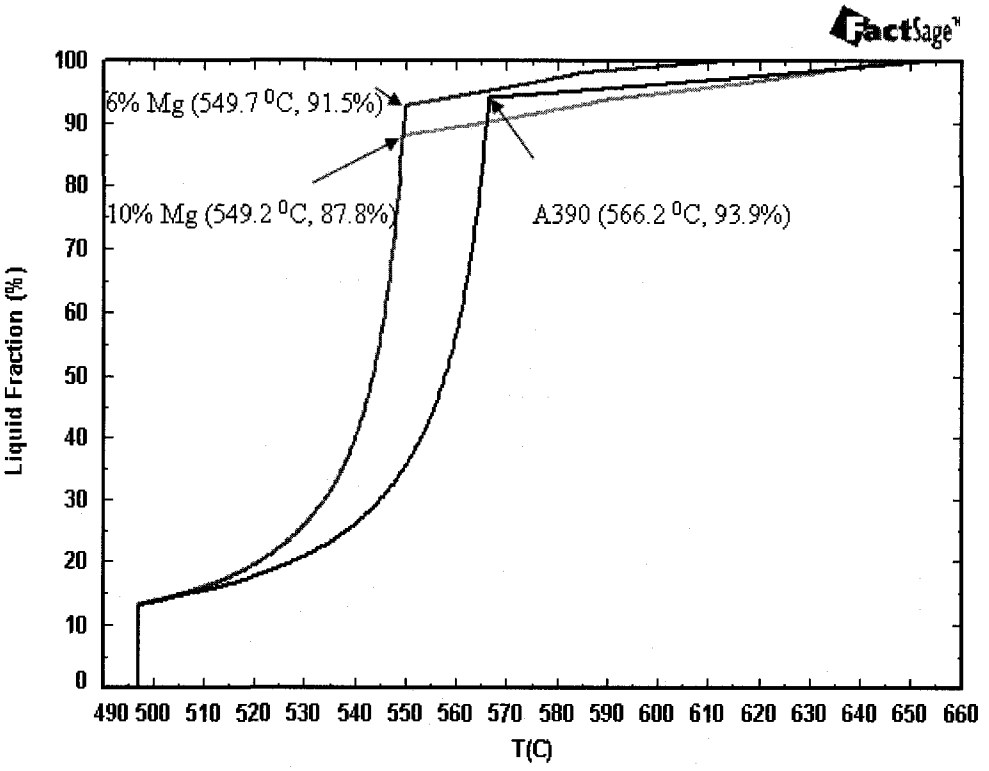

Fig.1: The liquid fraction versus temperature curves of A390, 6% Mg and 10 wt% Mg alloys calculated according to the thermodynamic predictions using the FACTSAGE software for the Scheil condition.

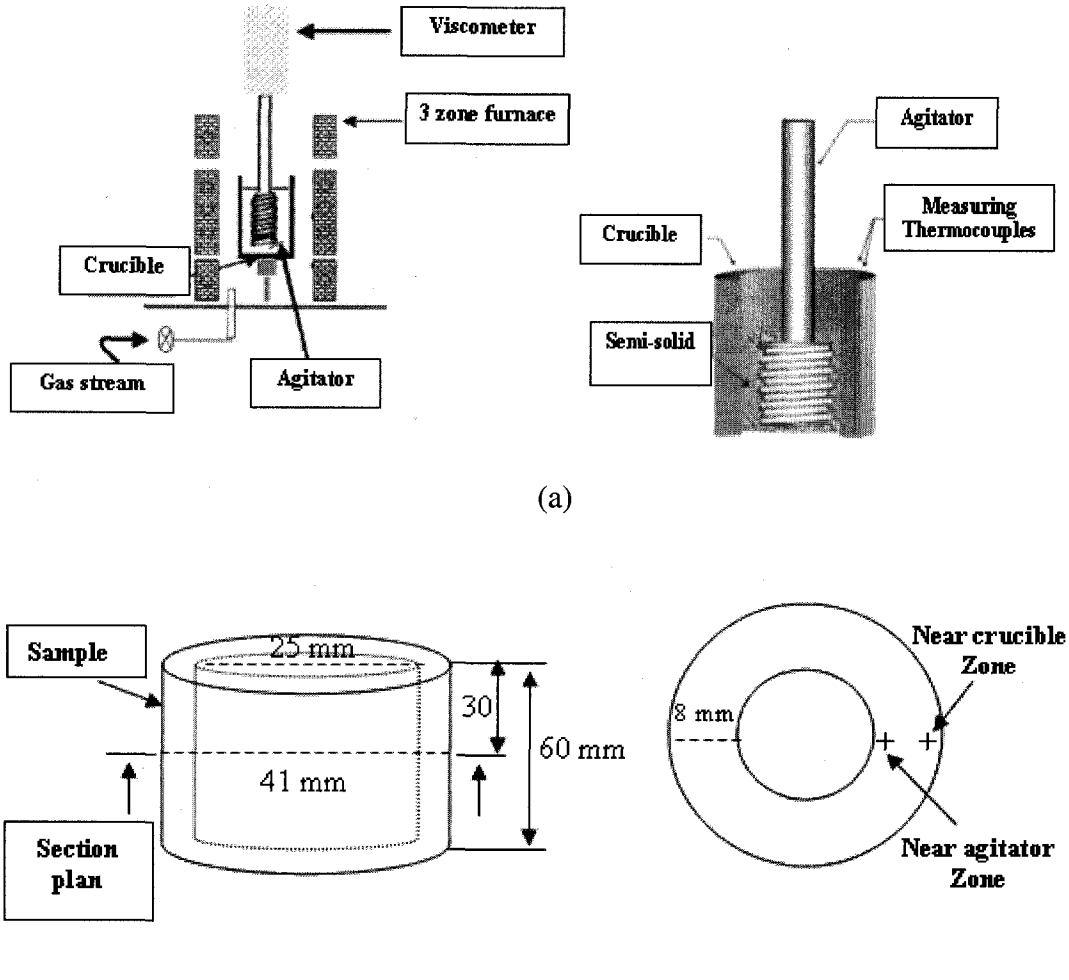

Fig. 2: (a) Schematic diagram of the apparatus used in this study and (b) the location of the sampled regions.

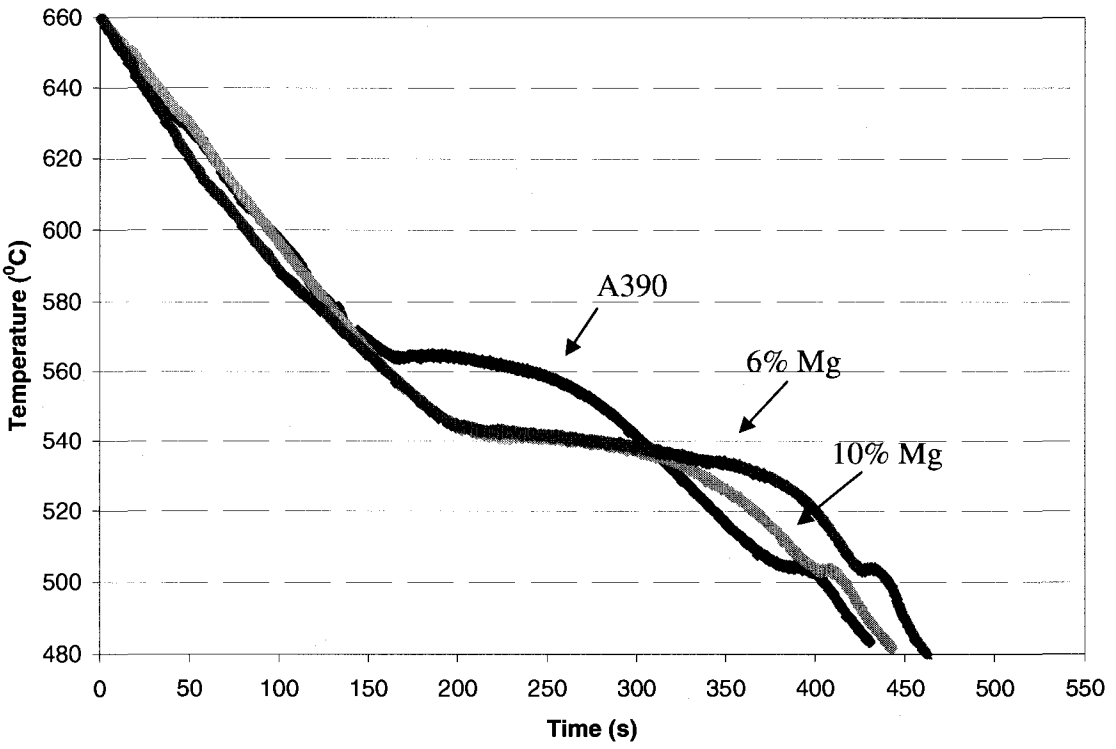

Fig. 3: Cooling curves for A390, 6% Mg and 10% Mg alloys for high cooling rate (HCR) condition as recorded from the thermocouple at the center of graphite crucible.

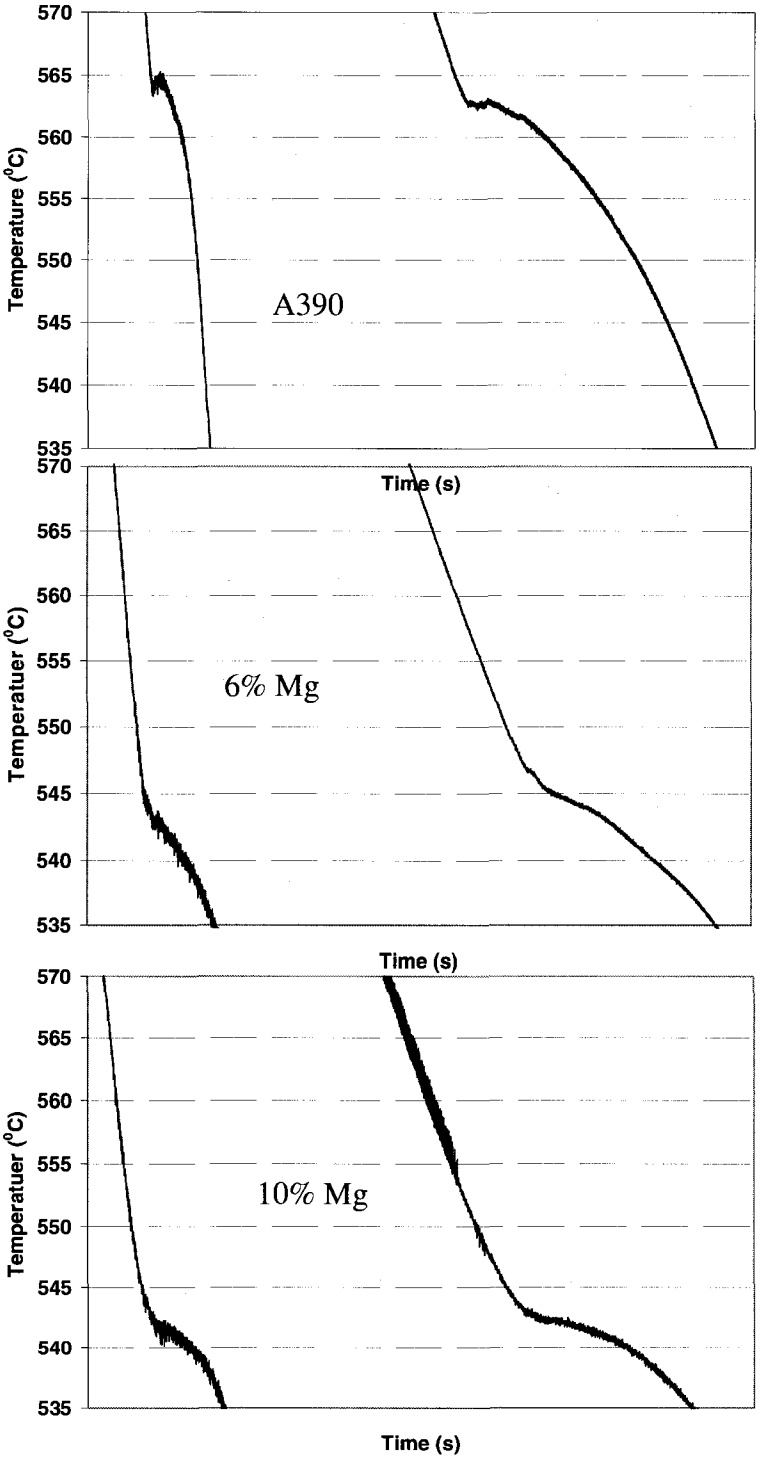

Fig. 4: The eutectic segment of the cooling curves tested at HCR (left curves) and LCR (right curves) for A390, 6% Mg and 10% Mg alloys.

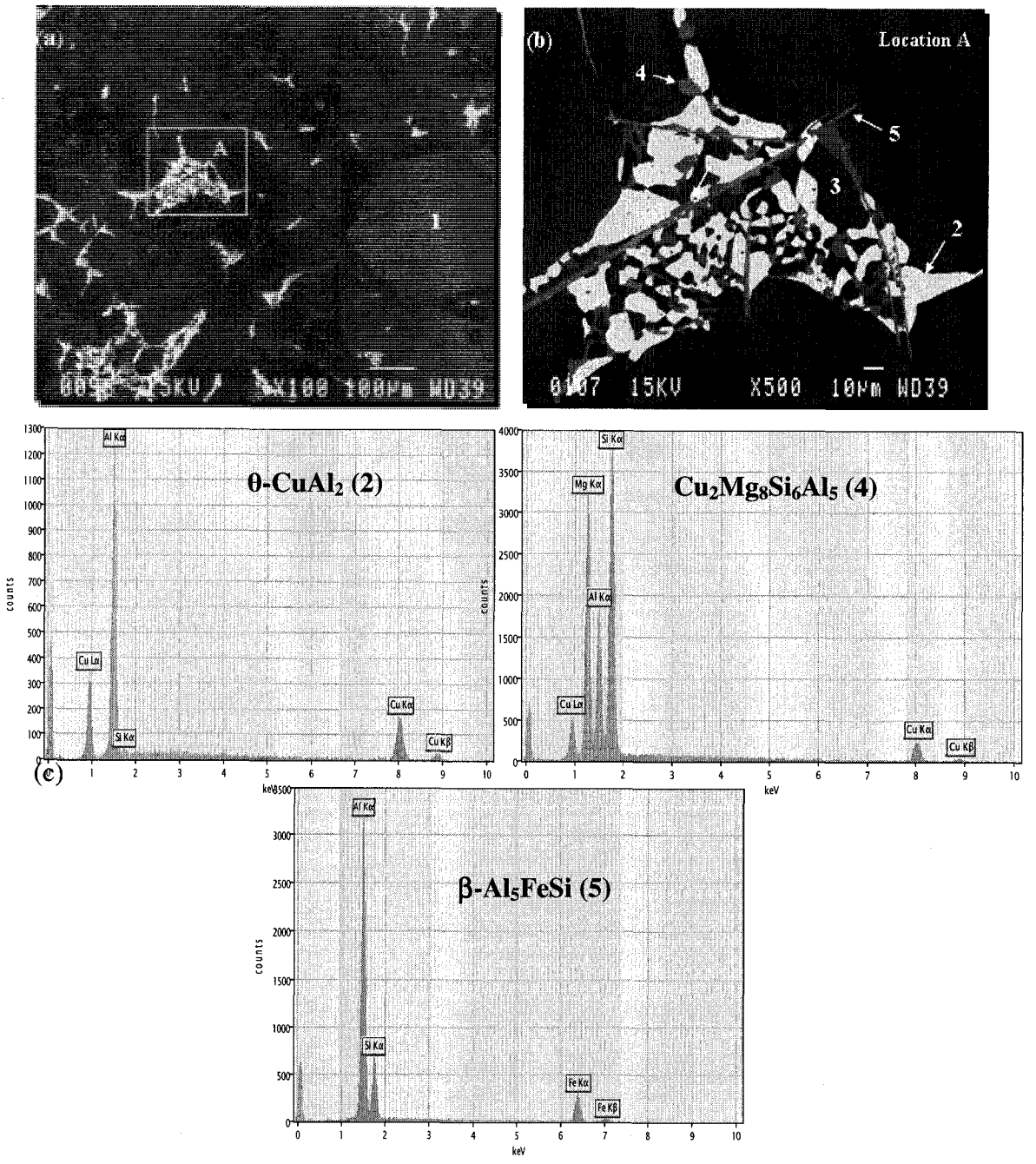

Fig.5: BSE (back scattered electron) image of A390 alloy for conventionally cast low cooling rate (LCR) sample. a) Large faceted primary silicon (1). The matrix consists of binary Al + Si eutectic as well as the additional phases found in location A. b) Magnified zone of location A showing θ-$CuAl_2$ (2), Al (3), $Cu_2Mg_8Si_6Al_5$ (Q phase, 4) and β-Al_5FeSi (5) as well as c) the EDX (energy dispersive x-ray) analysis of phases (2), (4) and (5).

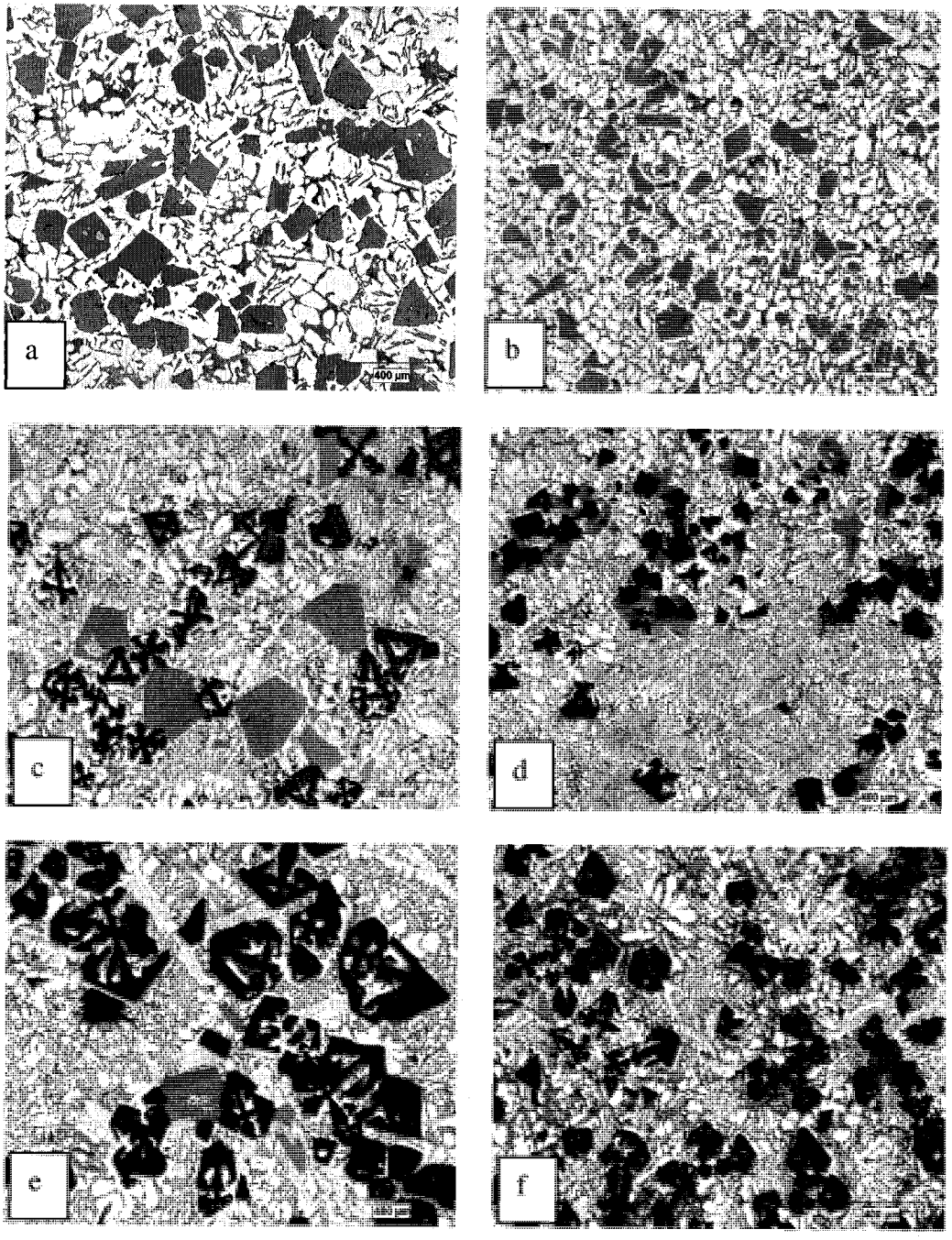

Fig.6: Overall microstructure of A390 alloy (a, b), 6% Mg alloy (c, d) and 10% Mg alloy (e, f) for different cooling rates. Right images for HCR samples and left images for LCR samples. The light grey phase is silicon, the dark phase is Mg_2Si and white phase are α-Al grains.(50X).

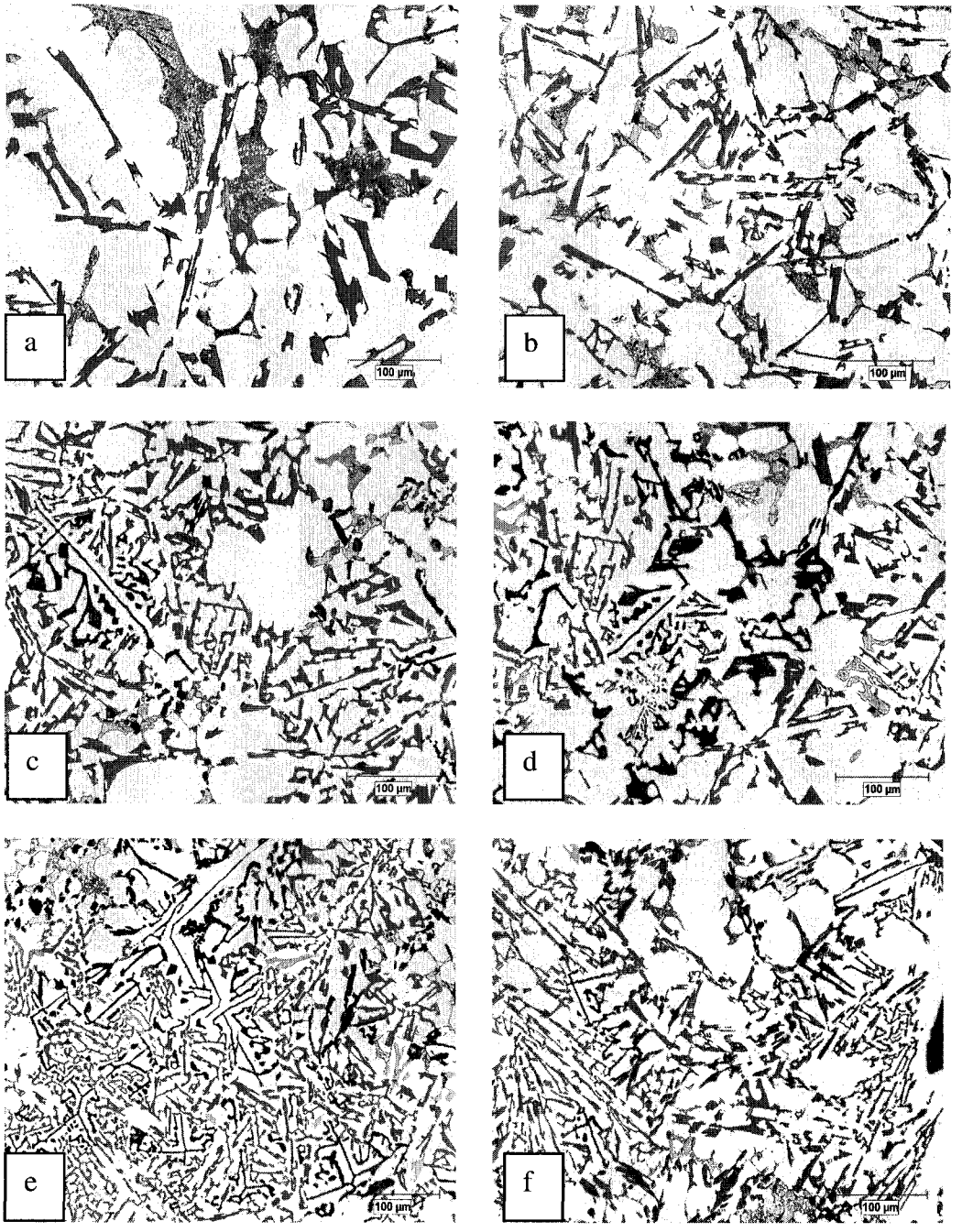

Fig. 7: The eutectic microstructure of A390 alloy (a, b), 6% Mg alloy (c, d) and 10% Mg alloy (e, f) alloys for different cooling rates. Right images for HCR samples and left images for LCR samples. Light grey phase is silicon, dark phase is Mg_2Si and white phase are α-Al grains (200X)

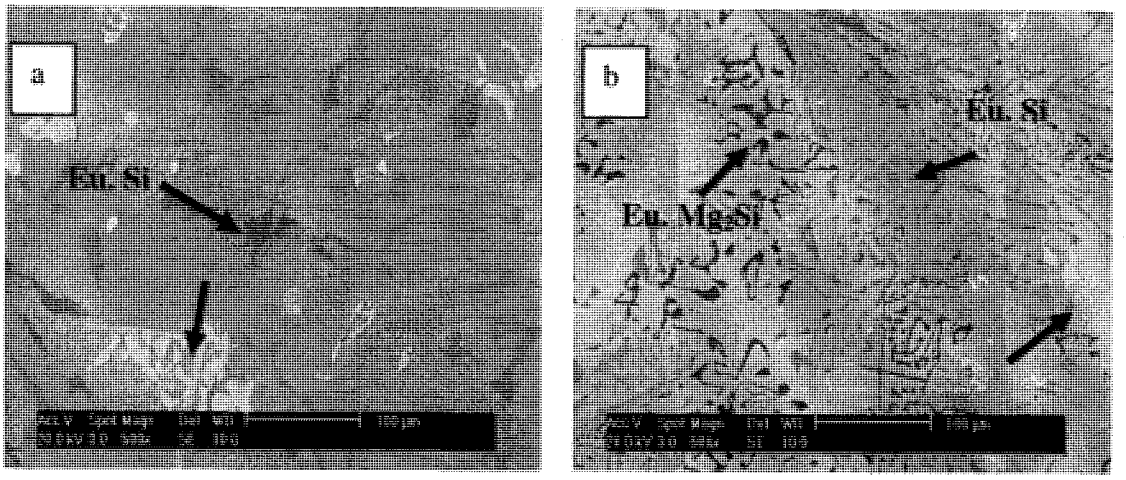

Fig.8: Comparison of the eutectic and intermetallic (arrows) microstructures solidified at LCR condition for (a) A390 alloy and (b) 10% Mg alloy at the same magnification.

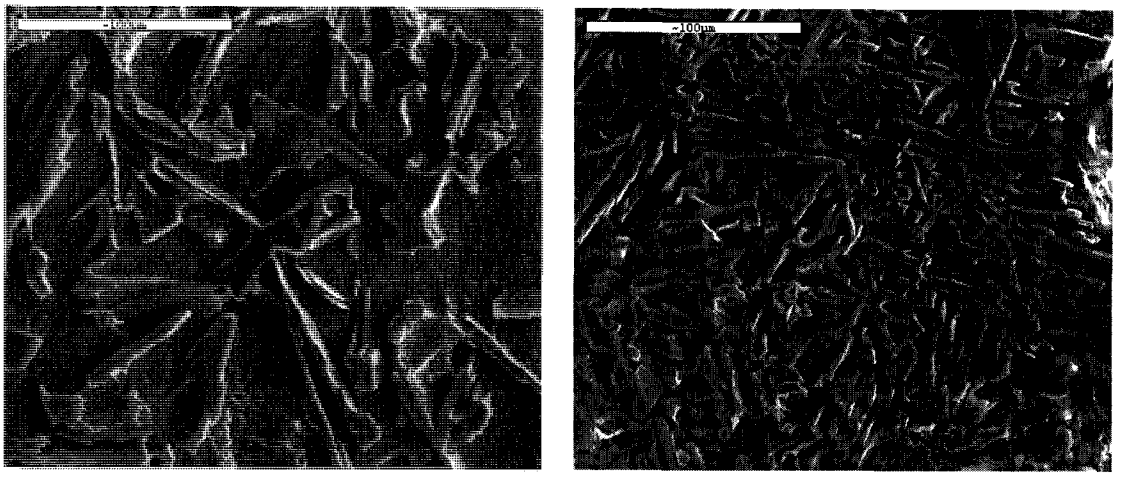

Fig.9: Deep etched images showing the morphology of the eutectic Si in A390 alloy (a) and 6% Mg alloy (b) for HCR condition at the same magnification.

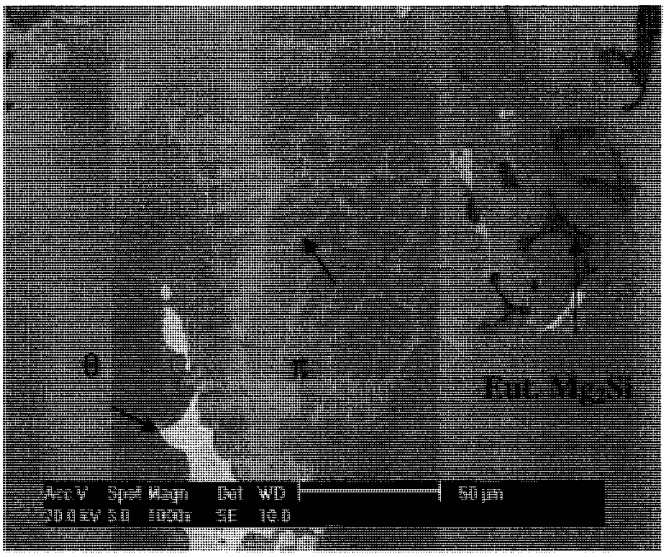

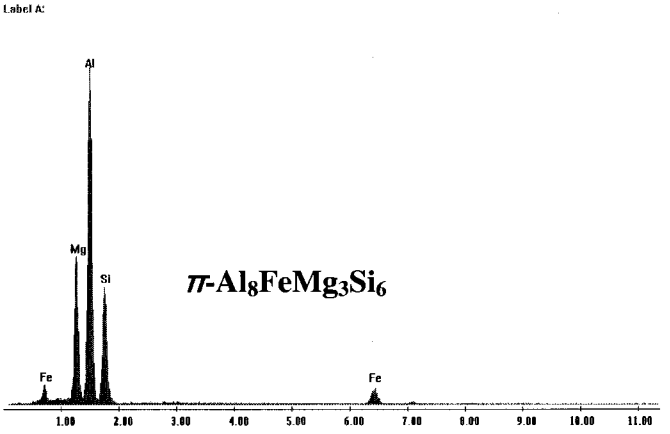

Fig.10: The phase π-$Al_8FeMg_3Si_6$ detected for 10% added Mg alloy at LCR condition.

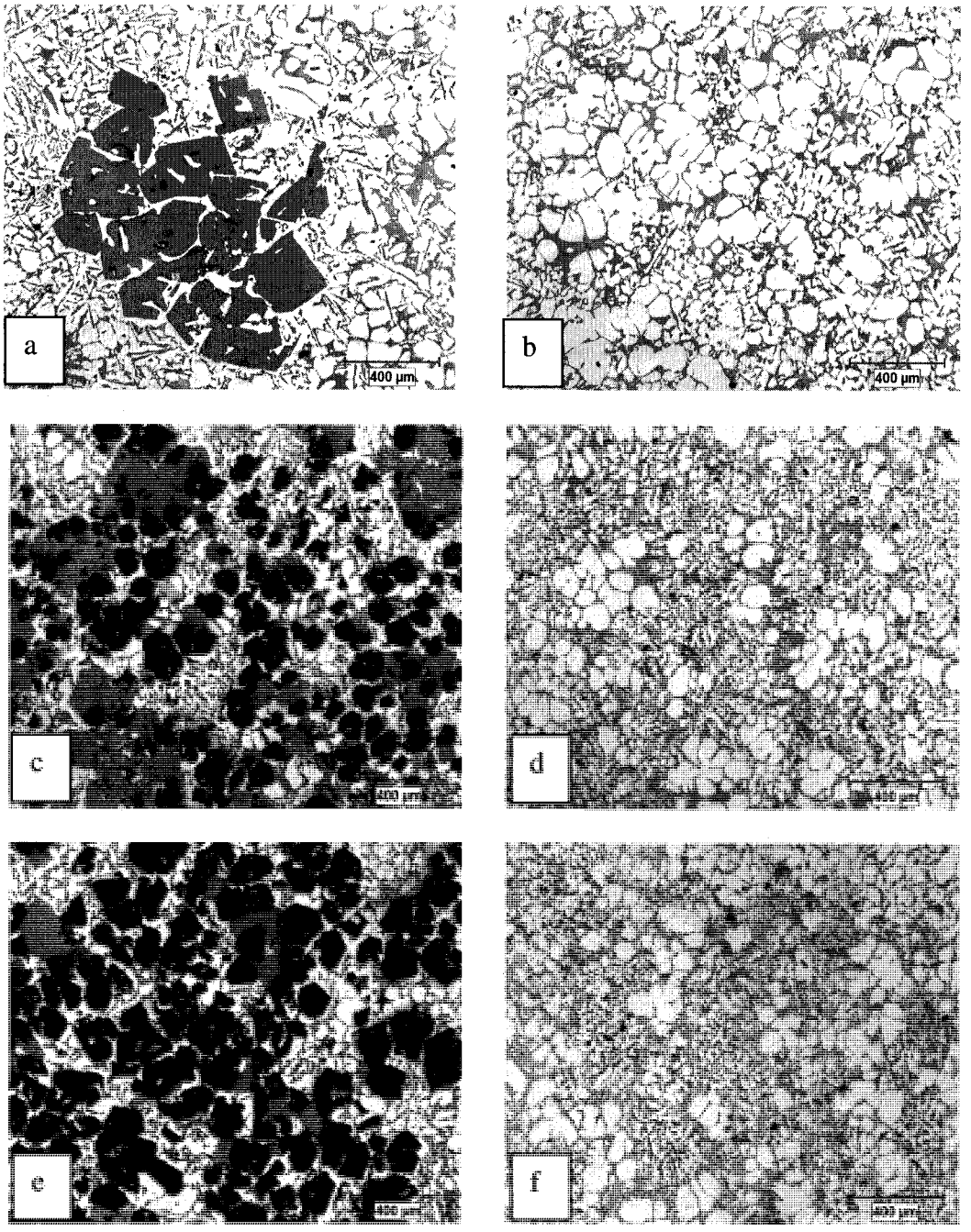

Fig.11: The stir cast microstructure of A390 alloy (a, b), added 6% Mg alloy (c, d) and added 10% Mg alloy (e, f). Left images represent the region near to the crucible wall (outer layer) and right images belong to the region near to the stirrer (inner layer).

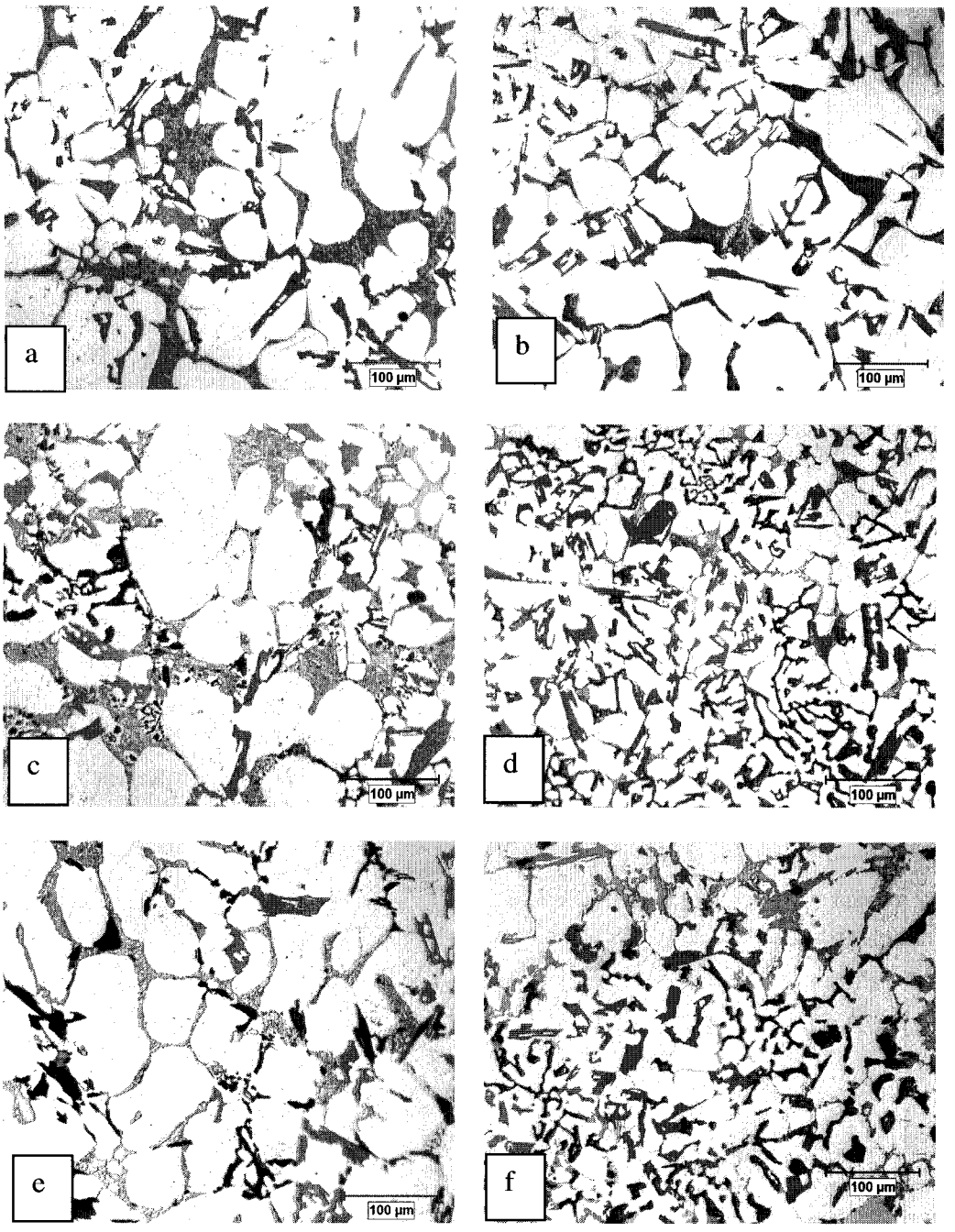

Fig.12: The microstructures near to the stirrer (inner layer) for stir cast samples. A390 alloy (a, b), added 6% Mg alloy (c, d) and added 10% Mg alloy (e, f). Left images represent the region within aggregation of the globular α-Al grains and right images belong to the region of eutectic microstructures.

References

[1] P. Kapranos, D.H. Kirkwood, H.V. Atkinson, J.T. Rheinlander, J.J. Bentzen, P.T. Toft, C.P. Debel, G.Laslaz, L.Maenner, S.Blais, J.M. Rodriguez-Ibabe, L. Lasa, P. Giordano, G. Chiarmetta and A. Giese, *J Mater Proc Tech* **135** (2003), p. 271.

[2] Y.G. Zhao, Q. D. Qin, Y. Q. Zhao, Y. H. Liang and Q. C. Jiang, *Materials Letters*, **58** (2004), p. 2192.

[3] C.L. Xu, Q.C. Jiang, Y.F. Yang, H.Y. Wang and J.G. Wang, *J Alloys and Compounds* **422**(2006), P. L1

[4] Jian Zhang, Zhongyun Fan, Yuqing Wang and Benlian Zhou, *Materials & Design* **21** (2000), P. 149.

[5] Q.C. Jiang, H.Y. Wang, Y. Wang, B.X. Ma and J.G. Wang, *Mater Sci Eng A* **392** (2005), P. 130.

[6] A.R. Hekmat and F. Ajersch, Thermodynamic evolution of hypereutectic Al-Si (A390) alloy with addition of Mg, (to be published).

[7] D. Liu, H.V. Atkinson and H. Jones, *Acta Mater* 53 (2005), P. 3807.

[8] Jian Li, M. Elmadagli, V.Y. Gertsman, J. Lo and A.T. Alpas, *Mater Sci Eng A* **421** (2006), P. 317.

[9] M. Elmadagli and A.T. Alpas, *Wear* **261** (2006), p. 367.

[10] S.S. Sreeja Kumari, R.M. Pillai, T.P.D. Rajan and B.C. Pai, *Mater Sci Eng A* **460-461**
(2007), p. 561.

[11] R. Taghiabadi, H.M. Ghasemi and S.G. Shabestari, *Mater Sci Eng A* **490** (2008), p. 162.

[12] S. Nafisi, D. Emadi, M.T. Shehata and R. Ghomashchi, *Mater Sci Eng A* **432** (2006), p. 71.

[13] Q.C. Jiang, H.Y. Wang, Y. Wang, B.X. Ma and J.G. Wang, *Mater Sci Eng A* 392 (2005), p. 130

[14] Q.D. **Qin**, Y.G. Zhao, W. Zhou and P.J. Cong, *Mater Sci Eng A* **447** (2007), P. 186.

[15] Jian Zhang, Zhongyun Fan, Yuqing Wang and Benlian Zhou. *Mater & Design* **21**(2000), p. 149.

[16] Shahrooz Nafisi, Reza Ghomashchi, *Mater Sci Eng A* **415** (2006), p. 273.

[17] J. Zhang, Z. Fan, Y.Q. Wang and B.L. Zhou, Mater Sci Tech 17 (2001), p. 494.

[18] J.I. Lee, H.I. Lee and M.I. Kim, *Scr Metal et Mater* **32** (1995), p. 1945.

Paper 3

Effect of isothermal ageing on the semi solid microstructure of rheoprocessed and partially remelted of A390 alloy with 10% Mg addition

Alireza, Hekmat-Ardakan and Frank Ajersch

Submitted for publication in Material Characterization

Feb 2009

5-4 Effect of isothermal ageing on the semi solid microstructure of rheoprocessed and partially remelted of A390 alloy with 10% Mg addition

Alireza, Hekmat-Ardakan and Frank Ajersch
École Polytechnique de Montréal, Dép. de Génie Chimique
Montreal, Quebec, Canada, H3C 3A7

Abstract

The semisolid microstructure of hypereutectic Al-Si alloy with 10% Mg was investigated for two different processing routes: 1) rheocasting after stirring at a rotation speed of 260 rpm and 2) partial remelting after fast cooling in a steel mould. The results show that the morphology of α-Al grains becomes more globular during isothermal holding time for both processing cases. However, at the same isothermal condition, the size of the α-Al phase particles for rheocast samples are larger and their morphology are more globular than for the samples examined after the partial remelting process. The microstuctural evolution, size and shape of the primary Mg_2Si as well as the silicon particles during isothermal ageing in the semi solid region was also investigated for the two processing conditions.

Keywords: Semi solid processing, Aluminium alloys, Isothermal heat treatment, globular, Magnesium.

1. Introduction

Semisolid metal (SSM) processing is an innovative technology for the treatment of alloys in the semi solid state. This technique takes advantage of the rheological characteristics of suspensions of solid materials in liquids. A low apparent viscosity can be achieved due to the thixotropic behaviour of the metallic slurry when high shear stresses are applied, generally resulting in shear thinning [1-2]. It is observed that the dendritic morphology is transformed into a globular or non dendritic form and the solid phase particles are dispersed in a liquid matrix resulting in better castability due to the lower viscosity. In addition, the forming temperature and heat content as well as the shrinkage of semi solid slurry are significantly reduced resulting in a "near net shaping" process [3]. Processing can be carried out by two methods: Rheocasting and Thixoforming [4]. In rheocasting, the molten liquid is mechanically or electromagnetically stirred while being cooled to produce non dendritic slurry for making a product. During thixoforming, reheated semi solid ingots which exhibit desirable microstructure are shaped into parts by using a die cast machine. The ingots (feed stocks) must be prepared with an appropriate microstructure as a starting material for this process. Magnetohydrodynamic (MHD) stirring [5], cooling slope casting (CS) [6] , strain induced melt activated (SIMA) [7] as well as recrystallisation and partial melting (RAP) [8] are other methods that can be used to produce a semi solid slurry.

Hypereutectic Al-Si alloys such as A390 alloy (Al-17%Si-4.5%Cu-0.5%Mg) exhibit outstanding wear and corrosion resistance, high thermal conductivity, excellent castability, high strength, together with reduced density which are widely used in the automotive, aerospace, and military industries [9-10]. This is due to the presence of the hard primary silicon particles dispersed in the matrix. However, for conventional casting, the primary silicon appears in the form of coarse polygonal crystals which lead to poor properties of these alloys. On the other hand, hypereutectic Al-Si alloys with high Mg content can also be used to form in situ Mg_2Si/Al-Si metal matrix composite alloys which also have high potential as a wear resistant materials. In terms of properties and solidification behaviour, many similarities exist between Mg_2Si and Si [11] resulting in super light wear resistant materials due to their low density when compared with aluminium. The hard intermetallic particles of Mg_2Si in the composite alloy act in the same way as the hard primary silicon particles and make it ideal for high wear resistance applications. This study presents the ageing characteristics of the alloy in terms of the evolution of two types of hard particles in the microstructure of hypereutectic Al-Si alloy with high Mg content.

2- Experimental procedure

The 10 wt% Mg alloy was produced by adding AZ91 Mg-base commercial alloy (this alloy is toxic) into the molten A390 alloy at 750 ^{o}C (about 100 ^{o}C above the melting temperature). About 20% additional AZ91 wrapped in Al foil was added the molten

A390 alloy to account for oxidation loss of Mg. The chemical compositions of the base alloys and the product alloy are shown in Table 1. Silicon and copper were also added to the melt in order to keep the chemical composition of these elements in the test alloy at the same level as formed in the A390 composition. The melt was degassed with argon and hand stirred for two minutes before pouring into a steel mould with three 35 ∅× 120 mm cylindrical cavities. These ingots were used as the starting material (feedstock) for the partial remelting (thixocast) experiments. Subsequently, 80 gram ingots was cut and placed into a 41 ∅× 120 mm graphite crucible with wall thickness of 10 mm. Two K-type thermocouples were placed in the crucible wall near the surface of melt and near the bottom of crucible in order to measure the temperature during the process. The samples were then heated at a rate of 0.25 °C/s in a 3 zone electrical resistance furnace to the semisolid temperature of 560± 1 °C where liquid, Mg_2Si and Si particles co-exist. In another test the sample was heated to 540 ± 1 °C where Mg_2Si, Si and Al co-exist in the liquid phase. These temperatures were selected on the basis of previous experimental studies of the cooling curves and the solidification behaviour of the A390 and with 10% Mg alloy and the DSC (Differential Scanning Calorimeter) mesurements which were also evaluated using Factsage® software [12-13]. For the thixocast tests, samples were taken from the melt by using a small spatula and quenching in the water after isothermal holding times of 30, 60 and 180 minutes in the semi solid region.

For the rheocast tests, the high Mg content alloy was continuously cooled from the liquid state at 750 °C and then held at the isothermal temperature of 540± 1 °C. The

semi solid material is then stirred by immersing a spiral grooved cylindrical stirrer at this temperature for a period of 30, 60 and 120 minutes at 260 rpm representing a shear rate of 52 s^{-1}. At the end of each period, the samples were quickly removed and quenched in the water.

All samples were mounted, polished conventionally and etched by using 0.5% HF solution for microstructural analyses. The Clemex software was used to analyse the evolution of the particle morphology and size observed in the microstructure. The shape factor is defined by the relation $F = \frac{4\pi A}{P^2}$ where A and P represent respectively the area and perimeter of the particles measured by the image analyser.

3. Results and discussion

3.1. Microstructural evolution during partial remelting

Fig.1 shows the microstructure of 10% Mg alloy rapidly solidified from the liquid state by pouring into a steel mould. This was used as the starting material for partial remelting process. The microstructure shows dendrites of Mg_2Si with a mean size of 47 μm, polygonal silicon crystals with a mean size of 80 μm and α-Al grains with a mean size of 32 μm. The remaining matrix network is composed of needle-like eutectic silicon particles and Chinese script Mg_2Si particles. It appears that all polygonal silicon

particles have nucleated and grown on the dendritic Mg_2Si particles which act as a heterogeneous nucleation site.

Fig.2a-c show the evolution of the semi solid microstructure of 10% Mg alloy held at an isothermal temperature of 560 °C for 30, 60 and 180 minutes. At this temperature the liquid phase co-exists with Si and Mg_2Si particles. As observed in Fig.2a, the morphology of primary Mg_2Si is transformed to irregularly shaped particles in the form of "rosettes", with an aspect that is between a dendritic and globular structure. The shapes become more elliptic (Fig.2b-c) with a mean size increasing from 61 to 79 μm with increasing holding time as shown in Fig.3. The coarsening of the particles first increases rapidly and then becomes more gradual up to a point where the particle size changes little with increased holding time. A number of Mg_2Si particles contain entrapped liquid (black arrows in Figs. 2 and 6) which decreases with the holding time. The coalescence of two or more Mg_2Si particles forming a 'neck' is indicative of a coarsening mechanism [14] as observed in Fig. 2a-c as well as in Fig. 4. The region indicated by the white arrow in Fig. 4 at a holding time of 180 minutes shows the coalescence of two Mg_2Si particles which eventually change into an elliptic shape. Nonetheless, it is believed that coalescence and Ostwald ripening mechanisms (dissolving of small particles and transferring their mass to the larger particles [24]) are the two important mechanisms that control grain coarsening in the semi solid state [15]. Fig. 4 also shows some Chinese script eutectic Mg_2Si phase particles (black arrows) together with the small α-Al grains (white phase) located in the matrix network. From

thermodynamic considerations, the presence of α-Al is not predicted at 560 °C. Its presence is possibly caused by the time interval of removing and handling of the samples resulting in a decrease of temperature and the start of solidification of α-Al phase before quenching in the water. These delays can be different for each test resulting in α-Al grains with different sizes. Qin et al. [16] have also observed these small α-Al grains during coarsening period of Mg_2Si/Al composite alloy.

On the other hand, the morphology of primary silicon particles does not change during this process and remained polygonal in all cases. However, the size distribution of silicon varies significantly whereas the mean size tends to decrease for holding times greater than 60 minutes as shown in Fig. 5. The reason for this anomaly is due to the nucleation of the silicon on Mg_2Si. The interface orientation between the two phases coincides with either {111} Si/ {001} Mg_2Si or {111} Si/ {111} Mg_2Si faceted planes because both of Mg_2Si and Si have similar crystal structures with {001}, {111} [17-18] and {111} close-packed facets [19-20], respectively. It was observed that the presence of Mg_2Si particles near the silicon particles limits their coarsening as shown in Fig. 6.a. With increasing holding time at isothermal conditions the coarsened and agglomerated Mg_2Si can limit and/or suppress the growth of silicon as shown in Fig. 6.b. Eventually, the fragmentation of silicon particles takes place resulting in decreasing their size, Fig. 6.c. The variation of the total solid fraction of silicon and Mg_2Si particles with increasing holding time was found to be essentially constant, as shown in Fig. 7.

The temperature of 540 °C corresponds to the region below the eutectic reaction temperature where α-Al, Mg_2Si and Si particles co-exist in the liquid phase (f_{Liquid} = 39%, $(f_s)_{Al}$ = 41%, $(f_s)_{Mg_2Si}$ = 13% and $(f_s)_{Si}$ = 7%). The solidification of the liquid phase (quenching from this state) shows a matrix network with a eutectic morphology. Fig.8a-c shows the evolution of the microstructure at this isothermal temperature with increasing holding time. The evolution of the morphology of Mg_2Si, the presence of the entrapped liquid and the coalescence of Mg_2Si at 540 °C are similar to their characteristics at 560 °C (Fig.2). However, the mean size of Mg_2Si particles varies less when compared with the coarsening of Mg_2Si at 560 °C as shown in Fig.3. For both cases, the coarsening rate first increases rapidly and then becomes gradual with increasing [16] holding time. However it is more pronounced at the higher temperature (high liquid fraction) of 560 °C. A lower coarsening rate is observed for lower liquid fraction [21] particularly during the period of time between 30 and 60 minutes. It was demonstrated that a temperature difference of ± 1 °C at this composition can change the liquid fraction by 13% according to the Factsage® calculations. However this variation of liquid fraction is negligible at 560 °C where the solidification rate of primary phases in this region is quiet slow.

The variation of holding time has also significant effect on the morphology and size of the α-Al particles. Fig.8a shows that they become more globular with mean size of about

80 μm. With increasing holding time, the particles become more spheroid and the mean size increases as well.

At 540 °C, small dispersed silicon particles (indicated by arrows in Fig.8a-c) were observed in the microstructure with increasing holding time with irregular shapes and the sizes between 10 and 40 μm. These silicon particles are typical of eutectic silicon which is transformed to irregular shapes during isothermal holding conditions and significantly decrease the mean size of the silicon particles. On the other hand, small rod shaped Mg_2Si particles [22] transformed from the Chinese script eutectic form was also detected in some regions in the microstructure as shown in Fig.9. Normally the eutectic silicon is the most important component of matrix network and the eutectic Mg_2Si is a minor constituent in the matrix network. This contribution is almost negligible compared to the eutectic silicon at 540 °C. With increased holding time this fraction becomes even smaller and indicates that the morphological transformation of these small particles takes place during the isothermal holding time.

3.2. Microstructural evolution during rheocasting

During the rheocasting process, the alloy was continuously cooled from the liquid state at a rate of 0.15 ± 0.05 °C s^{-1} down to the given isothermal temperature of 540 °C and then sheared at 260 rpm (52 s^{-1}). The microstructural evolution during shear was investigated for isothermal holding times of 30, 60 and 120 minutes. Fig.10 shows the microstructure of alloy after simple continuous cooling before isothermal shearing. The

microstructure shows large equiaxed dendrites of Mg_2Si, large polygonal silicon crystals nucleated on Mg_2Si, dendritic α-Al and a eutectic matrix network containing of eutectic silicon. This is representative of the microstructure at the beginning of the isothermal rheocasting process at 540 °C. Fig.11a-c shows the microstructural evolution with shear for isothermal stirring times of 30, 60 and 120 minutes. The fragmentation of Mg_2Si particles takes place during isothermal rheoprocessing. Fig.11a shows that the morphology of Mg_2Si becomes degraded by fragmentation of the large equiaxed dendrite shape solidified at the beginning of the isothermal process (see Fig.10) with increased stirring time. As a result, the Mg_2Si particle size for rheocast samples is certainly higher than for the partially remelted case. The rounded tip morphology is due to the breakdown of the dendrites by fragmentation and collision of particles of Mg_2Si during isothermal shearing. With increasing holding time, the fragmentation increases for all Mg_2Si particles and morphology tends to be globular as shown in Fig.11c. As shown in Fig 13a, b, some regions were observed after 120 minutes holding time where the high fraction of fragmentation debris has relocated in the melt around the α-Al grains. This behaviour was not detected the case of the tests with 30 and 60 minutes holding time.

Fig.12a-b compares the effect of holding time at 540 °C on the mean size and the shape factor of α-Al grains after rheocasting and after partial remelting. Both the particle size and shape factor for rheocast samples are higher than in the partial remelting samples. The coarsening of the particles for the rheocast case increases significantly with

increasing holding time in comparison with partially remelted samples as shown in Fig.12a. According to the theory of Ostwald ripening, the coarsening of the particles for isothermal conditions can be described by the Lifshitz-Slyozov-Wagner (LSW) equation [23]:

$$d^n - d_0^n = Kt \qquad (2)$$

Where d_0 is the initial particle size, d is the size at the holding time t, n is the coarsening exponent and K is the coarsening rate. For coarsening controlled by volume-diffusion only, the value of n equals 3. Ji et al. [24] have found that the coarsening exponent n in the LSW equation increases to 8.2 and 12.7 for AZ91D Mg base alloy when a rotation speed of 300 and 800 rpm are applied, respectively. The value of k also increases with increased rotation speed. Shear promotes the isothermal coarsening process as is clearly shown in Fig.12a for the rheocast samples when compared to the partial remelting case. The shape factors of α-Al particles in the rheocast samples are also more spherical than for the partially remelted samples as shown in Fig.12b. The globular shaped particles may be formed by fragmentation of dendrite arms at the beginning of the isothermal coarsening due primarily to forced convection caused by shear flow [24]. The isothermal coarsening can be attributed partly to the Ostwald ripening or to the collision and subsequent bonding of particles at a constant volume fraction during coarsening time [24]. On the other hand, shear can also reduce the agglomeration of particles. The semi solid slurry can therefore attain a dynamic equilibrium between agglomeration and de-

agglomeration. During the coarsening process the morphology changes from dendrite to rosette and eventually to globular shapes.

The fragmentation of silicon was not observed in the rheocast samples and the morphology changed little but increasing in size with stirring time. Some silicon particles with 120 minute stirring time were found to increase to 300 μm, as shown in Fig 13a as a result of the effect of rotation speed on particle coarsening. In contrast to the microstructure of partially remelted samples, the silicon particles tend to separate from the Mg_2Si particles due to the presence of intensive convective shear. On the other hand, the eutectic silicon illustrated in Fig 11a-c, forms small polygonal particles instead of a needle like network [25]. However, the size of these silicon particles is larger than the eutectic silicon phase particles for the partially remelted case with diameters between 30 and 70 μm with increasing stirring time.

4. Conclusions

The α-Al phase particles for the rheocast samplesof hyper-eutectic Al-Si alloy with 10% Mg, become more globular and increase in size when compared to the partially remelted samples at the same isothermal coarsening temperature of 540 ± 1 °C.

For the partially remelted samples, the Mg_2Si particles are transformed into irregular shapes after 30 minutes and become more elliptic with increasing holding time. However, the coarsening rate at higher liquid fractions (560 ± 1 °C) is greater than at

540 ± 1 °C, particularly at the holding times between 30 and 60 minutes. The fragmentation of Mg_2Si particles takes place during isothermal coarsening and the morphology of Mg_2Si transforms to a degraded form of the large equiaxed dendrite shapes solidified at the beginning of the isothermal process. The morphology becomes more globular with stirring time. The fragmentation debris of Mg_2Si particles was also observed with increasing stirring time specifically after 120 minutes.

In contrast, the polygonal silicon particles for the partially remelted samples decrease in size with holding time between 60 and 120 minutes. This phenomenon was not detected for sheared samples where the silicon particles coarsened with increasing stirring time. At 540 ± 1 °C, the morphology of the eutectic silicon is transformed from the needle like to small irregular and/or polygonal shape for both processing cases.

The microstructure of the rheoprocess and the thixoprocess samples indicated that, contrary to the considerable morphology evolution for Mg_2Si particles to globular form for thixoprecess, the significant morphology evolution of α-Al particles for the rheoprocess samples was observed when compared to the thixoprocess samples.

Acknowledgements

The authors gratefully acknowledge the financial support from the Fonds Quebecois de Recherche sur la Nature et les Technologies (FQRNT) and Natural Sciences and Engineering Research Council (NSERC) of Canada.

List of figures

Fig.11: Evolution of the microstructure at 540 °C (a) 30 (b) 60 and (c) 120 minutes for rheocast samples. Mg_2Si (black), polygonal silicon (grey), small eutectic silicon particles (pointed by arrows) and α-Al grains (white) are observed.

Fig.12: Comparison of the effect of isothermal holding time on the particle size (a) and the shape factor (b) of α-Al at 540 °C for partially remelted and rheocast samples.

Fig.13: Microstructure of some regions in the rheocast sample after 120 minutes holding time at 540 °C. (a) High debris of fragmentation of Mg_2Si particles (indicated by arrow) (b) fragmentation debris at high magnification.

Table 1: Chemical analysis of A390 base alloy, AZ91 Mg alloy and test ingot (wt. %).

	Al	Si	Cu	Mg	Fe
A390	77.8	16.7	4.58	0.58	0.32
AZ91	9.3	0.02	0.0007	90.6	0.0046
Test Alloy	69.0	16.83	4.12	9.73	0.28

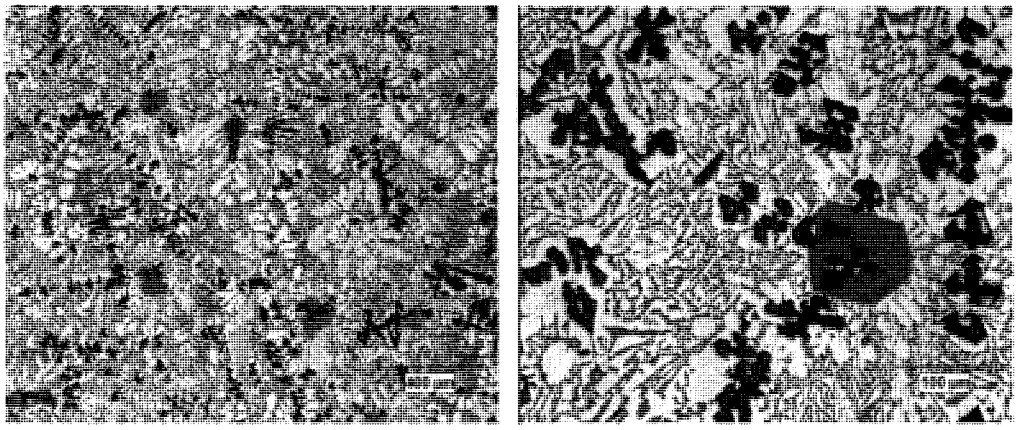

(a) (b)

Fig.1: Microstructure of 10% Mg alloy rapidly solidified from liquid by pouring into a steel mould (a) 50X and (b) 200X. The microstructure contains the dendritic grains of α-Al (white), equiaxed dendrites of Mg_2Si (black), polygonal silicon (grey) particles and the eutectic matrix.

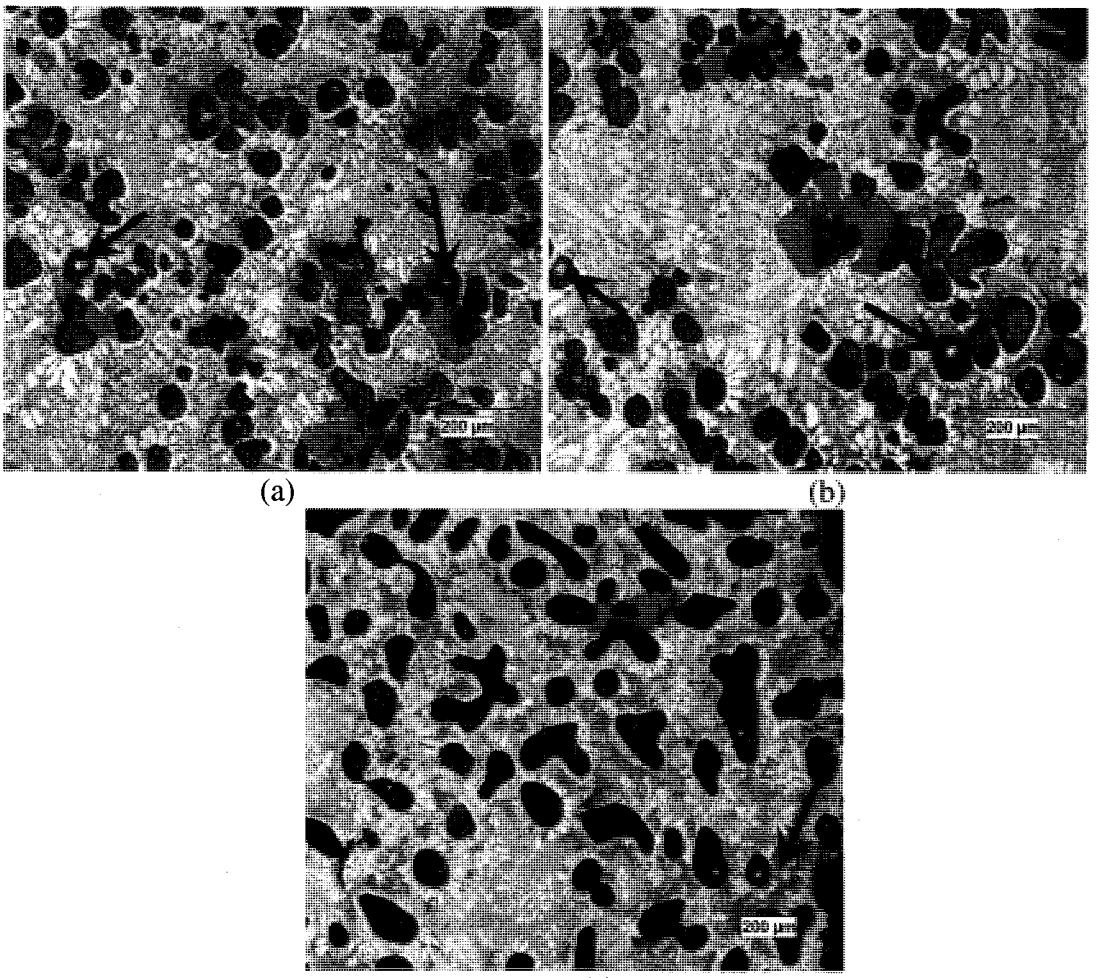

Fig.2: Evolution of the semi solid microstructure of the partially remelted 10% Mg alloy at isothermal temperature of 560 °C after holding times of (a) 30 (b) 60 and (c) 180 minutes. Mg_2Si (black), polygonal silicon (grey) and some small α-Al phase particles (white) are observed. The arrows show the Mg_2Si particles with entrapped liquid

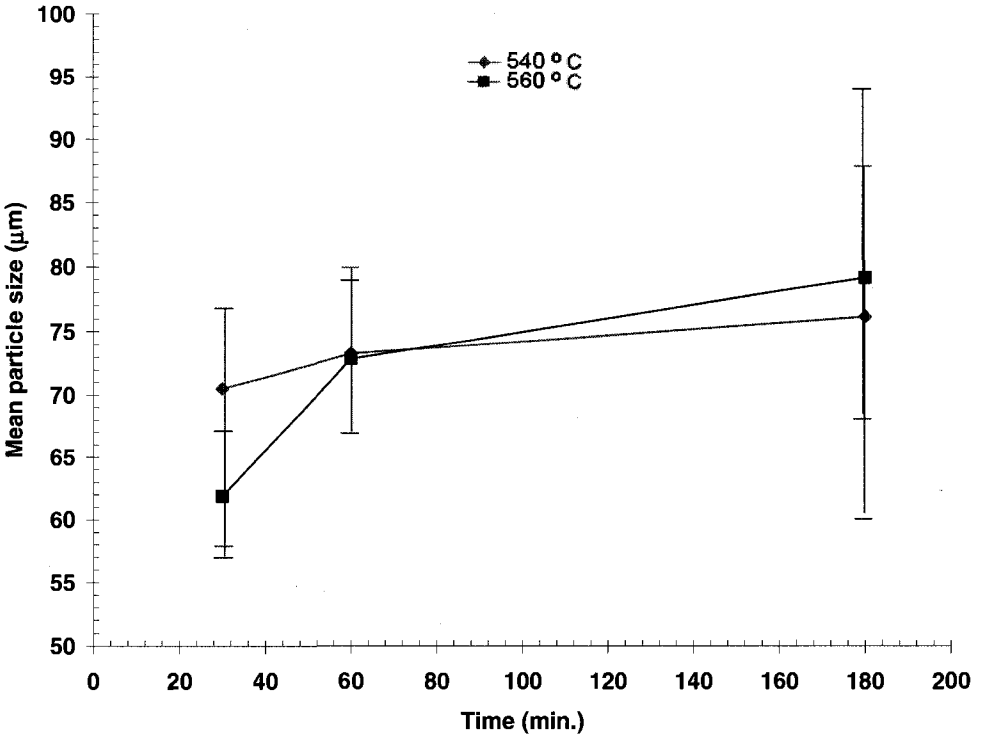

Fig.3: The variation of mean particle size of Mg_2Si with increasing holding time for two different temperatures for partially remelted samples.

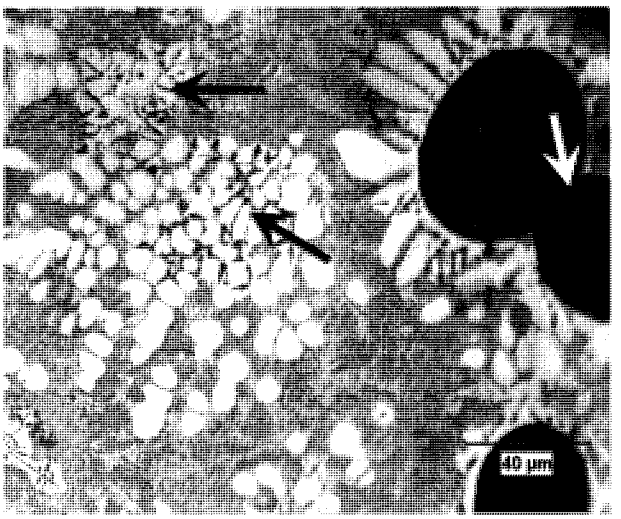

Fig.4: The coalescence of two Mg_2Si particles indicated by a white arrow as well as the emergence of the Chinese script eutectic Mg_2Si (black arrows) within the small α-Al phase particles (white) at holding times of 180 min at 560 °C.

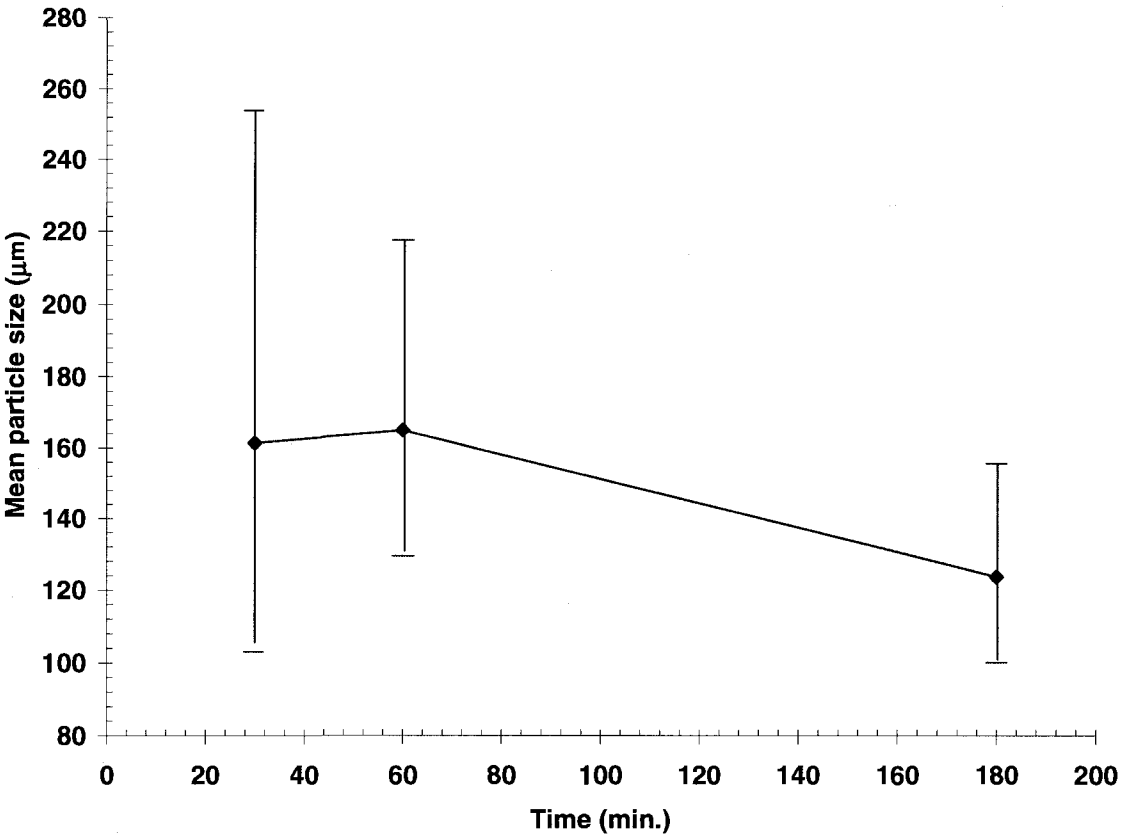

Fig.5: The variation of mean particle size of silicon with increasing holding time at 560 ^{o}C for partially remelted samples

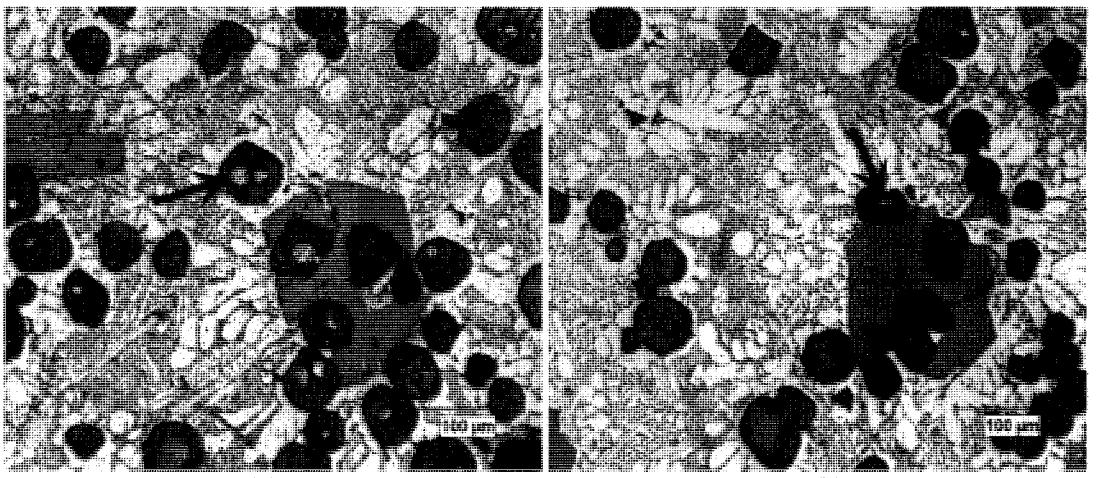

(a) (b)

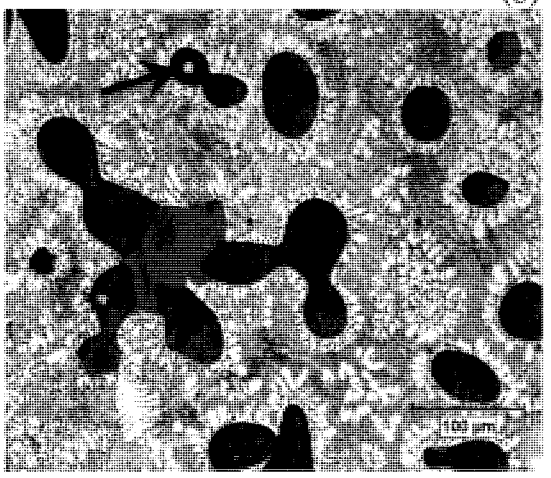

(c)

Fig.6: Growth suppression and eventually fragmentation of silicon phase particles by presence of Mg_2Si particles at the isothermal temperature of 560 °C after (a) 30 (b) 60 and (c) 180 minutes. Mg_2Si (black), polygonal silicon (grey) and some small α-Al particles phase (white) are observed. The arrows also show the Mg_2Si particles with entrapped liquid.

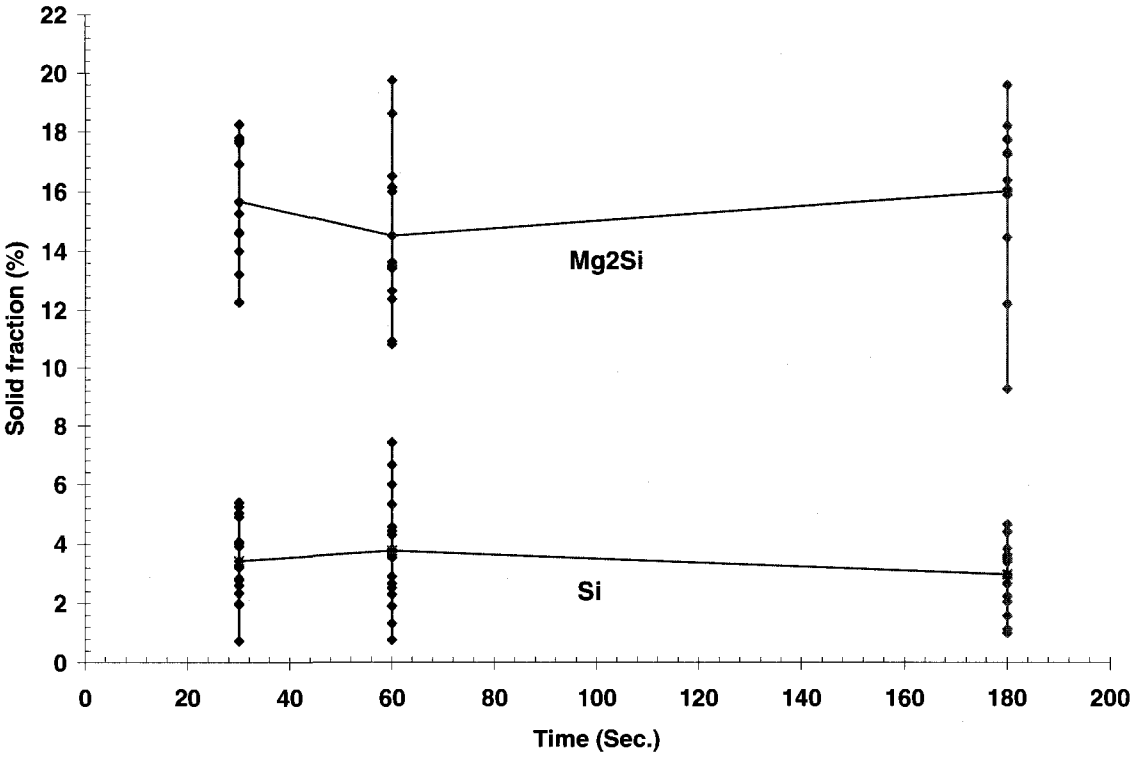

Fig.7: The variation in solid fraction of the silicon and Mg_2Si particles with increasing holding time at the isothermal temperature of 560 ^{o}C

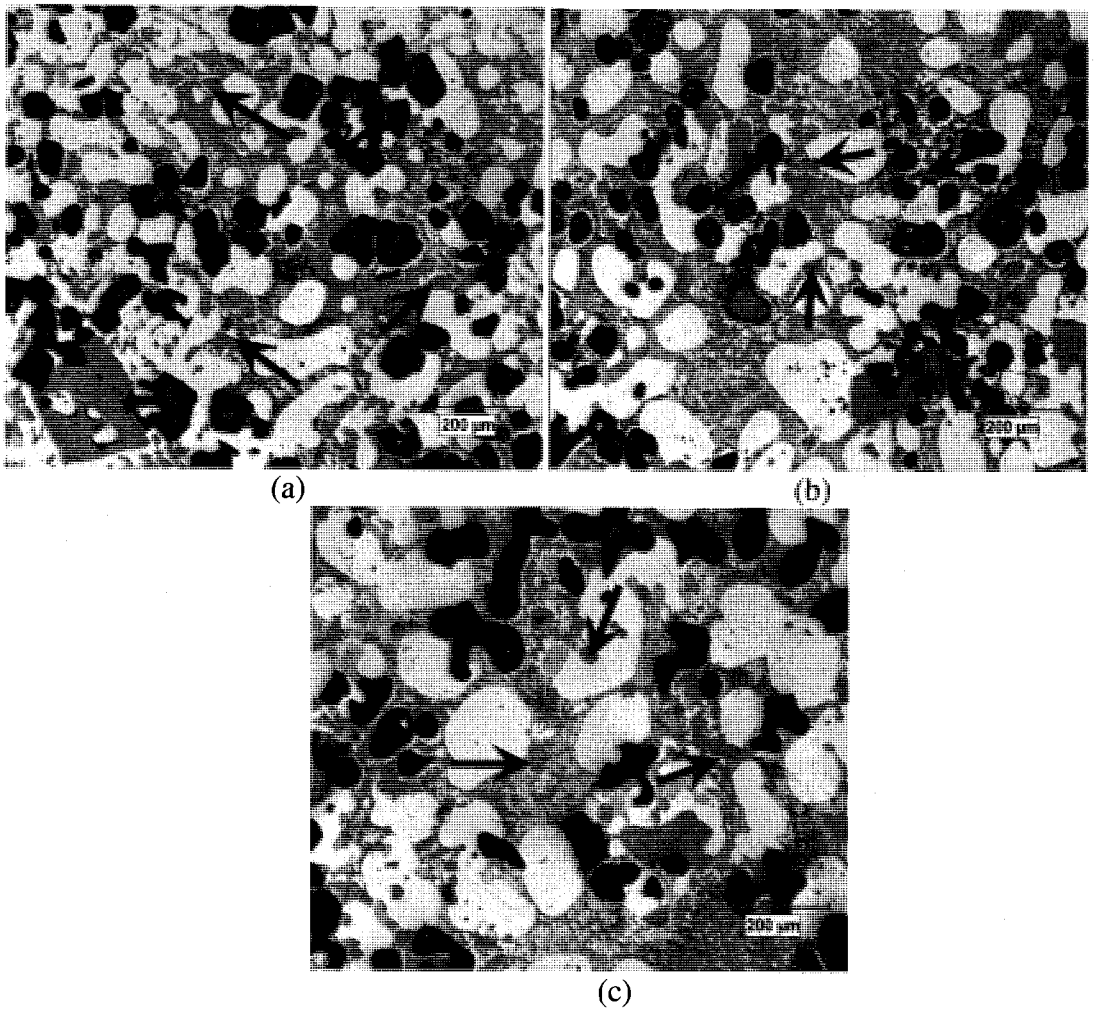

Fig.8: Evolution of the microstructure for isothermal holding at 540 °C (a) 30 (b) 60 and (c) 180 minutes. Mg_2Si (black), large polygonal silicon (grey), small eutectic silicon (pointed by arrows) and α-Al phase particles (white) particles are observed.

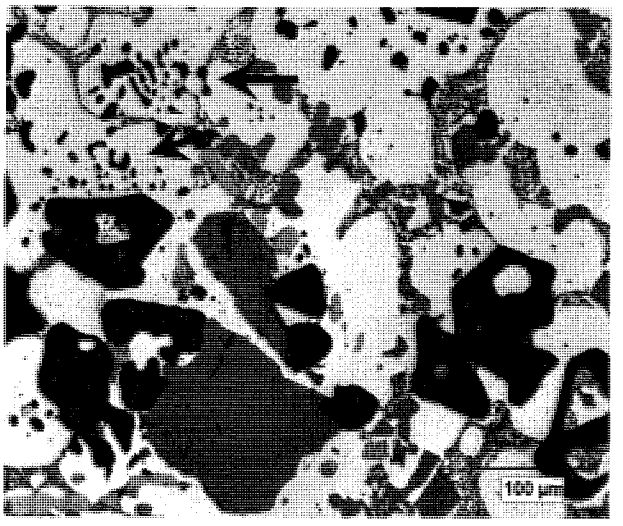

Fig.9: The presence of rod-shape eutectic Mg_2Si (arrow) in some regions transformed from Chinese script form the eutectic phase for isothermal holding time of 30 minutes.

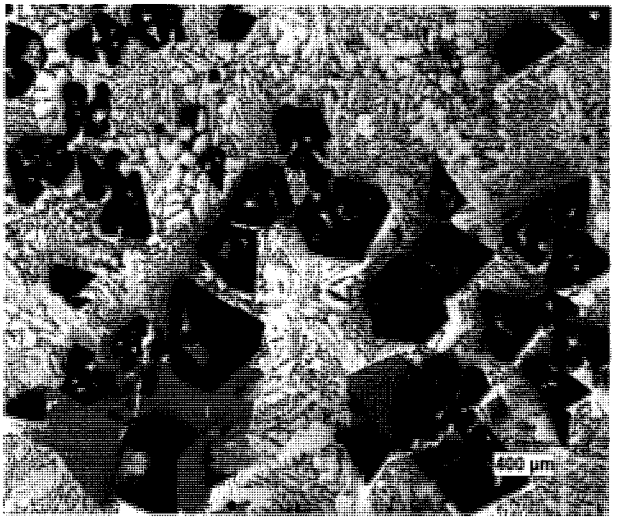

Fig.10: The microstructure of continuously cooled sample showing large equiaxed dendrites of Mg_2Si (black), large polygonal silicon particles (grey) nucleated on Mg_2Si, dendritic α-Al phase particles (white) and the eutectic matrix.

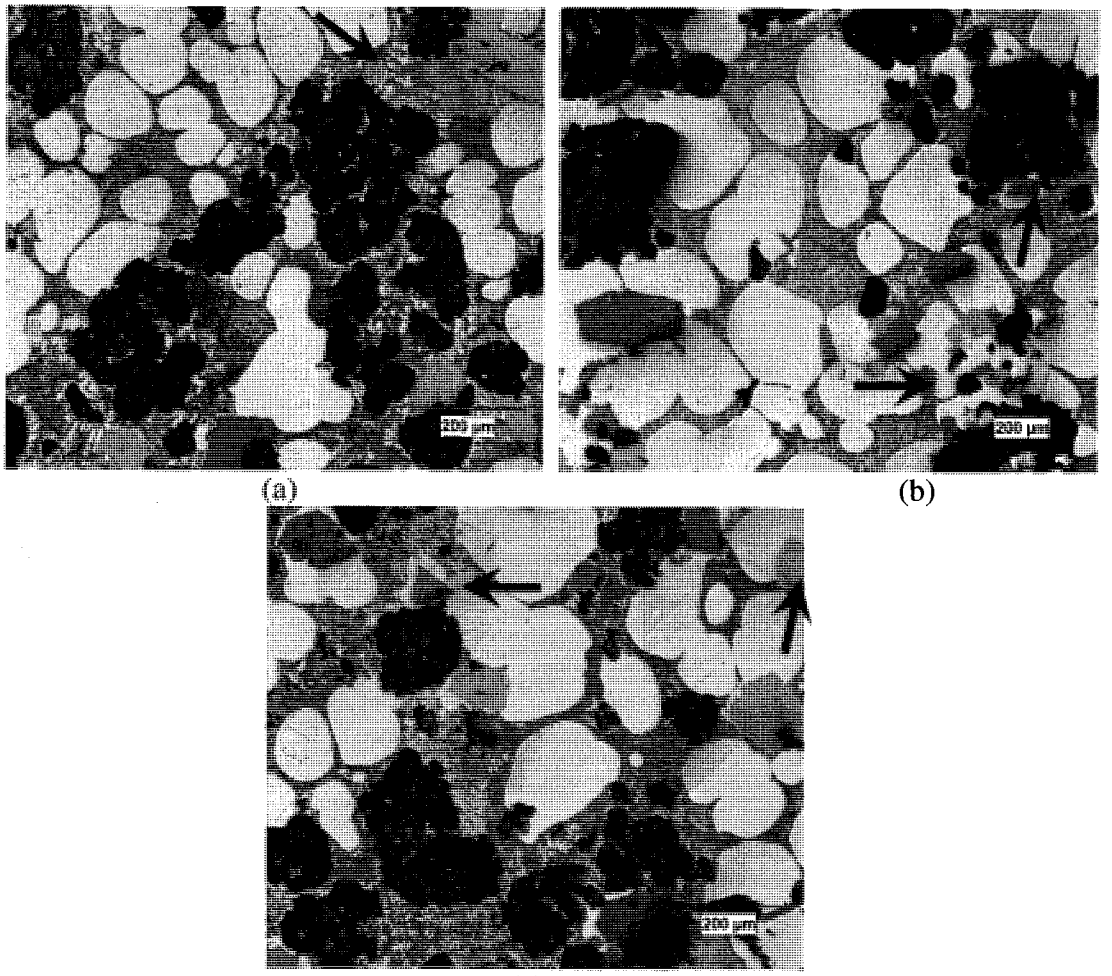

(a) (b)

(c)

Fig.11: Evolution of the microstructure at 540 °C after (a) 30 (b) 60 and (c) 120 minutes of rheoprocessing. Mg_2Si particles (black), polygonal silicon particles(grey), small eutectic silicon particles (pointed by arrows) and α-Al phase particles (white) are observed.

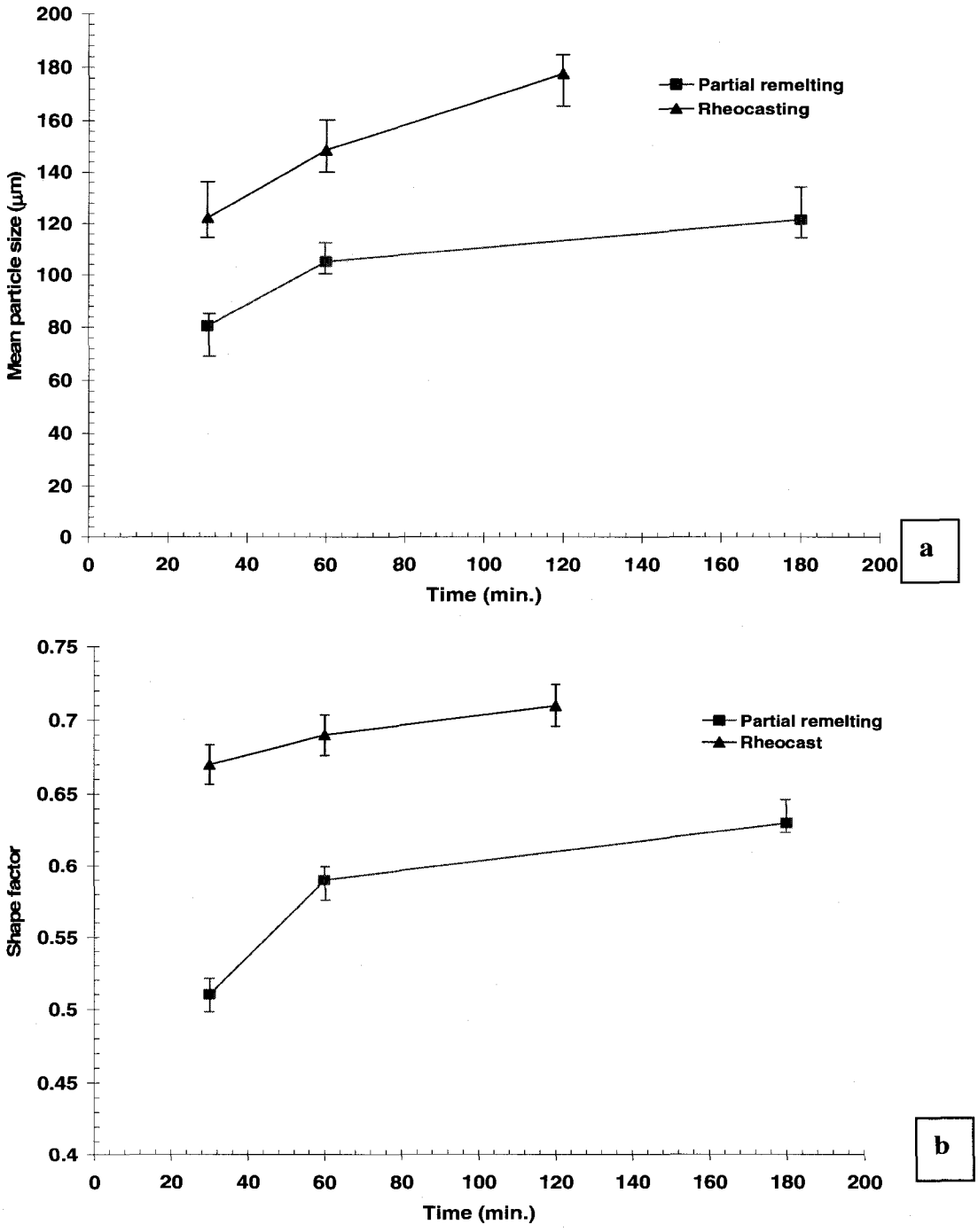

Fig.12: Comparison of the effect of isothermal holding time on the particle size (a) and the shape factor (b) of α-Al at 540 °C for partially remelted and rheocast samples.

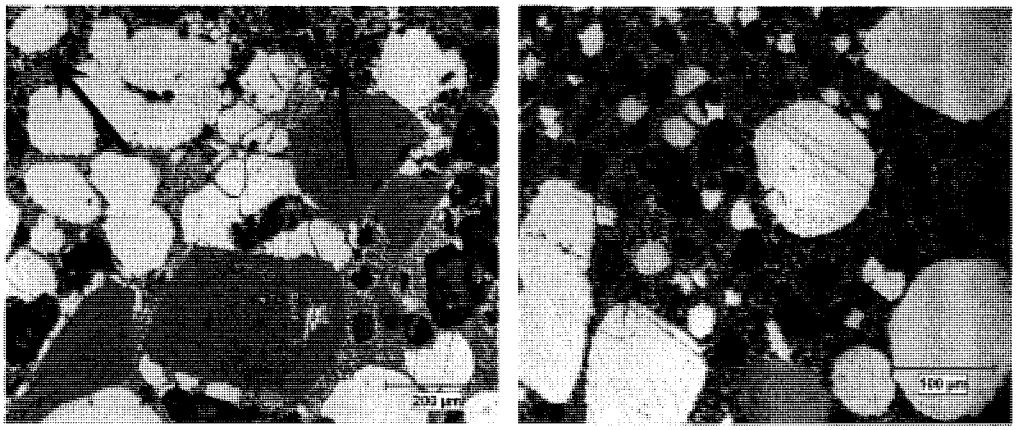

(a) (b)

Fig.13: Microstructure of some regions in the rheocast sample after 120 minutes rheoprocessing time at 540 °C. (a) debris of fragmented Mg_2Si particles (indicated by arrow) (b) fragmentation debris at high magnification.

References

[1] D.B. Spencer: PhD thesis, MIT, Cambridge, MA, 1971.

[2] D.B. Spencer, R. Mehrabian and M. C. Fleming, *Metall. Trans.* **3** (1972), p. 1952.

[3] P. Kapranos, D.H. Kirkwood, H.V. Atkinson, J.T. Rheinlander, J.J. Bentzen, P.T. Toft, C.P. Debel, G. Laslaz, L. Maenner, S. Blais, J.M. Rodriguez-Ibabe, L. Lasa, P. Giordano, G. Chiarmetta, A. Giese, *J Mater Proc Tech* **135** (2003), p. 271.

[4] Z.Fan, semi solid metal processing, International Materials Reviews Vol. 47 No. 2. (2002)

[5] P.A. Davidson, An Introduction to Magneto Hydrodynamics, Cambridge University press (2001).

[6] T. Haga, T. Kouda, H. Motoyama, N. Inoue and S. Suzuki, Proceedings of the ICAA7 on Aluminium Alloys: Their Physical and Mechanical Properties Charlottesville, VA, Publ. Trans. Tech. (1998).

[7] K.P. Young, C.P. Kyonka and J.A. Courtois, Fine grained metal composition', US Patent 4,415,374 (1982).

[8] D.H. Kirkwood, C.M. Sellars and L.G. Elias Boyed, Thixotropic materials, European Patent 0305375 B1 (1992).

[9] M. Gupta and S. Ling, *J. Alloys Compd.* **287** (1999), p. 284.

[10] L. Lasa and J.M. Rodriguez-Ibabe, Scripta Mater. **46** (2002), p. 477.

[11] J. Zhang, Z. Fan, Y.Q. Wang and B.L. Zhou, *Mater Sci Eng A* **281** (2000), p. 104.

[12] A.R. Hekmat and F. Ajersch, Thermodynamic evolution of hypereutectic Al-Si (A390) alloy with addition of Mg, to be published.

[13] A.R. Hekmat and F. Ajersch, Effects of Mg content on the evolution of eutectic microstructure for conventionally cast and rheocast hypereutectic Al-Si alloy, to be published.

[14] Nathalie Limodin, Luc Salvo, Michel Suéry and Marco DiMichiel, *Acta Mater* **55**, (2007), p. 3177.

[15] E. Tzimas and A. Zavaliangos, *Mater. Sci. Eng. A* **289** (2000), p 228.

[16] Q.D. Qin, Y.G. Zhao, P.J. Cong, W. Zhou and B. Xu, *Mater. Sci. Eng. A* **444** (2007), p. 99.

[17] Q.D. Qin, Y.G. Zhao, W. Zhou, and P.J. Cong, *Mater. Sci. Eng. A* **447** (2007), p. 186.

[18] Q.D. Qin, Y.G. Zhao, C. Liu, P.J. Cong and W. Zhou, *J. Alloys Compd.* **454** (2008), P. 142.

[19] C.L. Xu, H.Y. Wang, C. Liu and Q.C Jiang. *J Crystal Growth* **291** (2006), p. 540.

[20] Ru-yao Wang, Wei-hua Lu and L.M. Hogan, *J Crystal Growth* **207** (1999), p. 43.

[21] H.V. Atkinson and D. Liu, *Mater. Sci. Eng. A* **496** (2008), p. 439.

[22] M. Zha, H.Y. Wang, P.F. Xue, L.L. Li, B. Liu and Q.C. Jiang, Microstructural evolution of Mg–5Si–1Al alloy during partial remelting, *J. Alloys Compd.*, in Press, (2008).

[23] I.M. Lifshitz and V.V. Slyozov, *J. Phys. Chem. Solids* **19** (1961), p. 35.

[24] S. Ji, K. Roberts and Z. Fan, *Scr Mater* **55** (2006), p. 971.

[25] L. Lasa and J. M. Rodriguez-Ibabe, *Mater. Sci. Eng. A* **363** (20030, p. 193.

5-5 Rheological characterization of hyper-eutectic Al-Si alloy with 10% Mg addition

In this section, the rheological behavior of the test alloys was investigated during continuous cooling as well as for isothermal "step change" experiments. The experimental procedures were described in section 4-6. the effect of stirring time on evolution of solid phase particles was also investigated

5-5-1 Rheological characterizations

5-5-1-1 Continuous cooling tests

In this test, the 10% Mg alloy was continuously cooled from the liquid state at a rate of 0.15 ± 0.05 $^{o}C\ s^{-1}$ while stirring at a constant speeds of 512, 256, 128, 64 and 32 rpm in separate tests for each rotation speed (see section 4-5-2). The test was stopped when the upper limit of the viscometer torque is reached. By continuously measuring the torque during continuous cooling, the apparent viscosity of alloys as a function of temperature was measured for different rotational speeds.

Fig.53 shows the viscosity versus temperature curves for the 10 % Mg alloy for different rotation speeds. The results indicates that the viscosity gradually increases in the solidification interval from 630 ^{0}C where the solidification of the primary Mg_2Si phase first starts down to the eutectic formation temperature at $544 \pm 2^{\circ}C$. This interval was

observed to change to plateau when the rotation speed increases. At this formation temperature (knee point) which is due to the ternary eutectic reaction (Liq. $\rightarrow$ Al + Si + Mg_2Si), the viscosity abruptly increases when the upper limit of the viscometer torque is reached the stirrer is stopped to prevent damage to the viscometer due to high solid fraction. The calculated liquid fraction demonstrates that 82.3% of the liquid phase is transformed to ternary eutectic phases (Al, Si and Mg_2Si) and the resulting eutectic solidification structure for the high Mg content alloy corresponds to the ternary reaction. Fig.54 compares the viscosity curve during solidification under continuous cooling test for the A390 alloy and the 10% Mg alloy at the rotation speed of 32 and 64 rpm. At a rotation speed of 32 rpm where the average shear rate is 6.5 s^{-1}, the viscosity of A390 alloy is lower than for the 10% Mg alloy at the initial solidification stage down to the eutectic temperature. This is due to the low solid fraction of primary phase for the A390 alloy (6.1%) compared to the high Mg content alloy (12.2%). However at the knee point, the viscosity of both alloys increase significantly. As described before, the eutectic reaction temperature at the knee point decreases with increasing the Mg content. Both FACTSAGE prediction and DSC tests confirms such decrease as shown in Fig. 55. As shown in paper 2, this reduction can significantly modify the eutectic silicon morphology of the matrix of 10% Mg alloy.

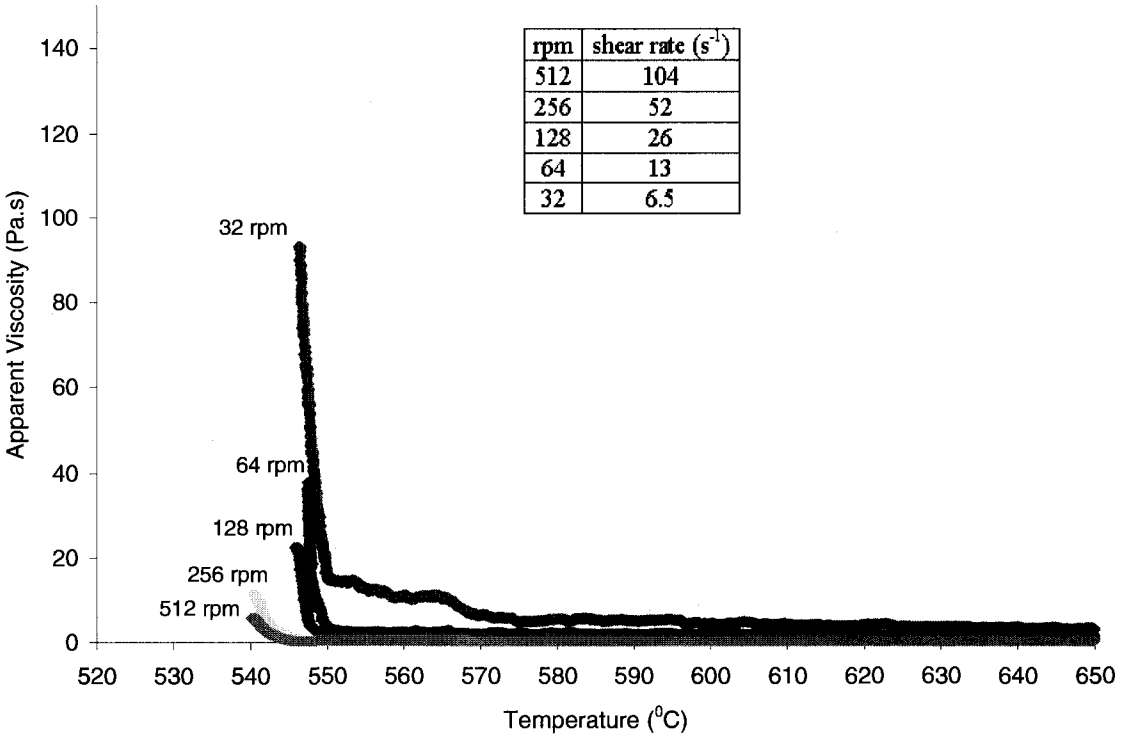

Fig. 53: The viscosity versus temperature curves for hyper eutectic Al-Si alloy with 10 % Mg at different rotation speed (cooling rate = 0.15± 0.05 ^{o}C s^{-1})

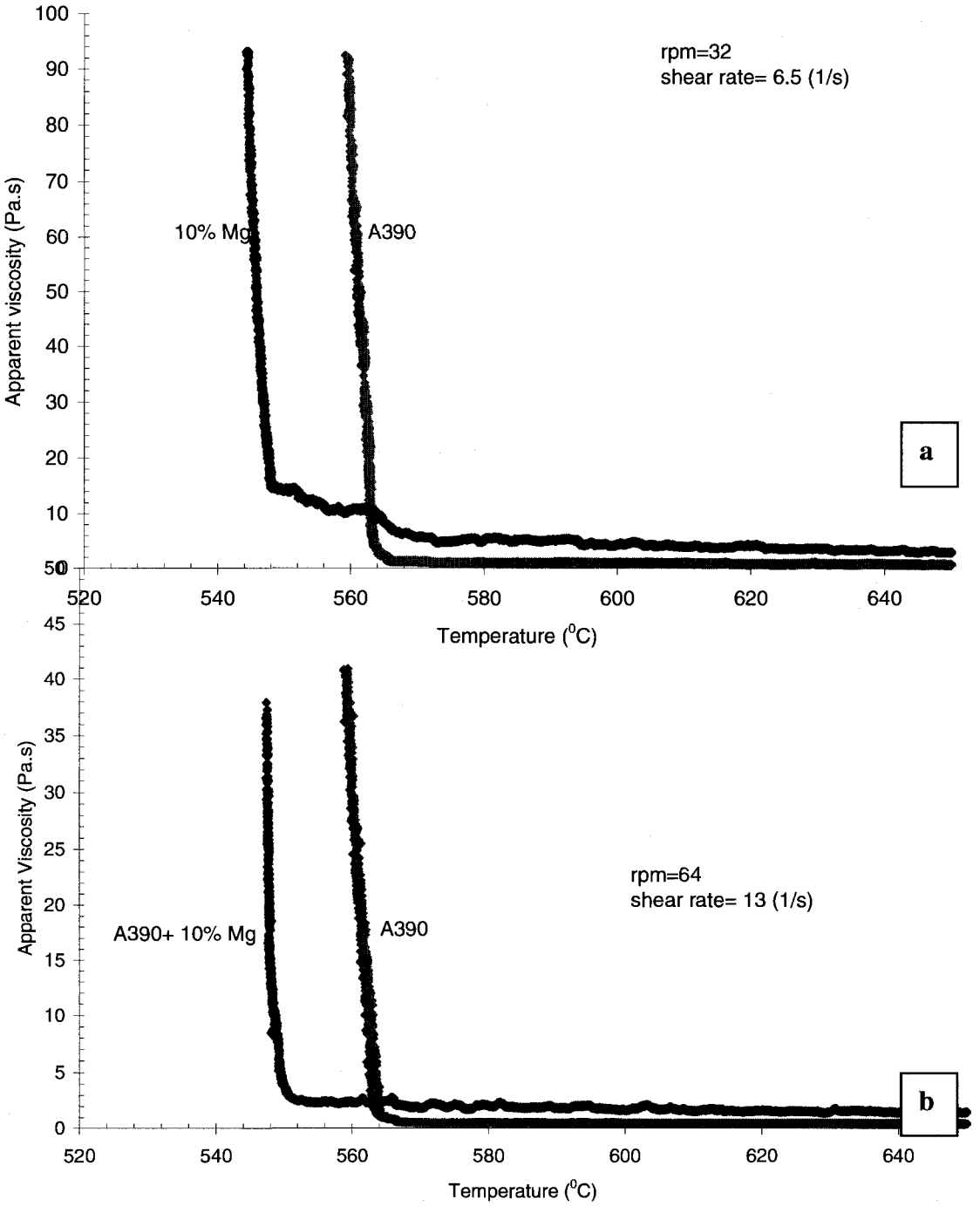

Fig. 54: Comparing the viscosity curve during continuous cooling for A390 and 10% Mg alloys at (a) 32 and (b) 64 rpm.

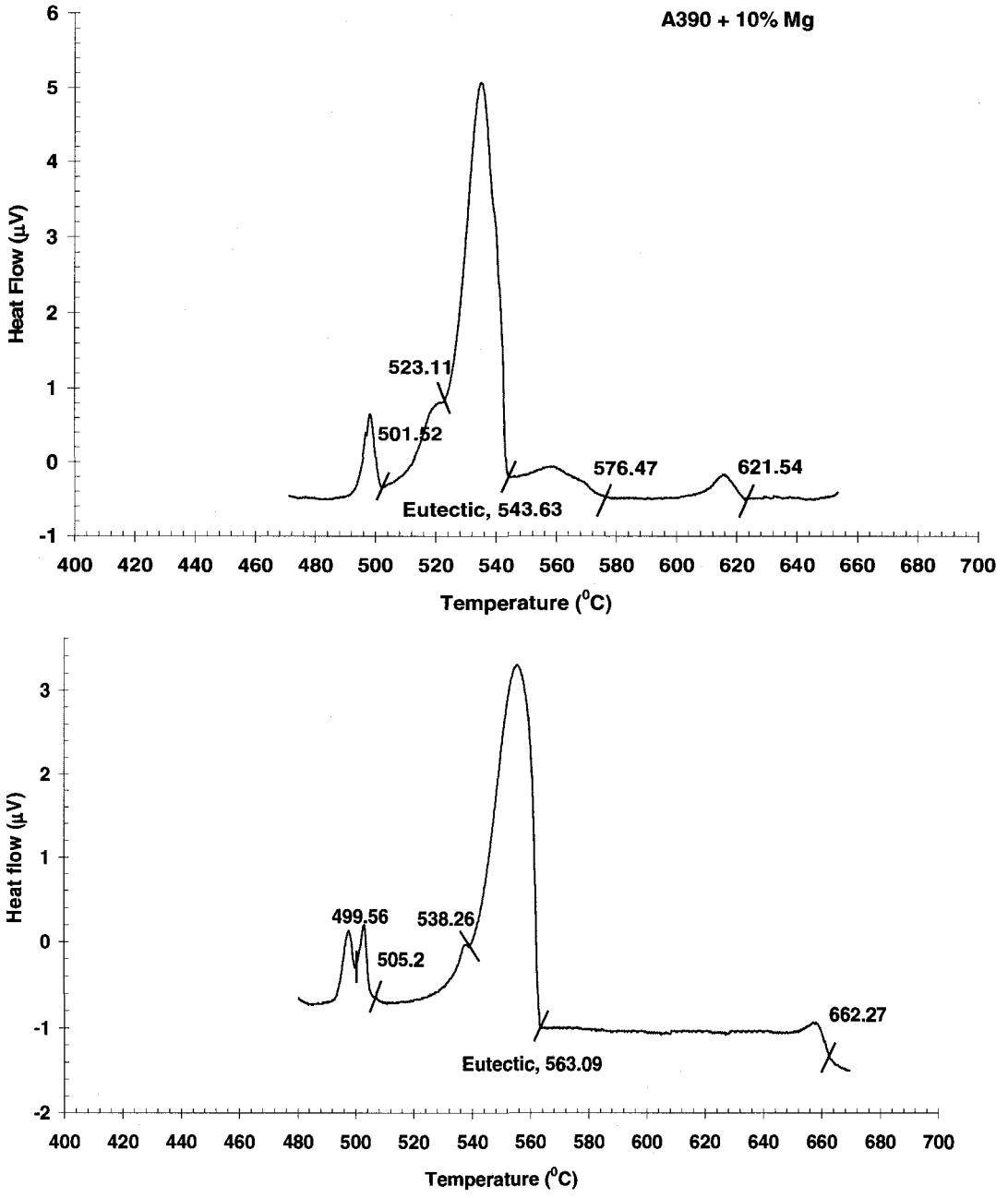

Fig. 55: The reduction of eutectic formation temperature (knee point) for A390 alloy and 10% Mg alloy measured by DSC (Differential Scanning Calorimeter) test

It can be observed that, the viscosity of the 10% Mg alloy in the liquid state (above liquidus point) at 650 ° C is also higher than that of the A390 alloy which is more related to the low enthalpy of solidification of Mg_2Si compared to Si.

5-5-1-2 Isothermal shear test (effect of stirring time)

For the isothermal or shear step tests, the sample was heated to a temperature of 700 ° C and then continuously cooled at the rate of -0.15± 0.05 $^{o}C\ s^{-1}$ without shearing to a temperature in the semi solid state. The alloy was then sheared at a given isothermal condition at a constant rotational speed. The variation of apparent viscosity vs. time, at given temperature, was investigated in order to characterize the "thixotropic behavior" of alloys.

In this study, the viscosity variation of the 10% Mg alloy was investigated at 550 ° C. This temperature is close to the eutectic formation temperature (544 ° C, according to the DSC test) with a solid fraction of almost 12%. Fig. 56 shows the corresponding curve for a rotational speed of 260 rpm and indicates that the apparent viscosity initially decreases significantly as the stirring time increases until it reaches a minimum value at 400 seconds after which it started to increase again very slowly as the stirring time continue to increase. Two phenomena have to be taken into account to explain this effect. Initially, the solid particles containing Mg_2Si and silicon would be fragmented and degraded by shear force resulting in a decrease of apparent viscosity. Fig 57a

schematically displays the degradation of particles resulting in a decrease of apparent viscosity. The reason for the increase in apparent viscosity with increased stirring time can be described by coarsening of small particles to form larger ones as a result of particle coalescence and Oswald ripening. Stirring can accelerate the coarsening by factor 3 or 4 depending on stirring speed as shown in the previous section (paper 3). This phenomenon was also observed for AZ91 D which is a Mg base alloy [84]. Fig 57b shows the schematic diagram of the variation of microstructure for the slowly increasing of viscosity shown in Fig 56.

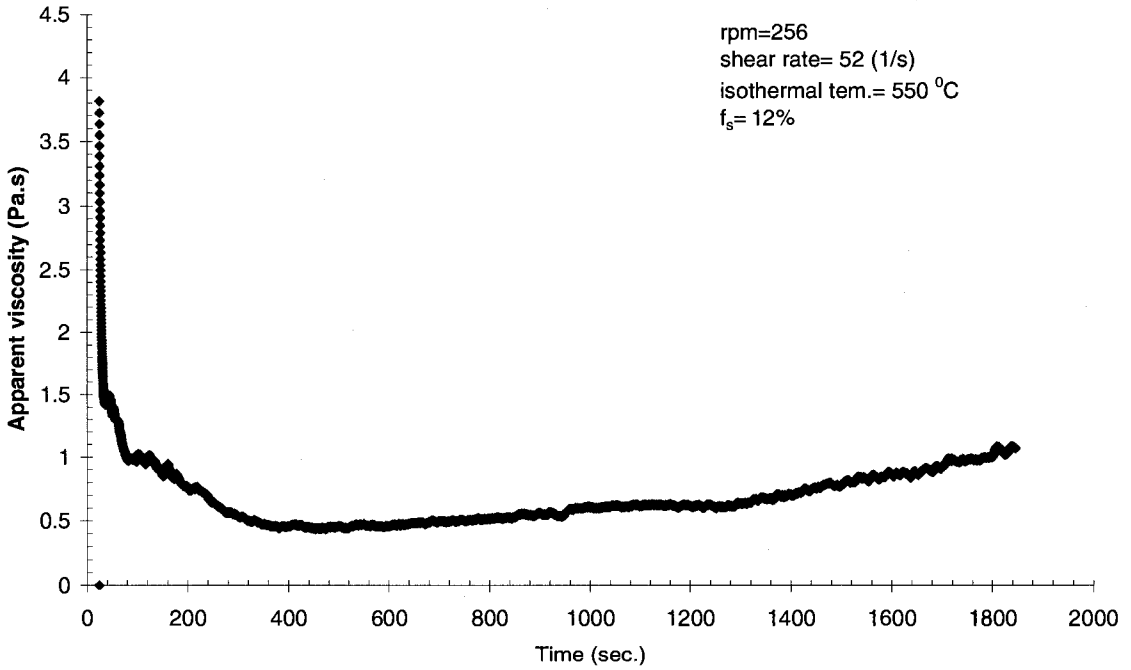

Fig. 56: The variation of viscosity of 10% Mg alloy as a function of time at isothermal semi solid temperature of 550 ° C.

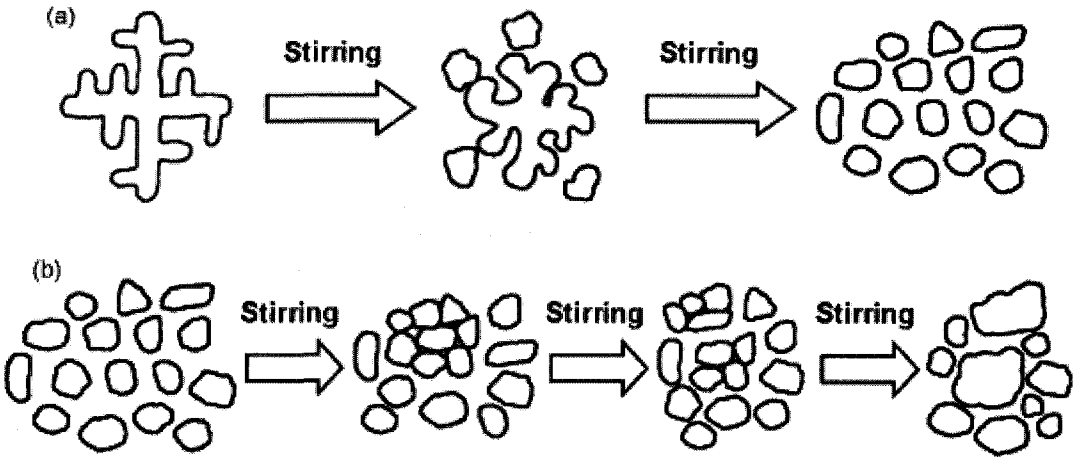

Fig. 57: Schematic diagram of the variation of microstructure for: (a) decreasing curve of apparent viscosity and (b) increasing curve of apparent viscosity in Fig. 54. [84]

5-5-1-3 Shear step change tests

The "step change" test makes it possible to evaluate the viscosity variation at isothermal condition and fixed solid fraction when the rotation speed (or shear rate) is suddenly changed. In this case, the viscosity curve is divided to two parts: the transient state viscosity and steady state viscosity. The transient state viscosity takes place during the initial period when the rotation speed changes. On increasing or decreasing rotation

speed, the viscosity respectively decreases or increases with time. When the viscosity no longer varies with prolonged shear time at a constant shear rate, the steady state apparent viscosity is established (see Fig. 51 in section 4-6-2). The results obtained from these tests can eventually be used to produce a curve of viscosity versus shear rate. This curve is a representation of the rheological behavior of alloy in the semi solid state showing the degree of deviation from Newtonian behavior for variable shear rate. The rheological behavior of metals in the semi solid state is often described by a power law equation relating the viscosity to the shear rate, $\eta = k\dot{\gamma}^{n-1}$ (see section 3-1-5-1) where n is a power law index. For alloys, in the semi solid state, the value of n is generally less than 1 and the rheological behavior becomes pseudo-plastic. For this alloy (10% Mg), the apparent viscosity η decreases with increase in shear rate.

A step change test was carried out at a semi solid temperature close to their eutectic reaction temperatures for the evaluation of the pseudo-plastic behavior of the A390 and with 10% Mg alloy. Fig 58 shows the result of the "step change" test for both A390 and the 10% Mg alloy at 566°C and 550°C, respectively. As can be observed, the 10% Mg alloy shows a larger variation of the apparent viscosity than the A390 alloy when the shear rate changes. The reason is due to the higher solid fraction of the 10% Mg alloy where f_s = 12 %, compared to the A390 alloy with only f_s = 6 %. This implies that the semi solid behavior of the A390 alloy is more Newtonian than the 10% Mg alloy at the temperature near the eutectic. In order to verify the semi solid behavior of alloys near

the eutectic temperature, the average apparent viscosity versus shear rate curve was plotted for both alloys using the results obtained by the "step change" tests. In this case, the mean value of the viscosity is plotted for each shear rate. Fig. 59 shows the average viscosity as a function of shear rate curve for the A390 and the 10% Mg alloy. Both alloys are represented by power law equations where the value of n, power law index, is less than 1 for both alloys. However, when the slope of the curve for the 10% Mg alloy is compared to A390 alloy the results indicate that the degree of pseudo-plasticity for the 10% Mg alloy is more predominate than for the A390 alloy resulting in a more negative value of n (n = -0.4816) compared to the A390 alloy (n = 0.4581). This is due to the relation of degree of pseudo-plasticity with the solid fraction. Since the 10% Mg alloy has high solid fraction than A390 at the eutectic temperature used for step change tests, the degree of pseudo-plasticity will be higher for the 10% Mg alloy. However, in the same semi solid condition (temperature and solid fraction) for two alloys, the 10% Mg alloy also show more degree of pseudo-plasticity compared to the A390 alloy because the evolution of the particle size and morphology is not identical for two alloys at the same condition.

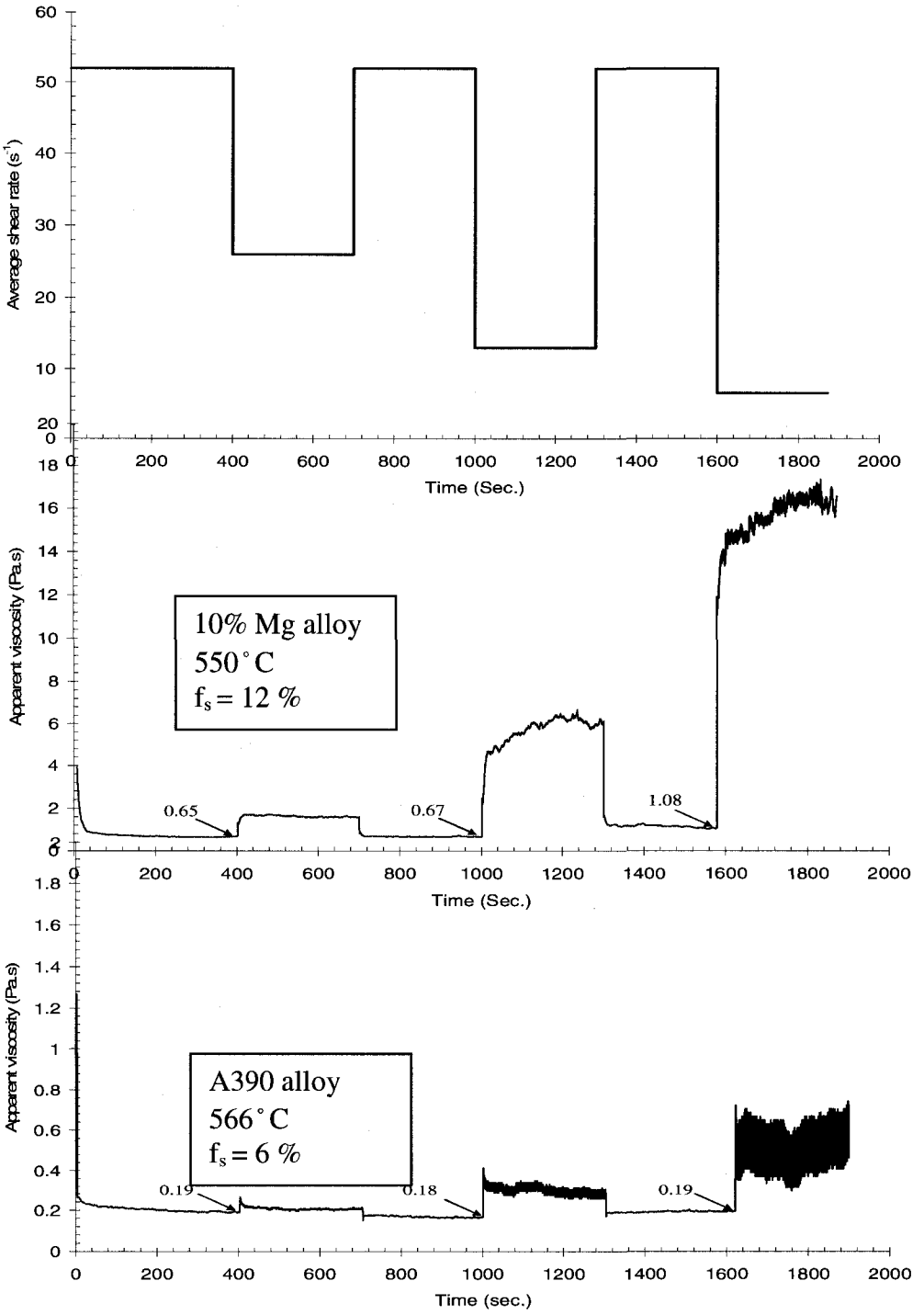

Fig 58: Result of step change tests for 10% Mg and A390 alloys near to the eutectic formation temperature, 550° C and 566° C, respectively.

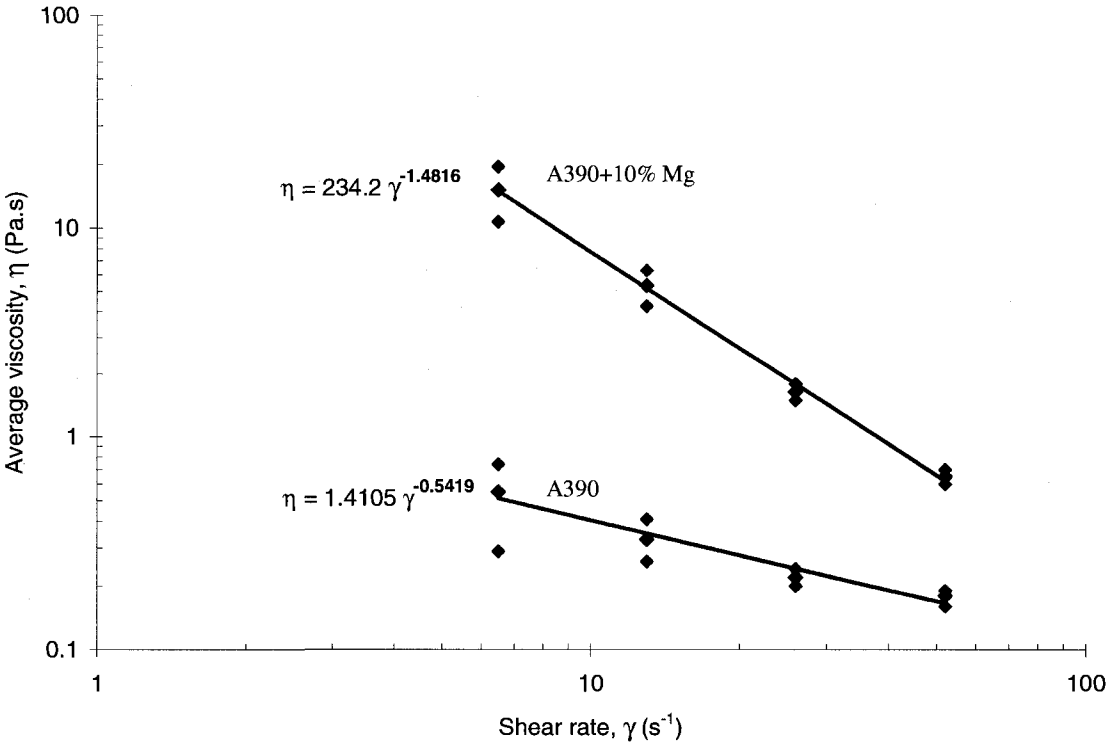

Fig. 59: The average apparent viscosity versus shear rate equations for A390 and 10% Mg alloy near their eutectic formation temperature.

5-6 Effect of Mg on hardness of A390 alloy

The methodology and the experimental procedures for measuring the hardness value have been thoroughly described in section 4-7. Fig 60 shows the values of Brinell hardness resulting from Rockwell B (100 kg load with 1/16 ball) hardness tests for conventionally cast samples using gravity permanent mould and T6 heat treatment samples of the A390 base alloy as well as the 6% and 10% Mg alloys. The average hardness values in a bar chart form are also shown in Fig 60 for the as cast and after T6 condition. The hardness value increases with increasing Mg content of alloys for the as-cast samples. Fig 61 shows the microstructure of as-cast A390 alloy. As described in the previous sections, it consists of polygonal primary silicon dispersed in the eutectic matrix of Al-Si phase. The eutectic silicon has a flake like morphology with a large inter-flake space. As it was described in Papers 1 and 2, the other intermetallic phases such as $CuAl_2$ (θ), $Cu_2Mg_8Si_6Al_5$ (Q), Al_5FeSi (β) are also presented in the microstructure of alloy. These intermetallics phases are always observed to form agglomerates dispersed in the matrix. Fig. 62 shows the as-cast microstructure of the 6% Mg alloy. It consists of the primary silicon and Mg_2Si phases with almost the same solid fraction distributed in the matrix. Therefore, both silicon and Mg_2Si are present in the primary and the eutectic phases for the high Mg content alloys. Fig. 63 shows the as-cast microstructure of the 10% Mg alloy. The eutectic morphology is similar to the 6% Mg alloy. However the solid fraction of the primary Mg_2Si is higher compared to the 6% Mg

alloy. Many reasons are attributed to the increase of hardness value with increasing Mg content. One of theses is due to the modification of the eutectic silicon. In this case, the matrix of the high Mg alloys consists of eutectic silicon with a very fine skeleton network whereas the eutectic microstructure of A390 alloy consists of eutectic silicon with a large individual needle morphology and high inter-needle spacing dispersed in matrix of α-Al.

Chinese script eutectics Mg_2Si morphology was also observed in the matrix of the high Mg alloys and was formed to increase the hardness value of alloy. Since the matrix with a eutectic morphology possesses the 81% and 75.4% of the solid fraction in the microstructure of A390 and the 10% Mg alloys respectively, the modification of the matrix, specifically the eutectic silicon, plays an important role in alloy hardness. Paper 2 has thoroughly investigated the evolution of the eutectic microstructure with increasing Mg content. Another reason is believed to be due to the increase of the solid fraction of hard primary particles such as silicon and Mg_2Si from 6.1% to 12.2% which is two times higher for A390 than for 10% Mg alloys.

Index	As cast			T6		
	390 1-2	6Mg 1-2	10Mg 1-2	390 6-1	6Mg 1-1	10Mg 1-1
Rockwell B	47.2	57.4	61.4	85.1	69.0	76.1
	60.0	59.1	73.2	80.6	77.2	80.8
	55.6	65.8	75.8	82.1	81.1	79.3
	60.3	58.2	73.1	85.5	79.7	71.1
	60.7	71.6	74.9	84.8	77.6	79.6
	60.5	64.6	68.5	85.1	75.9	77.2
	47.3	71.0	71.3	86.3	76.9	79.2
	62.0	68.0	72.2	87.9	76.0	80.8
Average	56.7	64.5	71.3	84.7	76.7	78.0
HB	90.7	101.5	112.6	141.4	123.4	126

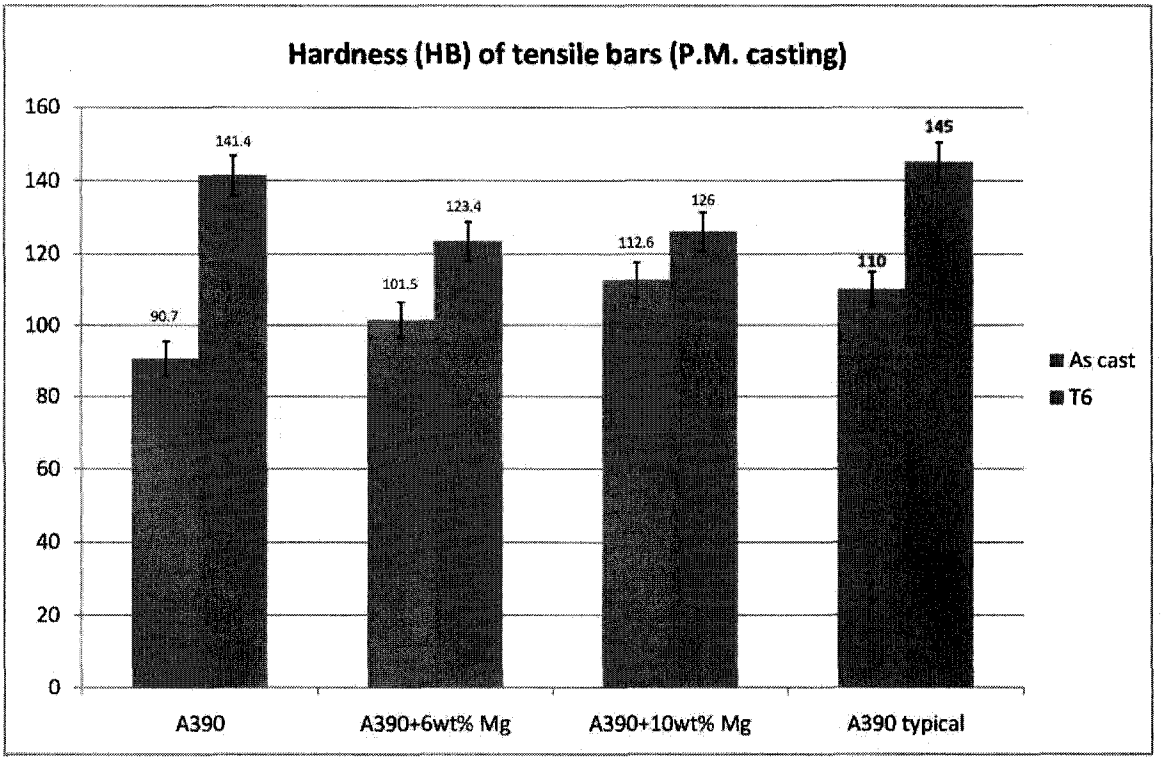

Fig 60: The result of hardness tests for conventionally cast using gravity permanent mould and after (T6) heat treatment samples of A390 base alloy as well as 6% and 10% Mg alloys. The results are compared to a typical hardness value of A390 alloy.

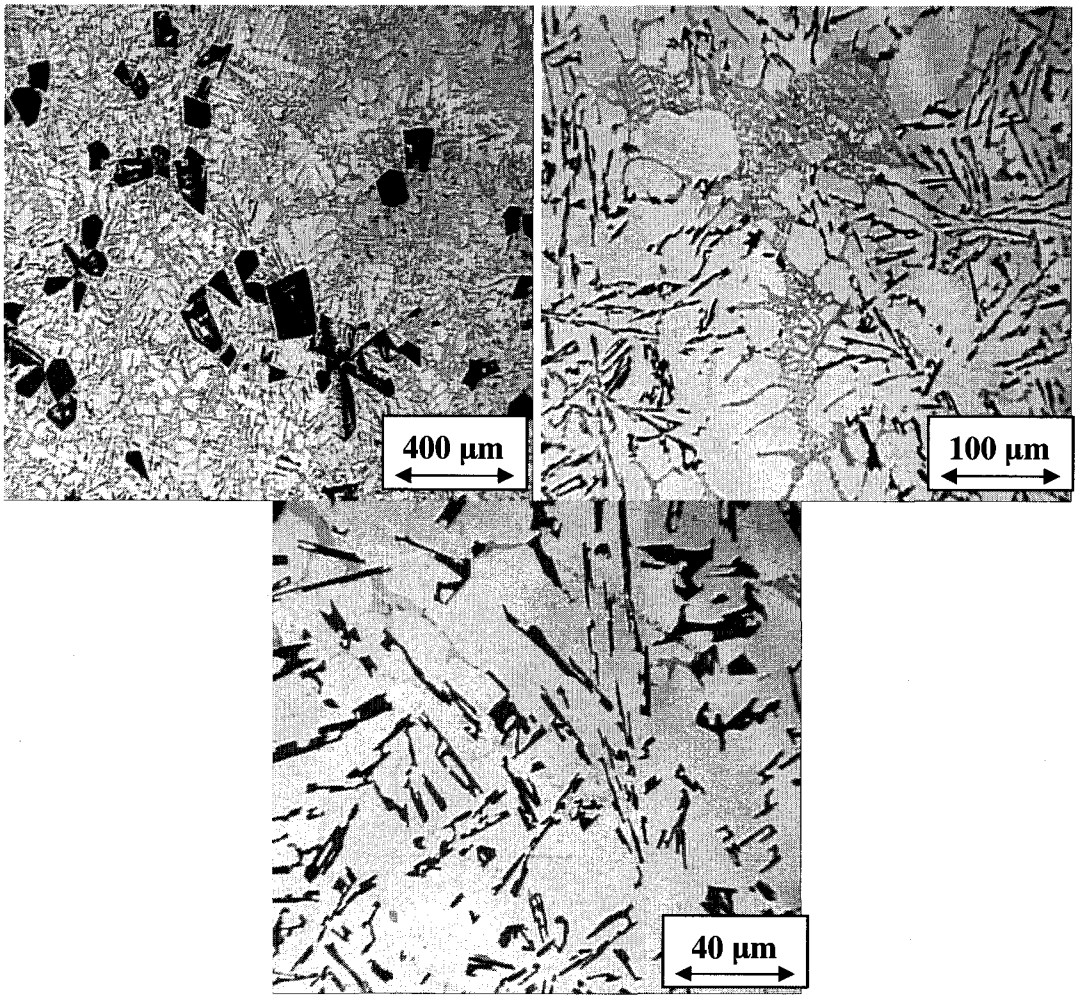

Fig 61: As-cast microstructure of A390 alloy at three different magnifications of 50X, 200X and 500X.

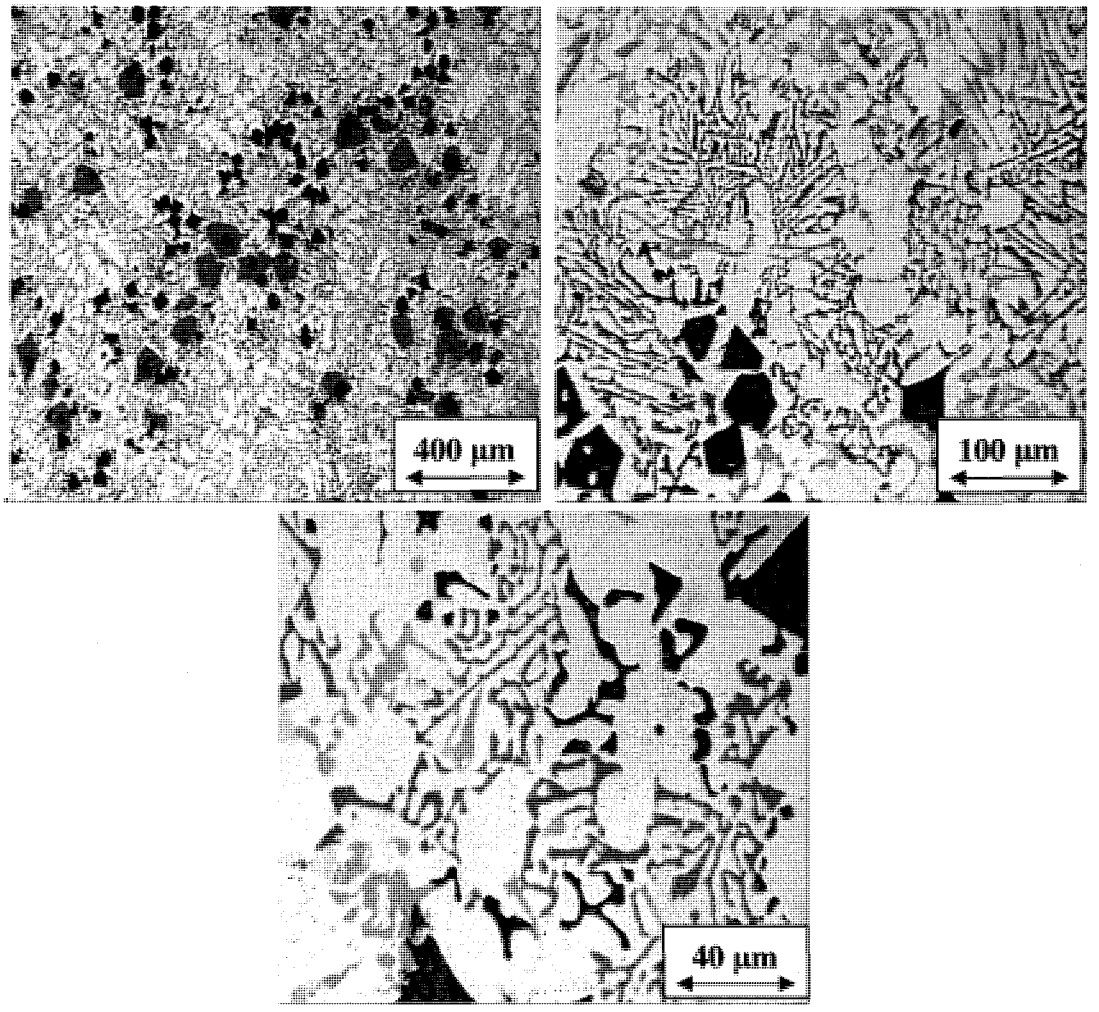

Fig 62: As-cast microstructure of 6% Mg at three different magnifications of 50X, 200X and 500X.

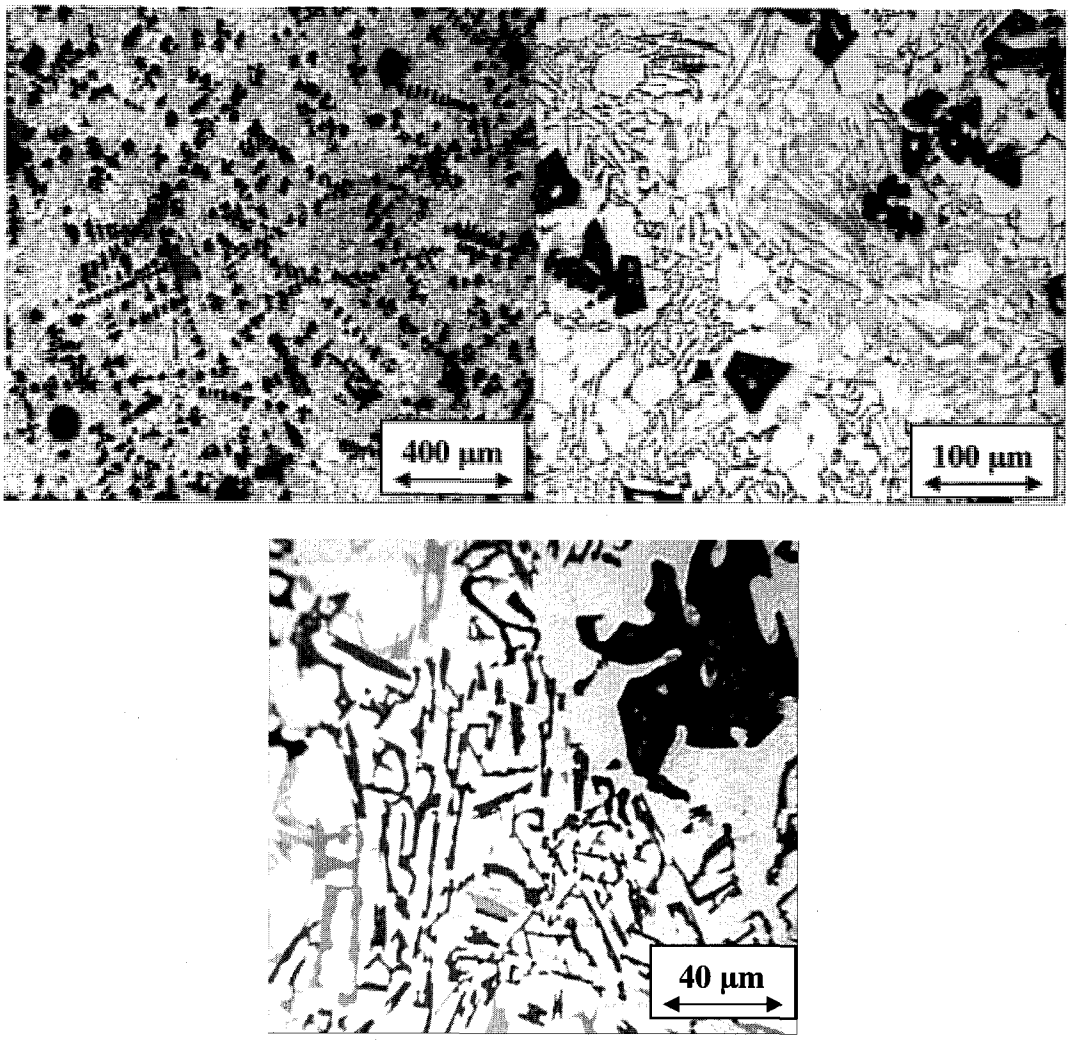

Fig 63: As-cast microstructure of 10% Mg at three different magnifications of 50X, 200X and 500X.

The hardness values for the samples after T6 heat treatment are all higher than for the as-cast samples. However, contrary to hardness value of the as-cast samples, the hardness decreases with increasing the Mg content. For example, the hardness value of A390 alloy under T6 condition greatly increases from 90.7 to 141.4 in HB scale while the 6% and 10% Mg alloy increase their hardness value from 101.5 to 123.4 (HB) and 112.6 to 126 (HB), respectively. Neither the 6 nor 10 wt% Mg alloy achieve the hardness value of A390 after heat treatment (T6). Fig. 64 shows the microstructure of A390 alloy after T6 heat treatment. The T6 heat treatment has no effect on morphology of primary phases such as silicon and Mg_2Si. However, the heat treatment affects the matrix of eutectic silicon, eutectic Mg_2Si and dendritic α-Al. It is believed that high temperature and long soaking times involved in the solution heat treatment promote rounding of the flake eutectic silicon, to form of fine globular Mg_2Si and hardening of the α-Al solid solution in the matrix. Fig. 64 clearly indicates that the needle silicon eutectic has changed to a rounded form by solution heat treatment. Moreover, a significant hardening can be expected for α-Al solid solution due to precipitation hardening effect. The T6 heat treatment is initialized with 8 hours solutionzing at 495 °C where α-Al forms a supersaturated solid solution of intermetallic phases, mainly $CuAl_2$ (θ). The intermetallic phases such as $CuAl_2$ (θ), $Cu_2Mg_8Si_6Al_5$ (Q), Al_5FeSi (β) are all present in the microstructure of A390 alloy. However, the $CuAl_2$ (θ) is the main intermetallic phase in the microstructure of A390 alloy with 6.6% solid fraction. The precipitation hardening continue by quenching the samples in water, followed by

another 8 hours ageing at 175 °C. Fig. 65 and Fig. 66 show the microstructure of the 6% and 10% Mg alloys after T6 heat treatment samples.

The hardness value for the heat treated samples indicates that heat treatment can affect the matrix of A390 alloy more significantly compared to the high Mg content alloys. Since the solid fraction of α-Al in the matrix of A390 alloy is higher than for the high Mg content alloys; the precipitation hardening during heat treatment has a greater effect on the hardness value. On the other hand, the morphology of the eutectic phase specifically the eutectic silicon and its distribution in the A390 alloy becomes quite different with addition of Mg. As described before; the eutectic silicon is in the form of a fine skeleton network with script morphology throughout the matrix of the high Mg content alloys. However, the matrix of A390 alloy consists of large flake eutectic silicon with high inter-flake spaces dispersed in α-Al. Comparing these microstructures, it is believed that the hardening of the α-Al has a greater effect on harness of the A390 alloy than the high Mg content alloys. The hardness value of 6% and 10% Mg alloys are similar.

In summary, the reason for the increase in hardness of as-cast high Mg content alloy is attributed to the modification of eutectic silicon, the presence of the eutectic Mg_2Si as well as the increase of solid fraction of primary phase. However, the hardness value of the samples after T6 heat treatment indicates that the high stiffness of α-Al due to the precipitation hardening effect as well as the eutectic morphology and its distribution in

matrix plays a predominant role. Therefore, the hardness value becomes more pronounced for A390 alloy due to high solid fraction of α-Al and large eutectic silicon particles compared to the high Mg content alloy with low solid fraction of α-Al. This can explain the values of almost the same hardness for 6% and 10% Mg alloys. Fig. 67 compares the microstructure of A390, 6% and 10% Mg alloy before and after T6 heat treatment at high magnification (500X).

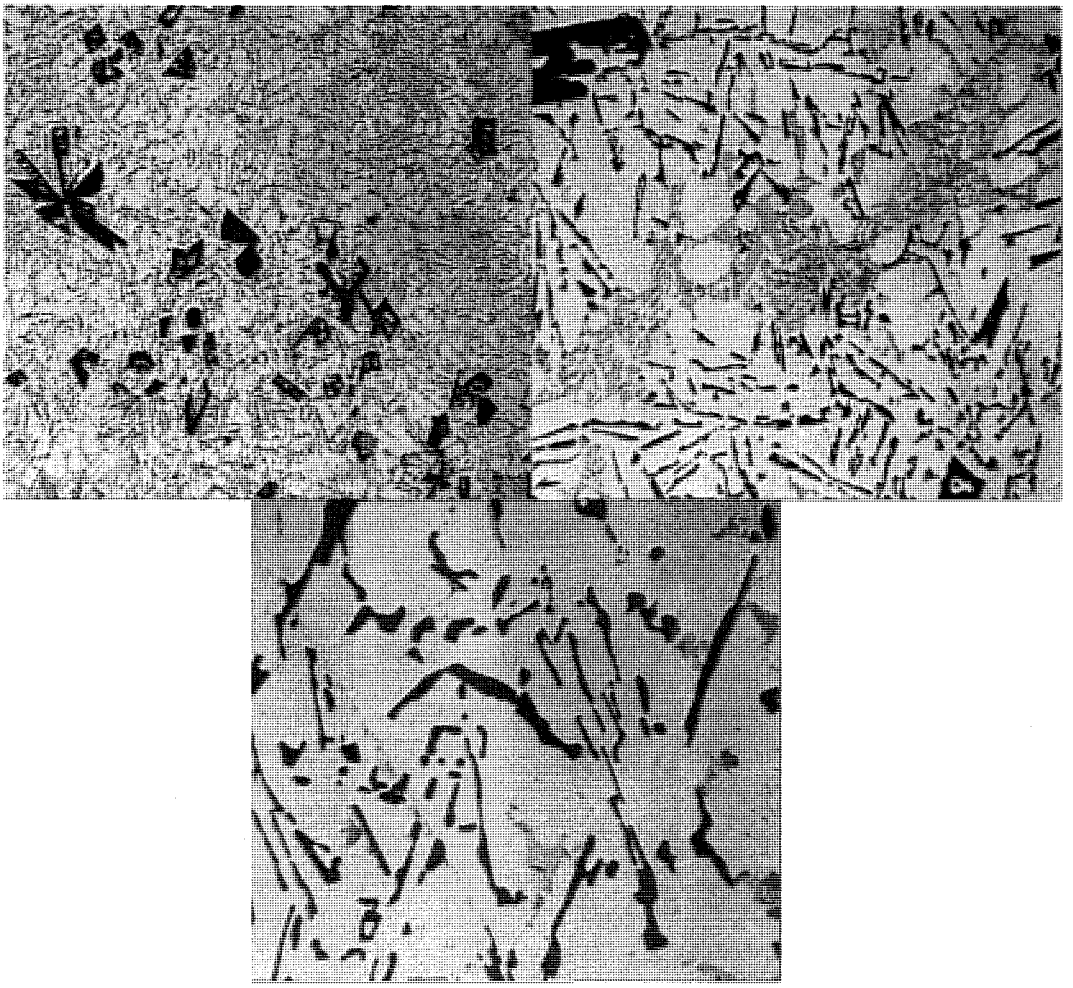

Fig. 64: The microstructure of A390 alloy after T6 heat treatment at three different magnifications of 50X, 200X and 500X.

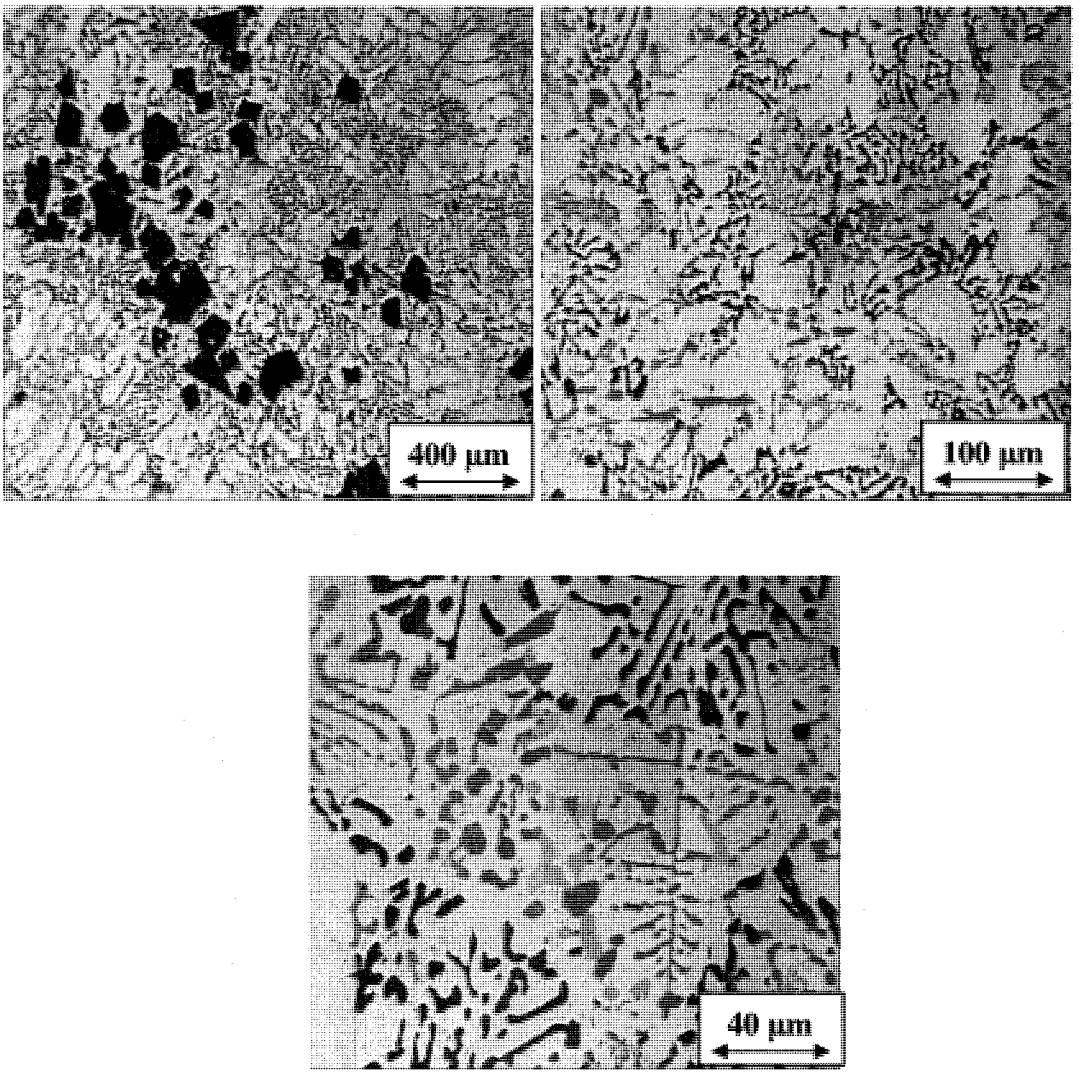

Fig. 65: The microstructure of 6% Mg alloy after T6 heat treatment at three different magnifications of 50X, 200X and 500X.

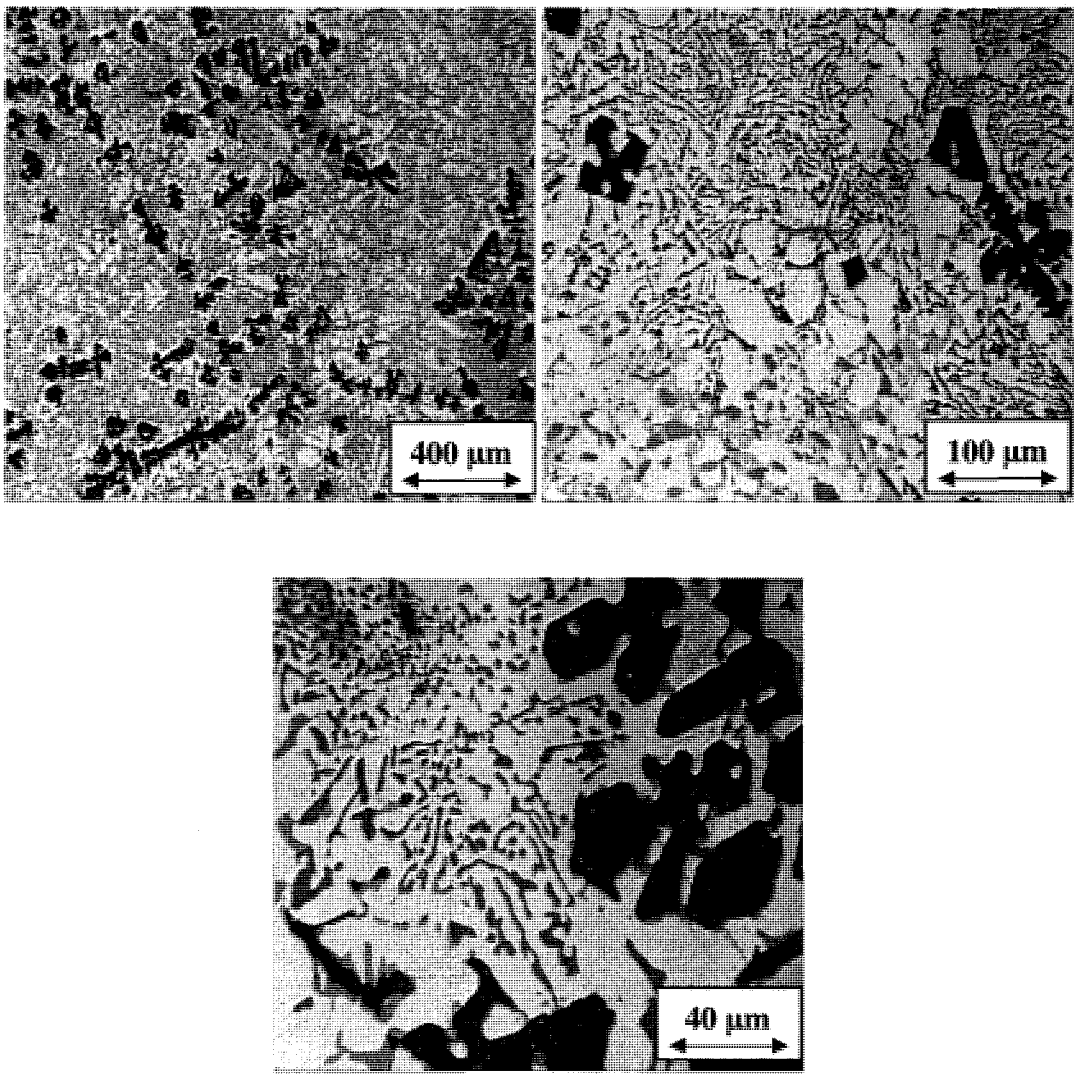

Fig. 66: The microstructure of 10% Mg alloy after T6 heat treatment at three different magnifications of 50X, 200X and 500X.

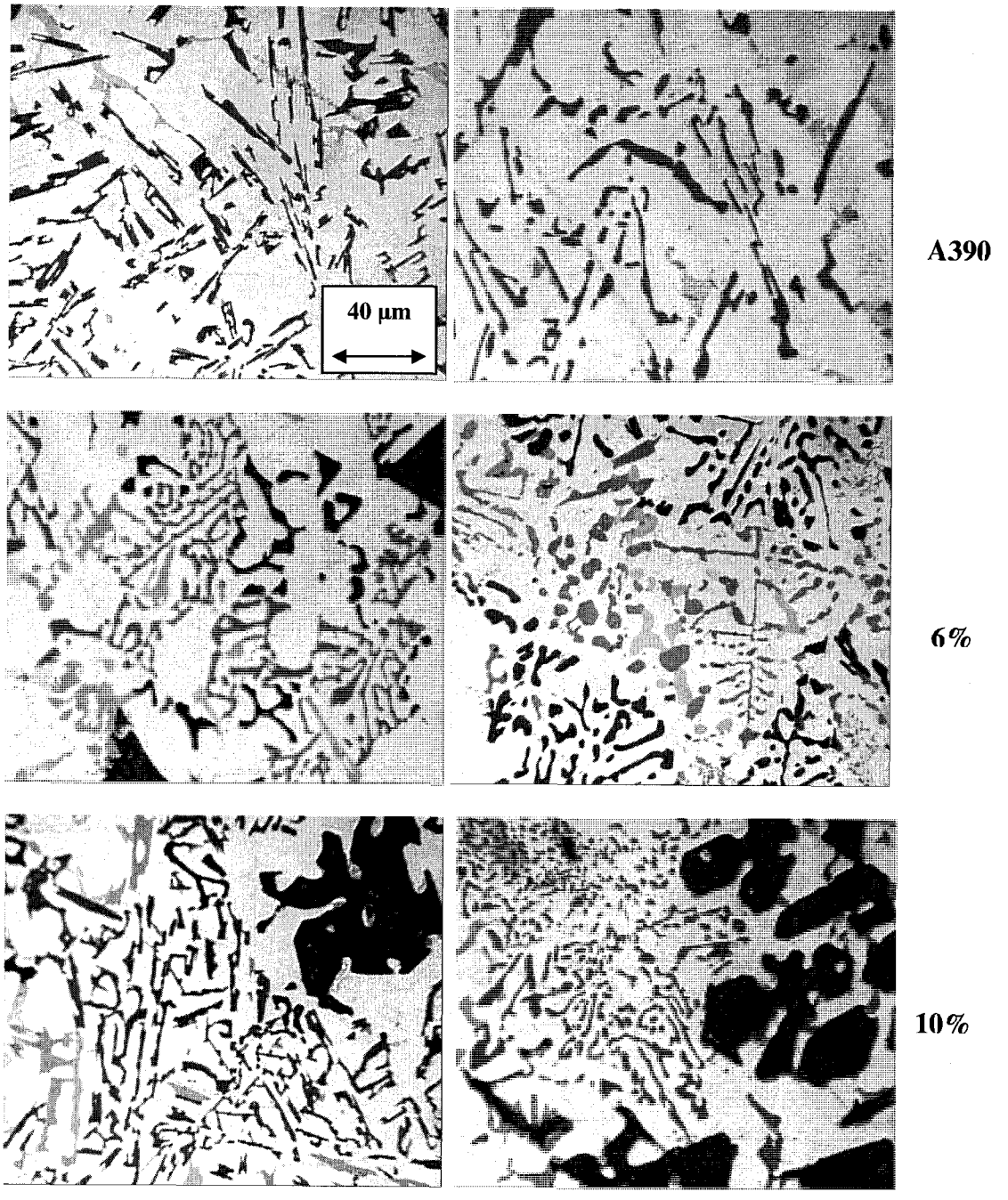

Fig. 67: The comparison of the microstructure of A390 alloy with 6% and 10% Mg alloy before and after T6 heat treatment at high magnification of 500X. The left and right columns represent the as-cast microstructures and after T6 heat treatment samples.

CHAPTER 6- GENERAL DISCUSSION

The objective of this study was to produce alloys with hardness and wear resistance higher than the A390 alloy and of a lower density. In support of this objective the thermodynamic properties and the microstructural characteristics of these alloys resulting from the semi solid processing were used. A decrease from 2.68 to 2.51 g/cm^3 was determined experimentally when the Mg content was increased from 0.5 wt% to 10 wt%. The reduced value is due to the formation of primary Mg_2Si intermetallic phase (density: 1.99 g/cm^3) as a result of reaction with silicon as well as the formation of eutectic Mg_2Si in the matrix of A390 alloy when Mg content is increased. This is of particular interest to the automobile industry for the production of fuel-efficient vehicles using light weight components produced from these alloys where the combination of high wear resistance and light weight is required.

The thermodynamic prediction using FACTSAGE software was carried out in order to thoroughly investigate the solidification characterization of the hyper-eutectic Al-Si alloys with Mg contents up to 10%. The results indicated that a minimum value of 7.2% Mg is required for the precipitation of Mg_2Si as a primary phase. For Mg content lower than 7.2%, silicon solidifies as a primary phase. Therefore, this value was identified as a critical Mg content for the solidification of these alloys with different Mg content. In order to obtain eutectic Mg_2Si in the matrix, a minimum value of 4.2% Mg is required. The results showed that the eutectic Mg_2Si (with Chinese script morphology) solidifies

in a eutectic network together with eutectic silicon and α-Al when the value of Mg in the alloy with a minimum of 4.2% Mg. For alloys with Mg content less than 4.2%, the matrix network consists of only a binary Al + Si eutectic structure. The FACTSAGE thermodynamic computation identified these two important critical Mg points for alloy with different Mg contents. Another important result obtained from the thermodynamic investigation is illustration of liquid fraction versus temperature curve for the solidification of alloys with different Mg contents. The comparison of curves indicated that the eutectic formation temperature significantly decreases with increasing the Mg content. The maximum reduction occurs at 4.2% Mg and then becomes almost constant. This is very important findings for the modification of the eutectic structure because the decrease of the eutectic formation temperature can promote the number of active nuclei in the melt and modify the eutectic microstructure, specifically that of eutectic silicon.

The results obtained by FACTSAGE were used as a starting point for the experimental work. Both Mg_2Si and Si particles are hard phases and are very similar in terms of physical properties and solidification behavior. This implies that high Mg content alloys can improve the hardness and wear resistance of alloy as well as decrease the density.

The experimental work compared the eutectic structure of the A390 alloy and the high Mg content alloys during solidification for continuous cooling tests. As expected, the eutectic silicon morphology was significantly modified from large flake morphology with high inter-flake space to a finely structured of eutectic network. As shown in the

results, the eutectic Mg_2Si with a Chinese script form (same as eutectic silicon) appeared in the matrix of eutectic network for the high Mg content alloys. Because the eutectic phase comprises nearly 80% of the microstructure, the modification of eutectic silicon is of high importance for the improvement of the alloy properties. On the other hand, the solid fraction of the primary phases doubles when the value of Mg increases from 0.5% to 10%. Therefore, it is predictable that the hardness value increases with addition of Mg content to the alloy. The results of the hardness test confirmed the increase of hardness value for high Mg content alloy.

Another set of experiments was carried out in order to verify the microstructure of the alloy with increasing Mg content using different semi solid forming method: thixoprocessing and rheoprocessing, for isothermal condition in the semi solid state. The goal was to focus on the evolution of morphology and size of primary Mg_2Si and Si particles. Excessive growth of primary silicon is expected using conventional casting of A390 alloy due to large solidification interval (about 150 ^{0}C). The large primary silicon can be easily detached from matrix when loads are applied resulting in poor mechanical properties. Therefore, the size and morphology of primary phase plays an important role in improving the mechanical properties. It was shown that the primary Mg_2Si in the microstructure of SSM cast samples of alloy with high Mg content is considerably modified when compared to the primary silicon in A390 alloy. The morphology and size of primary Mg_2Si particle is more globular and finely structured during the semi solid casting processes while the primary silicon remain faceted and large. In addition, the

eutectic phase, consisting of mainly eutectic silicon, is transformed during the rheocasting process from flake eutectic silicon and becomes more compact and polygonal during thixocasting process. As a result, the semi solid metal processes are accepted as an economically attractive and powerful alternative to conventional casting of there alloys with high Mg content. By comparing the microstructure of samples produced by the two semi solid processes, the thixocasting processes showed remarkable modification of primary Mg_2Si but not of Si. On the other hand, the outstanding modification was achieved for α-Al grains through rheocasting process. This implies that rheocasting can be used for forming of hypoeutectic Al-Si alloy where α-Al solidifies as primary phase.

The apparent viscosity was also measured for alloys with high Mg content during continuous solidification experiments and for increasing shear rates. Higher shear rates resulted in a lower viscosity at the same solid fraction which is indicative of the transforming of the primary particles of Mg_2Si and Si with more globular shapes as result of the shear rate. The results of 'step change' test showed that flow behavior of the A390 alloy in the semi solid region near to the eutectic formation temperature is more Newtonian than the 10% Mg alloy. This may be attributed to the higher solid fraction of the high Mg content alloy compared to the A390 alloy. However both alloys show the pseudo-plastic behavior (non Newtonian) and their viscosities can be presented by a power law equation. It was shown that greater modification of the microstructure can be achieved for high Mg content alloy using semi solid casting processes.

Finally, the hardness tests was investigated for conventionally cast samples using gravity permanent mould and T6 heat treatment samples of the A390 base alloy as well as the 6% and 10% Mg alloys. It was shown that for as-cast samples, the hardness value increases with increasing the Mg content of alloys. Many reasons are attributed to the increase of hardness value with increasing Mg content. One of theses is due to the modification of the eutectic silicon. In this case, the matrix of the high Mg alloys consists of eutectic silicon with a very fine skeleton network whereas the eutectic microstructure of A390 alloy consists of eutectic silicon with a large individual needle morphology and high inter-needle spacing dispersed in matrix of α-Al. Chinese script eutectics Mg_2Si morphology was also observed in the matrix of the high Mg alloys and was formed to increase the hardness value of alloy. Another reason is believed to be due to the increase of the solid fraction of hard primary particles such as silicon and Mg_2Si from 6.1% to 12.2% which is two times higher for A390 than for 10% Mg alloys.

The hardness values for the samples after T6 heat treatment are all higher than for the as-cast samples. However, contrary to hardness value of the as-cast samples, the hardness decreases with increasing the Mg content. This indicates that the high stiffness of α-Al due to the precipitation hardening effect as well as the eutectic morphology and its distribution in matrix plays a predominant role for sample heat treated. Therefore, the hardness value becomes more pronounced for A390 alloy due to high solid fraction of α-Al and large eutectic silicon particles compared to the high Mg content alloy with low

solid fraction of α-Al. This can explain the values of almost the same hardness for 6% and 10% Mg alloys.

CHAPTER 7- CONTRIBUTIONS AND RECOMMENDATION

7-1 Original contribution

The study has resulted in new and original contribution in the development and processing of a new class of alloys. The specific contributions are itemized as below:

1- Increasing the Mg content of hyper-eutectic Al-Si alloys (Al-17Si-4.5Cu) from 0.5 wt% to 10 wt% Mg, not only decrease the density but also changes the solidification structure and the resulting mechanical properties. This decrease of density is due to the formation of Mg_2Si intermetallic phase which has a lower density (1.99 g/cm^3) than primary silicon (2.33 g/cm^3).

2- Thermochemical computation using FACTSAGE has shown that the solidification of basic A390 alloy (Al-17Si-4.5Cu-0.5Mg) proceeds sequentially, where the primary, binary, ternary and quaternary reactions occur at formation temperatures of 653.1, 566.2, 502.4 and 496.9 °C, respectively. With the addition

of Mg, up to 10% Mg, two critical compositions were detected at 4.2% and 7.2% Mg where the formation temperatures for the liquidus, start of the binary and of the ternary reaction are changed.

3- The zone of precipitation of Mg_2Si intermetallic phase has been clearly illustrated by computation of phase diagram. From 0.5% Mg to 4.2% Mg, the Mg_2Si solidifies only in the ternary reaction zone. From 4.2% to 7.2%, the Mg_2Si solidifies in both binary and ternary reaction zones and for Mg contents greater than 7.2%, the Mg_2Si solidifies as a primary, binary and ternary phase. The liquid fraction-temperature curves showed that eutectic formation temperature decreases by 17 °C when the Mg content in A390 alloy increases to 10%.

4- The results obtained by FACTSAGE software also showed a good agreement with DSC (Differential Scanning Calorimeter) test as well as with cooling curves tests confirming the change in the eutectic formation temperature which decreases abruptly at 4.2% Mg. Above this value of Mg content, this temperature stays constant.

5- The microstructure of the matrix for the conventionally cast samples of the 6% and 10% Mg alloy was clearly characterized. Eutectic Mg_2Si with Chinese script morphology together with eutectic Si and dendritic α-Al were identified. This is in contrast to the eutectic microstructure of A390 (0.5% Mg) consists of binary Al + Si phases. A significant modification of the eutectic silicon was also observed for the high Mg content alloy due to reduction of the eutectic formation temperature. The large flake morphology of the eutectic silicon in the matrix of A390 alloy changes considerably with the addition of Mg content by forming a fine skeleton network with script morphology similar to the eutectic Mg_2Si. This morphology is the same for alloy with 6% and 10% Mg.

6- Rheoprocessing tests carried out by using a stirrer (rotation speed = 260 rpm, $\dot{\gamma}_{ave}$ = 52 s^{-1}) during solidification with continuous cooling resulted in a fragmentation of the eutectic silicon. The skeleton morphology observed in the matrix of an as-cast alloy with 6% and 10% Mg was completely transformed in the sheared samples resulting in finer structure.

7- Other intermetallic phases such as θ-$CuAl_2$, Q-$Cu_2Mg_8Si_6Al_5$ and β-Al_5FeSi were also identified in the microstructure of A390 alloy. The iron containing β

phase is the most detrimental to the mechanical properties. With increasing Mg content the β-Al_5FeSi phase is transformed to phase π ($Al_8FeMg_3Si_6$) with no unfavorable effect on the properties.

8- The rheological characterization of A390 and 10% Mg alloys showed that the viscosity gradually increases from the value of liquid state when the solidification of the primary Mg_2Si phase starts. Higher shear rates slow down this viscosity increase with temperature. At the ternary eutectic reaction (Liq. → Al + Si + Mg_2Si) temperature of 544 °C, the viscosity abruptly increases.

9- The viscosity variation of 10% Mg alloy at the isothermal semi solid temperature of 550 °C, near the eutectic formation temperature where the solid fraction is 12%, the shear at 260 rpm indicates that the apparent viscosity initially decreases to a steady state value at 400 seconds. After this period the viscosity increases very solely as result of particle coarsening.

10- The difference of the morphological evolution of the semi solid microstructure using rheoprocessing and thixoprocessing were clearly demonstrated by

comparing basic A390 and 10% Mg alloys. The morphology and size of α-Al grains in the rheoprocessed samples are more spheroidal and larger than the thixoprocessed samples at the same isothermal temperature. The difference in the morphology of Si and Mg_2Si primary particles was explained in terms of the effect of temperature, solid fraction ang ageing time. For both processes, the morphology of the eutectic silicon in the matrix is transformed from the needle like to a compact polygonal shape.

11- The increase in hardness of alloys with increasing the Mg content for conventionally cast samples is attributed to transformation of the eutectic phases as well as the increase of the solid fraction. After T6 heat treatment the hardness for all compositions was higher than for the as-cast samples. An anomaly was observed however to the heat treated samples where the hardness decreases with increasing the Mg content. The solution heat treatment promotes the rounding of the flake eutectic silicon and the eutectic Mg_2Si phase. The high hardness is due to the precipitation hardening effect of α-Al solid solution in the matrix. Since the solid fraction of α-Al in the matrix of A390 alloy is higher than for the high Mg containing alloys, the hardness is therefore higher.

7-2 Recommendations

More experiments need to be carried out in future in order to study the effect of Mg on other mechanical properties of A390 alloy. A thixoprocessing method can be used for these alloys because, contrary to primary silicon, the primary Mg_2Si intermetallic transforms to a fine globular morphology during this process. This process can eliminate the porosity if the alloy is formed by a pressure die-casting process. The microstructure of high Mg content alloy produced by the conventional liquid casting process showed the value of porosity 3 times higher than the A390 alloy. It was clearly observed that the high viscosity of the high Mg content alloys makes casting difficult, resulting in more porosity. This implies that conventional casting of high Mg content alloys is not advisable. Die filling at semi-solid temperature using applied pressure can eliminate the porosity. In addition, the shrinkage is much less than that of a fully molten alloy. Samples thixoformed in this way would also result in better wear resistance as well as hardness.

REFERENCES

[1] D.B. Spencer, R. Mehrabian and M.C. Flemings. (1972). Metal. Trans., Vol. 3, pages: 1925-32.

[2] P.A. Davidson, An Introduction to Magneto Hydrodynamics, Cambridge, 2001.

[3] T. Haga, T. Kouda, H. Motoyama, N. Inoue and S. Suzuki, Proceedings of the ICAA7 on Aluminium Alloys: Their Physical and Mechanical Properties Charlottesville, VA, Publ. Trans. Tech. Publications 2000 (1998), pp. 327–332 Part 1.

[4] K.P. Young, C.P.Kyonka, J.A. Courtois, Fine grained metal composition', US Patent 4,415,374 (30 March 1982).

[5] D.H. Kirkwood, C.M. Sellars, L.G. Elias Boyed, Thixotropic materials European Patent 0305375 B1 (28 October 1992).

[6] Lasa, L., & Rodriguez-Ibabe, J. M. (2003). Wear behavior of eutectic and hypereutectic Al–Si–Cu–Mg casting alloys tested against a composite brake pad. *Materials Science and Engineering A, Vol. 363*(Issues 1-2), 193-202.

[7] Kapranos, P., Kirkwood, D. H., Atkinson, H. V., Rheinlander, J. T., Bentzen, J. J., Toft, P. T., et al. (2003). Thixoforming of an automotive part in A390 hypereutectic Al–Si alloy. *Journal of Materials Processing Technology, Vol. 135*(2-3), 271-277.

[8] Wang, F., Ma, Y., Zhang, Z., Cui, X., & Jin, Y. (2004). A comparison of the sliding wear behavior of a hypereutectic Al–Si alloy prepared by spray-deposition and conventional casting methods. *Wear Vol. 256*, 342-345.

[9] Lee, J. I., Lee, H. I., & Kim, M. I. (1995). Formation of spherical primary silicon crystals during semi solid processing of hypereutectic Al-15.5wt%Si alloy. *Scripta Metallurgica et Materialia, Vol. 32*(12), 1945-1949.

[10] Zhao, Y. G., Qin, Q. D., Zhao, Y. Q., Liang, Y. H., & Jiang, Q. C. (2004). In situ Mg_2Si/Al–Si composite modified by K2TiF6. *Materials Letters, Vol. 58*(16), 2192-2194.

[11] J. Zhang, Z. F., Y. Q. Wang and B. L. Zhou. (2000). Microstructural development of Al– 15wt.%Mg2Si in situ composite with mischmetal addition. *Materials Science and Engineering A, Vol. 281*(1-2), 104-112.

[12] Q.D. Qin, Y.G. Zhao, W. Zhou, P.J. Cong, Effect of phosphorus on microstructure and growth manner of primary Mg_2Si crystal in Mg_2Si/Al composite. Materials Science and Engineering: A, Volume 447, Issues 1-2, 25 February 2007, Pages 186-191.

[13] Q.D. Qin, Y.G. Zhao, C. Liu, P.J. Cong, W. Zhou, Strontium modification and formation of cubic primary Mg_2Si crystals in Mg_2Si/Al composite, Journal of Alloys and Compounds, Volume 454, Issues 1-2, 24 April 2008, Pages 142-146.

[14] C.L. Xu, H.Y. Wang, C. Liu, Q.C. Jiang. Growth of octahedral primary silicon in cast hypereutectic Al–Si alloys, Journal of Crystal Growth, Volume 291, Issue 2, 1 June 2006, Pages 540-547.

[15] Ru-yao Wang, Wei-hua Lu, L. M. Hogan, Growth morphology of primary silicon in cast Al–Si alloys and the mechanism of concentric growth. Journal of Crystal Growth, Volume 207, Issues 1-2, November 1999, Pages 43-54.

[16] Jiang, Q. C., Xu, C. L., Lu, M., & Wang, H. Y. (2005). Effect of new Al-P-Ti-TiC-Y modifier on primary silicon in hypereutectic Al-Si alloys. *Materials Letters, Volume 59*(6), 624-628.

[17] Li, C., Liu, X., & Wu, Y. (2008). Refinement and modification performance of Al–P master alloy on primary Mg2Si in Al–Mg–Si alloys. *Alloys and Compounds.*

[18] Qin, Q. D., Zhao, Y. G., Zhou, W., & Cong, P. J. (2007). Effect of phosphorus on microstructure and growth manner of primary Mg2Si crystal in Mg2Si/Al composite. *Materials Science and Engineering A, Volume 447*(Issues 1-2), 186-191.

[19] Xu, C. L., Jiang, Q. C., Yang, Y. F., Wang, H. Y., & Wang, J. G. (2006). Effect of Nd on primary silicon and eutectic silicon in hypereutectic Al-Si alloy. *Journal of Alloys and Compounds, Volume 422*(1-2), L1-L4.

[20] Zhang, H., Haili DUAN, Guangjie SHAO, Luoping XU, Junlin YIN, & YAN, B. (2006). Modification mechanism of cerium on the Al-18Si alloy. *Rare Metals, Volume 25*(1), 11-15.

[21] Zhao, Y. G., Qin, Q. D., Zhao, Y. Q., Liang, Y. H., & Jiang, Q. C. (2004). In situ Mg2Si/Al–Si composite modified by K2TiF6. *Materials Letters, Vol. 58*(16), 2192-2194.

[22] Chen, C. M., Yang, C. C., & Chao, C. G. (2005). A novel method for net-shape forming of hypereutectic Al-Si alloys by thixocasting with powder preforms. *Journal of Materials Processing Technology, Volume 167,* (1), 103-109.

[23] Kapranos, P., Kirkwood, D. H., Atkinson, H. V., Rheinlander, J. T., Bentzen, J. J., Toft, P. T., et al. (2003). Thixoforming of an automotive part in A390 hypereutectic Al–Si alloy. *Journal of Materials Processing Technology, Vol. 135*(2-3), 271-277.

[24] Lee, J. I., Lee, H. I., & Kim, M. I. (1995). Formation of spherical primary silicon crystals during semi solid processing of hypereutectic Al-15.5wt%Si alloy. *Scripta Metallurgica et Materialia, Vol. 32*(12), 1945-1949.

[25] M.C Flemings. (1974). "Solidification processing", Mc Graw Hill Book Co., New York.

[26] K.P. Young and C.P. Kyonka, J.A. Courtis. (1984). U.S. Patent 4, 482, 012.

[27] A.Vogel, R.D. Dohetry and B. Canter. (1979). Proc. Int. Conf. on solidification and casting of metals. Eds., J.Hunt, Sheffield, The Metal Society, page: 581.

[28] R.D. Dohetry, H.I. Lee and E.E. Feest. (1984)."Microstructure of Stir-Cast Metals" Mat. Sci.& Eng. 65(1), pages 181-189.

[29] Omid Lashkari and Reza Ghomashchi, The implication of rheology in semi solid metal processes: An overview, Journal of Materials Processing Technology, Volume 182, Issues 1-3, 2 February 2007, Pages 229-240.

[30] M. Suéry, Mise en Forme des alliages métalliques a l'état semi solide, Lavoisier Publication, France (2002).

[31] M.C. Flemings, Behavior of metal alloys in the semi solid state, *Metal. Trans. A* 22A (1991) (May), pp. 952–981.

[32] D.H. Kirkwood, Semisolid metal processing, *Int. Mater. Rev.* 39 (1994) (5), pp. 173–189.

[33] O. Lashkari, R. Ghomashchi, The implication of rheological principles for characterization of semi solid aluminum cast billets, J. Mater. Sci., in press.

[34] J.Y. Chen and Z. Fan, Modeling of rheological behavior of semisolid metal slurries, part 3—transient state behavior, *Mater. Sci. Technol.* 18 (2002) (March), pp. 250–257.

[35] R.J. Kissling and J.F. Wallace, Grain refinement of aluminum castings, *Foundry* (1963) (June), pp. 78–82.

[36] D.R. Poirier and G.H. Geiger, Transport Phenomena in Materials Processing, TMS Publication (1994).

[37] H. Wang, C.J. Davidson, J.A. Taylor and D.H. St. John, Semisolid casting of AlSi7Mg0.35 alloy produced by low temperature pouring, *Mater. Sci. Forum* 396–402 (2002), pp. 143–148.

[38] O. Lashkari, Sh. Nafisi, R. Ghomashchi, Microstructural characterization of rheocast billets prepared by variant pouring temperatures, Mater. Sci. Eng. A, in press.

[39] D.B. Spencer, R. Mehrabian and M.C. Flemings, Rheological behavior of Sn-15Pct Pb in the crystallization range, *Metall. Trans.* 3 (1972), pp. 1925–1932.

[40] T.Z. Kattamis and T.J. Piccone, Rheology of semisolid Al–4.5% Cu–1.5% Mg alloy, *Mater. Sci. Eng. A* A131 (1991), pp. 265–272.

[41] Shahrooz Nafisi and Reza Ghomashchi, Effect of stirring on solidification pattern and alloy distribution during semi solid-metal casting, Materials Science and Engineering: A, Volume 437, Issue 2, 15 November 2006, Pages 388-395

[42] R. Wang, W. Lu and L.M. Hogan. (1999) "Growth Morphology of Primary Silicon in Cast Al-Si Alloys and The Mechanism of Concentric Growth". J. Cryst. Growth, 207, pages: 43-54.

[43] Q.C. Jiang, C.L. Xu, M. Lu and H.Y. Wang, Effect of new Al–P–Ti–TiC–Y modifier on primary silicon in hypereutectic Al–Si alloys, Materials Letters, Volume 59, Issue 6, March 2005, Pages 624-628

[44] P.J. Ward, H.V. Atkinson, P.R.G. Anderson, L.G. Elias, B.Garcia, L.Kahlen and J-M. Rodriguez-Ibabe. (1996)."Semisolid Processing of Novel MMCs Based on Hypereutectic Al-Si Alloys", Acta Mater. Vol.44, No.5, pages:1717-1727.

[45] H. V. Atkinson, S. C. Hogg and P. Kapranos. "Silicon Network in Al-High Silicon Alloys and Their Effect on Semi solid Processing". Thixoforming conference 2004, pages 241-245.

[46]H.S. Kang, W.Y. Yoon, K.H. Kim, M.H. Kim and Y.P. Yoon. (2005) "Micro structure Selections in the Undercooled Hypereutectic Al-Si Alloys", Material Science and Engineering, A, Volume 404, Issues 1-2, Pages 117-123.

[47] L. Lasa and J. M. Rodriguez-Ibabe, Wear behavior of eutectic and hypereutectic Al–Si–Cu–Mg casting alloys tested against a composite brake pad, Materials Science and Engineering A, Volume 363, Issues 1-2, 20 December 2003, Pages 193-202.

[48] Feng Wang, Yajun Ma, Zhengye Zhang, Xiaohao Cui, Yuansheng Jin, A comparison of the sliding wear behavior of a hypereutectic Al–Si alloy prepared by spray-deposition and conventional casting methods, Wear 256 (2004) 342–345.

[49] Attipon Diewwanit, 1996, Semi solid Processing of Hypereutectic Al-Si Alloys, Ph.D thesis, MIT.

[50] YücelBirol, Cooling slope casting and thixoforming of hypereutectic A390 alloy, *Journal of Materials Processing Technology, Volume 207, Issues 1-3, 16 October 2008, Pages 200-203*

[51] L.F. Mondolfo.(1978). "Manganese in Aluminum Alloys" , Syracuse University, USA. Publisher: The Centre, ISBN: 2901109012.

[52] P. Kapranos, D. H. Kirkwood, H. V. Atkinson, J. T. Rheinlander, J. J. Bentzen, P. T. Toft, C. P. Debel, G. Laslaz, L. Maenner, S. Blais *et al.* (2003)"Thixoforming of An Automotive Part in A390 Hypereutectic Al–Si Alloy", journal of Materials Processing Technology, Volume 135, Issues 2-3, Pages 271-277.

[53] Jian Li, M. Elmadagli, V.Y. Gertsman, J. Lo and A.T. Alpas. (2006), "FIB and TEM characterization of subsurfaces of an Al–Si alloy (A390) subjected to sliding wear", Materials Science and Engineering: A, Volume 421, Issues 1-2, Pages 317-327.

[54] C. M. Chen, C. C. Yang and C. G. Chao. (2004), "Thixocasting of hypereutectic Al–25Si–2.5Cu–1Mg–0.5Mn alloys using densified powder compacts", Materials Science and Engineering A, Volume 366, Issue 1, Pages 183-194.

[55] Christopher W. Bale and Arthur D. Pelton, FACTSAGE 5.4.1, C.R.C.T (Centre of Research for Computational Thermochemistry), École Polytechnique de Montréal.

[56] Lennart Backerud, GuoCai Chai, Jarmo Tamminen; Solidification Characteristics of Aluminum Alloys, Volume 2 – Foundry Alloys; University of Stockholm; Sweden

[57] L. Backerud, G. Chai and J. Tamminen. (1990). "Solidification Characteristics of Aluminium Alloys", Foundary Alloys, AFS/Skanaluminium , Des Plaines, IL, USA, Vol. 2, page 86.

[58] M.A. Moustafa, F.H. Samuel and H.W. Doty. (2003). "Effect of Solution Heat Traetment and Additives on the Microstructure of Al-Si (A413.1), Automotive Alloys", Journal of Materials Science, 38, 4507-4522.

[59] S. Spigarelli, E.Evangelista and S.Cucchieri. (2004). "Analysis of the Creep Respo nse of an Al-17Si-4Cu-0.55Mg alloy",Material Science and Engineering A 387-389, pages: 702-705.

[60] Dr. Sc, Ir.C. and Ir.E. Marc Van Lancker. (1967). "Metallurgy of aluminium alloy", translated [from the French] by E. Bishop, published by London, chapman-hall, pages: 469-476.

[61] Y. G. Zhao, Q. D. Qin, Y. Q. Zhao, Y. H. Liang and Q. C. Jiang, In situ Mg_2Si/Al–Si composite modified by K_2TiF_6, Materials Letters, Volume 58, Issue 16, June 2004, Pages 2192-2194.

[62] Q.D. Qin, Y.G. Zhao, P.J. Cong, W. Zhou, B. Xu Semisolid microstructure of Mg_2Si/Al composite by cooling slope cast and its evolution during partial remelting process, *Materials Science and Engineering: A, Volume 444, Issues 1-2, 25 January 2007, Pages 99-103*

[63] J. Zhang, Z. Fan, Y. Q. Wang and B. L. Zhou, Microstructure and mechanical properties of in-situ Al- Mg_2Si composites, Material Science and Technology, july-august 2000, vol. 16, page 913-918.

[64] Jae Joong Kim, Do Hyang Kim, K. S. Shin and Nack J. Kim, Modification of Mg_2Si morphology in squeeze cast Mg-Al-Zn-Si alloys by Ca or P addition, Scripta Materialia, Volume 41, Issue 3, 9 July 1999, Pages 333-340.

[65] L. Lasa and J. M. Rodriguez-Ibabe, Wear behavior of eutectic and hypereutectic Al–Si–Cu–Mg casting alloys tested against a composite brake pad, Materials Science and Engineering A, Volume 363, Issues 1-2, 20 December 2003, Pages 193-202.

[66] Shahrooz Nafisi, Omid Lashkari, Reza Ghomashchi, Frank Ajersch and Andre Charette, Microstructure and rheological behavior of grain refined and modified semi solid A356 Al–Si slurries, Acta Materialia, Volume 54, Issue 13, August 2006, Pages 3503-3511.

[67] Omid Lashkaria,, Frank Ajerschb, Andre Charettec, X.-Grant Chen, Microstructure and rheological behavior of hypereutectic semi solid Al–Si alloy under low shear rates compression test, Materials Science and Engineering A, 492 (2008) 377–382

[68] Yucel Birol, Feriha Birol, Sliding wear behavior of thixoformed AlSiCuFe alloys *Wear, Volume 265, Issues 11-12, 26 November 2008, Pages 1902-1908.*

[69] Q.C. Jiang, C.L. Xu, M. Lu and H.Y. Wang, Effect of new Al–P–Ti–TiC–Y modifier on primary silicon in hypereutectic Al–Si alloys, Materials Letters, Volume 59, Issue 6, March 2005, Pages 624-628.

[70] J. Valer Goñi, J. M. Rodriguez-Ibabe and J. J. Urcola, Strength and toughness of semi solid processed hypereutectic Al/Si alloys, Scripta Materialia, Volume 34, Issue 3, 1 February 1996, Pages 483-489.

[71] D.K. Dwivedi, A. Sharma and T.V. Rajan, Interface temperature under dry sliding conditions, *Mater Trans JIM* **43** (9) (2002), pp. 2256–2261.

[72] D.K. Dwivedi, Interface temperature and wear behavior of cast Al–Si alloys, *Mater Sci Technol* **19** (8) (2003), pp. 1091–1096.

[73] K.B. Shah, Sandeep Kumar and D.K. Dwivedi, Aging temperature and abrasive wear behavior of cast Al–(4%, 12%, 20%)Si–0.3% Mg alloys, *Materials & Design, Volume 28, Issue 6, 2007, Pages 1968-1974*

[74] C.M. Chen, C.C. Yang and C.G. Chao, Dry sliding wear behaviors of Al–25Si–2.5Cu–1Mg alloys prepared by powder thixocasting, *Materials Science and Engineering A, Volume 397, Issues 1-2, 25 April 2005, Pages 178-189*

[75] Q.C. Jiang, C.L. Xu, M. Lu and H.Y. Wang, Effect of new Al–P–Ti–TiC–Y modifier on primary silicon in hypereutectic Al–Si alloys, *Materials Letters, Volume 59, Issue 6, March 2005, Pages 624-628*

[76] Feng Wang, Yajun Ma, Zhengye Zhang, Xiaohao Cui and Yuansheng Jin, A comparison of the sliding wear behavior of a hypereutectic Al–Si alloy prepared by spray-deposition and conventional casting methods, *Wear, Volume 256, Issues 3-4, February 2004, Pages 342-345.*

[77] G. Timmermans and L. Froyen, Tribological performance of hypereutectic P/M Al–Si during sliding in oil, *Wear, Volume 231, Issue 1, June 1999, Pages 77-88*

[78] L. Lasa and J. M. Rodriguez-Ibabe ,Wear behavior of eutectic and hypereutectic Al–Si–Cu–Mg casting alloys tested against a composite brake pad, Materials Science and Engineering A, Volume 363, Issues 1-2, 20 December 2003, Pages 193-202.

[79] Dheerendra Kumar Dwivedi, Wear behavior of cast hypereutectic aluminium silicon alloys, *Materials & Design, Volume 27, Issue 7, 2006, Pages 610-616*

[80] Wang, R., Lu, W., & Hogan., L. M. (1999). Growth Morphology of Primary Silicon in Cast Al-Si Alloys and The Mechanism of Concentric Growth. *Crystal Growth, 207*, 43-54.

[81] Liu, D., Atkinson, H. V., & Jones, H. (2005). Thermodynamic prediction of thixoformability in alloys based on the Al–Si–Cu and Al–Si–Cu–Mg systems. *Acta Materialia, Vol. 53*(14), 3807-3819.

[82] Ward, P. J., Atkinson, H. V., Anderson, P. R. G., L.G. Elias, B. G., L.Kahlen, & Rodriguez-Ibabe., J.-M. (1996). Semisolid Processing of Novel MMCs Based on Hypereutectic Al-Si Alloys. *Acta materialla, Vol.44*(5), 1717-1727.

[83] Ajersch, F., Messaoud, F., & Azzi., L. (2003). Rheological Characteristics of AZ91E Alloys in Semi solid State. *TMS Aluminium Proceeding,* , 65-75.

[84] Hsueh-I Chen, Jyh-Chen Chen, Jyun-Jhong Liao, The influence of shearing conditions on the rheology of semi solid magnesium alloy *Materials Science and Engineering: A, Volume 487, Issues 1-2, 25 July 2008, Pages 114-119.*

[85] FAN Z. Semisolid metal processing [J]. International Materials Reviews, 2002, 47(2): 1–34.

[86] K. Ichikawa, S. Ichizuka and Y. Kinoshita, Trans. Japan Inst. of metals. 28 (1978) 135.

[87] G. Arakan, S. Takamori, Y. Ohsawa and A. Sato, J. Japan Inst. of metals. 59 (1995) 559.

[88] Alireza Hekmat-Ardakan, Rheological characterization of A390 alloy in the semi solid state, 2006, master thesis, École Polytechnique de Montréal.